EFFECTIVE CROSS-SECTIONS FROM TRANSPORT PROPERTY MEASUREMENTS

by

Martin James Ross, BSc(Eng), ACGI

A thesis submitted for the Degree of Doctor of Philosophy of the University of London and for the Diploma of Membership of the Imperial College.

Department of Chemical Engineering and Chemical Technology
Imperial College of Science, Technology and Medicine
London S.W.7.

November 1988

ABSTRACT

This thesis presents the measurement of the thermal conductivity of the gases helium, neon, hydrogen, carbon dioxide, nitrous oxide, tetrafluoromethane, methane, ethane and ethylene in the temperature range 308 K to 430 K at pressures up to 10 MPa. Also included are argon and nitrogen measurements in the range 170 K to 430 K at pressures up to 10 MPa. The measurements have been made using the transient hot-wire method in an instrument designed to return measurements with an estimated uncertainty of 0.3%. This estimated uncertainty has been confirmed with reference to independently-measured thermal conductivity data for the monatomic gases and, additionally, with reference to the exact kinetic theory relationship between low-density thermal conductivity and viscosity. The high-accuracy, low-density thermal conductivity data for argon, helium and hydrogen are used as an independent test of proposed intermolecular potentials. The low density thermal conductivity of the polyatomic gases is used to demonstrate the inadequacy of the available kinetic theory of polyatomic gases and to indicate areas for further development.

In order adequately to describe the thermal conductivity of monatomic gas mixtures, it is necessary to use high-order kinetic theory expressions. Anticipating that this is also necessary in the case of polyatomic gas mixtures, a development to infinite order of the formal kinetic theory for polyatomic gas mixture thermal conductivity is presented.

The available theories for predicitng the density dependence of thermal conductivity are tested against the new body of high accuracy

thermal conductivity data. Traditional macrosocpic theories are found to be inadequate. A new microscopic theory is used as a basis for a successful semi-empirical predictive scheme.

ACKNOWLEDGEMENTS

I would like to take this opportunity to express my gratitude to the many people who aided and abetted me during the course of this work. I am particularly indebted to my supervisor, Professor W.A. Wakeham, for his excellent guidance and advice in all aspects of the work. Special thanks are due to Dr. J. Millat, Dr. M. Mustafa and Dr. V. Vesovic for sharing their knowledge of kinetic theory with me, and to Dr. R. Craven for his assistance with the equations of state.

I would also like to thank my colleagues Dr. M. Zalaf, Dr. W. Cole, Dr. T. Retsina and Dr. R.D. Trengove, all of whom contributed to the progress of this work.

I would like to extend my gratitude to Mr. I.W. Drummond, Mr. M. Dix and Mr. R. Wood (in the Electronics Workshop) and to Mr. T. Stephenson and the staff of the Chemical Engineering Workshop for their advice and good work which contributed to the running of the thermal conductivity instrument.

I would also like to express my gratitude to Mrs. M. Lubbock for doing a good job of typing this thesis from my original manuscript.

Finally, financial assistance from the United Kingdom Science and Engineering Council is gratefully acknowledged.

CONTENTS

LIST OF TABLES

LIST OF FIGURES

CHAPTER 1

INTRODUCTION

The transport properties of gases have been the subject of intensive experimental and theoretical investigation for many years. The theory of dilute gases and gas mixtures is well advanced, but it is only recently that experimental work has been developed to such an extent that the predictions of theory can be rigorously tested.

The Chapman–Enskog kinetic theory of gases provides a successful theory for the transport of mass, momentum and energy for dilute noble gases. Here the transport coefficients are obtained as functions of fundamental properties of the atoms and well–defined functionals of the force between the atoms. The functional dependence of the transport coefficients on the interaction potential provides a route to the interaction potential. The statistical mechanics of equilibrium systems provides expressions for other macroscopic properties in terms of different functionals of the potentials. With the aid of transport property data and a wide variety of other information, including *ab initio* calculations, sophisticated interaction potentials have been obtained for the monatomic gases and their mixtures. The transport coefficients of particular interest here are the viscosity and thermal conductivity. The kinetic theory results for the viscosity and thermal conductivity of pure monatomic gases in the limit of zero density indicate that the ratio $\lambda RMM/\eta$ is proportional to the heat capacity

$$\frac{\lambda^{o}\ RMM}{\eta^{o}} \alpha\ C_{v}$$

where λ is the thermal conductivity, η the viscosity, RMM the relative molecular weight and C_v the constant volume heat capacity.

The constant of proportionality is a pure number almost totally independent of the interaction potential (with a value of 2.5 to within about 1%). Hence the thermal conductivity and viscosity of the noble gases have an almost identical functional dependence on the interaction potential. For this reason, the viscosity has been used almost exclusively for the determination of the interaction potential. In addition, accurate measurements of viscosity over a wide range of temperatures are much more readily available than equivalent thermal conductivity measurements.

Theories for the transport properties of polyatomic gases are also well advanced. Some time ago it was realized that the classical kinetic theory was insufficient for the prediction of the transport coefficients of polyatomic gases. The reason for this failure is that polyatomic gases have internal degrees of freedom within which energy may be stored, and the interaction potential is, in general, anisotropic. These features of polyatomic gases have important consequences. Energy may be transferred between internal degrees of freedom and translational degrees of freedom via the phenomenum of inelastic collisions, a phenomenum that cannot be accounted for satisfactorily by the classical kinetic theory.

The effects of inelastic collisions on the viscosity of polyatomic gases is anticipated to be small since the internal structure of the molecule is unlikely to affect appreciatively the transport of momentum. This intuitive argument has been verified by extensive model calculations and experiment. The effects of internal energy on thermal conductivity is, however, marked. Therefore, any theory wishing to predict the thermal conductivity of polyatomic

gases must account for the effects of inelastic collisions.

The traditional treatment of this problem follows from an idea originally proposed by Eucken in which two nearly-independent contributions to the thermal conductivity are identified with internal and translational fluxes of energy. The result is then corrected for the coupling of the two fluxes. The most sophisticated kinetic theory formulae of this type are those of Viehland *et al.* These equations are first-order relationships derived from the formal semi-classical theory of Wang Chang and Uhlenbeck, corrected for the effects of spin polarisation.

The expressions for the thermal conductivity are found to be functions of three effective cross-sections which contain all the information about the intermolecular potential. From a macroscopic viewpoint, these effective cross-sections are related to the decay of translational and internal fluxes and the coupling between them. It is important to note that these effective cross-sections provide different, and hence complementary, information about the intermolecular potential than provided by the effective cross-section appropriate to the transfer of momentum.

The calculation of these effective cross-sections for any realistic potential was for many years an almost hopeless task owing to the immense computational effort required. However, recent studies have demonstrated that such calculations may soon be practicable. The cross-sections appropriate to thermal conductivity are known to possess different sensitivities to the anisotropic and isotropic parts of the potential. Whilst experimental measurement of such cross-sections are unlikely to provide all the information necessary for the determination of sophisticated potential surfaces for real systems, they do provide an essential element in the final

definition of such surfaces.

In the absence of routine calculation for the effective cross-sections necessary for evaluation of the thermal conductivity of polyatomic gases, it is generally calculated from other transport property data, principally the viscosity and the collision number of internal energy relaxation (which may be obtained from sound absorption measurements). Also implicit in the formulae is the group

$$\frac{\rho D_{int}}{\eta}$$

where ρ is the gas density, η is the viscosity and D_{int} is the so-called diffusion coefficient of internal energy. The value of D_{int} is not accessible to independent measurements so it is customary to make use of the kinetic theory relationship

$$\frac{\rho D_{int}}{\eta} = \frac{6}{5} A^* \frac{D_{int}}{D}$$

where D is the hypothetical self-diffusion coefficient of the gas and A^* is a ratio of effective cross-sections thought to be independent of the form of the intermolecular potential. It is usual to assume that the ratio D_{int}/D is unity and to use an elastic value of the ratio of A^*.

In order to test the reliability of this scheme, it is necessary to compare the predictions with reliable experimental data. The highest accuracy is required because it is the treatment of a coupling phenomena that is being investigated. Even small errors in the primary quantities, thermal conductivity and viscosity will propagate to produce large errors in the important coupling terms or, more particularly, in $\rho D_{int}/\eta$. It is therefore important that

measurements of thermal conductivity enjoy an accuracy as nearly as possible equivalent to the accuracy obtainable for viscosity.

Following the pioneering work by Haarman and the developments made by Kestin, Wakeham and their collaborators, the transient hot-wire method has been developed as the most accurate method for measurement of the thermal conductivity of gases. Over a period of ten years a number of independent measurements have confirmed an accuracy of ± 0.3% is possible near room temperature. These high-accuracy thermal conductivity data have been used in conjunction with equally high-accuracy viscosity data to investigate the traditional predictive schemes. These comparisons have demonstrated a disappointing lack of agreement between theory and experiment. This situation can be turned to advantage since it demonstrates that the coupling effective cross-sections are sensitive to the anisotropy of the potential and may be used as probes of that part of the potential.

Following the observation made by Mason and Monchick that the presence of inelastic collisions merely increases the flux of internal energy and reduces the translational energy flux, leaving the total flux essentially unchanged, Thijsse *et al.* developed an alternative formulation for the thermal conductivity of polyatomic gases. This new formulation uses different effective cross-sections related to the total heat flux, a difference heat flux and the coupling between them. These effective cross-sections are related to the more usual Wang Chang and Uhlenbeck effective cross-sections found in the Viehland-Mason-Sandler formalism and may be calculated from them directly. A recent theoretical and experimental investigation, in addition to that originally performed by Thijsse *et al.*, has indicated that the Thijsse *et al.* formalism can be used as

the basis for the representation of thermal conductivity over a wide range of temperatures.

In addition to these observations about the usefulness of the zero-density thermal conductivity in the formulation of intermolecular potentials, and the failure of traditional methods of prediction, the theory of the density dependence of transport coefficients has recently been the subject of renewed interest. There has been considerable theoretical development in the region of very high density but the intermediate range has been largely neglected, presumably due to the complexity of density effects on the transport processes in gases. The prediction of dense gas transport coefficients is important to the chemical and process industries where accurate data is necessary for efficient design of process equipment. Available schemes for the prediction of the density dependence of thermal conductivity remain largely untested due to the lack of reliable experimental data.

A theory has recently been proposed for the first density coefficient of thermal conductivity of monatomic gases. The experimental data presented in this thesis are the first of sufficient accuracy to test it.

In view of these facts it is appropriate to carry out an extensive systematic study of the thermal conductivity of gases over a wide range of thermodynamic states. The accuracy of these measurements must, as near as possible, be characteristic of the accuracy obtainable near room temperature. However, there have been few measurements reported in which the transient hot-wire method has been employed away from room temperature. In most cases, excepting the instrument designed at Imperial College, the highest acuracy has not been maintained.

In this thesis the reasons for this failure are described and a new instrument is discussed, capable of measurement in the temperature range 80–430 K and at pressures up to 10 MPa. The accuracy of the measurements is confirmed to be generally ± 0.3% over the entire range except under certain circumstances, which are also explained. The present design is the result of many years of experience with previous installations providing high–accuracy data near room temperature, and it was found that the lack of success of the method away from room temperature turns out to be a problem in practice, rather than a problem in principle. This experience is an example of the great care and attention to detail necessary to attain the highest–accuracy measurements as significant errors may arise from the most subtle causes.

Also in this thesis, a new set of thermal conductivity data is presented for a variety of monatomic and polyatomic gases. This new data set is used in conjunction with other transport property data to obtain experimental effective cross–sections for the polyatomic gases and to make comparisons with the results obtained using recent potentials for the monatomic gases. The zero–density thermal conductivity gas data is used, along with equally reliable viscosity data to confirm the correct operation of the instrument via application of the exact kinetic theory Eucken factor relation (equation 1.1).

In addition, the data is used to investigate the concept of a temperature–independent excess thermal conductivity and to provide a rigorous test of the initial density dependence of the thermal conductivity. In particular, the new data is used to provide a semi–empirical correlation for the initial density dependence of thermal conductivity based on a new, systematic microscopic theory.

The accurate thermal conductivity data for monatomic gas mixtures performed at Imperial College demonstrated that a first-order analysis was insufficient to describe the data. For mixtures of monatomic and polyatomic gases, the available equations were found to be adequate if adjustments were made to some of the quantities found in the expressions. It was considered that a more accurate kinetic theory was needed so that derived quantities enjoyed greater precision and physical significance and that systems of gases with a large molecular mass ratio could be described. It is likely that polyatomic gas mixture data of high accuracy will soon become available, so in order that theory is not a barrier to progress, new higher-order expressions are obtained for the thermal conductivity of polyatomic gas mixtures.

CHAPTER 2

THE THEORY OF THE TRANSIENT HOT-WIRE METHOD

2.1 INTRODUCTION

As described previously, the lack of high-accuracy thermal conductivity data, of at least comparable accuracy to the available viscosity data, motivated the development of the transient hot-wire method. This method is based on measuring the temperature history of a wire suspended in the test fluid while it is subject to internal heating. Basically, the lower the thermal conductivity of the surrounding fluid, the more rapid the temperature rise of the wire. The thermal conductivity of the fluid can be deduced from the rate of temperature increase of the wire.

The method was pioneered by Haarman [1] and developed by Kestin and Wakeham and their collaborators [2-5]. The method is now considered the most accurate method for measuring the thermal conductivity of gases. This claim is justified by a large number of independent measurements near room temperature which have confirmed an accuracy of ± 0.3%; this is comparable to that of viscosity measurements. Prior to the work described in this thesis it has not been possible to maintain this high accuracy over an extended range of temperatures. The reason for this is a matter of experimental and practical detail, which will be discussed later, and not a problem in principle [6].

Because the theory of the transient hot-wire method has been treated in detail elsewhere the description presented here takes the form of a summary of the work carried out when the method was in its infancy.

2.2 THE IDEAL MODEL

The ideal model for the transient hot-wire method involves an infinitely thin, straight wire immersed vertically in an isotropic fluid of infinite extent with temperature-independent physical properties. Initially, the wire and the fluid are at equilibrium (T_0, P_0). The wire is then, at t = 0, subject to a step change in voltage applied to it. The wire then becomes a line source of heat with a constant heat generation, q, per unit length. The thin wire is considered to have zero heat capacity and infinite thermal conductivity. The temperature history of the gas surrounding the wire is obtained via the line source solution of the Fourier heat conduction equation

$$\frac{\partial T}{\partial t} = \alpha . \nabla^2 T \qquad (2.2.1)$$

where α ($= \lambda/\rho C_p$) is the thermal diffusivity of the fluid and is assumed to be constant.

Defining $\Delta T(r, t)$ as the temperature rise of the fluid at time t and radial position r from the wire (i.e. $\Delta T(r, t) = T(r, t) - T_0$), the boundary conditions for the solution of the Fourier equation in the ideal case are

(1) $$t \leq 0 \text{ for all } r \qquad \Delta T(r, t) = 0 \qquad (2.2.2)$$

(2) $$r = 0 \text{ and } t \geq 0 \qquad \lim_{r \to 0} \left[r \frac{\partial T}{\partial t} = - \frac{q}{2\pi\lambda} \right] \qquad (2.2.3)$$

(3) $$r \to \infty \text{ and } t \geq 0 \qquad \lim_{r \to \infty} (\Delta T(r, t)) = 0 \qquad (2.2.4)$$

This problem is standard and has the solution [7]

$$\Delta T(r, t) = \left[\frac{-q}{4\pi\lambda}\right] E_i \left[\frac{-r^2}{4\alpha T}\right] \qquad (2.2.5)$$

E_i is the exponential integral which for large values of $\alpha t/r^2$ may be expanded to yield

$$\Delta T(r, t) = \frac{q}{4\pi\lambda} \ell n \left[\frac{4\alpha t}{a^2 C}\right] + 0 \left[\frac{r^2}{4\alpha t}\right] + \ldots \qquad (2.2.6)$$

where $C = 1.781\ldots$ is the exponential of Euler's constant.

For practical purposes a wire radius is chosen such that the first term above dominates and the residual amounts to less than 0.1% of $\Delta T(r, t)$. Therefore the final equation for the ideal case is

$$\Delta T(r, t) = \frac{q}{4\pi\lambda} \ell n \left[\frac{4\alpha t}{r^2 C}\right] \qquad (2.2.7)$$

It is evident from the above equation that the thermal conductivity of a fluid may be obtained form the slope of a $\Delta T(r, t)$ v. $\ell n(t)$ plot. The thermal diffusivity may be obtained from the temperature rise at a particular time. The prospect of simultaneous thermal conductivity and thermal diffusivity measurements has been the subject of recent review [8].

Equation (2.2.7) is the equation which would describe the temperature history of the fluid field in the ideal case. The ideal case can only be approximated in practice. It is this degree of approximation that determines the performance of the practical instrument. The philosophy underpinning the design of a precision instrument capable of providing primary data is that imperfections in the mathematical model are fully understood. Hence, the instrument comes complete with a full working equation and a detailed knowledge of all the corrections is available. The next section gives a

summary of the corrections to the ideal model. Previous studies [3] have shown that many of the deviations are negligible in most practical instruments.

2.3 CORRECTIONS TO THE IDEAL MODEL

In order to investigate the effect of imperfections in the mathematical model, it is assumed that a set of $\Delta T(r, t)$ v. $\ell n(t)$ data has been obtained. Corrections usually take one of two forms: (i) those that modify the temperature rise and (ii) those which modify, and hence define, the thermodynamic state of the fluid appropriate to the reported thermal conductivity. These two divisions are further sub-divided. This further sub-division is based on the ultimate uncertainty required of the instrument and is therefore dependent on the purpose for which it is intended. If the ultimate uncertainty is of order 0.3%, then most corrections are negligible or can be reduced to a negligible level by careful design. Details of these corrections can be found elsewhere [2–5, 8–15].

Three corrections remain, and these are outlined below.

2.3.1 Heat Capacity of the Wire Correction

This correction modifies the measured temperature rises and results from consideration of a wire of finite radius, a, finite thermal conductivity, λ_w, and proper heat capacity, $(\rho C_p)_w$, per unit volume. The measured temperature rise of the wire at any instant time t corresponds to the average temperature of the wire. Defining $\Delta T_w(t)$ as the instantaneously measured temperature rise of the wire and $\Delta T^{id}(a, t)$ as the ideal temperature rise in the field at r = a, the following equations have been derived [9] for large values of $4\alpha t/r^2$.

$$\Delta T^{id} = \frac{q}{4\pi\lambda} \ell n \left[\frac{4\alpha t}{a^2 C}\right] + 0 \left[\frac{a^2}{\alpha t}\right] \qquad (2.3.1.1)$$

$$\Delta T_w(t) = \frac{q}{4\pi\lambda} \left\{1 + \frac{a^2}{2\lambda t} (\rho C_p - (\rho C_p)_w) \ell n \left[\frac{4\alpha t}{a^2 C}\right] + \frac{a^2}{2\alpha t} - \frac{a^2}{4\alpha_w t} + \frac{\lambda}{2\lambda_w}\right\} * \qquad (2.3.1.2)$$

The ratio of thermal conductivities is not time dependent to this order of approximation and merely shifts the ΔT's by a very small and constant amount (and is therefore ignored). The significant correction is due to the $a^2/2\lambda t$ $(\rho C_p - (\rho C_p)_w)$ term. Rearranging equation (2.3.1.2) and using the first term in equation (2.3.1.1) the following is obtained.

$$\Delta T_w(t) = \Delta T^{id}\left[1 + \frac{a^2}{2\lambda t} ((\rho C_p) - (\rho C_p)_w) + \frac{q}{4\pi\lambda} \cdot \frac{a^2}{4\alpha t} \left[2 - \frac{\alpha}{\alpha_w}\right]\right] \qquad (2.3.1.3)$$

Where α_w is the thermal diffusivity of the wire.

Generally, it is possible to ignore the second term in the above and obtain the measured temperature rise as a perturbation of the ideal solution

---

*Note: This result is at variance with the earlier result [2]. The contents of the ℓn term contains C not c = C/e which would lead to an inconsistent correction .

$$\Delta T_w(t) = \Delta T^{id} \left[1 + \frac{a^2}{2\lambda t} ((\rho C_p) - (\rho C_p)_w)\right] \qquad (2.3.1.4)$$

Thus, the above expression can be used to correct the measured temperature rise data set to an equivalent set of ΔT^{id} v. ℓn t data. In order to calculate the correction factor, estimates for the wire radius, the thermal conductivity and the heat capacity per unit volume of both wire and fluid are required. The magnitude of the correction decreases as the square of the wire radius which indicates that significant benefit is derived from the use of a thin wire. The magnitude of the correction also decreases as the time increases. In most practical instruments, the correction amounts to less than 1% of the measured temperature rise.

3.2 Outer Boundary Correction

This correction arises from the fact that the wire is positioned inside a container and not in a fluid of infinite extent. The effect of the outer boundary of the container is to modify the temperature field of the fluid. At short times the thermal wave emanating from the wire is unaware of the presence of the boundary, so the ideal solution is appropriate. At longer times the heat flux at the boundary may be significant, which would then modify the temperature history of $\Delta T(a, t)$. This line of thought led to the re-examination of the original problem with altered boundary conditions. Denoting the vessel radius by b the new boundary conditions are

$$\Delta T(r, t) = 0 \quad \text{at } r = b \text{ and } t \geq 0 \qquad (2.3.2.1)$$

$$\frac{\partial T}{\partial r} = -\frac{q}{2\pi a\lambda} \quad \text{at } r = a \text{ and } t \geq 0 \qquad (2.3.2.2)$$

This problem has been solved in the limit $b/a \gg 1$ and $4\alpha t/a^2 \gg 1$,

$$\Delta T(a,\ t)_b \ = \ \frac{q}{4\pi\lambda}\left\{2\ \ell n\left[\frac{b}{a}\right] - 4\sum_{\nu=1}^{\infty}\frac{\exp(-g_\nu^2\alpha t/b^2)}{\left[\frac{2}{\pi Y_0(g_\nu)}\right]^2 - \frac{a^2 g_\nu^2}{b^2}}\right\} \tag{2.3.2.3}$$

where g_ν represents the consecutive roots of a zero-order Bessel function of the first kind and Y_0 represents a zero-order Bessel function of the second kind. Equation (2.3.2.3) tends to the steady-state solution as $t \to \infty$.

$$\Delta T_\infty \ = \ \frac{q}{4\pi\lambda}\ 2\ \ell n\left[\frac{b}{a}\right] \tag{2.3.2.4}$$

Equation (2.3.2.3) must also tend to the line source solution when $\alpha t/b^2 \to 0$. This has not been confirmed analytically but has been verified by extensive numerical calculations [2, 3].

Writing the line source solution (equation 2.2.7)

$$\Delta T^{id}(a,\ t) \ = \ \frac{q}{4\pi\lambda}\ \ell n\left[\frac{\alpha t}{a^2 C}\right] \tag{2.3.2.5}$$

$$= \ \frac{q}{4\pi\lambda}\left\{2\ \ell n\left[\frac{b}{a}\right] + \ell n\left[\frac{4\alpha t}{b^2 C}\right]\right\} \tag{2.3.2.6}$$

then

$$\Delta T^{id}(a,\ t) \ = \ \Delta T(a,\ t)b + \delta T_2 \tag{2.3.2.7}$$

where

$$\delta T_2 \ = \ \frac{q}{4\pi\lambda}\left\{\ell n\left[\frac{4\alpha t}{b^2 C}\right] + 4\sum_{\nu=1}^{\infty}\frac{\exp(-g_\nu^2\alpha t/b^2)}{\left[\frac{2}{\pi Y_0(g_\nu)}\right]^2 - \frac{a^2 g_\nu^2}{b^2}}\right\} \tag{2.3.2.8}$$

or, alternatively

$$\Delta T^{id}(a,\ t) = \left\{ \frac{\ell n\left[\frac{4\alpha t}{a^2 C}\right]}{2\ \ell n\left[\frac{b}{a}\right] - 4 \sum_{\nu=1}^{\infty} \frac{\exp(-g_\nu^2 \alpha t/b^2)}{\left[\frac{2}{\pi Y_0(g_\nu)}\right]^2 - \frac{a^2 g_\nu^2}{b^2}}} \right\} \Delta T(a,\ t) \qquad (2.3.2.9)$$

This correction is generally small. Following the asymptotic analysis of Healy *et al.* [2] it has been shown that it is of order 0.01% of the temperature rise [9]. However, if the fluid has a high thermal diffusivity and the radius is not so small, such that $\alpha t/a^2 << 4000$ the correction can be as much as 0.2% of the temperature rise [12]. Hence, the correction is made whether it is necessary to do so or not, as this decision can only be made after a measurement is completed.

2.3.3 Variable Fluid Properties.

This correction arises from the fact that the fluid properties vary throughout the time of the measurement as a result of their dependence on temperature. This phenomena can be accounted for if the properties of the fluid are considered to be linear perturbations of the properties of the fluid at equilibrium. This may not be the case over the entire thermodynamic range of states of the fluid (and is especially suspect near the critical point). The effect of the non-constant fluid properties is to define a reference temperature for the measurement. The reference temperature is obtained via a correction to the equilibrium bath temperature (T_0). If the ΔT v. ℓn t data set is linear in ℓn t then the reference temperature is

$$T_{ref} = T_0 + \frac{1}{2}\left[\Delta T(t_i) + \Delta T(t_f)\right] \qquad (2.3.3.1)$$

where T_{ref} = reference temperature

T_0 = initial bath temperature

t_i = initial measurement time

t_f = final measurement time

2.3.4 Other Corrections

Along with the development of the transient hot-wire method there has been a parallel development of the theory. This development has been focussed on time-independent corrections necessary for the evaluation of the thermal diffusivity. These corrections have a negligible effect on the thermal conductivity measured using most practical instruments. Other older and well-known corrections have been found to be negligible with respect to the basic instrument used here [17]. They are therefore not considered further.

The corrections mentioned so far have assumed that the fluid is transferring heat from the wire by conduction alone. There is always the possibility of other modes of heat transfer being present. Therefore the effect of convection and radiation on the temperature history of the fluid field must be considered.

In the case of radiation the important point is whether or not the fluid absorbs radiation. If the fluid is transparent and it is assumed that all surfaces involved are black, then the analysis is straightforward. The energy lost to radiation modifies the heat generation q in equation (2.2.5). This then reduces the temperature rise of the wire by the amount

$$\delta T_{rad} = \frac{8\pi a \sigma T_0^3 (\Delta T^{id}(a, t))^2}{q} \qquad (2.3.4.1)$$

where σ is the Stefan–Boltzmann constant. The magnitude of the correction is small, typically 0.05% of the measured temperature rise. If, however, the fluid absorbs , especially in the infra–red, then a different and more complex analysis is necesary [14, 18].

The transient hot–wire method has a distinct advantage over other methods for measurement of thermal conductivity, because the effects of the final and most damaging heat transfer mode – convection – can be completely eliminated. This is the major reason for the method's success. There are various sources of convection in a practical instrument. Each of these sources can be eliminated by suitable choice of operating region and careful design and construction.

When dealing with the ideal model, the fluid was considered to be isotropic. This is a situation which is difficult to obtain. If, by some combination of circumstances the fluid at the bottom of the vessel is less dense than the fluid at the top of the vessel, then there are certain to be convection currents present in the fluid. This situation is avoided by keeping a positive temperature gradient in the vessel (i.e. the top is kept hotter than the bottom). This gradient usually amounts to 0.2–0.5 K over a cell length of 20 cm (approximately). Also, when considering the ideal model, the wire was of infinite length. Near the ends of the wire the correct heat transfer model for the fluid is no longer one–dimensional and there will also be conduction of heat from the measurement wire to its relatively massive supports. These end effects can be dealt with by using a compensating wire. The details of how this effects the measurement are of a practical nature and will be dealt with later. The principle of the compensating wire is that it becomes possible to observe the temperature history of a finite section of an infinite

wire by considering the change in the resistance of the diffference of the two wires. This approach goes some way to eliminating the effect of a cold front of fluid moving upwards along the wires and starts immediately heat generation is initiated. As long as this process affects both wires equally, then the effect on the finite section is eliminated. This phenomena is explained more easily in Figure 2.1.

Figure 2.1 shows a temperature gradient in the fluid before the introduction of heating. Some time after heating has begun, the temperature field is characterised by the temperatures T_1–T_4. The gas below the support is not directly heated by the wire and remains at the bath temperature. The gas further away from the wire, characterised by T_1'–T_3' has not been heated by the wire. It is possible therefore that $T_2 > T_1'$ and $T_3 > T_2'$ and hence convection will occur with a vertical velocity component. This vertical movement of the gas causes the cold gas below the support to be dragged up over the wire and hence cool it.

This convection process will occur when there is a temperature gradient applied to a fluid in a gravitational field. The fluid, however, is initially at rest and the buoyancy forces will require some time to accelerate the fluid. If the measurement is completed before the fluid has been accelerated then the effects of convection are eliminated. The time for the onset of convection can range between 0.5 s and 5 s depending on the fluid in question and its thermodynamic state. Convection is a serious departure from the mathematical model for the instrument. This departure takes the form of curvature of the ΔT v ℓn t plot and sudden enhancement of the thermal conductivity. By studying the ΔT v. ℓn t plot, it is possible to decide whether convection has occurred, and reject or

Figure 2.1

Convection.

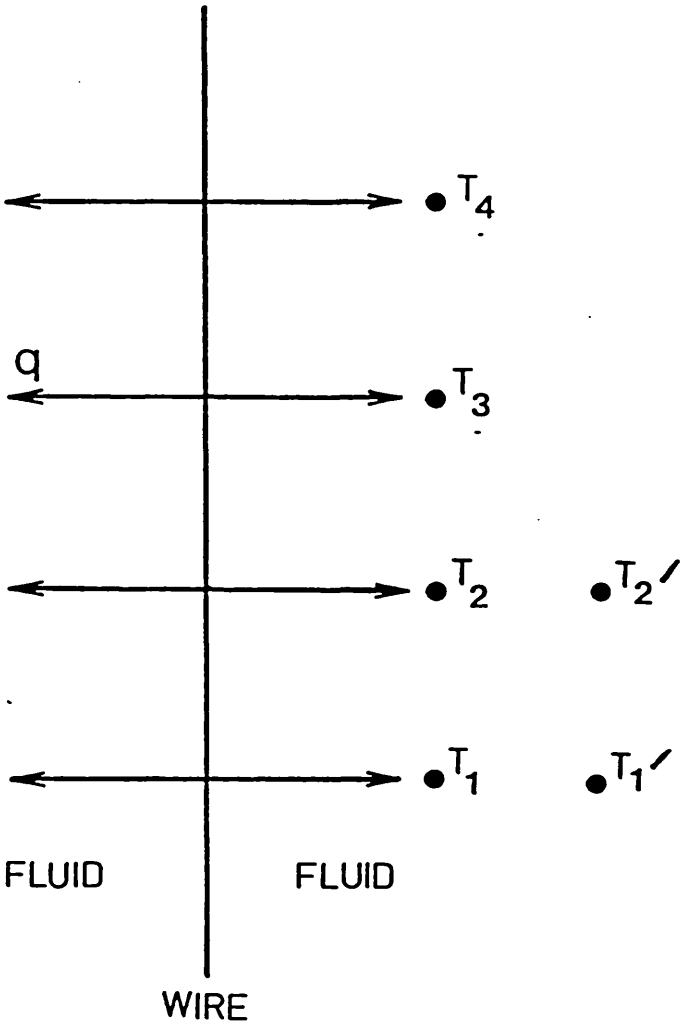

repeat the measurement under different conditions. Reduction of the effects of convection can be obtained by decreasing the power generation in the wire or by truncating the measurement at shorter times.

Finally, it is also possible for convection to be a problem if the wire is not held vertically or if the wire moves laterally when the heating begins [19, 20].

2.3.5 Summary

The result of studying the theory of the transient hot-wire method is that the thermal conductivity of a fluid may be obtained from the slope of a data set of ΔT v. $\ell n\ t$ information by application of the followimg set of equations

$$\Delta T^{id} = \frac{q}{4\pi\lambda_{ref}} \ell n \left[\frac{4\alpha_0 t}{a^2 C}\right] \qquad (2.3.5.1)$$

where λ_{ref} is the thermal conductivity at the reference condition (T_{ref}, P_0) and α_0 is the thermal diffusivity of the fluid at equilibrium. The reference temperature T_{ref} may be obtained from the equation,

$$T_r = T_0 + \frac{1}{2}\left[\Delta T(t_i) + \Delta T(t_f)\right] \qquad (2.3.5.2)$$

and the ideal temperature rise ΔT^{id} is obtained from the observed temperature rise according to the equation,

$$\Delta T^{id}(t) = \Delta T(t)_{observed} + \delta T_{ob} + \delta T_{HC} \qquad (2.3.5.3)$$

where

$$\delta T_{HC} = \frac{a^2((\rho C_p)_w - \rho C_p)}{2\lambda t} \Delta T^{id}(t) \qquad (2.3.5.4)$$

and

$$\delta T_{ob} = \frac{q}{4\pi\lambda}\left\{\ell n\left[\frac{4\alpha t}{b^2 C}\right] + 4\sum_{\nu=1}^{\infty}\exp\left[\frac{-(-g_\nu^2\alpha t}{b^2}\right](\pi Y_0(g_\nu))^2\right\}^{*} \qquad (2.3.5.5)$$

*(Note: This is the asymptotic form of the full equation [2]).

References

[1] J.W. Haarman, PhD Thesis, Technische Hogeschool Delft (1969).

[2] J.J. de Groot, J. Healy and J. Kestin, Physica 82C, 392 (1976).

[3] J.J. de Groot, J. Kestin and H. Sookiazian, Physica 75, 454 (1974).

[4] J. Kestin and W.A. Wakeham, Physica 92A, 102 (1978).

[5] A.A. Clifford, J. Kestin and W.A. Wakeham, Physica 100A, 370 (1980).

[6] G.C. Maitland, M. Mustafa, M. Ross, R.D. Trengove, W.A. Wakeham and M. Zalaf, Int. J. Thermophys. 7, No. 2, 245 (1986).

[7] H.S. Carslaw and J.C. Jaegar, 'Conduction of Heat in Solids', 2nd Edition (Oxford University Press), p. 261 (1959).

[8] C.A. Nieto de Castro, B. Taxis, H.M. Roder and W.A. Wakeham, (to be published.)

[9] J.M. Fareleira, PhD Thesis, Technical University of Lisbon (1986).

[10] J.W. Haarman, in 'Transport Phenomena', J. Kestin, Ed., AIP Conference Proceedings, Vol. II, 193 (1973).

[11] G.P. Anderson, J.J. de Groot, J. Kestin and W.A. Wakeham, J. Phys. E: Sci. Instrum. 7, 948 (1974).

[12] C.A. Nieto de Castro, J.C.G. Calado, W.A. Wakeham and M. Dix, J. Phys. E: Sci. Instrum. 9, 1073 (1976).

[13] M.J. Assael, M. Dix, A. Lucas and W.A. Wakeham, J. Chem. Soc. Faraday Trans. I 77, 439 (1981).

[14] C.A. Nieto de Castro, S.F.Y. Li, G.C. Maitland and W.A. Wakeham, Int. J. Thermophys. 14, 311 (1983).

[15] J.C.G. Calado, J.M. Fareleira, C.A. Nieto de Castro and W.A. Wakeham, Rev. Port. Quim. 26, 173 (1984).

[16] J. Fischer, Ann. Phys. 34, 669 (1939).

[17] M.J. Assael, PhD Thesis, University of London (1980).

[18] J. Menashe and W.A. Wakeham, Int. J. Heat & Mass Transf. 25, 61 (1982).

[19] C.A. Nieto de Castro and W.A. Wakeham, Proc. 1st Nat. Conf. on Pure and Applied Mathematics (Lisbon) (1974).

[20] P.G. Knibbe and R.D. Raal, Int. J. Thermophys. 8, 181 (1987).

CHAPTER 3

EXPERIMENTAL

3.1 INTRODUCTION

In Chapter 2, the ideal model of a transient hot-wire instrument was studied and the corrections found to be necessary for practical instruments, designed to achieve an uncertainty of 0.3% in thermal conductivity, were listed. The task now is to ensure that the practical instrument resembles as closely as possible the mathematical model for it and build an instrument capable of operation over all the thermodynamic states of interest. Finally, there must be a system for measuring the temperature rise of the hot-wire from which the thermal conductivity is obtained.

Identification of the thermodynamic range of interest follows from theoretical and engineering requirements. Theoretical development is most advanced in the dilute gas region (i.e. zero density) and there is some development in the moderately dense gas region (i.e. thermal conductivity is a linear function of density). In order to investigate these areas, accurate measurements are required as a function of temperature for both the zero-density thermal conductivity and its initial density dependence. Since measurements at low density are not possible because of temperature jump effects, it seems appropriate that measurements are made as a function of temperature and at sufficient densities such that the zero-density thermal conductivity may be obtained via extrapolation and the initial density dependence may be obtained via regression of the data. Engineers may be satisfied with lower-accuracy measurements, but covering a very large range of thermodynamic

states. To some extent, the objectives may be contradictory. They may, however, be reconciled by arguing that predictive schemes with a sound theoretical basis will save both time and effort in the long run and, hence, concluding that accurate measurements must be the first priority.

Close resemblance between the ideal model and the practical instrument is obtained by careful study of the corrections mentioned in Chapter 2, and arranging that as many as possible are negligible or can be estimated with confidence. Studies of this type have been made at Imperial College [1, 2] and elsewhere [3–5] where liquid– and gas–phase instruments have been in operation for some time. Near room temperature, consistent measurements have been made with instruments in various laboratories worldwide over a period of 10 years. This level of success was first achieved in 1980. Although measurements have been attempted at temperatures removed from room temperature, it has not been possible until recently to report data with an accuracy of 0.3%. The reasons for this were problems of a practical nature, not problems of principle. In the following sections, the design and operation of the instrument that enabled accurate measurements over the temperature range 170 K to 430 K and at pressures up to 10 MPa to be reported, is presented.

3.2 DATA ACQUISITION

In this section, the electrical system for measurment of the temperature rise from which the thermal conductivity of the fluid is obtained, is presented. The theory of the method indicates that the temperature rise of a wire must be measured as a function of time when it experiences a constant internally–generated heat flux. The application of a sudden voltage across a wire will cause ohmic

heating within the wire. The wire itself can then be used as a thermometer and its resistance measured using a bridge circuit. Once the resistance is obtained as a function of time, the temperature history can be obtained via the temperature–resistance characteristics of the wire material. In this instrument 7 μm nominal diameter platinum wire of 99.99% purity was used [6]. Platinum has well–defined temperature–resistance characteristics and has been used in high–accuracy resistance thermometers for many years [7]. The theory of the method refers to an infinite wire, whereas in practice of course, a finite wire must be used. In order to avoid the inevitable consequences of end effects, the resistance of a finite section of an infinite wire is approximated by the difference in resistance of two finite wires.

The problem then becomes the design of a circuit that initiates a heat flux in the wires and then is able to measure the resistance history of the difference of the two wires, and hence perform simultaneous elimination of the end effects. Such a circuit was developed in this laboratory [8, 9] and is shown in Figure 3.1. The left–hand arm of the bridge contains the measurement wires and remains unchanged from previous installations [1, 10]. The right–hand arm is, however, significantly altered and is a direct consequence of recent advances in electronics. The principle of operation of the bridge circuit is unaltered from previous instruments [1, 10], although there are alternatives [4, 11, 12].

Referring to Figure 3.1, R_L represents the resistance of the long wire and R_S represents the resistance of the short wire. Resistances R_8 and R_9 and capacitors C_1 and C_2 serve to centre–tap the bridge supply voltage, V_0, which is derived from a Hewlett Packard 6114A precision power supply. The other resistors are precision

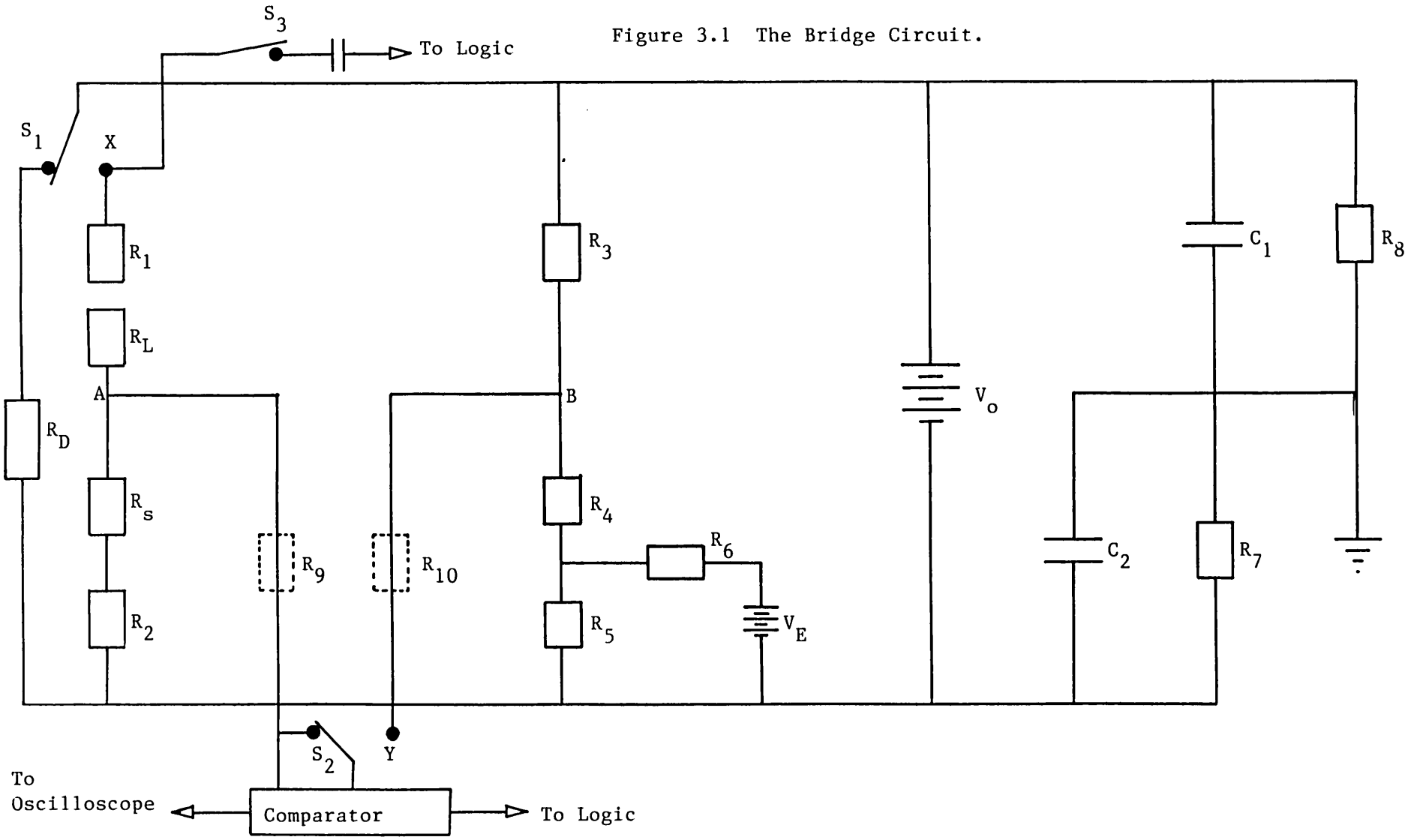

Figure 3.1 The Bridge Circuit.

resistors for which details are given in Table 3.1. Voltage V_E represents an additional voltage which is programmed to provide preset values in a prearranged sequence. This voltage source replaces the shunt resistors in the previous installation [1, 10].

Recent advances in electronics have allowed the measurement process to be computerised. The operation of the bridge is governed using specially-written Basic and Assembly language programs on an IBM-XT micro-computer. The voltage source V_E is a 12-bit D/A converter demarked into three 4-bit nibbles. The D/A is capable of 4096 discrete voltage outputs and uses as reference voltage a quarter of the bridge supply voltage V_0. In practice, approximately 50 discrete voltages are selected and stored in an array. Prior to the measurement, the value of resistor R_1 is chosen such that $R_1 \simeq R_L$. The bridge is then activated by switching S_1 from the dummy resistor R_D to position X and switching S_2 to position Y using relay drives governed by the Basic program. The bridge is then balanced using a supply voltage V_0 of 0.1 V (approximately) and varying resistor R_2 until a null is detected at the comparator output by a voltmeter or oscilloscope. The switches are then returned to their original positions. This corresponds to a steady-state measurement which will be discussed later. The transient measurement is then performed by incrementing R_2 slightly (usually 1-3 Ω results in a final temperature rise of 2-4 K) and initiating the heat flux by switching S_1 to position X. The current causes a pulse to flow via S_3 and C_3 to the logic circuit which starts a 24-bit 100 KHz clock which is divided into three 8-bit nibbles. Switch S_3 is then opened and remains so. In addition, S_2 is switched to position Y so that the comparator is in the circuit. Once the heat flux has been initiated, the wires will begin to heat up and increase in resistance. Since

$R_L > R_S$ the bridge will begin to approach a balance point. When the comparator registers a polarity change between points A and B in Figure 3.1, the clock time is stored in an array and the first D/A voltage is initiated. This voltage upsets the balance of the bridge but because the wires continue to increase in resistance, a new balance point is soon reached. Hence, a new time is stored in the time array and the second D/A array voltage is initiated. This process is repeated until all the D/A array voltages have been used and the measurement is complete. Built into the assembly language program that controls the transient measurement is a delay between the switching of any relays and the sending of the comparator output signal to the logic circuit. This avoids any unwanted false null detections due to switching. Also there is a time-out facility which avoids unnecessary heating of the wires if no balance point is observed for a period exceeding 4 s (approximately). When the measurement is complete, the computer has stored, in the form of two arrays, a set of D/A voltage values and the corresponding balance times of the bridge.

By carrying out a circuit analysis from Figure 3.1 it is possible to derive an expression for the out-of-balance voltage across A-B in terms of the resistance values and the D/A voltage [8, 9]

$$\frac{V_{AB}}{V_0} = \frac{R_1+R_L}{(R_1+R_L+R_2+R_S)} - \left[\frac{\left[\frac{R_3}{R_5}+\frac{R_3}{R_6}\right] - \frac{V_E}{V_0}\frac{R_3}{R_6}}{1+\left[\frac{R_3}{R_5}+\frac{R_4}{R_5}\right]\left[\frac{R_5}{R_6}+1\right]}\right] \qquad (3.2.1)$$

A schematic diagram of V_{AB} vs t is given in Figure 3.2. The saw-tooth pattern is obtained because when $V_{AB} = 0$, the value of V_E is incremented. At balance $V_{AB} = 0$, so rearrangement of equation

Figure 3.2 Schematic of Comparator input voltage

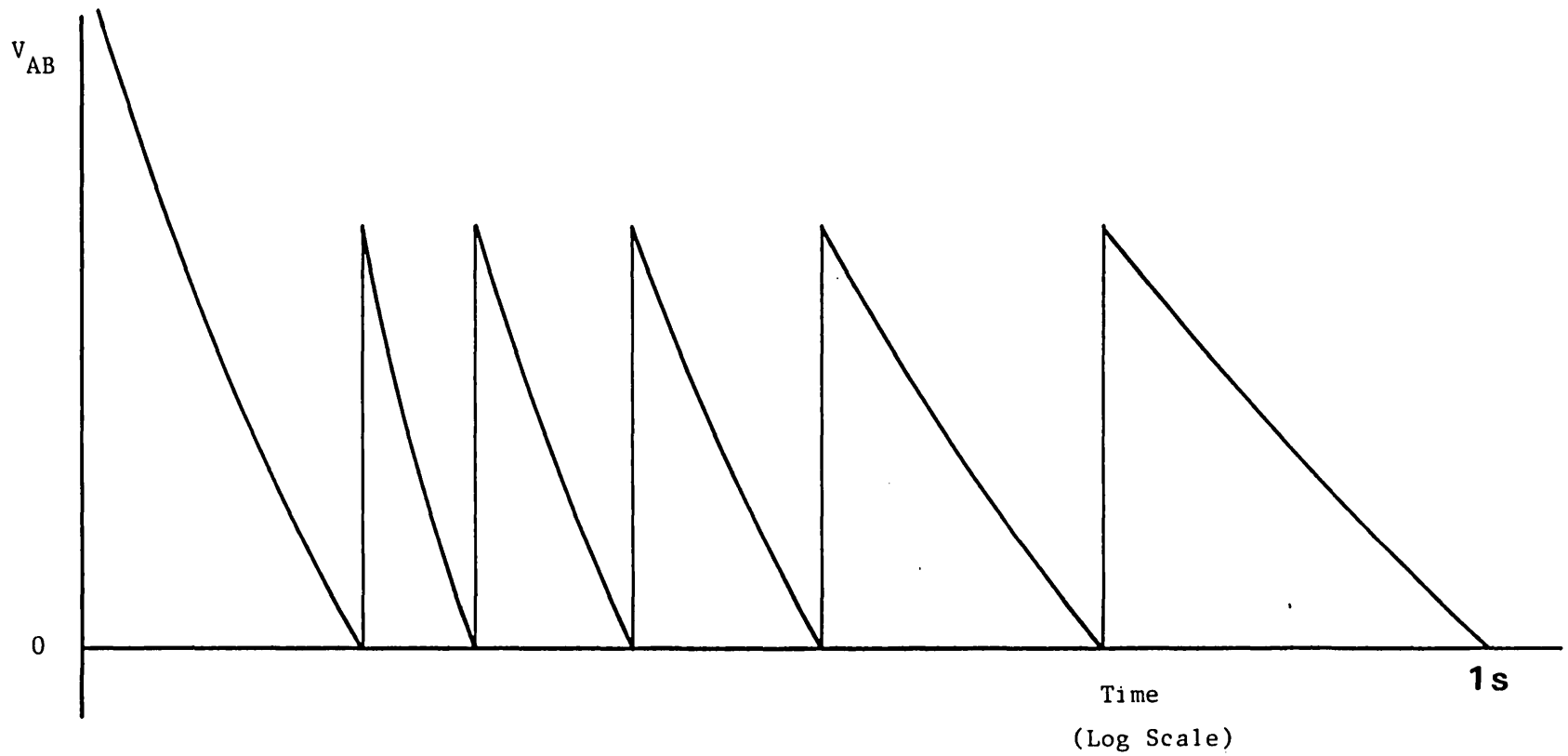

(3.2.1) provides an equation for the resistance difference of the wires:

$$R_L - R_S = \frac{\left[\frac{R_L}{R_S} - 1\right](CR_2 - (1-C)R_1)}{\frac{R_L}{R_S}(1-C) - C} \qquad (3.2.2)$$

where

$$C = \frac{\left[\frac{R_3}{R_5} + \frac{R_3}{R_6}\right] - \frac{V_E}{V_0}\frac{R_3}{R_6}}{\left[1 + \left[\frac{R_3}{R_5} + \frac{R_4}{R_5}\right]\left[\frac{R_5}{R_6} + 1\right]\right]} \qquad (3.2.3)$$

There are two important features of this circuit configuration. Firstly, because the perturbing voltage appears as a ratio V_E/V_0 and since V_E is a linear function of V_0 , the reference voltage, a wide range of fluids are able to be measured using the same bridge configuration and, secondly, explicit knowledge of V_E and V_0 is not necessary for the evaluation of the resistance difference. In addition, simulations, subsequently verified by experiment, have indicated that the bridge circuit produces a nearly-linear distribution of points in logarithm of time when a linear selection of V_E/V_0 is used. This is a natural consequence of the working equation for the instrument.

Equation (3.2.2) also contains the ratio R_L/R_S which is independent of time so long as the wires are identical apart from their lengths. Therefore, if independent measurements are performed for R_L and R_S in steady-state mode, as explained previously, equation (3.2.2) is, to zero order, explicit in R_L-R_S. The steady-state measurements are made by using a switching system which selectively positions the long wire or short wire in the top left arm of the bridge and short circuits the remaining wire. The bridge is then

balanced by using R_2 for a series of low bridge supply voltages V_0 and zero perturbation voltage V_E. The resistances are then extrapolated to zero power to provide the equilibrium values of R_L, R_S and $R_L - R_S$.

Finally, in this section on the operation of the bridge circuit, the heat flux is considered. The ideal model stipulates that the heat flux be constant throughout the time of the measurement. At any instant of time, the heat flux per unit length of wire is given by

$$Q(t) = \left[\frac{V_0}{R_1+R_2+R_L(t)+R_S(t)}\right]^2 \frac{R_L(t) + R_2(t)}{L_L + L_S} \qquad (3.2.4)$$

where L_L and L_S are the lengths of the long wire and the short wire respectively.

For simplicity, R_1 and R_2 are chosen such that

$$R_1 + R_2 = R_L(0) + R_S(0)$$

Equation (3.2.4) can be rearranged and simplified such that [5]

$$Q(t) = \left[\frac{V}{2R}\right]^2 \frac{R}{L_L+L_S} \left[1 - \left[\frac{\Delta R(t)}{2R}\right]^2\right] \qquad (3.2.5)$$

where

$$R = R_L(0) + R_S(0) \qquad (3.2.6)$$

and

$$\Delta R(t) = (R_L(t) - R_L(0) + (R_S(t) - R_S(0)) \qquad (3.2.7)$$

Therefore $Q(t)$ will change by a factor of order $(\Delta R(t)/2R)^2$ from its initial value during the entire measurement. At 170 K the value of $\Delta R(t)/2R$ is of order 0.01 so that even at this temperature the

correction to the heat flux from this source is of order 10^{-4}. At lower temperatuers, ΔR may be a considerable fraction of $2R$ especially if low resistance wires are used in the first place.

3.3 PRECISION

The ultimate objective of the measurement circuit is to regress a set of ΔT vs $\ell n\ t$ data in order to obtain the thermal conductivity from the slope. The quality of such a regression is determined by various factors, some of which are associated with the bridge circuit. Firstly, in the older installations, the number of data points obtained per measurement was restricted to six. Then the fluid was left to recover from the transient heating and the process was repeated a number of times in order to provide a suitable number of data points. This process may take as long as twenty minutes in total during which time the bath temperature must remain constant. This proved difficult to achieve at elevated temperatures and there was increased scatter amongst the data set. This problem is avoided with the new installation since a complete data set can be obtained in one second. This is a major contribution to the precision of the thermal conductivities reported away from room temperature. The precision of the measurements is also affected by the precision of the measured temperature rise and the time. The advantage of the present instrument is that these two factors can be related directly to the quality of the components used in the circuit and the noise level at the comparator input.

3.3.1 The Bridge Components

The target precision for the thermal conductivity measurements is $\pm$ 0.1%. This relates to a precision in the measurement of the

temperature rise of 0.05% which, in turn, places a precision requirement on the resistance difference

$$[R_L(t) - R_S(t)] - [R_L(0) - R_S(0)] \qquad (3.3.1.1)$$

Equation (3.2.2) forms the basis of a working equation for the instrument and can be used via a sensitivity analysis [8] to define the tolerances allowable for the resistance elements of the bridge and the D/A voltage V_E. The result of that study is summarised in Table 3.1. It is worth noting that R_1, R_2 and R_6 are made up of precision decades and R_5 contains a precision resistor and decade to allow a considerable degree of flexibility.

The other major component of the bridge is the comparator which detects the bridge balance condition, hence triggering a sequence of events that result in the time of balance being recorded. As mentioned previously, delays are built into the assembly language program to avoid false triggering due to switching. Other factors must, however, be considered to ensure that triggering of the comparator registers a true balance point. Firstly, the effect of the input impedance of the comparator on the operation of the bridge is discussed. The comparator input impedance modifies the circuit diagram for the bridge, as shown in Figure 3.1 by the dotted lines representing R_9 and R_{10}. In the previous analysis, it was implicitly assumed that $R_9 = R_{10} \rightarrow \infty$. A further circuit analysis including R_9 and R_{10} concludes that if $R_9 = R_{10} \simeq 10^9\ \Omega$ then the contribution to the error in the evaluation of $R_L(t)-R_S(t)$ is $1 \times 10^{-5}\%$ [8]. This input impedance is achieved by using, within the comparator, two input buffer amplifers which are balanced in a cross-coupled mode. The configuration adopted results in a high input impedance, high

Table 3.1

The Bridge Components

Resistor	Make/Model	Resistance Values	Tolerance
R_1, R_2	Cropico RB5	10x100, 10x10, 10x1, 10x0.1, 10x0.01	0.01 %
R_3	Vishay Welwyn 4812	2x1000	0.01 %
R_4	Vishay Welwyn 4812	1x1000	0.01 %
R_5	Vishay Welwyn 4812	1x1000	0.01 %
	Muirhead D-805-B	10x1	0.1 %
R_6	Muirhead D-805-G/I	10x100 000	0.05%
	D-805-F	10x10 000	0.05%

common mode rejection ratio device which maintains an internal noise level less than that intrinsic to the bridge itself [13].

3.3.2 Electrical Noise

Finally, the level of noise tolerated at the comparator input is considered. Proper earthing of the equipment has proved to be an important factor when precise measurements are required. The presence of a large noise component at the comparator input will result in a large scatter of the ΔT vs ℓn t data points. A sensitivity analysis based on equation (3.3.2) indicates that a noise level of order 1 μV is necessary at lower temperatures, whilst 10 μV may be tolerated at room temperature and above. In order to provide the most precise measurements, a target noise level of 1 μV was aimed for. The high common mode rejection ratio of the comparator ensures that common mode interference is passed at unit gain, whilst differential signals are amplified. Figure 3.2 shows a schematic diagram of the voltage decay observed at the comparator input. The centre tapping of the power supply means position V_B is kept near earth potential. As a balance point is approached, V_A approaches V_B and the comparator is triggered by the noise. At the earlier times, the slope of the voltage decay is steep so that a low level of noise will have little effect on the triggering time. At longer times, however, the slope is flatter so the noise level will affect the triggering time. It is the logarithm of time that is of interest and since the error in the logarithm is proportional to the inverse of time, the error in ℓn t due to the error in t decreases with increasing time.

In order to reduce interference pick-up by the comparator, the cell and frame containing the wires are earthed, as are all cable

screens and the cabinets containing the components. Great care was taken to ensure that all the earthing wires led to the same earthing point on the bridge and that there is no other route to earth, to avoid earth loops. The active components such as power supplies were kept in a separate cabinet from the resistive elements. All other ancillary equipment was isolated from earth during the period of the measurement using a contact relay. Having taken all these precautions and, additonally, arranging the geometry of the equipment in such a way as to null any remaining interference, the target level of 1 μV was attained. The noise level at the comparator output is constantly checked for the presence of previously unobserved interference, so that corrective action can be taken or measurements suspended until the source has either disappeared or can be identified.

3.4 THE WORKING EQUATIONS

The previous sections have described how the primary experimental measurements are made. All that remains is to convert the information gained from knowledge of the bridge balance at specific times to the thermal conductivity at a specific temperature. This process is inherently iterative because knowledge of the corrections required to convert experimental temperature rises to the ideal temperature rises requires *a priori* knowledge of the thermal conductivity. Secondly, solution for $R_L(t)-R_S(t)$ requires knowledge of the temperature dependence of the ratio $R_L(t)/R_S(t)$. In addition, a complication arises due to the non-ideality of the two-wire compensating system. In order that $[R_L(t)-R_S(t)]$ vs t epresents the true temperature history of a finite section of the long wire, the two wires must be identical in every detail apart from

their lengths. Manufacturing processes cannot guarantee that the resistance per unit length of the two wires is identical. In fact, there can be considerable departures from equality. Schemes have been developed which allow this problem to be avoided even if the departure in resistance per unit length is 4% [14]. If the difference in resistance per unit length is about 1%, a first-order analysis is sufficient. By assuming that incomplete compensation of conduction and convection end effects is negligible, the temperature rise of the finite section of the long wire may be written in the form

$$(\Delta T)_L = \Delta T' \left\{ 1 + \frac{R_S(0)}{R_L(0) + R_S(0)} \left[1 - \frac{(\Delta T)_S}{(\Delta T)_L} \right] \right\}^{-1} \qquad (3.4.1)$$

where supscript L and S refer to the long and short wires respectively and $\Delta T'$ is an experimentally-measured temperature rise defined by

$$\Delta T' = \frac{(R_L(t)-R_S(t)) - (R_L(0)-R_S(0))}{\alpha(T_0, T)(R_L(0)-R_S(0))} \qquad (3.4.2)$$

where $\alpha(T_0, T)$ is a linear coefficient of resistance defined by the equation

$$R_T = R_{T_0}(1 + \alpha(T_0, T)\Delta T) \qquad (3.4.3)$$

Where
$$\Delta T = T - T_0 \qquad (3.4.4)$$

and T_0 is the initial bath temperature.

equation (3.4.1) can be rearranged to contain experimentally-accessible quantities [14]

$$(\Delta T)_L = \frac{\Delta T'}{1 + \epsilon_3} \tag{3.4.5}$$

where

$$\epsilon_3 = \frac{R_S(0)}{(R_L(0)-R_S(0))} \cdot \epsilon_2 \tag{3.4.6}$$

$$\epsilon_2 = \frac{\epsilon_1\left\{1 + \ell n \left[\frac{4\alpha t}{a\ C}\right]\right\}}{\ell n\left[\frac{4\alpha t}{a_S^2\ C}\right]} \tag{3.4.7}$$

$$\epsilon_1 = 1 - \sigma_S\sigma_L \tag{3.4.8}$$

and

$$\sigma_L = \frac{R_L(0)}{L_L} \tag{3.4.9}$$

$$\sigma_S = \frac{R_S(0)}{L_S} \tag{3.4.10}$$

The bridge design ensures that the current flowing in the left-hand arm is essentialy constant but, once again, due to differences in resistance per unit length of the two wires, the heat flux will not be the same for both wires. However, the heat flux in the central portion of the long wire may be written in terms of experimental quantities [14]

$$q = \frac{q^*}{(1-\epsilon_4)^2(1+\epsilon_5)} \tag{3.4.11}$$

where

$$q^* = \frac{V_0^2(R_L-R_S)/(L_L-L_S)}{[R_1+R_2+(R_L-R_S)(L_L+L_S)/L_L-L_S)]^2} \tag{3.4.12}$$

$$\epsilon_4 = \frac{2\sigma_L\ \epsilon_1\ L_L\ L_S}{(L_L-L_S)(R_L+R_S) + (R_L-R_S)(L_L+L_S)} \tag{3.4.13}$$

and

$$\epsilon_5 = \frac{L_S \epsilon_1}{(L_L - L_S)} \qquad (3.4.14)$$

The application of the above equations requires knowledge of the lengths of the wires. The length is measured at approximately 20°C so correction is necesary when working at different temperatures. This correction is generally small ($\sim 10^{-4}\%$) and is made using the relation

$$L(T_0) = L(T_m)[1 + \gamma(T_0 - T_m)] \qquad (3.4.15)$$

where γ ($\gamma = 9 \times 10^{-6}$) is the coefficient of linear expansion of platinum and T_m is the temperature at which the wire lenght was measured. In addition, to knowledge of the wire lengths, the values of $4\alpha t/a_S^2 C$ and $\alpha(T_0, T)$ are required.

The value of $\alpha(T_0, T)$ is found from the resistance temperature characteristic of the wire which is given for temperatures above 0°C by an equation of the form [7]

$$R_{t_c} = R_0(1 + At_c + Bt_c^2) \qquad (3.4.16)$$

where

$$t_c = T - 273.15 \qquad (3.4.17)$$

R_0 is the resistance of the wire at 0°C and the constants A and B are specific to each wire and are obtained by calibration against an accurate thermometer at well-defined temperatures. In principle, this calibration could be performed for each of the hot-wires used in

the hot-wire cell. However, due to the extreme fragility of the hot-wires when *in situ*, this was not attempted. The wire is 99.99% pure platinum and studies have shown [1] that wires of this purity have a temperature resistance-characteristic experimentally compliant with the recommended temperature resistance-characteristic of pure platinum [7] . Therefore, equation (3.4.16) is used to obtain an expression for $\alpha(T, T_0)$

$$\alpha(T_0, T) = \frac{(A + B(2(T_0-273.15) + (T-T_0))}{1 + A(T_0-273.15) + B(T_0-273.15)^2} \qquad (3.4.18)$$

It is worth noting that equation (3.4.17) works using the reduced parameters A and B and does not require explicit knowledge of the resistance of the wire at 0°C. The recommended values of A and B for pure platinum are [7]

$$A = 3.98471 \times 10^{-3}\ K^{-1}$$

$$B = -5.874557 \times 10^{-7}\ K^{-2}$$

The recommended resistance-temperature characteriestic is more complicated below 0°C [7]

$$T_{68} = A_0 + \sum_{i=1}^{20} A_i\ [\ell n\ W_{CCT-68}]^i \qquad (3.4.19)$$

where the A_i's are constants and

$$W_{CCT-68} = W_{T_{68}} - \Delta W_{T_{68}} \qquad (3.4.20)$$

where

$$W_{T_{68}} = \frac{R_{T_{68}}}{R_{273.15}} \tag{3.4.21}$$

and $\Delta W_{T_{68}}$ is a temperature–dependent deviation function. Following the assumption made previously on the basis of purity

$$\Delta W_{T_{68}} = 0 \tag{3.4.22}$$

Hence equation (3.4.19) can be used directly to obtain an equation implicit in $\alpha(T_0, T)$

$$\Delta T = \sum_{i=1}^{20} A_i \left[(\ell n\, W_{T_0}(1 + \alpha(T_0, T)\Delta T))^i - (\ell n\, W_{T_0})^i\right] \tag{3.4.23}$$

Once again, knowledge of the resistance at 0°C is not required for application of equation (3.4.23). However, both equations (3.4.18) and (3.4.23) require knowledge of ΔT which is not known *a priori* so an iterative procedure is necessary in both cases.

As far as the group $4\alpha t/a_s^2 C$ is concerned, an estimate of the thermal diffusivity of the fluid is required. As this is not known *a priori*, the first–order correction for non–ideal compensation also requires an iterative procedure. The method of obtaining the thermal conductivity is therefore a nested iterative algorithm.

3.5 CALCULATION ALGORITHM

(1) In the first instance, the corrections to the ideal model are not included and are considered decoupled from all other effects.

(2) Zeroth–order solution of equation (3.2.2). The ratio of resistance R_L/R_S is considered independent of temperature and is assigned the value $R_L(0)/R_S(0)$ (i.e. the initial conditions ratio). Equation (3.2.2) is then solved for R_L–R_S at each balance time using the bridge resistance values and the preset V_E/V_0 ratios.

(3) Zeroth–order temperature rise and heat flux calculation. The dual wire compensation system is assumed to work perfectly, i.e. $\sigma_L = \sigma_S$ in equations (3.4.5)–(3.4.10) and (3.4.11)–(3.4.14).

(3a) An initial estimate of temperature is used to calculate a first estimate of $\alpha(T, T_0)$ either from equation (3.4.18) or (3.4.23). This estimate of $\alpha(T, T_0)$ is used to calculate a new temperature rise at each balance point using

$$\Delta T = \frac{[R_L(t)-R_S(t)] - [R_L(0)-R_S(0)]}{\alpha(T, T_0)[R_L(0)-R_S(0)]} \qquad (3.5.1)$$

This temperature rise is used to re–estimate $\alpha(T, T_0)$ until convergence. This usually takes about two iterations if the error in temperature rise tolerated is 0.01%.

(3b) The zeroth order heat flux is calculated for each temperature rise and then an average heat flux generation is obtained.

(3c) The initial estimates of the temperature rise at each balance point and the initial estimate of the average heat flux are used to estimate the thermal diffusivity via a linear regression to obtain the thermal conductivity and using the relation

$$\alpha = \frac{\lambda}{\rho C_p} \qquad (3.5.2)$$

(4) First–order solution of equation (3.2.2). The first–order

estimate of the resistance ratio $R_L(t)/R_S(t)$ is obtained from the relation

$$\frac{R_L(t)}{R_S(t)} = \frac{R_L(0)}{R_S(0)} [1 + \alpha(T_0, T)\Delta T.\epsilon_2] + 0(\Delta T^2) \qquad (3.5.3)$$

(4a) The temperature rise at each balance point is found by an interactive scheme similar to the zero–order case.

(4b) The first–order average heat flux is calculated.

(5) The first–order temperature rise vs ℓn t data is regressed to yield a first approximation of the thermal conductivity.

(6) The corrections to the ideal model are applied and the new ΔT vs ℓn t data are regressed again to obtain a second estimate of the thermal conductivity.

(7) If the deviation of the first approximation and the second approximation exceeds 0.1%, the first approximation scheme is repeated until there is convergence (i.e. go back to (4)). One iteration of this type is all that is usually necessary.

Having presented the data acquisition system, which is independent of the physical location and environment of the wires, and the method of extracting the thermal conductivity from the experimentally measured quantities, an account of the mechanical design and operation of the instrument is given.

3.6 THE INSTRUMENT

An instrument has been designed for operation between 80 K and 450 K and at pressures up to 10 MPa. Such an instrument contains a cell for the measurement wires, a pressure vessel for the fluid and a thermostat system to maintain temperature stability. The basis for the instrument was already in place at the beginning of the current

set of measurements [1, 15, 16]. Although the instrument has remained essentially unchanged, various important modifications were found necessary in order to extend the temperature range for accurate measurements. One of the most important modifications concerns the wire-mounting system; the other refers to extension of measurements to low temperatures. These two features are dealt with here in an uncoupled fashion for clarity, but in fact extension to temperatures away from room temperature required modification of the wire mountings.

3.6.1 The Measurement Cell

The transient hot-wire method requires the heating of the measurement wires whilst immersed in the test fluid. The wires are held vertically in a cell designed specially for the purpose. A considerable amount of effort has been put into the design of the cells since proper design will contribute to the accuracy of the data. Particular attention has been paid to the way in which the wires are suspended within the cell, since this has contributed directly to the attainment of accurate temperatures removed from room temperature.

The present cell design is the result of experience gained with previous installations [1, 15, 16]. The present cell is similar to that used successfully in the past for measurements from 300 K to 430 K [15, 16]. The cell design is shown in Fgiure 3.3. The cell is made up of two independent cylindrical enclosures which contain the measurement wires. The cells are made from a single stainless-steel (EN57B) cylinder (1) by drilling two cylindrical holes of diameter 13 mm centred along a diameter of the cylinder. The cylinder is then divided into two halves along a diametral plane. The two halves have

Figure 3.3

The measurement cell.

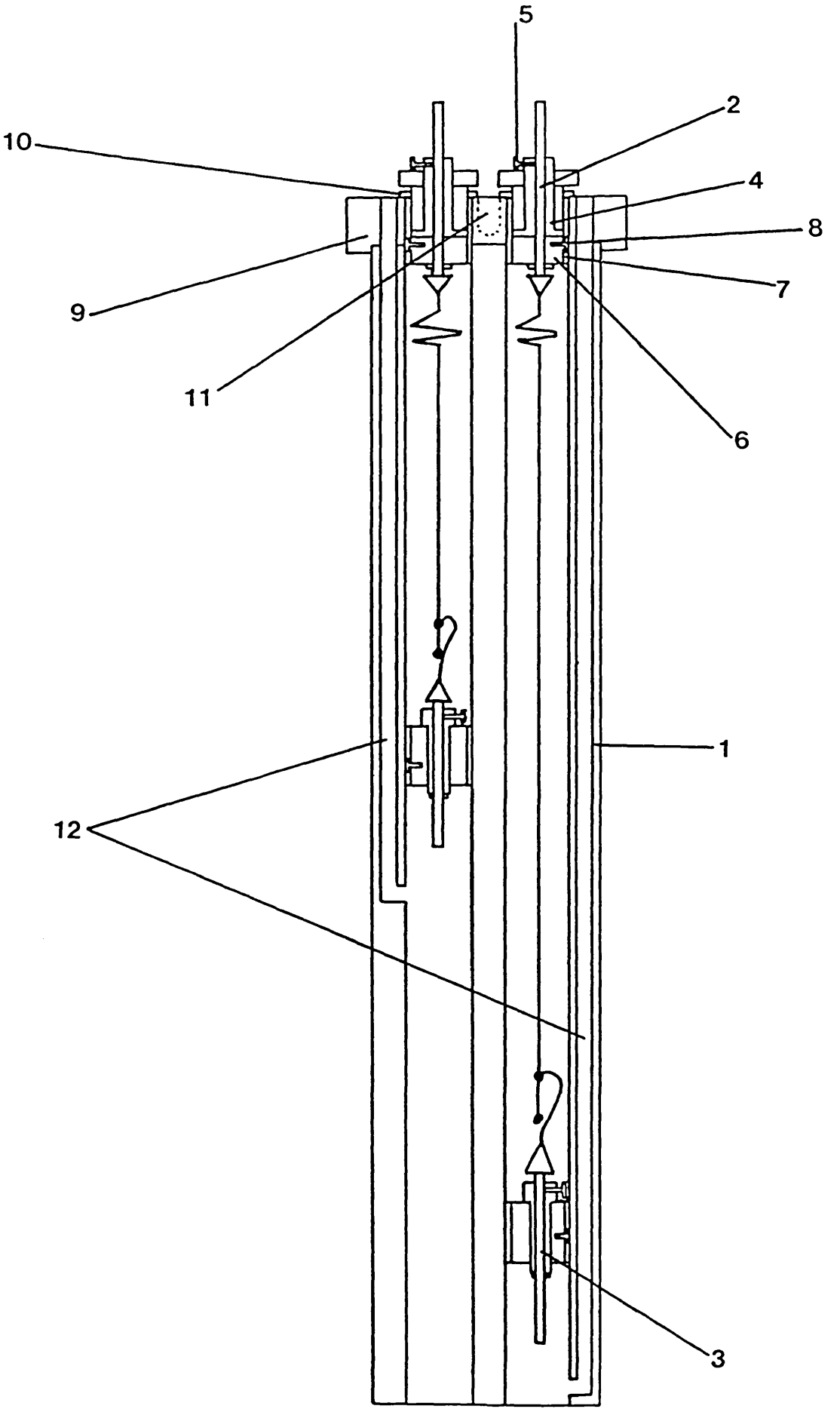

been lapped so that they fit together well. One half contains the wire supports, the other acts as a cover providing individual cylindrical enclosures for the wires. The cell design allows easy access to the wire supports during the wire mounting operation.

The supports for the two wires are made from an assembly of stainless-steel components (2), (3). The upper support (2) is fixed using a threaded stainless-steel cylinder (4) and set screw (5). The support is insulated from the cell by fixing the threaded cylinder inside a ceramic bush (6) and stainless steel sleeve (7) which is held together by a further set screw (8). The wire support assembly is then fixed to a mounting flange (9) by a retaining plate (10) and a bolt (11). The lower supports (3) are constructed in a similar manner except that the sleeve is attached directly to the side wall of the cell. The cover is fixed in position using a vertical bolt screwed through the mounting flange and a horizontal bolt near the bottom of the cell. The electrical leads from the bottom of the wire supports are glass-insulated copper wires which pass along channels in the cell wall (12) to terminal posts fixed to the mounting flange (9).

3.6.2 The Wire/Weight Assembly

The wire used in the present instrument is platinum wire of 99.99% purity and with a nominal diameter of 7 μm. Measurement of the wire diameter using a scanning electron microscope indicates that the actual diameter is 7.2 ± 0.1 μm. The thermal conductivity of the fluid is calculated from the resistance history of the hot wires. Care must be taken to ensure that there is no other contribution to the resistance change of the wires other than that which is a direct consequence of the temperature rise of the wires. Also the only heat

transfer mechanism present must be conduction.

The cell design proposed by de Groot *et al.* [5, 17] had the wire fixed to both ends of the rigid supports. This design is shown schematically in Figure 3.4a. After some years, it was realised that the axial thermal expansion of the wire caused by the transient heating results in the wire moving laterally through the gas. This movement is tantamount to a convective contribution to the heat transfer. This motion is observed as a discontinuity in the slope of the line of ΔT vs $\ell n\ t$ which accompanies the change from a moving wire to a stationary wire in an off-axis position [18].

This problem was overcome by using the wire assembly shown in Figure 3.4b [18]. Here the extension of the wire during the transient heating is accommodated by contraction of a weak gold spring. The tension on the wire was chosen to be no more than 20% of the yield stress of the wire and providing that allowance is made for the varying tension in the wire during a measurement [19] the design has proved successful near room temperature [10, 18]. This design has proved difficult to adapt to a wide range of temperatures because of the unreliable thermal characteristics of gold springs when exposed to a number of cycles of temperature and the difficulty in ensuring that the wire is always under a tension of a known, but not excessive, amount [15]. An alternative design, shown in Figure 3.4c, has been proposed where the spring is fixed at the top of the cell and designed such that the tension in the wire remains within preset limits over a defined temperature range [15]. The useful life time of such a design is restricted by creep in the wire limiting its long-term stability [15]. A further disadvantage of these cell arrangements was encountered when a large current flows in the

Figure 3.4 The Wire Mountings.

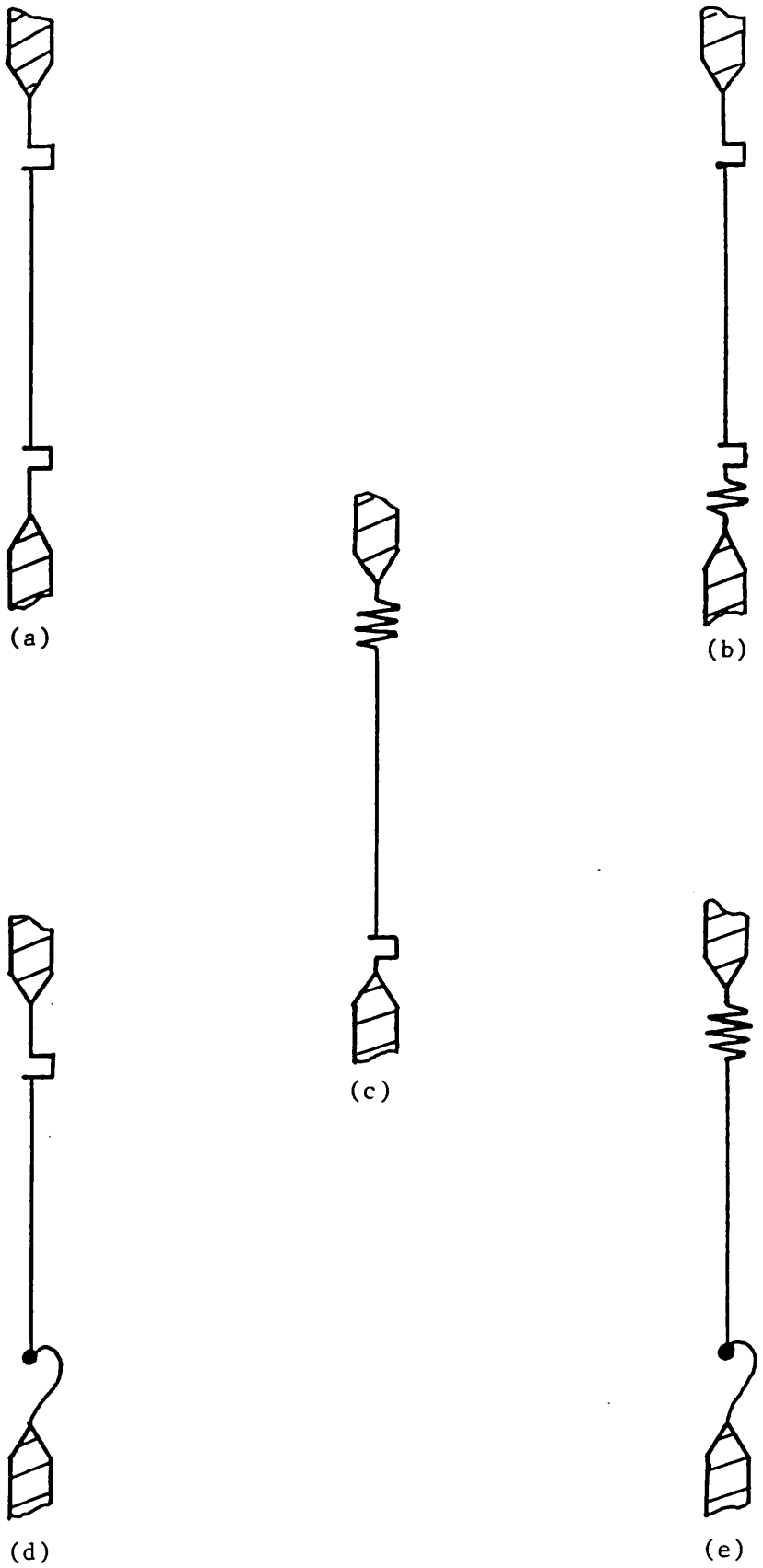

spring. The spring was observed to show a tendency to contract, owing to magnetic forces, which causes an additional longitudinal tension in the wire of an oscillatory nature. This tension induces resistance oscillations in the wire of a few milliohms or less, but they cause oscillations in the measured temperature rise of about 0.1%.

These considerations led to the cell design shown in Figure 3.4d being adopted for gases. In this design, the wire hangs from the top fixed support and carries a small platinum weight (70–120 mg) at the bottom end to provide a constant tension in the wire throughout the measurement. Electrical continuity is provided by using a soft gold loop attached to the small weight and the lower support. This design has been used successfully in liquids for some time [20]. The relatively low damping in gases means that special precautions have to be taken elsewhere in the apparatus in order to prevent the wire/weight assemby undergoing a pendulum–like oscillation driven by extraneous building vibrations.

Assuming that the effects of extraneous vibration can be avoided, this design solves many of the problems associated with the other designs. It does, however, introduce a further difficulty. Most of the temperature rise of the wire occurs during the first few hundredths of a second, as does the inevitable axial extension. The effect of the heating is therefore the same as dropping the weight on the end of the elastic wire. Once again the thermal expansion of the wire induces axial oscillations of the wire/weight assembly. These oscillations cause resistostrictive oscillations of the wire resistance at the level of a few milliohms. These oscillations have been observed using a fast recovery storage oscilloscope and are illustrated in Figure 3.5. The oscillations are superimposed on the

Figure 3.5 Schematic of Comparator input voltage showing effects of resisto-strictive oscillations.

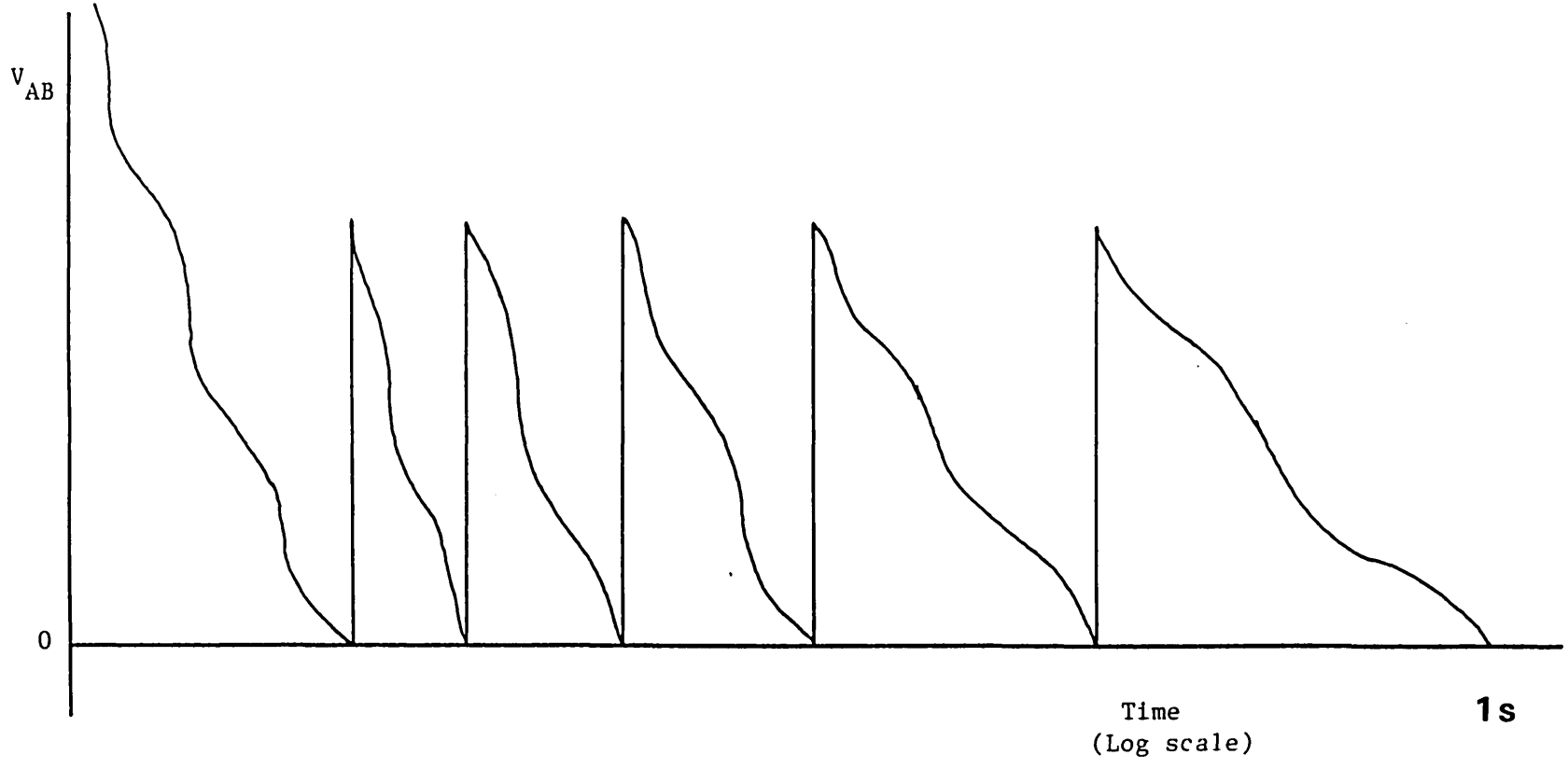

usual voltage decay and have a frequency of 150 Hz ± 50 Hz and amplitude in excess of the background noise at the comparator ouput (10 mV). These oscillations will cause systematic triggering of the comparator and will seriously affect the precision of the reported thermal conductivity. Further evidence for the presence of this effect can be inferred from a study of the deviations of the experimental temperature rise from that calculated from the linear regression of the ΔT vs ℓn t data. The instrument will sample the oscillations at a frequency less than that of the oscillations themselves so it is difficult to discern any oscillatory behaviour in the deviation plots, which appear to be random, but the plots do demonstrate increased deviations at lower times where the effect will be more pronounced. Figure 3.6 shows a typical deviation plot with the cell configuration given in Figure 3.4d.

The final problem was overcome by using the design shown in Figure 3.4e. Here the wire/weight assembly is suspended from a very weak gold spring. The tension in the wire is kept constant using the weight and electrical continuity is once more ensured by the gold loop. The spring constant for a tightly-wound helical spring is given by

$$K_{sp} = \frac{Gd^4}{8D^3nK} \qquad (3.6.2.1)$$

where

$$K = \frac{C}{C-1} + \frac{1}{4C} \qquad (3.6.2.2)$$

and

$$C = \frac{D}{d} \qquad (3.6.2.3)$$

Here G is the rigidity of the material used for the spring, d is the diameter of the wire used for the spring, D is the diameter of the

Figure 3.6

Deviations from the least squares fit for cell design 3.4d

$$DEV = ((\Delta T_{EXP} - \Delta T_{CALC})/\Delta T_{CALC}) \times 100\ \%$$

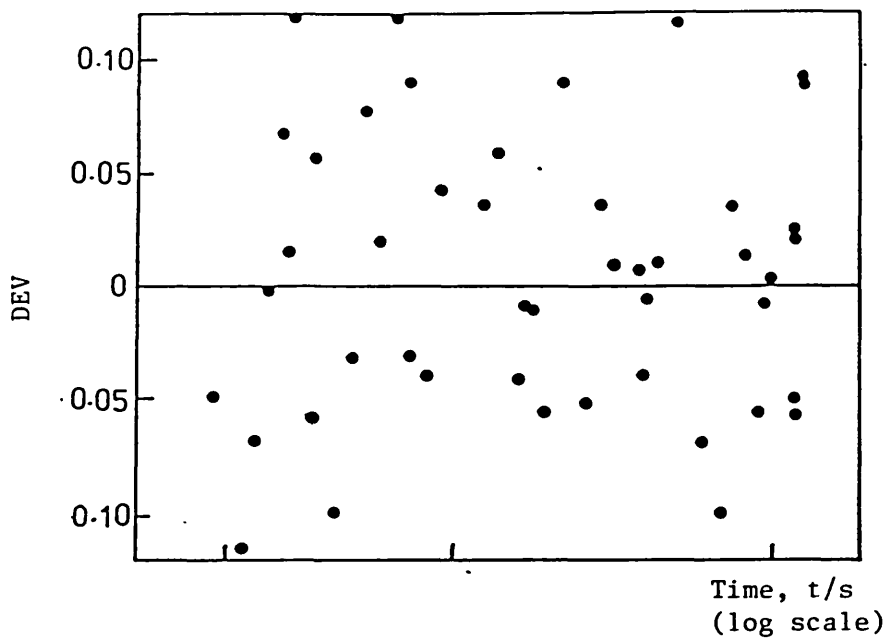

Figure 3.7

Deviations from the least squares fit for cell design 3.4e

$$DEV = ((\Delta T_{EXP} - \Delta T_{CALC})/\Delta T_{CALC}) \times 100\ \%$$

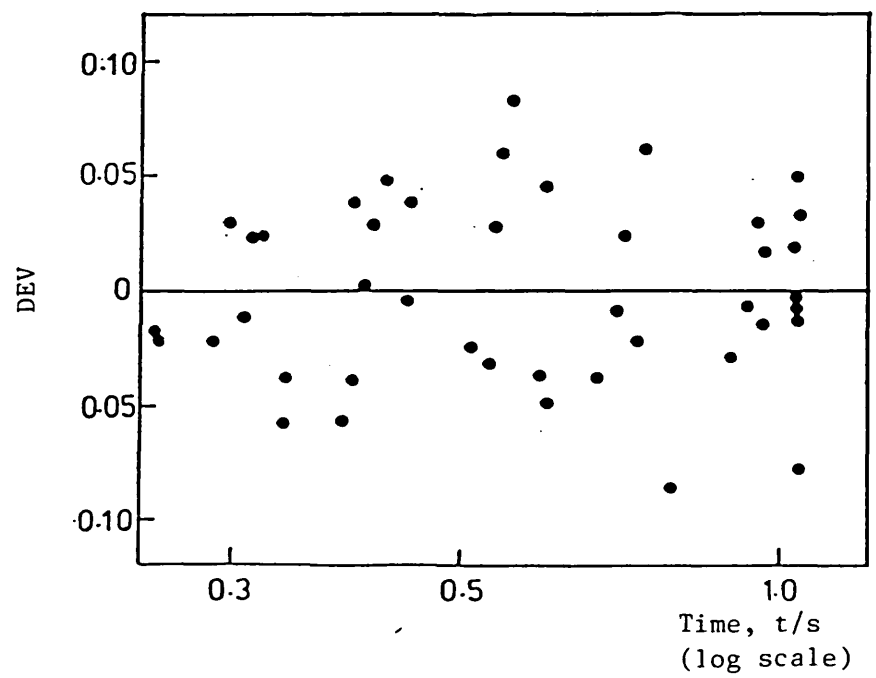

spring and n is the number of turns. The spring constant for the wire is given by

$$K = \frac{AE}{L} \qquad (3.6.2.4)$$

where E is the Young's Modulus, A is the cross-sectional area and L is the length. The principle behind the use of the gold spring is that the potential energy of the falling weight is tranferred to the spring rather than the platinum wire. The spring will then cause the entire wire/weight assembly to oscillate vertically by an amount insufficient to effect the heat transfer from it. It is proposed that the energy is transferred to the spring in preference to the wire if the spring constant for the spring is much less than the spring constant for the elastic wire. The springs used in the present installation comply with the design criterion.

$$K_{sp} \simeq \frac{K_w}{10} \qquad (3.6.2.5)$$

The springs have the approximate dimensions:

D = 3 mm

d = 0.122 mm

N = 5

The effects discussed above are very small. They cannot contribute to more than 0.1% of the measured temperature rise of the wire, which is generally the resolution of many instruments. The effect is, however, of a systematic nature and very reproducible and, as such, can have a substantial effect on the measurement of thermal conductivity. Figure 3.7 shows the improved deviation plot obtained when switching from the cell design of type 3.4d to 3.4e. The

precision of the measurement is greatly improved.

3.6.3 Construction of the Wire/Weight Assembly

In this section, the sequence of events that result in a set of hot-wires contained within the measurement cell is discussed. The manufacturing process is the result of many years of experience with previous designs [1, 10, 15]. The first components to be made are the springs and weights. The weights are made from a piece of platinum rod of diameter 0.5mm and length about 10 mm. A small blob of gold is then melted onto both ends of the platinum rod using a microtorch. The heat is applied for a sufficient length of time to produce a platinum-gold alloy near the pure metal boundary, but not enough to cause significant oxidation of the gold. The weight is then weighed to ensure that the weight will not apply an excessive stress to the wires. A weight of 70-120 mg is usually used. The spring is manufactured from 40 SWG gold wire by hand winding it around a ~ 3 mm diameter rod to produce five tightly-wound turns. A length of gold wire is retained at one end of the spring and a hook is formed at the other end for subsequent attachment of the platinum wire. The platinum wire is removed from the spool being careful to avoid kinks in the wire and contamination due to dust particles on the surface. The platinum wire is then soldered to the hook of the gold spring using a 4:1 gold-tin solder. This solder was used because it allowed fixing of the platinum wire to the spring without the gold spring dissolving into the solder, whilst providing a good electrical contact between the gold spring and the platinum wire. The weight is then attached to the platinum wire by using the microtorch to heat and melt the gold blob whilst the platinum wire is laid over the top of the blob. Surface tension draws the wire into

the melted gold and a low resistance platinum–gold alloy is produced. A gold loop is manufactured by compressing about 20 mm of the 40 SWG gold wire and annealing it in an oven at about 1010°C for six hours. The resultant gold loop has very little mechanical strength and will apply no lateral force on the wire/weight assembly. The gold loop is soldered onto the gold blob using the 4:1 ratio gold–tin solder. The resultant wire/weight assembly is shown in Figure 3.4e.

The wire/weight assembly is then transferred into a jig for mounting in the hot–wire cells. The assembly is held between the points of a pair of tweezers and allowed to hang freely. This is a good test of the mechanical strength of the wires and the joints. The assembly is then brought up to the supports of the hot–wire cells using the controls of the jig then the spring is soldered to the top support and the free end of the gold loop is soldered to the bottom support. The wire/weight asesmbly is now in position. Any residual stress in the wires is removed by annealing them by heating to red heat using ohmic dissipation. The annealing process lasts about an hour and is carried out with the wire slack. This concludes the construction and installation of the wires. Before the cell is closed and placed inside the pressure vessel, the length of the wires is measured using a cathatometer with a precison of ± 0.02 mm. Accurate identification of the exact end of the wires is necessary and the cell may have to be rotated during this operation in order to spot the exact ends of the wire. Any solder or gold that may have travelled down the wire causes the resistance of that section to be greatly reduced and must be considered part of the supports. Finally, the resistance of each of the wires is measured to check if the resistances per unit length agree to within 1%. As a final check before assembly of the cell, the wires are tested for electrical

insulation from the cell body.

3.6.4 The Pressure Vessel

The cell containing the measurement wires is placed inside a pressure vessel manufactured from a stainelss-steel cylinder (EN58B), designed for pressures up to 150 Atmospheres, as shown in Figure 3.8. the mounting flange is held to the shoulder of the pressure vessel using two screws. At temperatures above room temperature the flanged cap of the pressure vessel (1) is sealed by a rubber 'O' ring (2). Below room temperature the 'O' ring is replaced by an annealed copper gasket which is preloaded using six high-tensile steel bolts (3). The cap is equipped with a gas/vacuum port (4) which also serves to allow electrical leads to pass from the cell to a high-pressure seal which is outside the main body of the instrument and is kept at room temperature. The port is sealed to the cap using a gold 'O' ring above room temperature (5). Below room temperature an indium wire 'O' ring is used. Two holes are drilled, one at the bottom of the cylinder, the other in the cap, for two calibrated Degussa platinum resistance thermometers (6), (7).

3.6.5 The Constant Temperature Enclosure

The temperature stability of the test fluid is maintained at a level of better than ± 1 mK over the temperature range 170 K to 430 K for the 10 minutes necessary for a complete measurement cycle by placing the pressure vessel inside a relatively massive copper block, as shown schematically in Figure 3.9. The copper block, which has a mass of approximately 30 kg, is divided into two sections (1), (2). The two halves are sealed above room temperature using a gold 'O' ring and, at lower temperatures, using an 'O' ring made from

Figure 3.8 The Pressure Vessel.

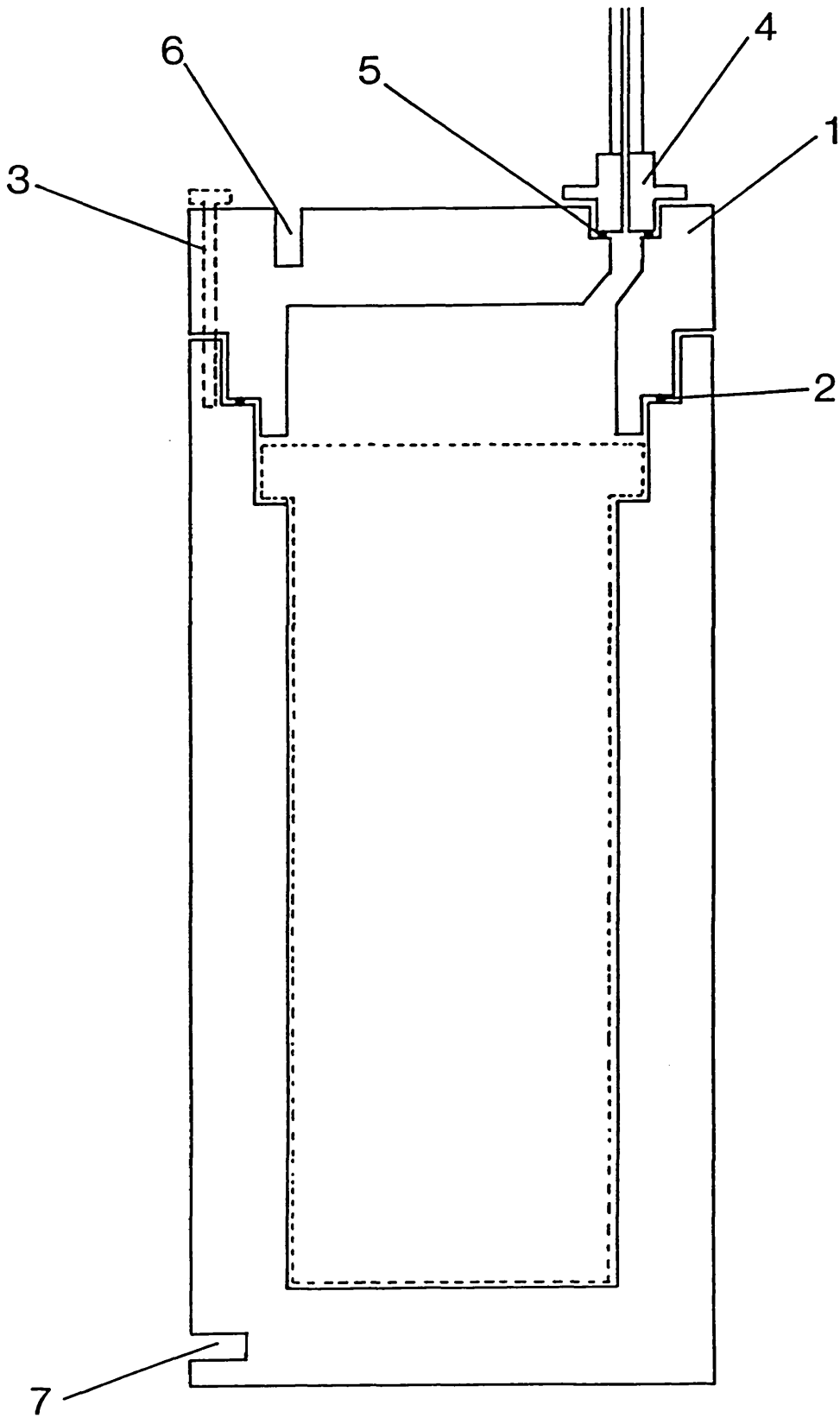

Figure 3.9 The present Instrument.

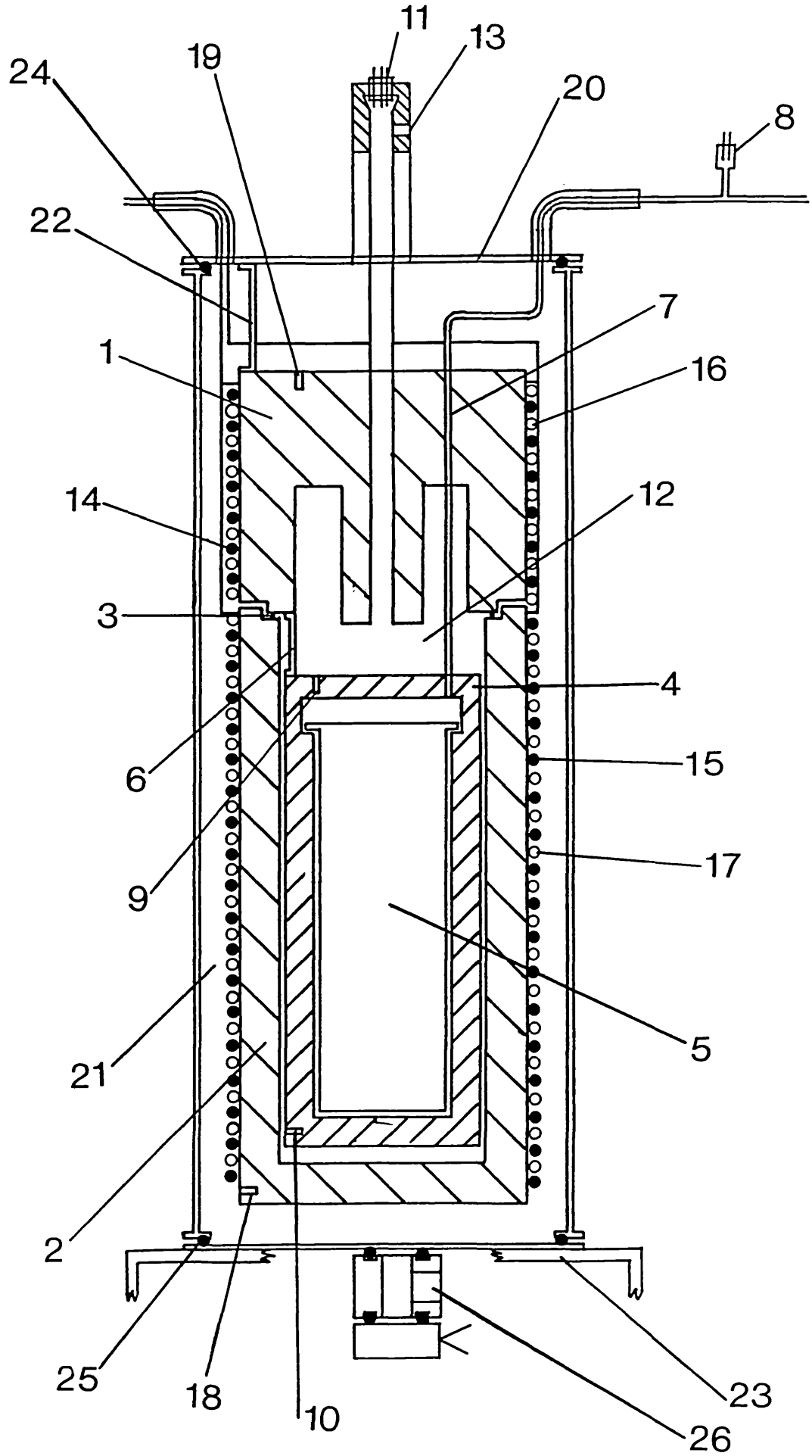

electrical solder (3). The pressure vessel (4) containing the cell (5) is suspended from the top half of the copper block using a thin strut (6). The electrical leads from the cell are fed through the gas feed tube (7) to a conax high-pressure seal (8) maintained at room temperature. The seal to the leads from the platinum resistance thermometers, positioned in the pressure vessel (9), (10), is also made at room temperature (11). The space between the copper block enclosure and the pressure vessel (12) may be filled with an exchange gas or vacuum via a port (13). The copper enclosure is fitted with bifilar windings of heating cable, comprising two separate heaters for the top and bottom sections (14), (15) and cooling coils which are also divided to cool the top and bottom sections (16), (17). The temperature of the enclosure is monitored using probes positioned in the top and bottom sections (18), (19). The copper block is suspended from the top plate (20) of a vacuum jacket (21), by means of thin strut (22). The vacuum jacket is sealed to top and base plates (20), (23) using rubber 'O' ring seals (24), (25). The vacuum jacket is attached to a high vacuum system comprised of Edwards rotary and diffusion pumps via a roughing line port (26) and butterfly valve using rubber 'O' ring seals placed in the grooves of a vacuum ring . A liquid nitrogen cold trap is installed to prevent back-streaming of the diffusion pump fluid. Finally, the whole assembly is bolted to a thin strutted frame .

The effects of building vibrations are reduced by the use of relatively massive components suspended on thin struts. Further precautions were taken by isolating the frame from the building using absorbent Tico pads and pneumatic isolation feet supplied by Barry Controls Ltd., which have a resonant frequency of 3 Hz.

3.6.6 The Gas Handling System

The pressure vessel is attached to the gas handling system shown in Figure 3.10. Where possible, the high-pressure components are contained within a $\frac{1}{4}$" steel cage and isolated from building vibrations using the Tico pads and isolation feet mentioned previously. Before filling the pressure vessel with gas, the line is evacuated using the vacuum pumps according to the following procedure. V_4 and V_9 are kept shut. The line, including the compressor up to V_4, is evacuated using an Edwards rotary pump. The pressure vessel and the rest of the line is evacuated using the Edwards rotary/diffusion pump combination. The vacuum obtained in both lines is monitored using the Pirani gauges P_1–P_3. A vacuum better than 10^{-2} torr is expected in the pressure vessel side. An inferior vacuum is obtained in the compressor line owing to the compressor seals not being designed for vacuum service. The effects of impurities may be reduced by successive filling and purging of the compressor line with the test gas. After leaving the system to evacuate for about six hours, the pressure vessel is filled to the required pressure using the compressor and by throttling the gas flow into the vessel using V_{10}. All the fittings used in the present installation are either Aminco or swaged high-pressure fittings and the valves are either Aminco type or Hoke high-pressure valves. the vacuum system contains Edwards high vacuum components and fittings. In the present installation, the high-pressure gauge reads 0–2000 PSIG and was calibrated by the manufacturers, Burnet Instruments. The low-pressure gauge reads from 30" Hg vacuum to 100 PSIG and was supplied and calibrated by Budenburg.

Figure 3.10 The Gas Handling System

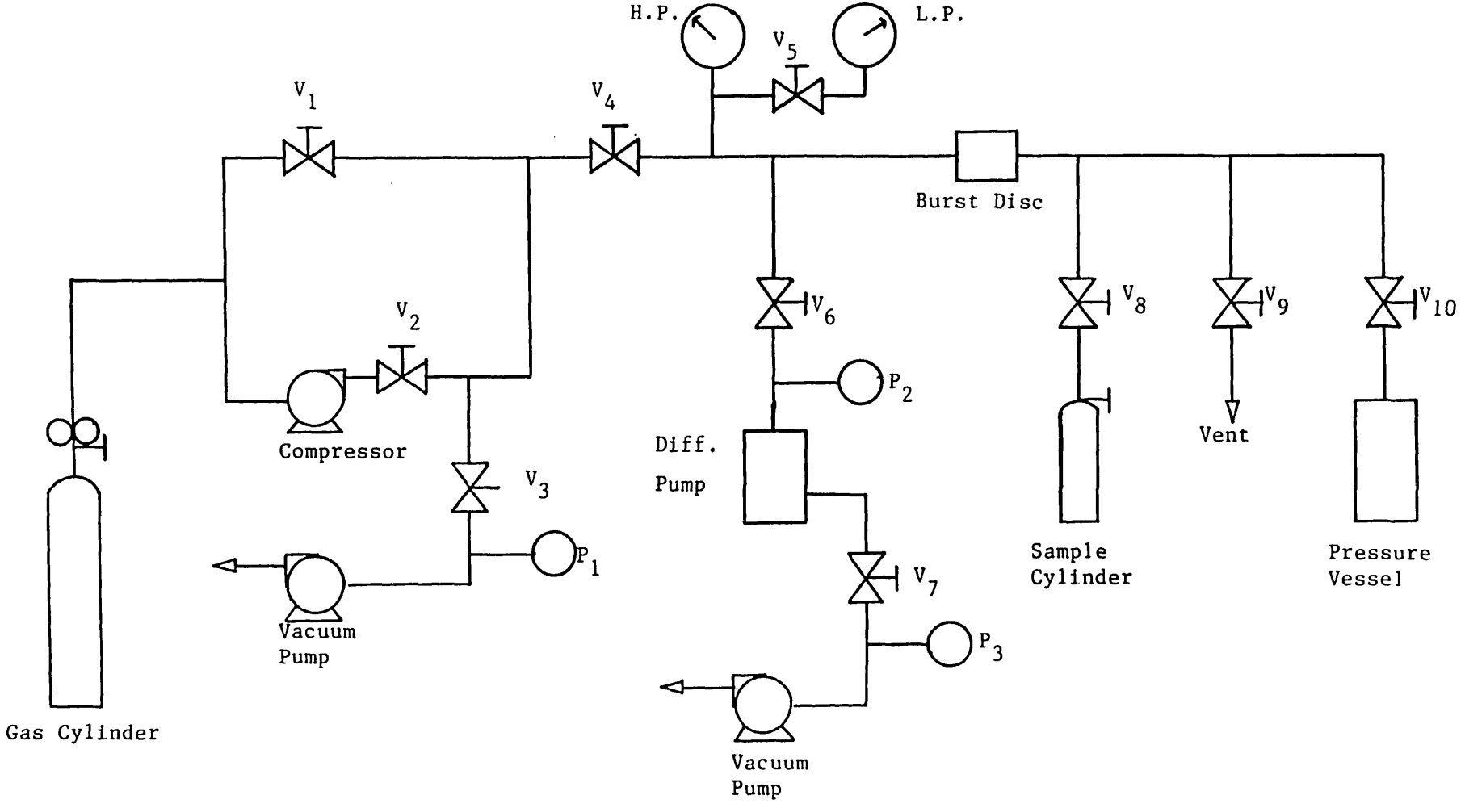

3.6.7 Temperature Control and Measurement

An important feature of this installation is the extended range of temperatures available. The system is inherently stable owing to the large thermal interia associated with the massive copper block which forms the temperature enclosure. The heating coils fixed to the two halves of the copper block are connected to two independent 30 V d.c. power supplies which are regulated using two PID controllers. Above room temperature, the controller probes are Chromel–Alumel thermocouples imbedded in the top and bottom of the copper blcok. The set points of the controllers are chosen such that there is a temperature gradient of approximately 0.5 K in the pressure vessel. This inhibits the creation of density–driven convection currents in the pressure vessel.

Below room temperature, cool nitrogen vapour or liquid nitrogen is passed through the cooling coils fixed to the copper block. The liquid nitrogen is supplied from a self–pressurising 75 L dewar which is kept topped up using a smaller 30 L shuttle dewar. The supply dewar is fitted with a level indicator and self–pressurising valve as shown in Figure 3.11. The dewar pressure is kept constant within the range 0–30 PSIG. This will ensure a constant flowrate of liquid or vapour to the cryostat. The flowrate is fine–tuned using a self–compensating flowrate control valve, V1, and measured after passing through an expansion coil using a standard rotameter. A flowrate in the range 7–20 L/min (gas at 760 mmHg and 15^{o}C) was found to be suitable for measurements in the range 273–170 K. The consumption of liquid nitrogen may be reduced by using short,lagged transfer tubes wherever possible and maintaining a good vacuum in the vacuum jacket. The principle of operation is that the coolant provides a background cooling element to the temperature control which is then fine–tuned

Figure 3.11 The Coolant System.

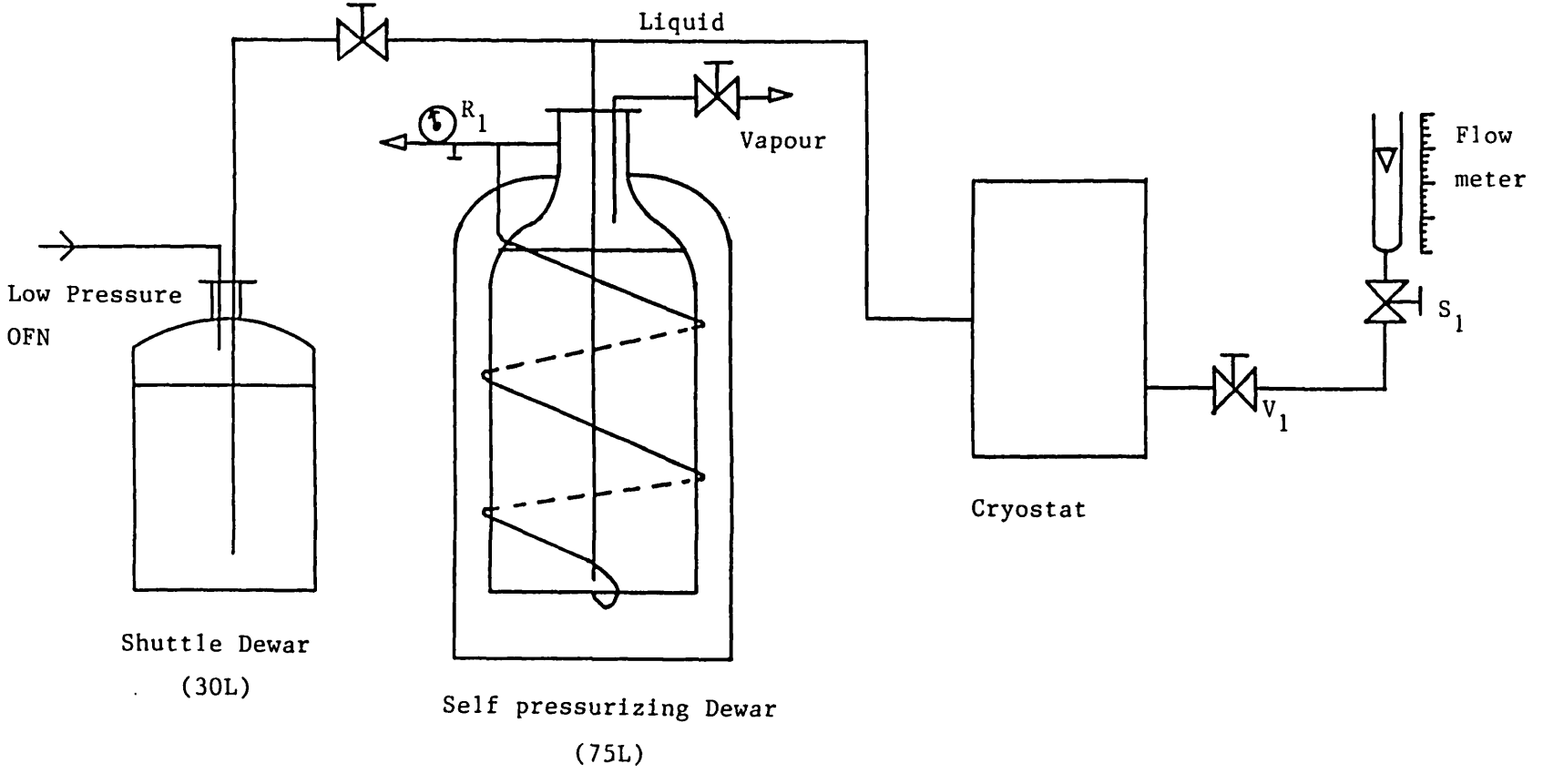

by using the heating coils. For the low temperature measurements, the thermocouples were replaced by silicone diode probes. The voltage across the forward biased junction of the semi–conductor is temperature–dependent and offers improved temperature sensitivity over that of a Chromel–Alumel thermocouple (typically 2 mV K^{-1} as opposed to 0.04 mV K^{-1}). The PID controllers were designed, however, to be used in conjunction with thermocouples above room temperature. A circuit was therefore designed such that the diodes mimic the behaviour of the more usual thermocouples. The attenuation of the diode signal necessary meant that the improved sensitivity was used to improve the signal to noise ratio of the device. The circuit used for this purpose is shown in Figure 3.12. D1 is the sensing diode and D2 is a reference voltage kept in a thermostatically–controlled constant temperature environment. The voltage signal from these components forms the input of a differential amplifier (gain ~ 1/50), the output signal from which is sent unaltered to the input of the PID controller.

As a further precaution to maintain good temperature stability during the measurement, a normally closed solenoid valve S1 (see figure 3.11) is fitted in the coolant line. The solenoid valve is energised and hence kept open during normal operation. However, during a measurement the heaters are switched off so as to avoid electrical interference. This switching operation also de–energises the solenoid valve, hence closing it and avoiding unnecessary cooling of the copper block.

The temperature measurement is performed using two calibrated degussa thermometers imbedded in the top and bottom of the pressure vessel. The temperature of the test fluid is taken to be the average temperature of the pressure vessel. Above room temperature, the

Figure 3.12 Diode Sensor Circuit.

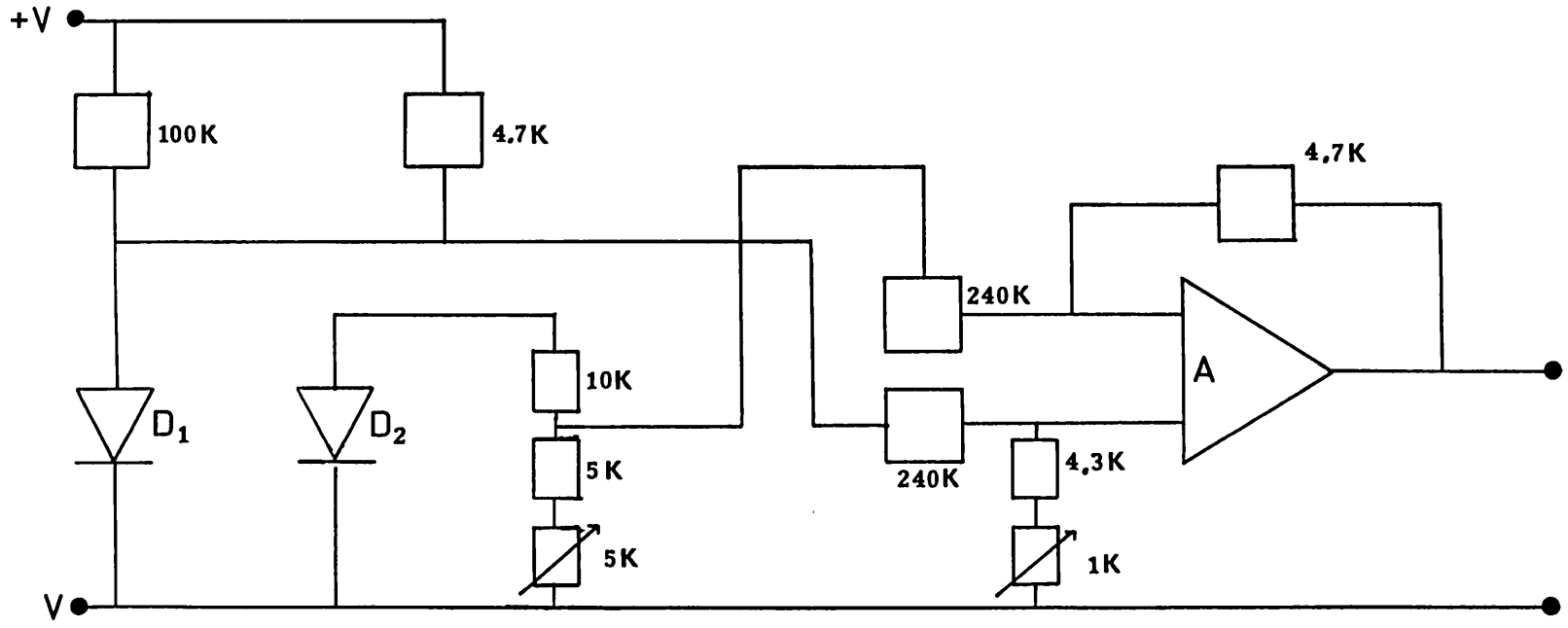

temperature–resistance characteristic of the Degussa thermometers is of the form

$$R(t) = R(0)[1 + At + Bt^2] \qquad (3.6.7.1)$$

The constants A and B used were those recommended by the manufacturers. The value of R(0) was measured experimentally for each thermometer. Below room temperature the thermometers required calibration. For this purpose, the Deugssa's and an NPL–calibrated Tinsley platinum resistance thermometer were immersed in a bath containing a well–stirred solid–liquid mixture of a pure organic compound immersed in a bath of liquid nitrogen. Suitable compounds can be selected to cover the range 77–273 K adequately. The results where fitted to a polynomial of the form,

$$R(t) = R(0)[\ 1 + At + Bt^2 + Ct^2]$$

The resistance of the Degussa's and the Tinsley were then measured using a Comark 6800 micro–processor thermometer. The overall uncertainty in the temperature measurement below room temperature is ± 0.03 K and 0.01 K above room temperature. The calibration constants are given in table 3.2.

3.7 TESTING THE BRIDGE

Before commissioning of the new computer–controlled bridge, the components were tested as far as possible. The bridge was then used to measure the thermal conductivity of argon at various temperatures as a function of pressure. Previous isotherms were measured using the older bridge circuit. The results of these test measurements confirmed the operation of the bridge circuit and are presented in Chapter 4, along with the other experimental results.

Table 3.2

Degussa calibration constants.

Above $0^{o}C$

Top

$R(0) = 100.041$; $A = 3.90784 \times 10^{-3}$; $B = -5.78408 \times 10^{-7}$

Bottom

$R(0) = 100.036$; $A = 3.90784 \times 10^{-3}$; $B = -5.78408 \times 10^{-7}$

Below $0^{o}C$

Top

$R(0) = 99.934$; $A = 3.9124 \times 10^{-3}$;

$B = -5.0033 \times 10^{-7}$; $C = 1.5189 \times 10^{-9}$

Bottom

$R(0) = 100.014$; $A = 3.9136 \times 10^{-3}$;

$B = -4.7946 \times 10^{-7}$; $C = 1.5896 \times 10^{-9}$

References

[1] M.J. Assael, PhD Thesis, University of London (1980).

[2] J. Menashe, PhD Thesis, University of London (1980).

[3] J.M. Fareleira, PhD Thesis, Technical University of Lisbon (1986).

[4] H.M. Roder, J. Res. NBS 86, 5, 457 (1981).

[5] J.J. de Groot, J. Kestin, H. Sookiazian, Physica 75, 454 (1974).

[6] Sigmund Cohn Corporation, New York, U.S.A.

[7] The International Temperature Scale of 1968 (HMSO, London) (1969).

[8] W.A. Wakeham (private communication).

[9] M. Zalaf, PhD Thesis, University of London (1988).

[10] M. Assael, M. Dix, A. Lucas and W.A. Wakeham, J. Chem. Soc. Faraday Trans. I 77, 439 (1981).

[11] E.F. Buyukbicer, J.E.S. Venart and R.C. Prasad, High Temp.-High Press. 18, 55 (1986).

[12] B.Taxis *et al* (to be published)

[13] M. Dix (private communication).

[14] J. Kestin and W.A. Wakeham, Physica 92A, 102 (1974)

[15] E.N. Haran and W.A. Wakeham, J. Phys. E: Sci. Instrum. 15, 839 (1982).

[16] E.N. Haran, G.C. Maitland, M. Mustafa and W.A. Wakeham, Ber. Bunsenges. Phys. Chem. 87, 657 (1983).

[17] J.J. de Groot, J. Kestin, H. Sookiazian and W.A. Wakeham, Physica 92A, 117 (1978).

[18] J. Kestin, R. Paul, A.A. Clifford and W.A. Wakeham, Physica 100A, 349 (1980).

[19] A.A. Clifford, J. Kestin and W.A. Wakeham, Physica 100A, 370 (1980).

[20] J. Menashe and W.A. Wakeham, Ber. Bunsenges. Phys. Chem. 85, 340 (1981).

CHAPTER 4

RESULTS

4.1 INTRODUCTION

In this chapter the thermal conductivity results obtained, using the previously-described instrument, are presented. The new computer-controlled instrument was used for the majority of the measurements presented, although some of the isotherms were obtained using the older bridge circuit. The distinction between the two instruments is only in terms of the increased precision of the newer instrument. The uncertainty associated with the thermal conductivity obtained using either bridge is generally unchanged. It is worth recalling that the primary motivation for the new bridge circuit was to increase the temperature range over which the highest accuracy was to be maintained and not necessarily to improve the uncertainty of the final result. In view of these facts, no distinction is made between the measurements reported here.

The measurements of thermal conductivity generally range from 308 to 430 K and pressures up to 10 MPa. However, the measurements for argon and nitrogen extend from 170 to 430 K (with pressures also up to 10 MPa). By virtue of the transient nature of the experiment, the reference temperature for each individual measurement is unique. In order to represent the data along isotherms it is necessary to correct each data point to a nominal temperature. The nominal temperature is generally never more than a degree celsius away from the reference temperature, so a simple linear correction is employed

$$\lambda^0(T_{nom}) = \lambda^0(T_{ref}) + \left[\frac{d\lambda}{dT}\right]_{\rho=0} \times (T_{ref} - T_{nom}) \qquad (4.1.1)$$

Application of the above equation assumes that the density dependence of the thermal conductivity is independent of temperature. This concept is generally accurate away from the critical region. Even so, the correction never usually amounts to more than 1% of the thermal conductivity and is often much smaller than that. It is therefore assumed that errors associated with the application of equation (4.1.1) will be negligible.

For purposes of interpolation, it is useful to represent the experimental thermal conductivity data by means of a finite polynomial in density

$$\lambda = \sum_{i=1}^{n} C_i \rho^i \qquad (4.1.2)$$

For each gas, along each isotherm, the coefficients C_i that secure the optimum fit to the data by means of equation (4.1.2) are given. This information is found in table 4.1.1. Deviation plots illustrating the deviation of the experimental data from the correlation of equation (4.1.2) are also presented for each gas. In addition, these figures serve as a common reference with which to compare the earlier results of other workers. For this purpose, the earlier results are generally selected along isotherms close to those reported here, and corrected to these nominal temperatures in the manner described previously.

4.2 THE THERMAL CONDUCTIVITY RESULTS

4.2.1 Argon

The argon used for these measurements was supplied by the British Oxygen Company plc with a stated purity of 99.998%. For the

density, there were two sources of information employed. Above 300 K the density was derived via interpolation among the (P, V, T) data of Michels and his collaborators [1]. The heat capacity was obtained from the same source using standard thermodynamic results. Below 300 K an equation of state, derived from many thermodynamic measurements, obtained by Stewart *et al.* [2], was employed for calculation of density and heat capacity. The estimated uncertainty of the density is better than 0.1% in both cases. Tables 4.2.1–4.2.7 list the thermal conductivity of argon along seven isotherms. These tables also include the pressure and reference temperature, since it is these quantities which determine the thermodynamic state appropriate to each datum.

Although measurements were possible up to 10 MPa for each isotherm studied, the measurements made at the highest pressures along the lowest isotherm proved difficult due to the onset of convection. This difficulty is explained in terms of the proximity of the density at these temperatures and pressures to the critical density. The instrument is not specifically designed to operate under these conditions and the working equations are invalidated. The measurements made in this region are burdened with an error of ± 2%. It is estimated that all other measurements enjoy an uncertainty of ± 0.3%.

Table 4.1.1 shows the optimum parameters of the correlating equation (4.1.2) at each temperature. The standard deviation of the least squares fit is consistent with the estimated uncertainty of 0.3%. Figure 4.1a and 4.1b show the deviation of each datum from the correlating equation. The maximum deviation of the present data is 1.2 % which reflects the decreased precision near the critical region. Figure 4.1a also shows the deviation of previous

Figure 4.1a

Deviations, $\epsilon = [(\lambda_{expt} - \lambda_{corr})/\lambda_{corr}] \times 100$, of the thermal conductivity of argon from the correlation of the present data by means of eq. 4.2.1

Present work: • 308.15 K; ▲ 333.15 K; ■ 378.15 K; ◆ 428.15 K.

Haran *et al.*[3] : ⊙ 308.15 K; Δ 333.15 K; □ 378.15 K; ◇ 428.15 K.

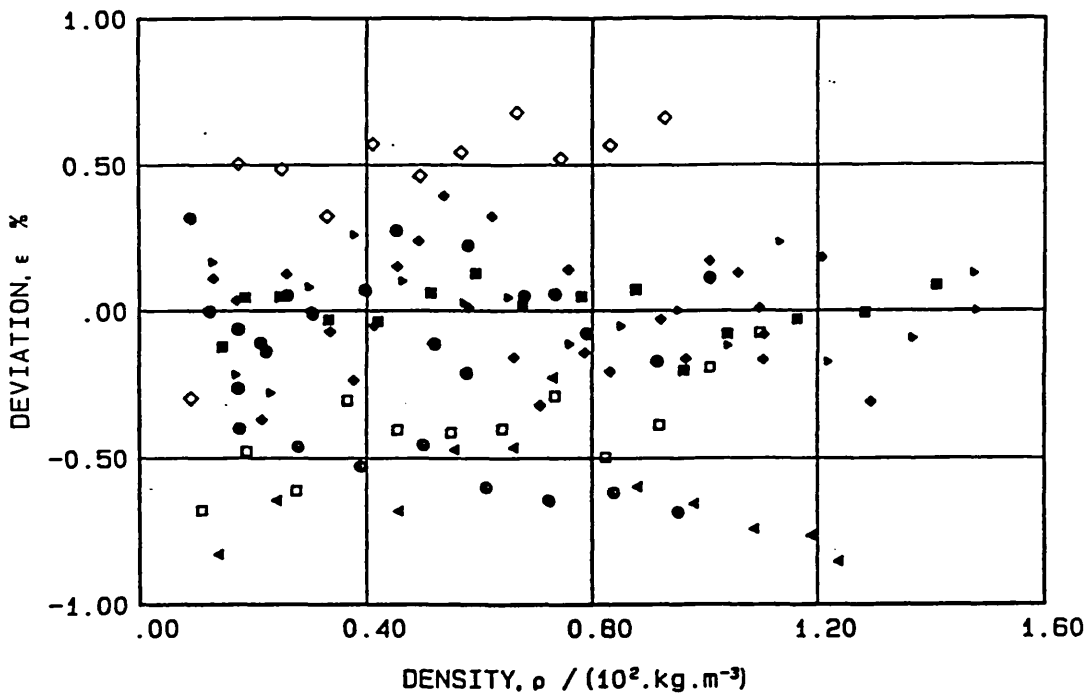

Figure 4.1b

Deviations, $\varepsilon = ((\lambda_{EXP} - \lambda_{CORR})/\lambda_{CORR}) \times 100$, of the thermal conductivity of argon from the correlation of eqn. 4.2.1

Present work: ▲174 K; ▼223.15 K; ◀266.65 K; ▶308.15 K;

■333.15 K; +378.15 K; ×428.15 K.

Lisbon[4]: △174.15 k; ▽225 K; ◁308.15 K;

▷378.15 K; ⊡429.15 K.

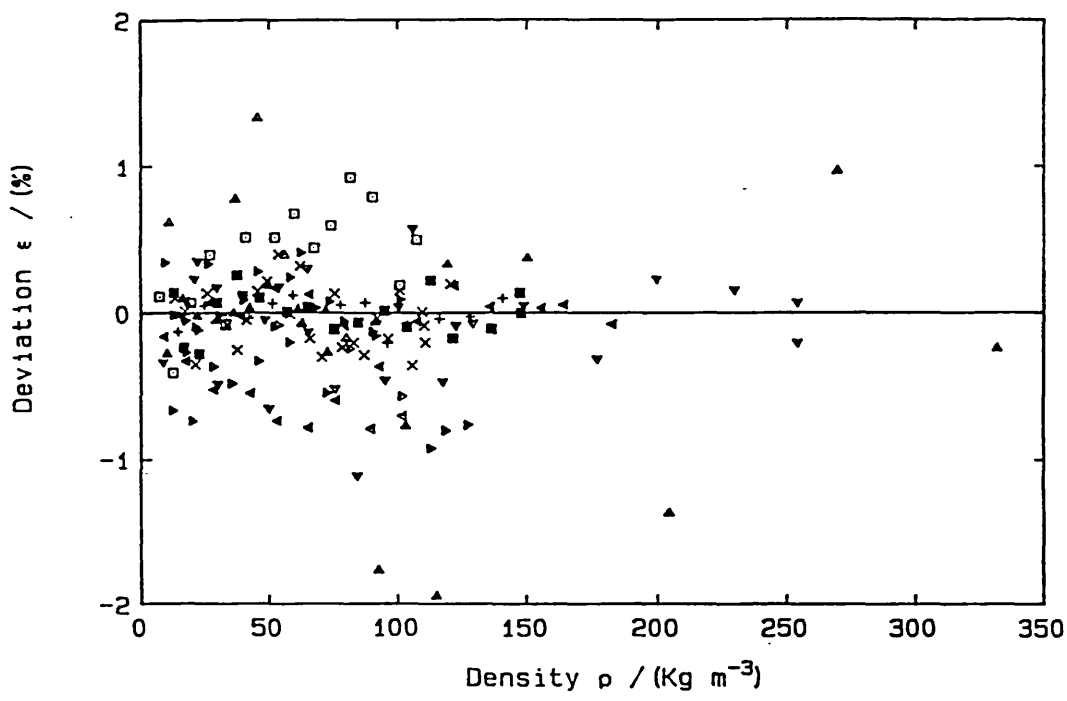

measurements made in the same laboratory [3]. These measurments deviate by at most 0.8% from the present correlation, although the estimated standard deviation of the entire data set is only ± 0.5%. This final figure is commensurate with the mutual uncertainty of the two independent sets of measurements (0.6%). Shown in Figure 4.1b are the deviations of a set of accurate measurements made in Lisbon [4]. These results extend across the entire temperature–pressure range of the present measurements, and show a level of agreement once more consistent within their muutal uncertainty of 0.6%, except at the lowest temperature where the deviation is as much as 1%. Discussions with the authors have indicated that this isotherm may be in error [5]. It is interesting to note that the differences between the two sets of measurements made at Imperial College are noticeably systematic. This shows that the accuracy of the results is not quite as good as their precision. Considering that three different types of wire mounting and two measurement bridges have been used to obtain this body of data, the agreement is considered satisfactory.

4.2.2 Helium

The helium used for these measurements was supplied by the British Oxygen Company plc and had a stated purity in excess of 99.999%. The measurements were made in the temperature range 308–430 K and, in general, from a maximum pressure of 10 MPa down to the lower limit set by the need to avoid Knudsen effects [6]. During the measurements extreme care was taken to avoid the effects of convection. In this respect, the new bridge circuit was most useful because it allowed precise measurements to be made with a temperature rise of only 2 K instead of the 4–5 K characteristic of earlier

versions of the instrument. The density of helium was calculated from the (P, V, T) measurements of Michels and his collaborators [7, 8], whereas the heat capacity required for the small corrections in the data reduction was estimated from the same source. It is estimated that the uncertainty in the reported thermal conductivity is one of ± 0.3% at the lowest temperatures, deteriorating slightly to ± 0.5% at the highest temperatures.

Tables 4.2.8–4.2.11 list the thermal conductivity of helium, along with the experimental pressure and reference temperature required to determine the density of the fluid. As usual, the experimental data are correlated along each isotherm. The optimum correlating parameters of equation (4.1.2) are given in Table 4.1.1 for each isotherm. A linear fit was all that was necessary to represent the thermal conductivity of helium over the entire temperature and pressure range.

Figure 4.2 shows the deviations of the present data from these optimum correlations. The maximum deviation is no more than 0.6%, whilst the standard deviation is one of ± 0.2%. These figures are consistent with the estimated precision of the measurement. The same figure also shows the deviations of earlier work from the present correlations [9–13]. There is good agreement (generally within the mutual uncertainty) between the present data and that reported by Kestin *et al.* [10] and the earlier measurements made at Imperial College [9].

4.2.3 Neon

The neon used for these measurements was provided by the British Oxygen Company plc and had a stated purity in excess of 99.995%. The density and heat capacity have been derived from the (P, V, T) data

Figure 4.2

Deviations of experimental thermal conductivity of helium from correlation of eqn. 4.1.2,

Present work: ● 35°C. ■ 65°C. ▲ 106.5°C. ◆ 155°C;

Earlier work: 35°C - Δ [9]. O [10]. □ [11].◇ [12]. ▽ [13]

65°C - ▽ [13]

106.5°C - □ [13]

155°C - ◇ [13]

$$\epsilon = [(\lambda_{expt} - \lambda_{corr})/\lambda_{corr}] \times 100\%.$$

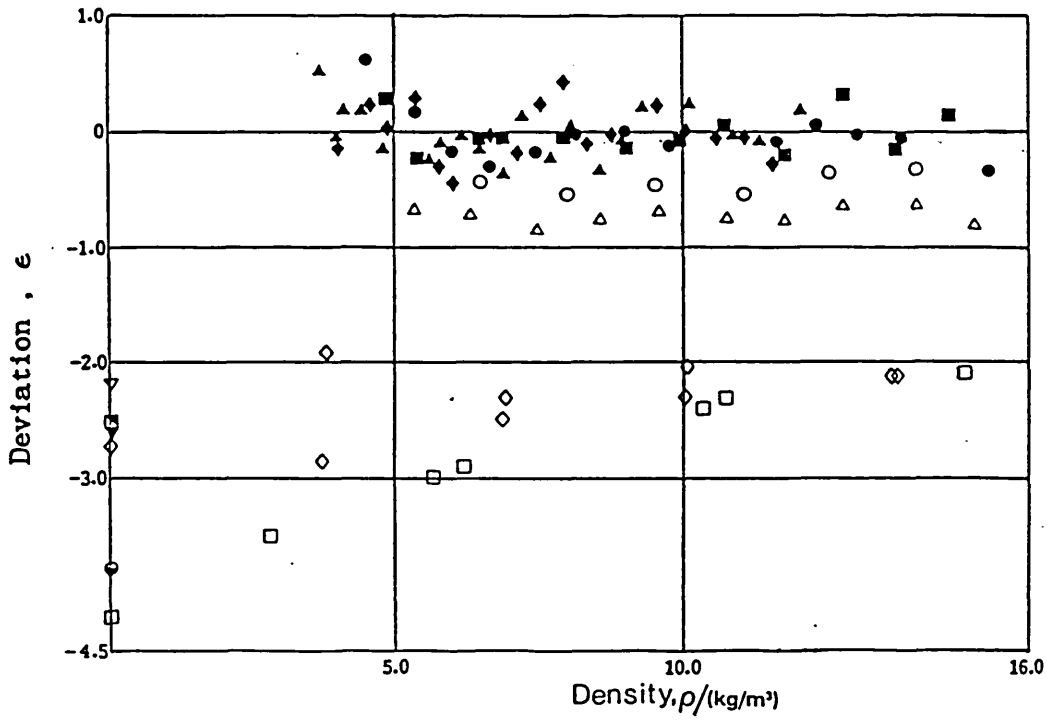

of Michels *et al.* [14]. Measurements were performed along four isotherms in the temperature range 308–430 K and at pressures up to 10 MPa. Tables 4.2.12–4.2.15 list the results. It is estimated that the uncertainty associated with these measurements is one of ± 0.3%. Again, the data is correlated using equation (4.1.2). The set of parameters securing the optimum fit to the data along each isotherm is presented in Table 4.1.1. Figure 4.3 shows the deviation of each data point from the correlation. The maximum deviation is 0.4%, while the standard deviation is ± 0.2%, which is consistent with the estimated uncertainty. The same figure also shows the results of earlier work with hot–wire instruments [9, 10]. Here the deviations are slightly larger and systematic amounting to almost 0.6%. This is still consistent with the mutual uncertainty of ± 0.6%. The comparison with other, older measurements [15, 16], obtained by other methods, is rather poor but is generally within the larger error band.

4.2.4 Hydrogen

The hydrogen used for these measurements was supplied by the British Oxygen Company plc and had a stated purity in excess of 99.999%. The density was obtained from the accurate (P, V, T) measurements of Michels *et al.* [7, 8] and the heat capacity was obtained from the same data along with an ideal gas value. Tables 4.2.16–4.2.19 list the results for hydrogen obtained along four isotherms from 10 MPa down to the lower limit set by the need to avoid the temperature jump effects. It is estimated that the uncertainty in these measurements is 0.3%, deteriorating slightly to 0.5% at the highest temperatures.

Figure 4.3

The deviations of the thermal conductivity data for neon from the correlation of eq. 4.1.2.

Present work: ▶ 308 K; • 337.65 K; ◆ 379.65 K; ■ 428 K. Assael et al.[9] : ◤ 308 K. Kestin et al.[10] : + 300.65 K. Sengers et al.[15] : x 298 K; □ 348 K. Tufeu[16] : ◇ 305 K; ⊙ 347 K.

$$\epsilon = [(\lambda_{expt} - \lambda_{corr})/\lambda_{corr}] \times 100$$

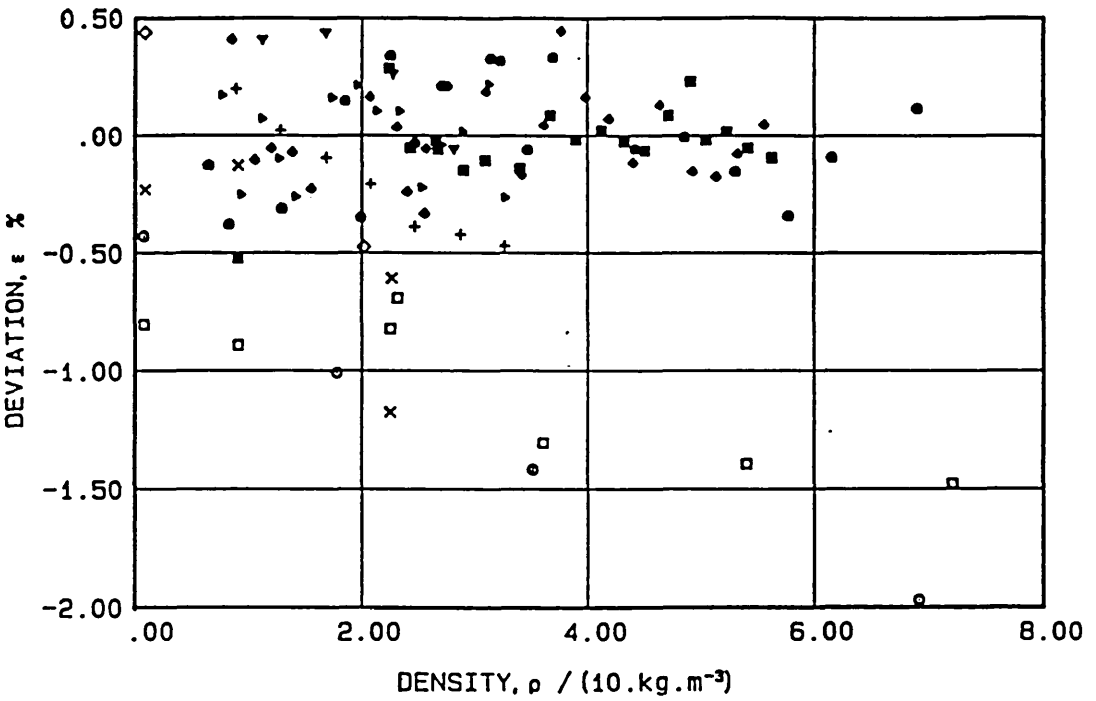

The thermal conductivity has been fitted to polynomials in density in order to obtain the optimum correlating parameters. It was found that a linear fit was all that was necessary to represent the thermal conductivity over the entire range studied. The optimum parameters are listed in Table 4.1.1. Figure 4.4 shows the deviations of the present data from the correlation. The maximum deviation is 0.6%, whereas the standard deviation is one of ± 0.2%. These values are consistent with the estimated uncertainty in the measurements. The same figure shows the deviations of older measurements from the present correlation [17–20]. The agreement between this work and other measurements performed at Imperial College [18] is satisfactory. On the other hand, the results of Clifford *et al.* [19] obtained using a similar instrument lie significantly below those obtained here and those obtained earlier over most of the temperature range. The origin of this discrepancy is unclear, notwithstanding the discussion of this point given by Clifford *et al.* [19].

4.2.5 Carbon Dioxide

The carbon dioxide used for these measurements was supplied by Argo International with a stated purity in excess of 99.995%. For carbon dioxide, the proximity of the range of measurements to the critical point means that a full equation of state must be employed to provide both the density and heat capacity. The most suitable equation available for the present purposes is that developed by Bender [21]. Tables 4.2.20–4.2.23 show the results for carbon dioxide in the temperature range 300–430 K and at pressures up to 10 MPa. As usual, the thermal conductivity data for each isotherm is corrected to the nominal temperature by application of a small linear

Figure 4.4

Deviations of experimental thermal conductivity of hydrogen from correlation of eqn. 4.1.2.

Present work: ● 35°C. ■ 64.5°C. ▲ 106.5°C. ◆ 155°C;

Earlier work: 35°C - O [19]. Δ [18]. O [20]. □ [17]

64.5°C - □ [19]

106.5°C -◇ [19]

$$\epsilon = [(\lambda_{expt} - \lambda_{corr})/\lambda_{corr}] \times 100\%.$$

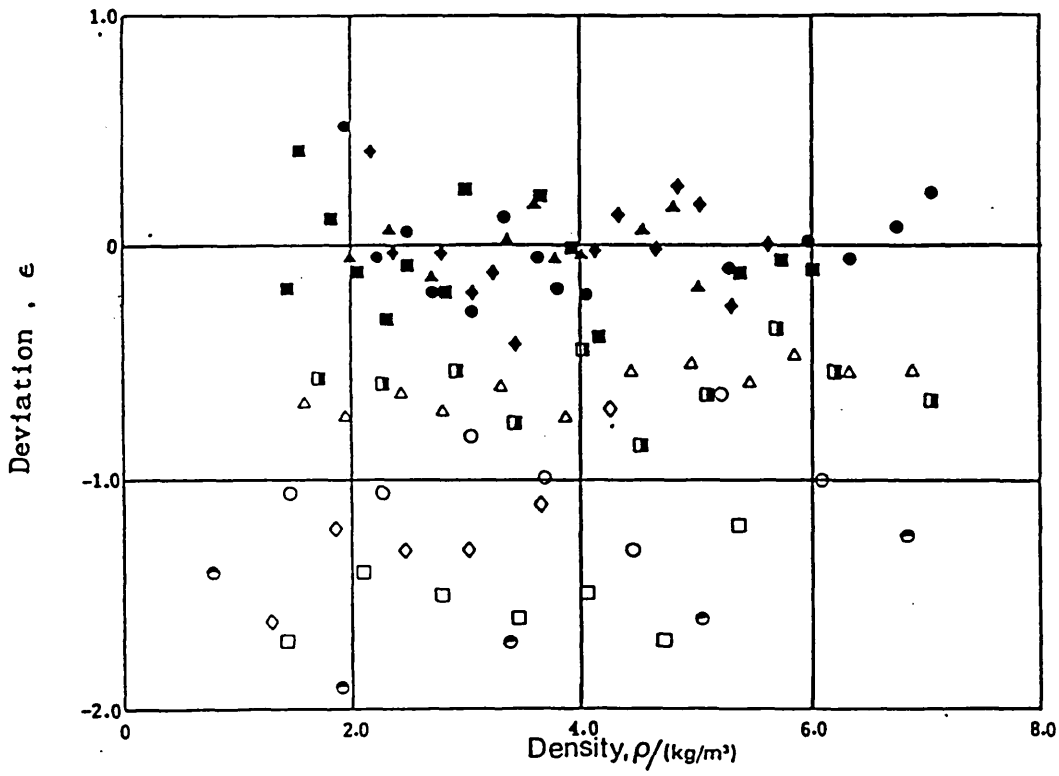

correction. This correction is small and is only 0.5% in regions far removed from the critical point. However, for the lowest isotherm and the highest pressure, a much reduced temperature rise was used so as to avoid the premature onset of convection. In these cases, the correction amounts to nearly 1% of the thermal conductivity. The uncertainty in the carbon dioxide data is estimated to be ± 0.3% over most of the range. However, due to experimental difficulties in the critical region and the large correction applied to the data in this region, the likely error is substantially higher at pressures in excess of 4 MPa along the lowest two isotherms, where it rapidly rises to ± 2% at the extreme pressures.

The data for carbon dioxide were correlated with a polynomial in density and the optimum parameters for each isotherm are listed in Table 4.1.1. Figure 4.5 illustrates the deviations of the present data from the correlation and also shows the deviations of other previous work. The figure shows that at all but the lowest temperature, the deviations of the present results from the correlation never exceed 0.5%. For the lowest isotherm, the scatter in the experimental data at the highest pressures amounts to 1.5%. This decreased precision is a consequence of the experimental difficulties observed near the critical point. The measurements of Johns *et al.* [22] are generally consistent with the present data within the mutual uncertainty band. On the other hand, the few measurements of Le Neindre *et al.* [23] that fall within the density range of interest reveal a substantially different density dependence and a value near zero density, approximately 3% below that reported here.

Figure 4.5

Deviations, $\epsilon = [(\lambda_{expt} - \lambda_{corr})/\lambda_{corr}] \times 100$, of the thermal conductivity of carbon dioxide from the correlation of the present data by means of eq. 4.1.2.

Present work: • 308.15 K; ▶ 333.15 K; ■ 379.15 K; ◆ 425.65 K.

Johns. et al.[22] : □ 379.15 K; ◇ 425.65 K.

Le Neindre et al.[23] : ⊙ 308.15 K.

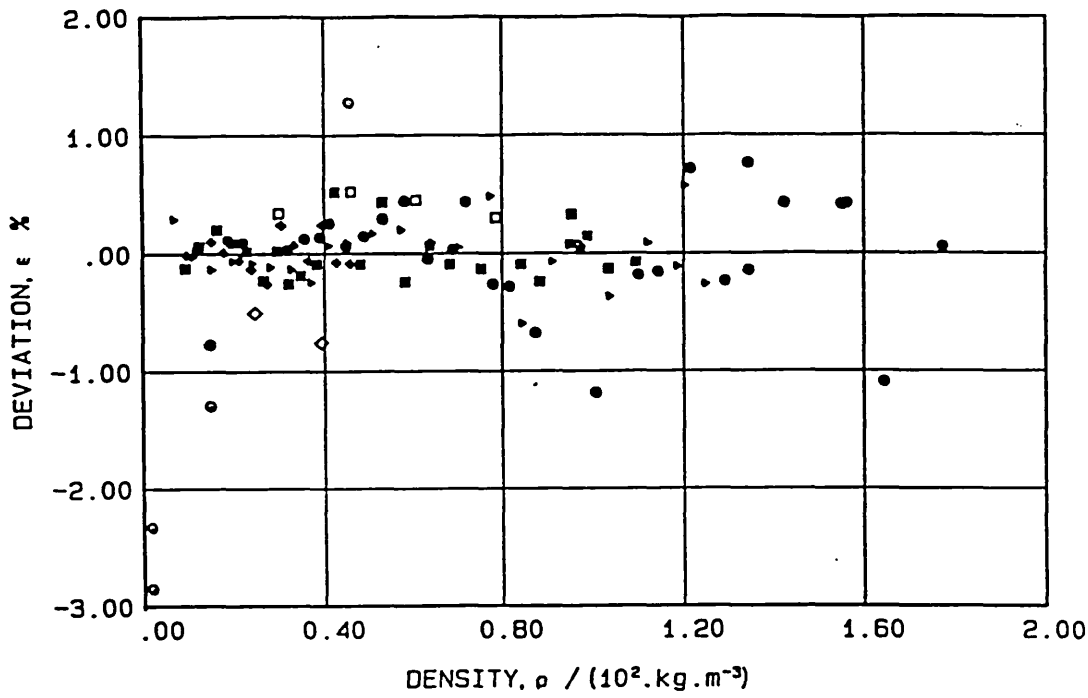

4.2.6 Nitrous Oxide

The nitrous oxide used for these measurements was supplied by the British Oxygen Company plc and had a stated purity of 99.9%. For nitrous oxide, the problem of the thermodynamic properties is more difficult than for carbon dioxide. The measurements were performed close to the critical point, hence a simple interpolation between isotherms is precluded. Furthermore, there is no complete equation of state for this fluid in the open literature. This situation forces the development of an equation of state suitable for the thermodynamic range covered by the thermal conductivity measurements. There are two reasonably extensive series of measurements of the density of nitrous oxide in the gas phase. The first was carried out by Schamp *et al.* [24], over the temperature range 273–423 K for pressures up to 15 MPa, and the second performed by Couch *et al.* [25] in the temperature range 243 to 423 K for pressures up to 31.5 MPa. These two sets of primary data are mutually consistent within their uncertainty but, for the purpose of developing an equation of state, from which only the density is required with good accuracy, then the data set due to Couch has been used alone.

By means of the techniques developed by de Reuck and Armstrong [26] from an idea by Wagner [27], the data may be represented by the following series of equations

$$Z = \frac{P}{\rho RT} = 1 + \omega\left[\frac{\partial \alpha^R}{\partial \omega}\right]_\tau \qquad (4.6.1)$$

where Z is the compression factor,

$$\omega = \frac{\rho}{\rho_c} \qquad (4.6.2)$$

is the reduced density, with ρ_c representing the critical molar density,

$$\tau = \frac{T_c}{T} \tag{4.6.3}$$

is a reduced temperature with T_c representing the critical temperature, and

$$\alpha^R = \frac{A(\omega, \tau) - A^{id}(\omega, \tau)}{RT} \tag{4.6.4}$$

in which A is the Helmholtz free energy of the gas and the superscript 'id' indicates the ideal gas state. The symbol R represents the universal gas constant.

As a result of the fitting procedure it has been found that the following function

$$\begin{aligned} Z = {} & 1 + \omega[a_{11} + a_{12}\tau^{\frac{1}{2}} + a_{13}\tau] + 2\omega^2[a_{21} + a_{22}\tau^{\frac{1}{2}} + a_{23}\tau] \\ & + 3\omega^3 a_{31} + 4\omega^4[a_{41} + a_{43}\tau] + b_{31}\omega^3(3-2\omega^2)\exp(-\omega^2) \end{aligned} \tag{4.6.5}$$

represents the data to within a maximum deviation of 0.3% except very near the critical point. The coefficients of the equation are given in Table 4.2.24, together with the critical constants employed in the reduction. Equation (4.6.5) has been used to calculate all of the density data for nitrous oxide reported here. The equation is not intended as a full equation of state for nitrous oxide and should not be used for the evaluation of all thermodynamic properties or for evaluation outside the range of thermodynamic states within which it has been fitted.

Table 4.2.24

The coefficients of equation (4.6.5) for the density of Nitrous oxide.

		a_{ij}	
j	1	2	3
i			
1	-24.24259831	59.616791902	-44.383007315
2	57.58333831	-144.95796463	91.191728652
3	153.95633731	0	0
4	-62.995286041	0	-35.5208207

$b_{31} = -128.69118722$

$T_c = 309.584$

$\rho_c = 50.2146 \times 10^3 \text{ mol m}^{-3}$

$R = 8.31434 \text{ J mol}^{-1} \text{ K}^{-1}$

The thermal conductivity of nitrous oxide has been measured along four isotherms in the temperature range 300–430 K. The range of pressures over which measurements has been made is restricted by the reported explosive character of the gas at high combined pressure and temperature [24]. The measurements are listed in Tables 4.2.25–4.2.28. The results for nitrous oxide are correlated with a polynomial in density to yield the parameters best representing the data. The optimum prarameters are given in Table 4.1.1 for each isotherm. Figure 4.6 shows the deviations of the present data from the correlations. The present data depart from the correlations by no more than 0.4% at any temperature up to moderate pressures. However, at higher pressures, the deviations increase, for the same reasons described earlier for carbon dioxide, and reflect a loss of precision in this region. The estimated uncertainty for nitrous oxide is similar to that claimed for carbon dioxide although in this case there may also be an error in the density amounting to as much as ± 0.2%.

Figure 4.6 also serves as a reference for comparison with earlier work. The results of Fleeter *et al* [28] at a temperature of 298.65 K are broadly consistent with the present measurements at low pressures, but there is a large systematic increase in the deviation at the highest pressures well beyond the limits of uncertainty. This is almost certainly due to the correction applied to the data, over a range of 7.5°C, being large (~ 3%) and uncertain because of the proximity of the critical density at higher pressures. The results of Richter and Sage [29] deviate markedly (up to 10%) from the present correlation and it must be concluded that these results are that much in error.

Figure 4.6

Deviations, $\epsilon = [(\lambda_{expt} - \lambda_{corr})/\lambda_{corr}] \times 100$, of the thermal conductivity of nitrous oxide from the correlation of the present data by means of eq. 4.1.2.

Present work: • 308.15 K; ■ 337.65 K; ▲ 379.15 K; ◆ 426.15 K.

Fleeter et al.[28] : ⊖ 308.15 K.

Richter and Sage[29]: □ 308.15 K; 337.65 K; △ 379.15 K; ◫ 426.15 K.

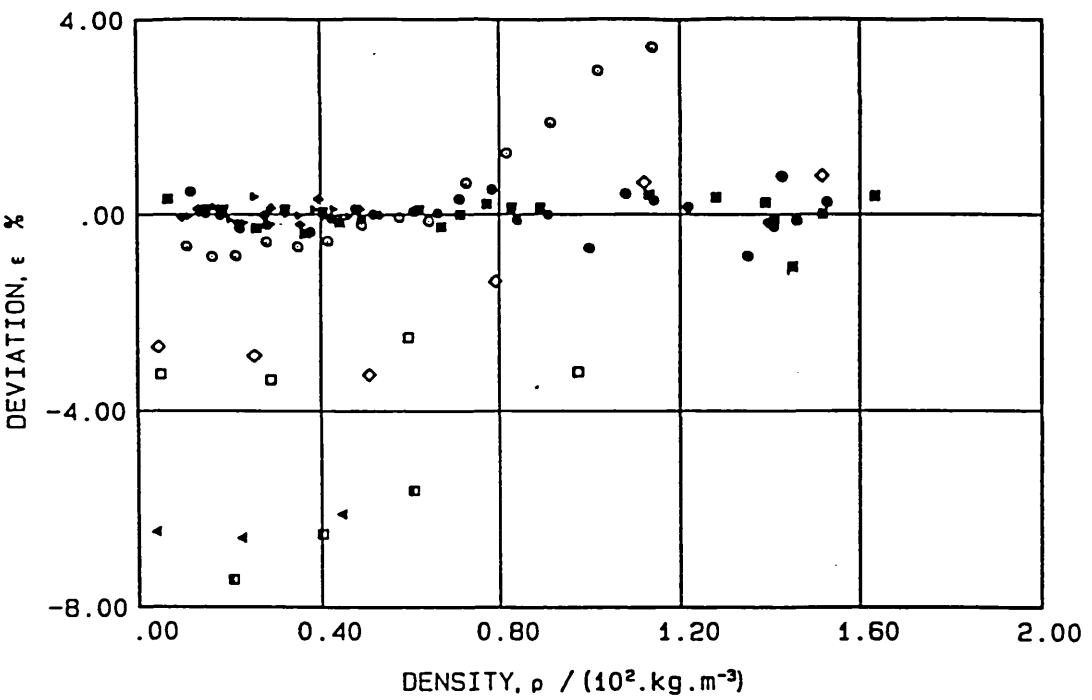

4.2.7 Methane

The methane used for all the measurements reported here was supplied by the British Oxygen Company plc and had a stated purity in excess of 99.995%. The density and heat capacity were obtained from an equation of state developed by Angus *et al.* [30]. The thermal conductivity was measured along four isotherms in the temperature range 300–430 K and at pressures up to 10 MPa. The results are given in Tables 4.2.29–4.2.32 for each temperature. The results have been fitted to a polynomial in density. The coefficients securing the best representation of the data are given in Table 4.1.1. Figure 4.7 shows the deviation of the present data from the correlation. The scatter of the present results show a maximum deviation of about 0.4% and a standard deviation of ± 0.2%. These figures are consistent with a claimed uncertainty for these measurements of ± 0.3% over the entire range.

The same figure also displays the deviations of the results of earlier transient hot–wire results [18, 31, 32]. These show a systematic deviation below the present data along the lowest isotherm by between 1 and 1.5%. Because this exceeds the mutual uncertainty of the measurements the 309 K isotherm for methane was repeated during the course of this work. The repeated measurements confirm the correlation given here to within ± 0.3%. Furthermore, the methane measurements reported here were preceded and followed by measurements on neon and argon respectively. These checks confirmed the correct operation of the instrument. The reason for the discrepancy with respect to earlier work with similar instruments is obscure because although the present series is the first to be performed on methane with the improved cell configuration, the change has had essentially no effect on other gases. The measurements made

Figure 4.7

The deviations of the thermal conductivity data for methane from the correlation of eq. 4.1.2.

Present work: ▶ 308 K; • 337.65 K; ◆ 379.15 K; ■ 425.65 K. Assael and Wakeham[18]: ◇ 308 K. Clifford et al.[32] : □ 300.65 K. Roder[31]: ▼ 310 K. Le Neindre et al.[44] : x 298 K. Tufeu et al.[45] : + 298 K. Misic and Thodos[46]: ▫ 297.7 K; ▪ 316.7 K.

$$\epsilon = [(\lambda_{expt} - \lambda_{corr})\lambda_{corr}] \times 100$$

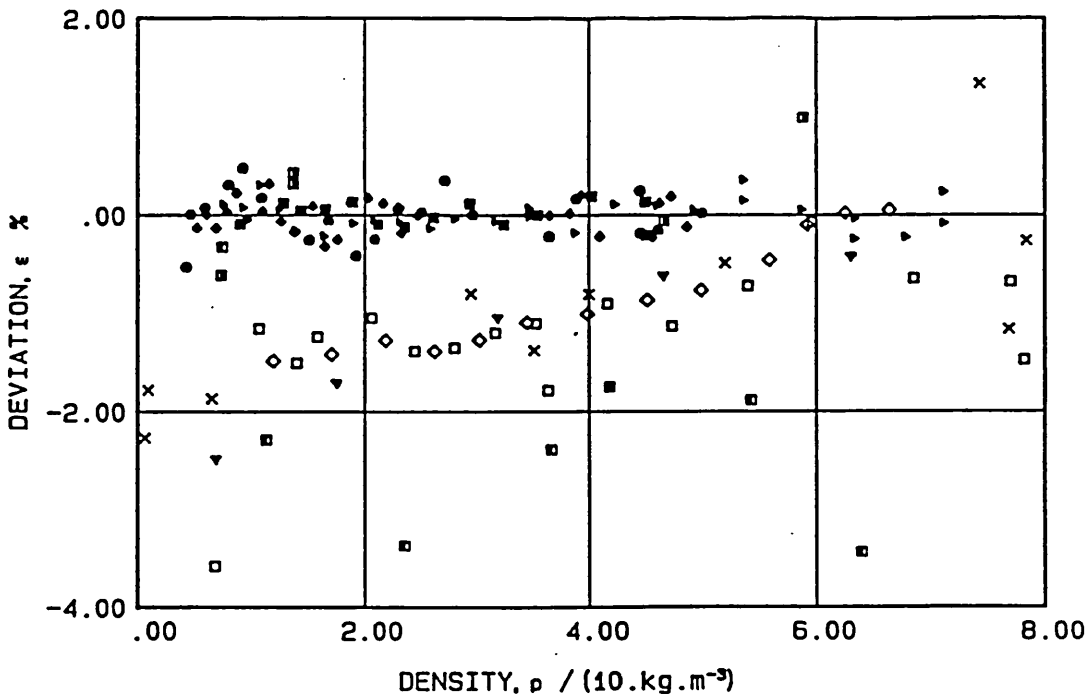

by other techniques [44,45] lie even further from the present correlation and generally display a far greater scatter.

4.2.8 Tetrafluoromethane

The gas used for the measurements on tetrafluoromethane was supplied by the British Oxygen Company plc and had a stated purity in excess of 99.7%. For the density and heat capacity, the results of Douslin *et al.* [33] have been employed. The thermal conductivity of tetrafluoromethane has been measured in the temperature range 300–430 K and at pressures up to 10 MPa. the results of these measurements are given in Tables 4.2.33–4.2.36 for each isotherm. The results were then fitted to a polynomial in density. The coefficients securing the best fit to the experimental data along each isotherm are given in Table 4.1.1.

Figure 4.8 shows the deviations of the present data from the correlations and reveals a maximum deviation of 0.4% and a standard deviation of ± 0.2%. These figures are consistent with a claimed uncertainty of 0.3% over the entire thermodynamic range. The figure also shows the two sets of results obtained by the same technique at 300.65 K by Kestin *et al.* [34]. These results depart from the correlation by up to 1.2% but this is approximately the same as the scatter in their data for this gas. Earlier measurements by Oshen *et al.* [35] and Lambert *et al.* [36] lie systematically below the present data.

4.2.9 Ethane

The samples of ethane used for the present measurements were supplied by Argo International with a stated purity of 99.99%. The measurements on ethane extend from 308 to 425 K and at pressures up to 10 MPa. For reduction of the data the density and heat capacity

Figure 4.8

The deviations of the thermal conductivity data for tetrafluoromethane from the correlation of eq. 4.1.2.

Present work: ▶ 309 K; • 331.65 K; ◆ 371.15 K; ■ 425.65 K. Imaishi *et al.*[34] : □, ◇ 300.65 K. Lambert *et al.*[36] : + 339 K. Oshen *et al.*[35] : x 296.9 K; ▼ 314.8 K.

$$\epsilon = [(\lambda_{expt} - \lambda_{corr})/\lambda_{corr}] \times 100$$

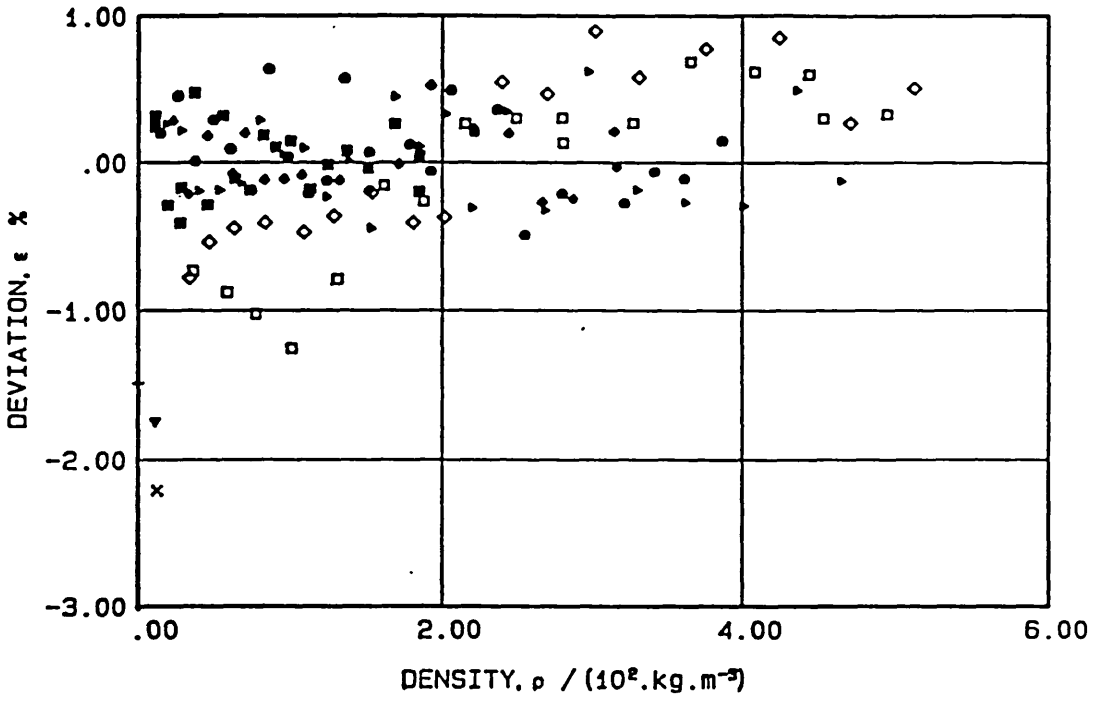

were obtained from an equation of state developed by Bender [37]. It is important to note that there was no evidence of systematic departures of the behaviour of the instrument from the theoretical model for it. However, at the lowest temperatures and the highest pressures, near the critical point, it was more difficult to retain high precision owing principally to the high compressibility of the gas. For this reason, it is estimated that the uncertainty in the thermal conductivity is ± 0.3% at moderate pressures for all temperatures, while at the lowest temperature and highest pressure the uncertainty may be as much as ± 2%.

Tables 4.2.37–4.2.40 list the thermal conductivity for ethane along the four isotherms. Each of these isotherms were fitted to a polymomial in density. The coefficients best representing the data for each isotherm are given in Table 4.1.1. It is useful to note at this stage that the higher–order coefficients for ethane are larger than the corresponding coefficients for argon. Although the coefficients derived by simple regression have no physical significance, this observation does indicate that the determination of lower–order coefficients by statistical analysis of the data is significantly more difficult for hydrocarbons than for argon.

Figure 4.9 shows the deviations of the present data from the correlation and, in addition, features a selection of earlier measurements. The present data departs by no more than 0.6% from the correlation and the standard deviation is one of ± 0.3%. These figures are consistent with the estimated uncertainty in the thermal conductivity. The comparison of the present correlations with earlier results is somewhat difficult for ethane, particularly at the lowest temperature and at elevated pressures, because of the proximity of the critical point. This means that the temperature

Figure 4.9

Deviations of measurements of the thermal conductivity of ethane from the present correlation.

$\epsilon = [(\lambda_{expt} - \lambda_{corr})/\lambda_{corr}] \times 100\%$.

This work: ▲ 308.15 K; ■ 331.65 K; ◆ 380.15 K; ● 425.65 K.

Roder [38]: Δ 305 K; ▽ 312 K. Tufeu *et al.* [39]: X 312 K.

Lenoir *et al.* [40]: ⊡ 329.8 K; ◇ 315 K.

Fleeter *et al.* [28]: + 300.6 K.

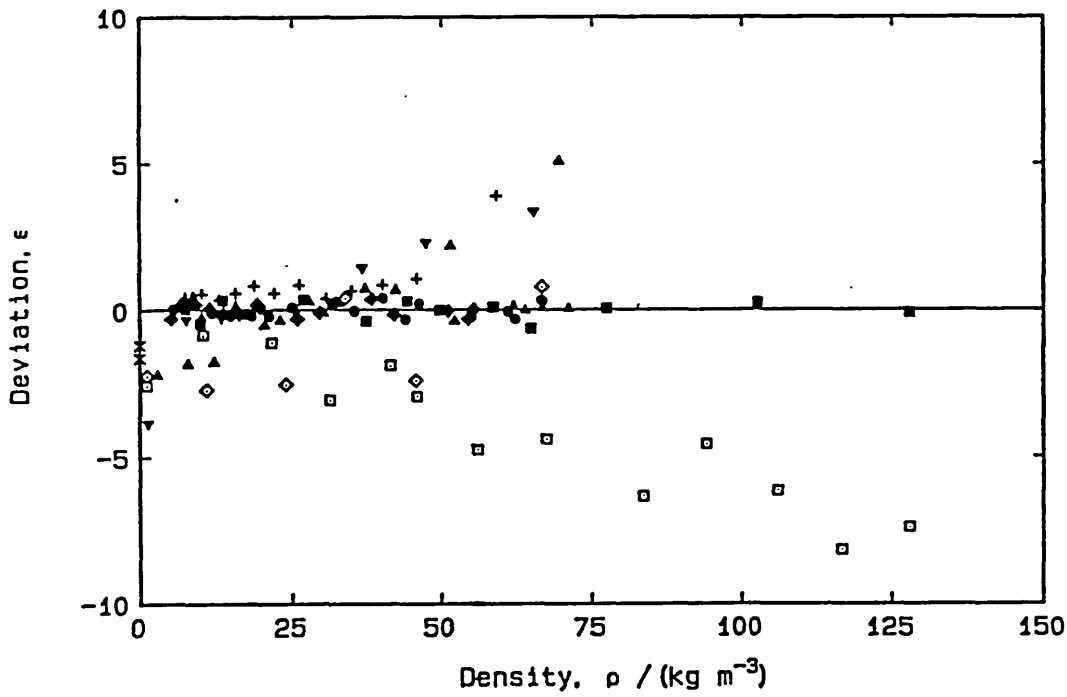

derivative of thermal conductivity is strongly temperature- and density-dependent. Furthermore, there is no representative equation for $\lambda(\rho, T)$ which is as accurate as the present measurements [38]. For these reasons, the comparisons found in Figure 4.9 are somewhat crude because estimates of $(d\lambda/dT)_{\rho = 0}$ have been used to adjust data of other workers from their experimental temperatures to those employed here. In some cases, the temperature correction amounts to a 10% change in the reported thermal conductivity and cannot be made with any certainty.

For ethane, Fleeter *et al.* [28] and Roder [20, 38] have used the transient hot-wire technique and obtained results at 300.65 K, and 305 K and 312 K respectively. At the low density where the temperature correction is most accurate, the agreement with the results of Fleeter *et al.* [28] is good and within the mutual uncertainty of the two sets. At higher densities, the discrepancies are larger and positive, probably as a result of an inadequate temperature correction. Similar comments apply to the results of Roder [20, 38] although these deviations are somewhat larger. The measurements of Tufeu *et al.* [39] in the limit of zero density lie about 1.5% below the present results which may be interpreted as satisfactory agreement. Finally, the results of Lenoir *et al.* [40] fall up to 8% below the present correlation, almost certainly because of undetected errors in the earlier measurements.

4.2.10 Ethylene

The ethylene used for the measurements reported here was supplied by the British Oxygen Company plc and had a stated purity of 99.92%. As for ethane, the density and heat capacity required for the reduction of the data were obtained from the equation of state

developed by Bender [41]. This equation proved indistinguishable from a more recent equation in the temperature and pressure range of interest. The conditions for measurement of ethylene were similar to those of ethane, the fluid being near the critical point. No sign of degradation of the ethylene samples was observed as has been reported elsewhere [42]. The uncertainty ascribed to these measurements is similar to that ascribed to ethane.

The results for ethylene are listed in Tables 4.2.41–4.2.44 for each isotherm. Measurements were made in the range 300–430 K and at pressures up to 10 MPa. These data were also fitted to polynomials in density and the coefficients securing the optimum representation of the data are given in Table 4.1.1. The same observations about the magnitude of successive coefficients were made for ethylene as for ethane.

Figure 4.10 shows the deviation of the present data from the correlation for each isotherm and the deviations of older data from the same correlations. The departure of the present data is never more than about 0.6% and the standard deviation is ± 0.3%. These figures are consistent with the claimed uncertainty. As noted for ethane, comparison with earlier work can ony be crude. The measurements of Prasad and Venart [42] (the most recent and extensive for ethylene) are significantly higher at all densities than those reported here. The deviations increase to as much as 20% at the highest densities but even at low densities, where the correction from one isotherm to another is most secure, the deviations are of order 3%. The earlier results of Lenoir and Commings [43] are, in contrast, significantly lower than the present data at both 308 K and 333 K by as much as 5%. In view of the higher accuracy of the present data they are to be preferred in their range of thermodynamic

Figure 4.10

Deviations of measurements of the thermal conductivity of ethylene from the present correlation.

$\epsilon = [(\lambda_{expt} - \lambda_{corr})/\lambda_{corr}] \times 100\%$.

This work: ▲ 308.15 K; ■ 333.15 K; ♦ 371.15 K; • 425.65 K.

Lenoir and Comings [43]: + 314.2 K; x 340.3 K.

Prasad and Venart [42]: ⊡ 299 K.

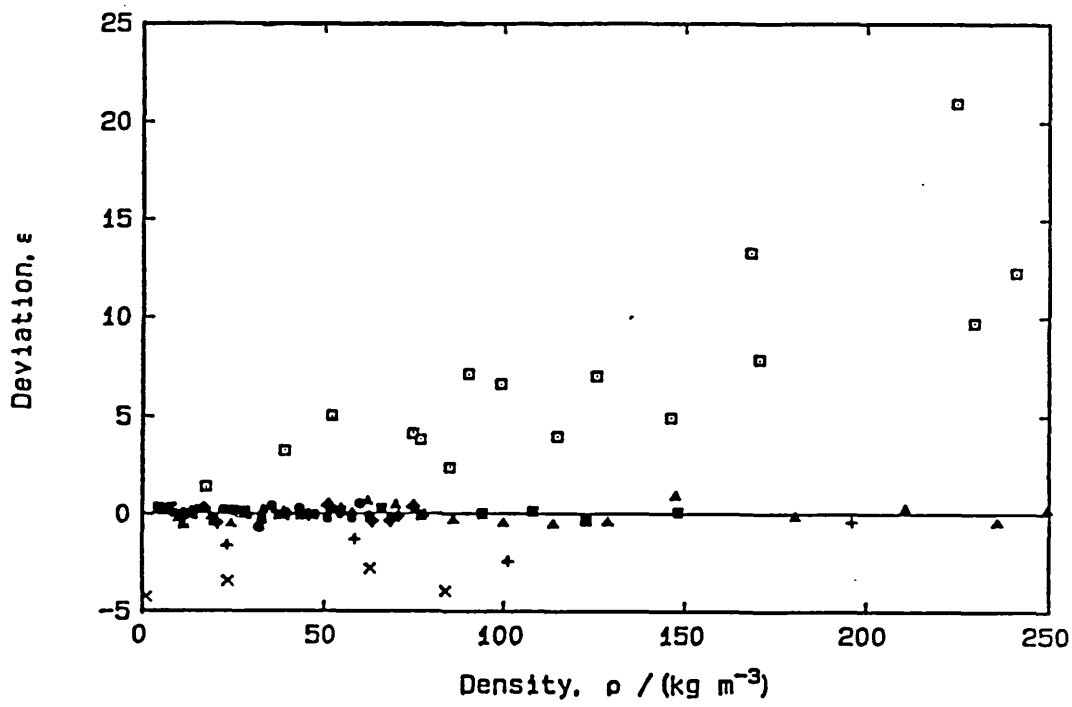

states, although they do not encompass the critical region.

4.11 Nitrogen

The nitrogen used for these measurements was supplied by Cambrian gases and had a stated purity in excess of 99.998 %. The density and heat capacity have been obtained from the equation of state developed by Angus et al [47]. The results for nitrogen are listed in tables 4.4.45 – 4.4.47 at each temperature. The data are fitted to a polynomial in density, the optimum correlating parameters are given in table 4.1.1. The maximum deviation is 0.9 % whilst the standard deviation is ± 0.2 %. These figures are comensurate with an estimated uncertainty of ± 0.3 %, under most conditions, deteriorating to perhaps ± 2 % at the lowest temperature and highest pressures. The deviations of the data from the present correlation are shown in figure 4.11 These new results are believed to be the only reliable low temperature nitrogen data available.

Figure 4.11

The deviations of the thermal conductivity for nitrogen from the correlation of eqn. 4.1.2.

▲ 177.50 K ■ 225.15 K ◆ 270.15 K

$$\varepsilon = ((\lambda_{EXP} - \lambda_{CORR})/\lambda_{CORR}) \times 100\ \%$$

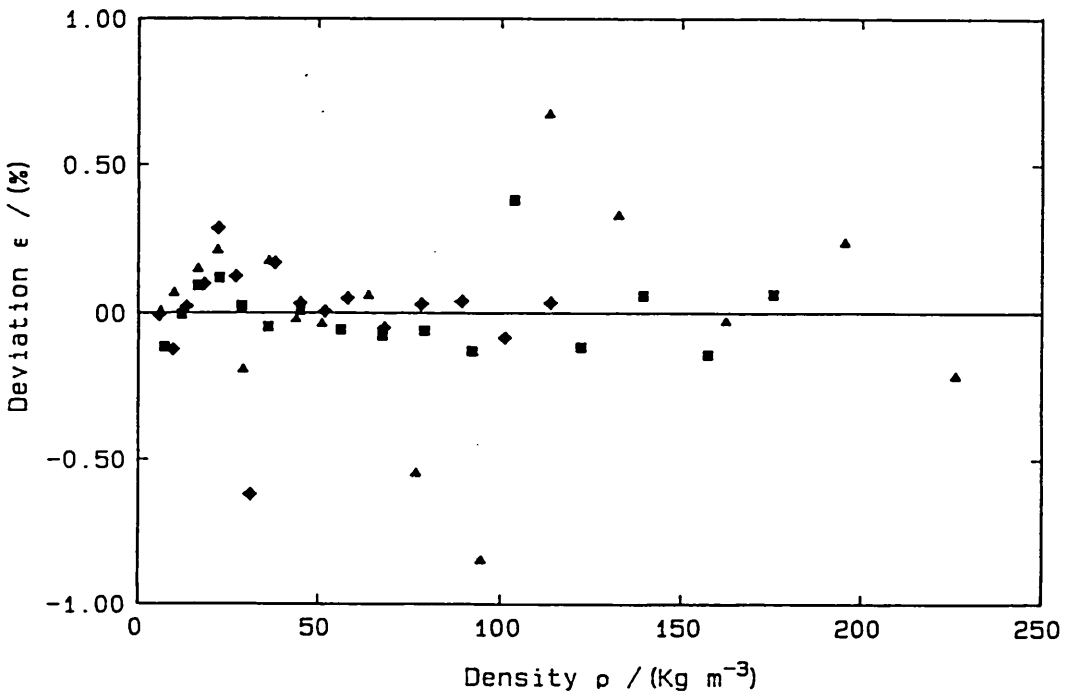

Rerences

[1] A. Michels, J.M. Levelt and W. de Graaff, Physica 24, 659 (1958).

[2] R.B. Stewart, R.T. Jacobsen, J.H. Becker, J.C.J. Teng and P.K.K. Mui, Paper presented at the Eighth Symposium on Thermophysical Properties, NBS, Gaithersburg (June 1981).

[3] E.N. Haran, G.C. Maitland, M. Mustafa and W.A. Wakeham, Ber. Bunsenges. Phys. Chem. 87, 657 (1983).

[4] U.V. Mardolcar, C.A.N. de Castro and W.A. Wakeham, Int. J. Thermophys. 7, 2, 259 (1986).

[5] C.A.N. de Castro (private communication).

[6] J.J. Healy, J.J. de Groot and J. Kestin, Physica 82C, 392 (1976).

[7] A. Michels and H. Wouters, Physica's Grav. 8, 923 (1941).

[8] A. Michels and H. Groudeket, Physica's Grav. 8, 347 (1941).

[9] M.J. Assael, M. Dix, A. Lucas and W.A. Wakeham, J. Chem. Soc. Faraday Trans. I 77, 439 (1981).

[10] J. Kestin, R. Paul, A.A. Clifford and W.A. Wakeham, Physica 100A, 349 (1980).

[11] B. Le Neindre, P. Bury, R. Tufeu, P. Johannin and B. Vodar, Nat. Bur. Stand. (U.S.) Spec. Publ. 302, 579 (1968).

[12] H.M. Roder, J. Res. Nat. Bur. Stand. 86, 457 (1981).

[13] B.J. Jody, P.C. Jain and S.C. Saxena, Trans. ASME, J. Heat Trans. 76-HT-C (1976).

[14] A. Michels, T. Wassenaar and P. Louwerse, Physica 26, 539 (1960).

[15] J.V. Sengers, W.T. Bolk and C.J. Stigter, Physica 30, 1018 (1964).

[16] R. Tufeu, PhD Thesis, University of Paris IV (1971).

[17] A.A. Clifford, J. Kestin and W.A. Wakeham, Ber. Bunsenges. Phys. Chem. 84, 9 (1980).

[18] M.J. Assael and W.A. Wakeham, J. Chem. Soc. Faraday Trans. I 77, 697 (1981).

[19] A.A. Clifford, P. Gray, A.I. Johns, A.C. Scott and J.T.R. Watson, J. Chem. Soc. Faraday Trans. I 77, 2679 (1981).

[20] H.M. Roder, NBS 112 84–3006 (1984).

[21] E. Bender, Proc. 5th Symp. on Thermophys. Props. (ASME, New York) 227 (1970).

[22] A.I. Johns, S. Rashid, J.T.R. Watson and A.A. Clifford, J. Chem. Soc. Faraday Trans. I 82, 2235 (1986); A.C. Scott, A.I. Johns, J.T.R. Watson and A.A. Clifford, J. Chem. Soc. Faraday Trans. I 79, 733 (1983).

[23] B. Le Neindre, R. Tufeu, P. Bury and J.V. Sengers, Ber. Bunsenges. Phys. Chem. 77, 262 (1973).

[24] H.W. Schamp, E.A. Mason and K. Su, Phys. Fluids 5, 769 (1962).

[25] E.J. Couch, L.J. Hirth and K.A. Kobe, J. Chem. Engng. Data 6, 229 (1961).

[26] K.M. de Reuck and B. Armstrong, Cryogenics 19, 509 (1979).

[27] W. Wagner, Fortsh.–Ber. VDI–Z Reihe 3 39 (1974).

[28] R. Fleeter, J. Kestin and W.A. Wakeham, Physica 103A, 521 (1980).

[29] G.N. Richter and B.H. Sage, J. Chem. Engng. Data 13, 221 (1963).

[30] S. Angus, B. Armstrong and K.M. de Reuck, International Tables of the Fluid State – 5: Methane (Pergamon, Oxford) (1978).

[31] H.M. Roder, Int. J. Thermophys. 6. 119 (1985).

[32] A.A. Clifford, J. Kestin and W.A. Wakeham, Physica 97A, 287 (1979).

[33] D.R. Douslin, R.H. Harrison, R.T. More and J.P. McCullough, J. Chem. Phys. 35, 1357 (1961).

[34] N. Imaishi, J. Kestin and R. Paul, Int. J. Thermophys. 6, 3 (1985).

[35] S. Oshen, B.M. Rosenbaum and G. Thodos, J. Chem. Phys. 46, 2939 (1967).

[36] J.D. Lambert, K.J. Cotton, M.W. Pailthorpe, A.M. Robinson, J. Scrivens, W.R.F. Vale and R.M. Young, Proc. Roy. Soc. Lond. A231, 280 (1955).

[37] E. Bender, Cryogenics 21, 157 (1981).

[38] H.M. Roder and C.A. Nieto de Castro, High Temp.-High Press. 17, 447 (1985).

[39] R. Tufeu, Y. Garrabos and B. Le Neindre, Thermal Conductivity 16, 605 (1980).

[40] J.M. Lenoir, W.A. Jonk and E.W. Comings, Chem. Eng. Prog. 49, 539 (1953).

[41] E. Bender, Cryogenics 7, 591 (1977).

[42] R.C. Prasad and J.E.S. Venart, Proc. 8th Symposium on Thermophysical Properties, Vol. I.

[43] J.M. Lenoir and E.W. Comings, Chem. Eng. Prog. 47, 2 (1951).

[44] B. Le Neindre, P. Bury, R. Tufeu, P. Johanin and B. Vodar, Proc. 7^{th} conf. on Thermal Conductivity, (N.B.S., Washington U.S.A.) 579 (1976).

[45] R. Tufeu, B. Le Neindre and P. Bury, Physica, 44, 81 (1969)

[46] D. Misc and G. Thodos, Physica 32, 885 (1960)

[47] S. Angus, B. Armstrong and K.M. de Reuck, International Thermodynamics of the Fluid State – 6: Nitrogen (Pergamon press Oxford) (1979).

Table 4.1.1

Coefficients used in the correlation of the thermal conductivity data

T (K)	C_0 $mWm^{-1}K^{-1}$	C_1 $\mu Wm^{2}Kg^{-1}K^{-1}$	C_2 $nWm^{5}Kg^{-2}K^{-1}$	C_3 $pWm^{8}Kg^{-3}K^{-1}$
Argon				
174	11.01	21.7	36.8	29
223.15	13.73	24.0	13.9	32
266.65	16.06	26.6	-20.0	14.6
308.15	18.13	25.0	4.0	——
333.15	19.49	22.3	27.0	——
378.15	21.66	22.0	25.0	——
428.15	23.94	19.0	40.0	——
Helium				
308.15	159.6	257	——	——
338.15	170.2	304	——	——
379.65	183.6	211	——	——
428.15	201.9	255	——	——
Neon				
308.15	49.97	54.79	——	——
337.65	53.55	42.15	——	——
379.65	57.37	75.80	-515.8	——
428.15	63.05	43.95	——	——

cont.

T (K)	C_0 $mWm^{-1}K^{-1}$	C_1 $\mu Wm^2Kg^{-1}K^{-1}$	C_2 $nWm^5Kg^{-2}K^{-1}$	C_3 $pWm^8Kg^{-3}K^{-1}$
Hydrogen				
308.15	193.7	893	—	—
337.65	209.0	813	—	—
379.65	226.7	724	—	—
428.15	245.3	1278	—	—
Carbon Dioxide				
308.15	17.57	15.0	290.0	-80.0
333.15	19.55	22.0	150.0	-300.0
379.15	23.32	13.0	300.0	-900.0
425.65	27.56	4.0	500.0	—
Nitrous Oxide				
308.15	18.16	29.0	148.0	—
337.65	20.59	26.0	138.0	—
379.15	24.89	43.0	-1100.0	16000
426.15	29.64	25.9	1240.0	-9680
Methane				
309.15	35.97	92.43	607.9	—
337.65	40.77	98.45	425.2	—
379.15	47.38	109.8	-1151	27510
425.65	57.00	16.23	2432.5	-15091

cont.

T (K)	C_0 $mWm^{-1}K^{-1}$	C_1 $\mu Wm^{2}Kg^{-1}K^{-1}$	C_2 $nWm^{5}Kg^{-2}K^{-1}$	C_3 $pWm^{8}Kg^{-3}K^{-1}$
Tetrafluoromethane				
308.15	16.74	11.49	31.69	-15.10
331.65	18.67	10.03	45.78	-38.41
371.15	21.74	12.18	31.67	——
425.65	26.16	12.41	43.61	——
Ethane				
308.15	22.87	58.4	418.0	2618.0
331.15	26.27	36.2	1095	-2305
380.15	34.18	16.8	1937	-15310
425.65	42.23	-0.99	2075	-14801
Ethylene				
308.15	22.61	19.3	1162	-2478
333.15	25.67	46.8	749	-1507
371.15	31.76	21.42	685	2438
425.65	41.82	-7.52	1213	-3765
Nirtogen				
177.50				
225.16				
270.15				

Table 4.2.1

The thermal conductivity of Argon at T_{nom} = 174 K.

Pressure	Ref. Temp.	Density at Ref. Temp.	Thermal conductivity $\lambda(T_r,\rho_r)$	$\lambda(T_{nom},\rho_r)$
P/MPa	T_r/K	$\rho_r(T_r,P)$/Kgm^{-3}	mWm^{-1}K^{-1}	mWm^{-1}K^{-1}
0.36	174.77	9.956	11.25	11.20
0.57	174.70	16.09	11.43	11.38
0.77	174.90	21.91	11.56	11.51
1.02	174.86	29.32	11.73	11.68
1.23	174.65	35.90	11.88	11.84
1.43	174.63	42.15	12.04	12.00
1.67	174.65	49.64	12.25	12.49
2.01	174.62	61.02	12.54	12.49
2.33	174.51	71.94	12.81	12.78
2.86	174.32	91.25	13.34	13.32
3.58	174.32	119.4	14.25	14.23
4.29	174.31	150.3	15.27	15.26
5.36	174.34	204.4	17.32	17.00
6.42	174.42	269.5	20.32	20.30
7.26	174.47	331.4	23.27	23.24

Table 4.2.2

The thermal conductivity of Argon at T_{nom} = 223.15 K.

Pressure P/MPa	Ref. Temp. T_r/K	Density at Ref. Temp. $\rho_r(T_r, P)$/Kgm^{-3}	Thermal conductivity $\lambda(T_r, \rho_r)$ mWm^{-1}K^{-1}	$\lambda(T_{nom}, \rho_r)$ mWm^{-1}K^{-1}
0.38	222.45	8.359	13.89	13.93
0.61	222.36	13.38	14.05	14.10
0.94	222.39	20.76	14.27	14.31
1.32	222.46	29.33	14.48	14.52
1.76	222.28	39.52	14.72	14.76
2.14	222.34	48.22	14.93	14.96
2.85	222.29	65.42	15.36	15.39
4.24	222.34	100.1	16.31	16.36
5.10	222.38	122.65	16.95	16.97
6.05	222.23	148.7	17.71	17.76
7.04	222.27	176.6	18.52	18.57
7.82	222.26	199.3	19.36	19.41
8.82	222.25	229.2	20.38	20.43
9.68	222.91	254.0	21.24	21.26
9.68	222.81	253.9	21.30	21.31

Table 4.2.3

The thermal conductivity of Argon at T_{nom} = 266.65 K.

Pressure	Ref. Temp.	Density at Ref. Temp.	Thermal conductivity	
P/MPa	T_r/K	$\rho_r(T_r, P)$/Kgm^{-3}	$\lambda(T_r, \rho_r)$ mWm^{-1}K^{-1}	$\lambda(T_{nom}, \rho_r)$ mWm^{-1}K^{-1}
0.51	266.89	9.195	16.29	16.28
0.97	266.94	17.63	16.55	16.54
1.47	266.30	26.98	16.76	16.78
2.14	266.33	39.36	17.07	17.08
2.83	266.33	52.56	17.44	17.45
3.53	266.34	65.92	17.78	17.79
4.24	266.28	79.74	18.09	18.11
4.93	266.28	93.18	18.41	18.41
5.66	266.59	107.7	18.86	18.86
6.39	266.59	122.4	19.31	19.32
7.07	266.64	136.2	19.67	19.68
8.04	266.66	155.9	20.28	20.28
8.45	266.68	164.4	20.55	20.55
9.34	266.84	182.7	21.13	21.12

Table 4.2.4

The thermal conductivity of Argon at T_{nom} = 308.15 K.

Pressure	Ref. Temp.	Density at Ref. Temp.	Thermal conductivity	
P/MPa	$T_r/^oC$	$\rho_r(T_r, P)/Kgm^{-3}$	$\lambda(T_r,\rho_r)$ $mWm^{-1}K^{-1}$	$\lambda(T_{nom},\rho_r)$ $mWm^{-1}K^{-1}$
0.58	36.12	8.990	18.54	18.42
0.79	36.06	12.34	18.56	18.44
1.11	36.15	17.31	18.69	18.56
1.35	35.80	21.13	18.74	18.65
1.41	36.15	22.08	18.79	18.67
1.65	35.94	25.80	18.90	18.80
1.93	35.58	30.30	18.96	18.90
2.51	35.55	39.63	19.22	19.16
2.86	35.43	45.15	19.36	19.34
3.27	35.23	51.82	19.45	19.44
3.64	35.37	57.78	19.68	19.66
3.64	35.91	57.67	19.61	19.57
4.27	35.25	67.82	19.90	19.88
4.60	35.41	73.25	20.05	20.03
4.96	35.68	78.88	20.18	20.15
5.71	35.62	91.13	20.48	20.45
6.31	36.55	100.6	20.83	20.75

Table 4.2.5

The thermal conductivity of Argon at T_{nom} = 333.15 K.

Pressure P/MPa	Ref. Temp. $T_r/^oC$	Density at Ref. Temp. $\rho_r(T_r, P)/Kgm^{-3}$	Thermal conductivity $\lambda(T_r, \rho_r)$ $mWm^{-1}K^{-1}$	$\lambda(T_{nom}, \rho_r)$ $mWm^{-1}K^{-1}$
0.87	59.01	12.66	19.76	19.80
1.16	59.22	16.77	19.78	19.82
1.56	58.97	22.72	19.90	19.95
2.02	58.87	29.48	20.12	20.18
2.57	59.04	37.45	20.36	20.41
3.16	59.14	46.05	20.55	20.59
3.89	59.05	56.84	20.80	20.84
4.42	59.05	64.79	21.00	21.05
5.16	58.98	75.63	21.25	21.30
5.76	58.92	84.66	21.50	21.55
6.44	58.86	94.72	21.78	21.84
7.04	59.01	103.6	22.00	22.06
7.66	59.01	112.8	22.34	22.39
8.24	59.00	121.5	22.50	22.55
9.24	58.92	136.4	22.95	23.00
9.96	58.94	147.2	23.32	23.38
9.96	58.18	147.6	23.27	23.36

Table 4.2.6

The thermal conductivity of Argon at T_{nom} = 378.15 K.

Pressure	Ref. Temp.	Density at Ref. Temp.	Thermal conductivity	
P/MPa	$T_r/^oC$	$\rho_r(T_r, P)/Kgm^{-3}$	$\lambda(T_r,\rho_r)$ $mWm^{-1}K^{-1}$	$\lambda(T_{nom},\rho_r)$ $mWm^{-1}K^{-1}$
1.13	104.84	14.42	21.94	21.95
1.44	105.00	18.39	22.07	22.08
1.92	104.95	24.48	22.22	22.22
2.58	104.57	33.09	22.38	22.40
3.27	104.71	41.84	22.60	22.61
3.99	104.66	51.16	22.84	22.86
4.61	104.54	59.16	23.05	23.07
5.26	104 69	67.49	23.24	23.26
6.06	104.63	77.89	23.51	23.53
6.80	104.50	87.34	23.76	23.78
7.46	104.81	95.88	23.93	23.94
8.07	104.95	103.7	24.18	24.18
9.04	104.95	116.1	24.53	24.53
9.97	104.68	128.1	24.86	24.87
10.95	104.56	140.6	25.23	25.26

Table 4.2.7

The thermal conductivity of Argon at T_{nom} = 428.15 K.

Pressure P/MPa	Ref. Temp. $T_r/^oC$	Density at Ref. Temp. $\rho_r(T_r,P)/Kgm^{-3}$	Thermal conductivity $\lambda(T_r,\rho_r)$ $mWm^{-1}K^{-1}$	$\lambda(T_{nom},\rho_r)$ $mWm^{-1}K^{-1}$
1.11	154.48	12.88	24.20	24.22
1.45	154.23	16.91	24.25	24.28
1.82	154.19	21.27	24.24	24.28
2.20	154.17	25.64	24.45	24.49
2.56	154.38	29.86	24.52	24.54
2.85	154.54	33.35	24.58	24.60
3.21	154.27	37.59	24.62	24.65
3.51	154.26	41.19	24.75	24.78
3.86	154.28	45.28	24.89	24.92
4.17	154.49	48.96	25.00	25.02
4.55	154.53	53.49	25.15	25.17
4.91	154.27	57.87	25.14	25.17
5.26	154.58	61.99	25.33	25.35
5.59	154.48	65.98	25.30	25.32
5.98	154.93	70.63	25.37	25.40
6.38	154.40	75.47	25.61	25.63
6.62	154.49	78.47	25.59	25.61
6.99	154.32	82.91	25.70	25.73
7.32	154.52	86.92	25.79	25.81
7.71	154.50	91.72	25.98	26.00
8.08	154.47	96.18	26.06	26.08
8.43	154.49	100.5	26.23	26.28
8.84	153.93	105.5	26.36	26.41
9.15	153.96	109.3	26.43	26.48
9.22	153.79	110.2	26.43	26.48
10.05	153.92	120.4	26.79	26.84

Table 4.2.8

The thermal conductivity of Helium at T_{nom} = 308.15 K.

Pressure P/MPa	Ref. Temp. $T_r/^oC$	Density at Ref. Temp. $\rho_r(T_r, P)/Kgm^{-3}$	Thermal conductivity $\lambda(T_r, \rho_r)$ $mWm^{-1}K^{-1}$	$\lambda(T_{nom}, \rho_r)$ $mWm^{-1}K^{-1}$
2.90	34.96	4.475	161.7	161.7
3.45	35.04	5.311	161.2	161.2
3.88	35.16	5.955	160.8	160.8
4.32	35.18	6.619	160.9	160.8
4.84	35.06	7.397	161.2	161.2
5.38	35.09	8.210	161.7	161.6
5.85	35.08	8.907	161.9	161.8
6.40	35.16	9.721	161.9	161.9
7.66	35.06	11.57	162.4	162.4
8.19	35.13	12.34	162.8	162.8
8.63	35.12	12.98	162.9	162.9
9.15	35.09	13.73	163.0	163.0
10.22	35.32	15.25	164.2	164.1

Table 4.2.9

The thermal conductivity of Helium at T_{nom} = 338.15 K.

Pressure	Ref. Temp.	Density at Ref. Temp.	Thermal conductivity	
P/MPa	$T_r/^oC$	$\rho_r(T_r, P)/Kgm^{-3}$	$\lambda(T_r,\rho_r)$ $mWm^{-1}K^{-1}$	$\lambda(T_{nom},\rho_r)$ $mWm^{-1}K^{-1}$
3.03	65.01	4.264	172.2	172.2
3.45	64.96	4.847	172.3	172.3
3.82	65.12	5.359	171.6	171.5
4.60	64.89	6.435	172.0	172.1
4.93	64.86	6.882	172.2	172.3
5.68	64.86	7.906	172.6	172.6
6.43	64.86	8.928	172.7	172.7
7.12	64.93	9.863	173.2	173.2
7.77	64.79	10.74	173.6	173.6
8.53	64.85	11.74	173.4	173.5
9.27	64.79	12.73	174.6	174.7
9.98	64.99	13.66	174.1	174.1
10.67	65.04	14.56	174.9	174.9
10.68	65.04	14.58	174.9	174.9

Table 4.2.10

The thermal conductivity of Helium at T_{nom} = 379.65 K.

Pressure	Ref. Temp.	Density at Ref. Temp.	Thermal conductivity	
P/MPa	$T_r/^oC$	$\rho_r(T_r, P)/Kgm^{-3}$	$\lambda(T_r,\rho_r)$ $mWm^{-1}K^{-1}$	$\lambda(T_{nom},\rho_r)$ $mWm^{-1}K^{-1}$
2.92	106.39	3.682	185.3	185.3
3.11	106.59	3.921	184.3	184.3
3.24	106.64	4.075	184.1	184.1
3.46	106.48	4.351	184.9	184.9
3.72	106.65	4.674	184.3	184.3
4.44	106.45	5.563	184.3	184.3
4.67	106.49	5.843	184.6	184.6
4.91	106.51	6.139	184.8	184.8
5.17	106.55	6.461	184.8	184.8
5.46	106.40	6.818	184.3	184.3
5.77	106.33	7.199	185.3	185.3
6.12	106.40	7.627	184.7	184.8
6.40	106.51	7.961	185.2	185.2
6.82	106.53	8.471	184.8	184.8
7.13	106.46	8.848	185.2	185.2
7.49	106.32	9.285	185.9	186.0
8.19	106.41	10.13	186.1	186.2
8.82	106.29	10.88	185.9	185.9
9.17	106.32	11.31	186.1	186.2
9.70	106.33	11.93	186.4	186.4

Table 4.2.11

The thermal conductivity of Helium at T_{nom} = 428.15 K.

Pressure	Ref. Temp.	Density at Ref. Temp.	Thermal conductivity	
P/MPa	$T_r/^oC$	$\rho_r(T_r, P)/Kgm^{-3}$	$\lambda(T_r, \rho_r)$ $mWm^{-1}K^{-1}$	$\lambda(T_{nom}, \rho_r)$ $mWm^{-1}K^{-1}$
3.49	152.29	4.013	201.9	202.6
3.85	152.33	4.420	202.6	203.4
4.23	152.33	4.849	202.3	203.0
4.65	152.37	5.323	203.0	203.8
5.05	152.30	5.766	202.0	202.7
5.45	152.49	6.081	202.0	202.7
5.82	152.56	6.628	202.8	203.5
6.23	152.63	7.081	202.6	203.3
6.59	152.65	7.488	203.6	204.2
6.96	152.67	7.893	204.1	204.7
7.33	152.27	8.309	203.0	203.8
7.67	152.24	8.638	203.2	203.9
8.08	152.29	9.130	203.5	204.2
8.44	152.41	9.522	204.4	205.1
8.89	152.45	10.01	203.6	204.4
9.36	152.45	10.53	203.9	204.6
9.88	152.30	11.10	203.8	204.6
10.28	153.44	11.51	203.7	204.2

Table 4.2.12

The thermal conductivity of Neon at T_{nom} = 308.15 K.

Pressure	Ref. Temp.	Density at Ref. Temp.	Thermal conductivity	
P/MPa	$T_r/^oC$	$\rho_r(T_r, P)/Kgm^{-3}$	$\lambda(T_r, \rho_r)$ $mWm^{-1}K^{-1}$	$\lambda(T_{nom}, \rho_r)$ $mWm^{-1}K^{-1}$
0.95	34.80	7.559	50.44	50.47
1.18	34.80	9.281	50.33	50.35
1.42	34.69	11.16	50.58	50.62
1.62	34.71	12.66	50.58	50.61
1.80	34.84	14.10	50.59	50.61
2.22	34.74	17.31	50.97	51.00
2.51	34.71	19.55	51.12	51.15
2.74	34.81	21.29	51.17	51.19
3.00	34.79	23.30	51.28	51.30
3.25	34.67	25.27	51.20	51.24
3.48	34.79	27.00	51.53	51.43
3.72	34.76	28.84	51.75	51.56
4.02	34.62	31.16	51.75	51.79
4.22	34.80	32.61	51.60	51.62

Table 4.2.13

The thermal conductivity of Neon at T_{nom} = 337.65 K.

Pressure P/MPa	Ref. Temp. $T_r/^oC$	Density at Ref. Temp. $\rho_r(T_r, P)/Kgm^{-3}$	Thermal conductivity $\lambda(T_r, \rho_r)$ $mWm^{-1}K^{-1}$	$\lambda(T_{nom}, \rho_r)$ $mWm^{-1}K^{-1}$
0.89	64.91	6.394	53.80	53.75
1.15	64.76	8.212	53.72	53.69
1.81	64.63	12.91	53.94	53.92
2.60	64.34	18.46	54.39	54.41
2.80	64.49	19.91	54.20	54.20
3.18	64.36	22.52	54.67	54.68
3.49	64.45	24.73	54.57	54.58
3.82	64.43	27.04	54.80	54.80
4.44	64.24	31.36	55.02	55.05
4.57	64.45	32.20	55.08	55.08
4.93	64.44	34.67	54.97	54.98
5.25	64.39	36.91	55.17	55.18
5.64	64.43	39.69	55.28	55.29
6.31	64.44	44.16	55.37	55.38
6.97	64.40	48.61	55.58	55.60
7.62	64.49	53.02	55.70	55.70
8.32	64.66	57.71	55.80	55.79
8.90	64.66	61.53	56.11	56.10
10.02	64.64	68.92	56.53	56.52

Table 4.2.14

The thermal conductivity of Neon at T_{nom} = 379.65 K.

Pressure P/MPa	Ref. Temp. $T_r/^oC$	Density at Ref. Temp. $\rho_r(T_r, P)/Kgm^{-3}$	Thermal conductivity $\lambda(T_r, \rho_r)$ $mWm^{-1}K^{-1}$	$\lambda(T_{nom}, \rho_r)$ $mWm^{-1}K^{-1}$
1.32	106.62	8.438	58.22	58.21
1.65	106.59	10.54	58.06	58.05
1.89	106.66	12.02	58.19	58.18
2.18	106.42	13.86	58.27	58.28
2.44	106.53	15.50	58.29	58.29
3.25	106.43	20.70	58.81	58.81
3.65	106.36	23.12	58.85	58.87
3.80	106.44	24.01	58.74	58.75
4.04	106.26	25.53	58.75	58.77
4.06	106.21	25.66	58.91	51.94
4.36	106.30	27.54	59.17	59.19
4.91	105.80	30.94	59.26	59.33
5.43	106.34	34.13	59.24	59.26
5.76	106.30	36.13	59.44	59.46
6.00	106.39	37.64	59.75	59.76
6.36	106.46	39.82	59.63	59.67
6.70	106.47	41.88	59.65	59.68
7.04	106.40	43.98	59.63	59.64
7.44	106.44	46.40	59.85	59.85
7.93	106.46	49.32	59.76	59.76
8.27	106.64	51.37	59.81	59.80
8.59	106.61	53.27	59.91	59.90
8.97	106.62	55.58	60.03	60.02

Table 4.2.15

The thermal conductivity of Neon at T_{nom} = 428.15 K.

Pressure	Ref. Temp.	Density at Ref. Temp.	Thermal conductivity	
P/MPa	$T_r/^oC$	$\rho_r(T_r, P)/Kgm^{-3}$	$\lambda(T_r,\rho_r)$ $mWm^{-1}K^{-1}$	$\lambda(T_{nom},\rho_r)$ $mWm^{-1}K^{-1}$
3.87	152.83	22.41	63.99	64.22
4.21	152.84	24.33	63.86	64.09
4.60	152.81	26.53	63.97	64.20
4.62	152.50	26.70	63.92	64.19
5.02	152.49	28.92	63.96	64.23
5.36	152.49	30.87	64.07	64.34
5.91	152.87	33.96	64.23	64.45
6.40	152.85	36.67	64.49	64.72
6.81	153.20	38.96	64.56	64.75
7.22	153.14	41.23	64.68	64.88
7.58	152.98	43.23	64.72	64.93
7.91	153.01	45.06	64.78	64.99
8.29	152.97	47.19	64.96	65.18
8.65	153.12	49.16	65.00	65.20
8.90	153.18	50.52	65.06	65.26
9.22	153.02	52.30	65.15	65.36
9.56	153.01	54.15	65.18	65.40
9.95	153.05	56.26	65.25	65.46

Table 4.2.16

The thermal conductivity of Hydrogen at T_{nom} = 308.15 K.

Pressure	Ref. Temp.	Density at Ref. Temp.	Thermal conductivity	
P/MPa	$T_r/^oC$	$\rho_r(T_r, P)/Kgm^{-3}$	$\lambda(T_r, \rho_r)$ $mWm^{-1}K^{-1}$	$\lambda(T_{nom}, \rho_r)$ $mWm^{-1}K^{-1}$
2.49	34.65	1.937	196.2	196.4
2.84	34.72	2.200	195.4	195.5
3.19	34.71	2.468	195.9	196.0
3.54	34.82	2.728	195.6	195.7
3.93	34.79	3.030	196.0	196.1
4.33	34.89	3.324	196.8	196.9
4.73	34.83	3.623	196.7	196.8
4.91	34.74	3.763	196.6	196.7
5.29	34.85	4.038	196.8	196.9
6.96	34.81	5.265	198.1	198.2
7.93	34.77	5.964	198.9	199.0
8.46	34.91	6.336	199.2	199.2
9.03	34.92	7.003	200.3	200.4

Table 4.2.17

The thermal conductivity of Hydrogen at T_{nom} = 337.65 K.

Pressure	Ref. Temp.	Density at Ref. Temp.	Thermal conductivity	
P/MPa	$T_r/^oC$	$\rho_r(T_r, P)/Kgm^{-3}$	$\lambda(T_r,\rho_r)$ $mWm^{-1}K^{-1}$	$\lambda(T_{nom},\rho_r)$ $mWm^{-1}K^{-1}$
1.98	64.46	1.410	209.8	209.8
2.18	64.46	1.545	211.2	211.2
2.53	64.40	1.796	210.7	210.8
2.85	64.43	2.018	210.1	210.2
3.26	64.36	2.301	210.2	210.2
3.52	64.36	2.482	210.6	210.6
3.84	64.42	2.705	210.8	210.8
4.20	64.40	2.952	210.9	210.9
5.20	64.40	3.634	212.4	212.4
5.63	64.39	3.924	212.3	212.3
5.95	64.38	4.142	212.5	212.6
7.70	64.38	5.304	213.1	213.1
8.20	64.14	5.702	213.4	213.5
8.65	64.35	5.991	213.6	213.6

Table 4.2.18

The thermal conductivity of Hydrogen at T_{nom} = 379.65 K.

Pressure P/MPa	Ref. Temp. T_r/°C	Density at Ref. Temp. $\rho_r(T_r, P)$/Kgm^{-3}	Thermal conductivity $\lambda(T_r, \rho_r)$ mWm^{-1}K^{-1}	$\lambda(T_{nom}, \rho_r)$ mWm^{-1}K^{-1}
3.13	106.68	1.979	228.1	228.0
3.67	106.75	2.313	228.6	228.5
4.30	106.79	2.700	228.5	228.3
5.35	106.61	3.343	229.2	229.2
5.74	106.85	3.580	229.9	229.7
6.02	106.77	3.752	229.3	229.2
6.34	106.73	3.945	229.5	229.4
7.30	106.67	4.522	230.2	230.1
7.69	106.50	4.759	230.5	230.5
8.03	106.56	4.960	229.9	229.9

Table 4.2.19

The thermal conductivity of Hydrogen at T_{nom} = 428.15 K.

Pressure P/MPa	Ref. Temp. T_r/°C	Density at Ref. Temp. $\rho_r(T_r, P)$/Kgm^{-3}	Thermal conductivity $\lambda(T_r, \rho_r)$ mWm^{-1}K^{-1}	$\lambda(T_{nom}, \rho_r)$ mWm^{-1}K^{-1}
3.73	155.17	2.152	247.8	248.9
4.07	155.18	2.344	247.4	248.4
4.85	155.18	2.782	247.8	248.8
5.28	155.19	3.023	247.8	248.7
5.63	155.15	3.220	248.1	249.1
6.03	155.17	3.447	248.0	249.0
7.21	155.43	4.112	249.6	250.5
7.62	155.43	4.336	250.3	251.2
8.11	155.54	4.613	250.3	251.1
8.47	155.62	4.810	251.3	252.1
8.86	155.63	5.029	251.4	252.2
9.36	155.67	5.306	250.6	251.5
9.89	155.68	5.602	251.7	252.5

Table 4.2.20

The thermal conductivity of Carbon Dioxide at T_{nom} = 308.15 K.

Pressure P/MPa	Ref. Temp. $T_r/^oC$	Density at Ref. Temp. $\rho_r(T_r, P)/Kgm^{-3}$	Thermal conductivity $\lambda(T_r, \rho_r)$ $mWm^{-1}K^{-1}$	$\lambda(T_{nom}, \rho_r)$ $mWm^{-1}K^{-1}$
0.68	35.07	12.06	17.81	17.81
0.83	34.98	14.87	17.73	17.73
1.05	34.91	18.89	17.99	17.99
1.21	34.82	22.07	18.05	18.07
1.69	34.88	31.65	18.35	18.36
1.88	34.68	35.52	18.48	18.50
2.05	34.97	41.04	18.77	18.978
2.31	34.80	44.80	18.84	18.84
2.50	34.99	48.90	19.03	19.03
2.68	34.86	53.19	19.24	19.25
2.90	35.04	58.19	19.51	19.51
3.11	34.96	63.31	19.67	19.67
3.35	34.84	68.86	19.96	19.74
3.34	34.83	68.87	19.72	19.74
3.45	34.97	71.81	20.21	20.22
3.69	35.11	77.91	20.43	20.42
3.82	35.03	81.51	20.65	20.63
4.02	35.08	87.26	20.91	20.90
4.47	35.01	100.4	21.66	21.66
4.71	32.69	110.0	22.39	22.59
4.82	32.52	114.3	22.71	22.92
5.01	32.46	121.3	23.47	23.68
5.22	32.56	129.1	23.90	24.10
5.35	32.23	134.5	24.36	24.59
5.36	32.52	134.3	24.59	24.80
5.62	32.35	142.3	25.26	25.44
5.80	32.19	155.0	26.41	26.65
5.82	32.29	156.1	25.53	26.76
5.98	32.17	164.2	26.92	27.16
6.20	32.17	176.9	28.59	28.83

Table 4.2.21

The thermal conductivity of Carbon Dioxide at T_{nom} = 333.15 K.

Pressure P/MPa	Ref. Temp. T_r/°C	Density at Ref. Temp. $\rho_r(T_r, P)$/Kgm^{-3}	Thermal conductivity $\lambda(T_r, \rho_r)$ mWm^{-1}K^{-1}	$\lambda(T_{nom}, \rho_r)$ mWm^{-1}K^{-1}
0.43	62.13	6.815	19.87	19.77
0.68	62.05	11.00	19.91	19.81
0.93	62.04	15.15	20.00	19.90
1.20	62.21	19.84	20.15	20.05
1.44	62.12	24.09	20.26	20.17
1.67	62.07	27.94	20.38	20.28
1.92	62.08	32.53	20.52	20.42
2.16	62.09	36.84	20.64	20.55
2.36	62.10	40.71	20.84	20.75
2.58	62.11	44.90	21.00	20.91
2.88	62.13	50.67	21.25	21.42
3.20	62.15	57.15	21.52	21.42
3.53	62.19	63.96	21.80	21.70
3.82	62.13	70.12	22.07	21.98
4.16	62.07	77.54	22.51	22.42
4.45	62.07	84.09	22.64	22.54
4.74	62.04	90.86	23.13	23.03
5.00	62.24	96.88	23.52	23.42
5.26	62.17	103.4	23.81	23.71
5.59	62.16	111.9	24.48	24.38
5.84	62.22	118.4	24.88	24.78
5.90	62.21	120.1	25.08	25.07
6.06	62.10	124.6	25.28	25.18

Table 4.2.22

The thermal conductivity of Carbon Dioxide at T_{nom} = 379.15 K.

Pressure	Ref. Temp.	Density at Ref. Temp.	Thermal conductivity $\lambda(T_r,\rho_r)$	$\lambda(T_{nom},\rho_r)$
P/MPa	$T_r/^oC$	$\rho_r(T_r,P)/Kgm^{-3}$	$mWm^{-1}K^{-1}$	$mWm^{-1}K^{-1}$
0.67	105.99	9.548	23.44	23.44
0.88	106.02	12.54	23.54	23.54
1.15	106.11	16.46	23.67	23.66
1.38	106.02	19.93	23.71	23.71
1.58	105.94	22.93	23.77	23.77
1.83	105.84	26.68	23.81	23.81
2.02	105.95	29.51	23.95	23.95
2.18	105.85	32.06	23.96	23.96
2.36	106.06	34.72	24.05	24.05
2.58	105.93	38.30	24.19	24.19
2.84	105.81	42.35	24.47	24.47
3.20	105.81	48.12	24.53	24.53
3.49	105.65	53.09	24.84	24.84
3.81	105.68	58.26	24.87	24.87
4.13	105.79	63.70	25.17	25.17
4.40	105.99	68.26	25.32	25.32
4.80	105.80	75.28	25.61	25.61
5.30	105.79	84.13	26.01	26.01
5.53	105.86	88.25	26.16	26.16
5.89	105.89	94.98	26.56	26.56
5.91	105.86	95.25	26.64	26.64
6.00	105.87	97.05	26.64	26.64
6.09	105.99	98.56	26.75	26.75
6.33	105.77	103.4	26.90	26.90
6.66	106.12	109.4	27.21	27.21

Table 4.2.23

The thermal conductivity of Carbon Dioxide

at T_{nom} = 425.65 K.

Pressure P/MPa	Ref. Temp. $T_r/^oC$	Density at Ref. Temp. $\rho_r(T_r, P)/Kgm^{-3}$	Thermal conductivity $\lambda(T_r,\rho_r)$ $mWm^{-1}K^{-1}$	$\lambda(T_{nom},\rho_r)$ $mWm^{-1}K^{-1}$
0.77	152.43	9.687	27.64	27.64
0.98	152.49	12.32	27.69	27.69
1.18	152.40	15.16	27.75	27.75
1.40	152.41	17.92	27.78	27.79
1.68	152.62	21.32	27.86	27.85
1.88	152.59	24.03	27.91	27.90
2.13	152.56	27.30	27.96	27.96
2.37	153.04	30.37	28.23	28.20
2.57	152.63	33.17	28.26	28.25
2.82	152.58	36.51	28.34	28.34
3.04	152.56	39.50	28.55	28.55
3.28	152.59	42.68	28.61	28.60
3.50	152.56	45.71	28.74	28.74

Table 4.2.25

The thermal conductivity of Nitrous oxide at T_{nom} = 308.15 K.

Pressure P/MPa	Ref. Temp. T_r/°C	Density at Ref. Temp. $\rho_r(T_r, P)$/Kgm^{-3}	Thermal conductivity $\lambda(T_r, \rho_r)$ mWm^{-1}K^{-1}	$\lambda(T_{nom}, \rho_r)$ mWm^{-1}K^{-1}
0.67	34.91	11.84	18.60	18.61
0.84	34.71	15.04	18.60	18.63
1.01	34.82	18.30	18.72	18.73
1.23	34.81	22.56	18.81	18.83
1.50	34.70	27.92	19.04	19.05
1.52	34.84	28.32	19.04	19.05
1.97	34.70	37.69	19.35	19.38
2.18	34.81	42.34	19.61	19.62
2.42	34.70	47.75	19.87	19.89
2.60	34.76	51.76	20.02	20.04
2.97	34.64	60.83	20.43	20.46
3.18	34.47	66.16	20.66	20.71
3.36	34.68	70.99	20.98	21.00
3.62	34.45	78.32	21.37	21.42
3.82	34.73	83.93	21.56	21.58
4.05	34.68	90.83	21.95	21.98
4.34	34.80	100.0	22.33	22.35
4.58	34.71	108.2	23.06	23.09
4.76	34.87	114.4	23.42	23.42
4.93	34.67	121.7	23.85	23.87
5.25	34.70	135.1	24.50	24.51
5.36	34.74	139.7	24.99	25.00
5.38	33.98	140.7	25.01	25.05
5.42	34.52	142.6	25.42	25.44
5.49	34.37	145.9	25.43	25.45
5.62	34.49	152.7	26.03	26.04

Table 4.2.26

The thermal conductivity of Nitrous Oxide at T_{nom} = 337.65 K.

Pressure P/MPa	Ref. Temp. $T_r/^oC$	Density at Ref. Temp. $\rho_r(T_r,P)/Kgm^{-3}$	Thermal conductivity $\lambda(T_r,\rho_r)$ $mWm^{-1}K^{-1}$	$\lambda(T_{nom},\rho_r)$ $mWm^{-1}K^{-1}$
0.43	65.14	6.866	20.89	20.83
0.94	65.40	15.24	21.11	21.03
1.16	64.74	19.00	21.16	21.14
1.58	64.75	26.18	21.31	21.29
1.92	64.92	32.33	21.62	21.58
2.16	64.78	36.65	21.65	21.62
2.36	64.72	40.54	21.88	21.86
2.56	64.77	44.21	21.98	21.95
2.80	64.56	49.08	22.16	22.16
3.44	64.74	61.95	22.74	22.72
3.67	64.70	66.96	22.88	22.86
3.89	65.05	71.49	23.15	23.11
4.14	64.67	77.20	23.45	23.43
4.38	64.67	82.74	23.70	23.68
4.64	64.70	89.19	24.01	24.00
5.59	65.05	113.2	25.40	25.36
6.10	64.85	127.9	26.23	26.21
6.46	64.81	138.9	26.88	26.87
6.50	64.22	140.9	26.89	26.90
6.63	64.57	144.8	27.28	27.28
6.85	64.64	151.7	27.65	27.65
7.17	64.51	163.2	28.88	28.55

Table 4.2.27

The thermal conductivity of Nitrous oxide

at T_{nom} = 379.15 K.

Pressure	Ref. Temp.	Density at Ref. Temp.	Thermal conductivity $\lambda(T_r,\rho_r)$	Thermal conductivity $\lambda(T_{nom},\rho_r)$
P/MPa	$T_r/^oC$	$\rho_r(T_r,P)/Kgm^{-3}$	$mWm^{-1}K^{-1}$	$mWm^{-1}K^{-1}$
0.78	106.27	11.34	25.28	25.25
0.97	106.26	13.84	25.35	25.33
1.18	106.18	16.99	25.44	25.42
1.40	106.01	20.27	25.42	25.42
1.61	105.93	23.39	25.45	25.46
1.79	105.91	26.10	25.63	25.64
1.99	106.12	29.15	25.57	25.56
2.20	106.13	32.46	25.70	25.69
2.38	105.92	35.18	25.74	25.74
2.57	105.76	38.47	25.85	25.87
2.72	105.76	40.68	25.88	25.90
2.84	105.89	42.66	25.99	26.01
3.06	105.86	46.14	26.10	26.11

Table 4.2.28

The thermal conductivity of Nitrous Oxide

at T_{nom} = 426.15 K.

Pressure	Ref. Temp.	Density at Ref. Temp.	Thermal conductivity	
P/MPa	$T_r/^oC$	$\rho_r(T_r, P)/Kgm^{-3}$	$\lambda(T_r, \rho_r)$ $mWm^{-1}K^{-1}$	$\lambda(T_{nom}, \rho_r)$ $mWm^{-1}K^{-1}$
0.79	152.89	9.94	29.46	29.47
1.07	152.92	13.47	29.51	29.52
1.40	152.92	17.83	25.54	29.55
1.73	152.80	22.07	29.59	29.51
2.27	152.83	29.28	29.72	29.74
2.75	152.71	35.70	29.77	29.79
3.04	152.97	39.62	30.05	30.06
3.36	152.95	43.99	30.13	30.13
3.69	153.02	48.69	30.24	30.02
4.01	153.08	53.16	30.32	30.32

Table 4.2.29

The thermal conductivity of Methane at T_{nom} = 309.15 K.

Pressure P/MPa	Ref. Temp. $T_r/^oC$	Density at Ref. Temp. $\rho_r(T_r, P)/Kgm^{-3}$	Thermal conductivity $\lambda(T_r,\rho_r)$ $mWm^{-1}K^{-1}$	$\lambda(T_{nom},\rho_r)$ $mWm^{-1}K^{-1}$
1.17	35.96	7.442	36.73	36.73
1.17	35.97	7.442	36.76	36.77
1.43	36.06	9.142	36.90	36.89
1.67	36.20	10.67	37.16	37.14
1.92	36.37	12.34	37.26	37.22
2.14	36.51	13.76	37.34	37.30
2.51	36.32	16.26	37.58	37.55
2.89	36.39	18.86	37.93	37.89
3.17	36.36	20.74	38.16	38.13
3.52	36.26	23.17	38.44	38.41
3.52	36.26	23.17	38.49	38.47
3.91	36.32	25.85	38.74	38.71
3.91	36.32	25.85	38.82	38.79
4.22	36.49	28.01	39.07	39.02
4.73	36.62	31.61	39.53	39.48
5.14	36.74	34.56	39.96	39.89
5.14	36.62	34.58	39.98	39.92
5.71	36.67	38.67	40.44	40.38
6.18	36.35	42.22	41.03	41.00
6.67	36.34	45.80	41.55	41.52
7.11	36.52	49.12	42.05	42.00
7.70	36.47	53.56	42.77	42.73
7.70	36.50	53.55	42.86	42.82
8.37	36.58	58.63	43.56	43.50
8.97	36.61	63.29	44.20	44.15
8.97	36.54	63.31	44.29	44.24
9.54	36.50	67.70	44.96	44.92
10.00	37.03	71.05	45.66	45.57
10.00	37.10	71.02	45.81	45.71

Table 4.2.30

The thermal conductivity of Methane at T_{nom} = 337.65 K.

Pressure	Ref. Temp.	Density at Ref. Temp.	Thermal conductivity $\lambda(T_r,\rho_r)$	$\lambda(T_{nom},\rho_r)$
P/MPa	$T_r/^oC$	$\rho_r(T_r,P)/Kgm^{-3}$	$mWm^{-1}K^{-1}$	$mWm^{-1}K^{-1}$
0.74	64.44	4.240	40.97	40.98
0.81	64.41	4.654	41.23	41.24
1.12	64.30	5.902	41.38	41.39
1.37	64.34	7.952	41.69	41.70
1.58	64.77	9.160	41.93	41.90
1.86	64.42	10.85	41.95	41.96
2.56	64.50	15.01	42.24	42.24
2.84	64.43	16.72	42.50	42.51
3.25	64.37	19.20	42.62	42.64
3.53	64.56	20.91	42.91	42.91
3.88	64.53	23.07	43.30	43.29
4.22	64.52	25.16	43.53	43.53
4.54	64.46	27.18	43.91	43.91
4.93	64.37	29.65	44.05	44.06
5.68	64.28	34.83	44.70	44.72
6.01	64.34	36.44	44.81	44.82
6.39	64.38	38.86	45.30	45.31
7.26	64.43	44.42	46.09	46.10
7.27	64.37	44.52	45.90	45.91
7.50	64.36	46.00	46.12	46.13
8.11	64.34	49.93	46.74	46.76

Table 4.2.31

The thermal conductivity of Methane at T_{nom} = 379.15 K.

Pressure P/MPa	Ref. Temp. $T_r/^oC$	Density at Ref. Temp. $\rho_r(T_r, P)/Kgm^{-3}$	Thermal conductivity $\lambda(T_r, \rho_r)$ $mWm^{-1}K^{-1}$	$\lambda(T_{nom}, \rho_r)$ $mWm^{-1}K^{-1}$
1.02	105.95	5.201	47.86	47.86
1.18	105.96	6.017	48.00	48.00
1.34	105.89	6.871	48.01	48.02
1.52	105.94	7.796	48.19	48.20
1.68	105.85	8.618	48.35	48.36
1.86	105.90	9.547	48.32	48.33
2.13	106.05	10.94	48.51	48.50
2.44	105.99	12.56	48.60	48.60
2.67	105.97	13.73	48.65	48.66
2.96	105.84	15.31	48.91	48.93
3.17	105.95	16.39	48.83	48.84
3.61	105.92	18.72	49.27	49.27
3.91	105.90	21.29	49.44	49.45
4.18	105.88	21.72	49.55	49.56
4.48	105.88	23.37	49.56	49.58
4.72	105.91	24.84	49.81	49.82
6.92	105.97	36.44	51.18	51.18
7.26	105.93	38.27	51.44	51.45
7.44	105.93	39.28	51.68	51.69
7.75	105.96	40.92	51.71	51.72
8.59	105.93	45.50	52.46	52.46
8.70	105.97	46.09	52.75	52.75
8.89	105.92	47.15	52.97	52.98
9.15	105.92	48.58	53.08	53.09

Table 4.2.32

The thermal conductivity of Methane at T_{nom} = 425.65 K.

Pressure P/MPa	Ref. Temp. $T_r/^oC$	Density at Ref. Temp. $\rho_r(T_r, P)/Kgm^{-3}$	Thermal conductivity $\lambda(T_r, \rho_r)$ $mWm^{-1}K^{-1}$	$\lambda(T_{nom}, \rho_r)$ $mWm^{-1}K^{-1}$
1.97	152.97	8.958	57.32	57.28
2.80	153.30	12.76	57.69	57.64
3.14	152.95	14.28	57.75	57.71
3.60	152.98	16.43	57.94	57.89
4.13	153.14	18.87	58.21	58.15
4.64	152.98	21.23	58.29	58.24
5.17	152.97	23.64	58.52	58.47
5.72	153.04	26.19	58.86	58.81
6.41	152.96	29.38	59.31	59.26
7.06	152.94	32.38	59.55	59.91
7.71	153.05	35.41	60.01	59.96
8.75	152.89	40.20	60.76	60.72
9.77	152.98	44.90	61.40	61.35
9.78	152.95	44.98	61.20	61.15

Table 4.2.33

The thermal conductivity of Tetrafluoromethane.
at T_{nom} = 308.15 K.

Pressure P/MPa	Ref. Temp. $T_r/^oC$	Density at Ref. Temp. $\rho_r(T_r,P)/Kgm^{-3}$	Thermal conductivity $\lambda(T_r,\rho_r)$ $mWm^{-1}K^{-1}$	$\lambda(T_{nom},\rho_r)$ $mWm^{-1}K^{-1}$
0.51	35.26	17.73	17.02	17.00
0.78	35.17	27.62	17.13	17.12
1.09	35.16	38.97	17.21	17.20
1.45	35.22	52.10	17.41	17.39
1.81	35.23	66.10	17.63	17.61
2.13	35.21	78.55	17.90	17.88
2.51	35.24	93.77	18.11	18.09
2.84	35.19	107.4	18.35	18.34
3.19	35.20	122.3	18.56	18.55
3.53	35.19	136.8	18.88	18.87
3.87	35.18	151.7	19.09	19.07
4.23	35.21	168.2	19.60	19.58
4.59	35.23	184.7	19.89	19.87
4.94	35.11	201.4	20.29	20.28
5.32	35.23	219.5	20.58	20.56
5.78	35.18	242.3	21.26	21.24
6.30	35.22	268.2	21.76	21.74
6.86	35.25	296.9	22.71	22.69
7.47	35.25	328.8	23.43	23.36
8.09	35.27	361.5	24.28	24.25
8.82	35.10	400.6	25.39	25.38
9.49	35.19	435.3	26.65	26.63
10.06	35.23	464.4	27.38	27.36

Table 4.2.34

The thermal conductivity of Tetrafluoromethane.
at T_{nom} = 331.65 K.

Pressure P/MPa	Ref. Temp. T_r/°C	Density at Ref. Temp. $\rho_r(T_r, P)$/Kgm^{-3}	Thermal conductivity $\lambda(T_r, \rho_r)$ mWm^{-1}K^{-1}	$\lambda(T_{nom}, \rho_r)$ mWm^{-1}K^{-1}
0.43	58.32	13.96	18.84	18.86
0.78	58.17	25.55	19.02	19.04
1.12	58.28	36.87	19.08	19.10
1.47	58.19	48.89	19.30	19.32
1.78	58.31	59.63	19.42	19.44
2.17	58.27	73.27	19.58	19.60
2.49	58.26	84.91	19.94	19.95
2.83	58.33	97.21	20.04	20.05
3.20	58.30	110.8	20.23	20.25
3.52	58.32	123.0	20.48	20.50
3.82	58.27	134.3	20.79	20.81
4.25	58.29	150.6	21.09	21.11
4.60	58.29	164.3	21.14	21.16
4.95	58.25	178.7	21.71	21.73
5.29	58.26	192.6	21.99	22.01
5.61	58.23	205.6	22.42	22.44
5.99	58.24	221.2	22.74	22.76
6.36	58.18	236.7	23.01	23.18
6.80	58.22	254.9	23.42	23.46
7.38	58.27	279.5	24.14	24.16
7.86	58.25	300.0	24.90	24.92
8.35	58.23	320.8	25.24	25.26
8.83	58.23	341.0	25.85	26.00
9.31	58.26	361.3	26.41	26.43
10.00	59.62	386.9	27.31	27.34

Table 4.2.35

The thermal conductivity of Tetrafluoromethane.

at T_{nom} = 371.15 K.

Pressure P/MPa	Ref. Temp. T_r/°C	Density at Ref. Temp. $\rho_r(T_r, P)$/Kgm^{-3}	Thermal conductivity $\lambda(T_r, \rho_r)$ mWm^{-1}K^{-1}	$\lambda(T_{nom}, \rho_r)$ mWm^{-1}K^{-1}
0.77	97.86	22.25	22.08	22.09
1.11	97.92	32.39	22.11	22.12
1.54	97.84	44.91	22.38	22.39
2.07	98.03	60.90	22.58	22.58
2.33	98.00	68.90	22.78	22.78
2.76	98.10	82.04	22.93	22.92
3.17	98.06	94.92	23.16	23.16
3.54	98.09	106.6	23.47	23.38
4.30	98.09	130.7	23.85	23.84
4.91	98.10	150.4	24.25	24.24
5.20	98.12	171.0	24.76	24.75
6.20	98.06	192.5	25.40	25.39
7.06	98.08	220.6	26.04	26.03
7.77	97.90	244.1	26.64	26.65
8.44	97.76	266.5	27.14	27.16
9.06	97.92	286.6	27.76	27.76
9.90	97.58	314.2	28.71	28.75
9.96	97.85	315.8	28.72	28.74

Table 4.2.36

The thermal conductivity of Tetrafluoromethane.

at T_{nom} = 425.65 K.

Pressure P/MPa	Ref. Temp. $T_r/^oC$	Density at Ref. Temp. $\rho_r(T_r, P)/Kgm^{-3}$	Thermal conductivity $\lambda(T_r, \rho_r)$ $mWm^{-1}K^{-1}$	$\lambda(T_{nom}, \rho_r)$ $mWm^{-1}K^{-1}$
0.42	152.17	10.62	26.33	22.36
0.42	152.10	10.63	26.35	26.38
0.75	152.01	18.95	26.29	26.33
1.08	152.11	27.14	26.38	26.42
1.11	152.09	27.84	26.46	26.49
1.45	152.20	36.59	26.77	26.80
1.78	152.24	45.03	26.71	26.73
2.16	152.22	54.58	27.03	27.05
2.47	152.23	62.57	27.05	27.08
2.82	152.37	71.81	27.21	27.22
3.20	153.15	81.29	27.56	27.51
3.51	153.19	89.50	27.71	27.65
3.89	153.07	99.22	27.91	27.86
4.38	153.04	112.0	28.09	28.04
4.82	152.82	123.6	28.38	28.36
5.29	152.88	136.0	28.71	28.68
5.84	152.90	150.5	29.04	29.00
6.53	152.84	168.4	29.59	29.56
7.15	152.77	184.7	29.90	29.88
7.15	152.75	184.8	29.98	29.96

Table 4.2.37

The thermal conductivity of Ethane at T_{nom} = 308.15 K.

Pressure P/MPa	Ref. Temp. T_r/°C	Density at Ref. Temp. $\rho_r(T_r, P)$/Kgm^{-3}	Thermal conductivity $\lambda(T_r, \rho_r)$ mWm^{-1}K^{-1}	$\lambda(T_{nom}, \rho_r)$ mWm^{-1}K^{-1}
0.62	34.56	7.60	23.27	23.34
0.71	34.54	8.81	23.46	23.52
0.82	34.65	10.22	23.40	23.45
0.95	34.58	11.98	23.55	23.60
1.08	35.01	13.76	23.75	23.75
1.22	34.44	15.73	23.85	23.93
1.36	34.50	17.72	23.95	24.02
1.53	34.48	20.23	24.16	24.23
1.70	34.35	22.95	24.28	24.37
1.87	34.48	25.57	24.55	24.62
2.00	34.47	32.92	24.98	25.06
2.30	34.47	32.92	25.32	25.39
3.23	34.49	52.16	27.25	27.32
3.33	34.60	54.47	27.56	27.62
3.61	34.52	61.91	28.67	28.74
3.67	34.45	63.84	28.89	28.97
3.77	34.37	66.80	29.34	29.43
3.90	34.39	71.11	30.00	30.08

Table 4.2.38

The thermal conductivity of Ethane at T_{nom} = 333.65 K.

Pressure P/MPa	Ref. Temp. $T_r/^oC$	Density at Ref. Temp. $\rho_r(T_r, P)/Kgm^{-3}$	Thermal conductivity $\lambda(T_r, \rho_r)$ $mWm^{-1}K^{-1}$	$\lambda(T_{nom}, \rho_r)$ $mWm^{-1}K^{-1}$
0.66	58.35	7.478	26.59	26.61
0.87	58.41	10.03	26.61	26.62
1.12	58.46	13.68	27.05	27.05
1.48	58.54	17.65	27.21	27.21
2.16	58.65	26.93	28.11	28.09
2.47	58.63	31.63	28.52	28.51
2.84	58.64	37.39	28.94	28.92
3.25	58.33	44.26	29.88	29.91
3.55	58.38	49.72	30.48	30.50
4.01	58.65	58.65	31.75	31.73
4.30	58.62	64.83	32.40	32.39
4.82	58.40	77.46	34.58	34.60
5.69	58.78	102.8	39.20	39.16
6.31	58.77	128.0	44.01	42.97

Table 4.2.39

The thermal conductivity of Ethane at T_{nom} = 380.15 K.

Pressure P/MPa	Ref. Temp. $T_r/^oC$	Density at Ref. Temp. $\rho_r(T_r, P)/Kgm^{-3}$	Thermal conductivity $\lambda(T_r, \rho_r)$ $mWm^{-1}K^{-1}$	$\lambda(T_{nom}, \rho_r)$ $mWm^{-1}K^{-1}$
0.54	106.96	5.27	34.22	34.22
0.72	106.86	7.06	34.45	34.47
0.94	106.34	9.30	34.46	34.56
1.16	106.82	11.49	34.60	34.62
1.36	106.84	13.66	34.66	34.68
1.62	106.94	16.37	34.85	34.86
1.88	106.56	19.24	35.11	35.18
1.91	106.87	19.60	35.16	35.18
2.47	106.87	25.92	35.52	35.54
2.78	106.87	29.52	35.92	35.94
3.50	106.70	38.30	36.89	36.94
3.80	106.83	42.06	37.09	37.11
4.48	106.94	51.12	38.03	38.04
4.78	106.78	55.37	38.42	38.45

Table 4.2.40

The thermal conductivity of Ethane at T_{nom} = 425.65 K.

Pressure P/MPa	Ref. Temp. $T_r/^oC$	Density at Ref. Temp. $\rho_r(T_r, P)/Kgm^{-3}$	Thermal conductivity $\lambda(T_r, \rho_r)$ $mWm^{-1}K^{-1}$	$\lambda(T_{nom}, \rho_r)$ $mWm^{-1}K^{-1}$
0.65	152.63	5.63	42.32	42.30
0.98	152.48	8.57	42.48	42.48
1.34	152.48	11.80	42.43	42.44
1.67	152.43	14.83	42.53	42.54
2.05	152.44	18.30	42.73	42.74
2.35	152.41	21.18	42.90	42.91
2.76	152.44	25.10	43.30	43.31
3.49	152.47	32.36	43.99	43.99
3.78	152.52	35.37	44.12	44.12
4.24	152.43	40.09	44.74	44.75
4.60	152.51	43.87	44.79	44.79
4.82	152.54	46.23	45.26	45.25
5.62	152.81	54.95	45.93	45.89
6.16	152.77	61.03	46.55	46.51
6.25	152.68	62.15	46.52	46.49
6.64	152.73	66.69	47.18	47.15
6.64	152.73	66.69	47.30	47.26

Table 4.2.41

The thermal conductivity of Ethylene at T_{nom} = 308.15 K.

Pressure P/MPa	Ref. Temp. T_r/°C	Density at Ref. Temp. $\rho_r(T_r, P)$/Kgm^{-3}	Thermal conductivity $\lambda(T_r, \rho_r)$ mWm^{-1}K^{-1}	$\lambda(T_{nom}, \rho_r)$ mWm^{-1}K^{-1}
0.51	34.95	5.71	22.77	22.78
0.85	35.07	9.77	22.86	22.85
1.25	35.08	14.69	23.19	23.18
1.57	35.08	18.77	23.34	23.33
1.98	35.01	24.26	23.60	23.60
2.29	35.04	28.65	24.05	24.04
2.58	35.07	32.39	24.47	24.46
2.94	35.08	38.62	24.98	24.97
3.85	34.97	54.43	26.78	26.77
4.22	34.94	61.98	27.84	27.85
4.58	34.92	69.77	28.88	28.89
4.92	34.93	77.80	29.95	29.96
5.24	35.10	85.92	31.18	31.17
5.70	34.96	99.81	33.47	33.48
6.10	34.98	113.7	34.58	35.98
6.47	34.95	128.7	38.87	38.88
6.86	35.03	147.2	43.11	43.10
7.46	35.05	180.5	49.30	49.29
7.98	34.98	210.7	55.21	55.21
8.48	34.98	235.7	58.96	58.97
8.82	35.11	249.4	61.37	61.36

Table 4.2.42

The thermal conductivity of Ethylene at T_{nom} = 333.15 K.

Pressure P/MPa	Ref. Temp. $T_r/^oC$	Density at Ref. Temp. $\rho_r(T_r, P)/Kgm^{-3}$	Thermal conductivity $\lambda(T_r, \rho_r)$ $mWm^{-1}K^{-1}$	$\lambda(T_{nom}, \rho_r)$ $mWm^{-1}K^{-1}$
0.42	58.61	4.331	25.80	25.97
0.74	58.55	7.793	25.99	26.16
1.06	58.69	11.27	26.00	26.16
1.78	58.13	19.65	26.58	26.78
2.19	59.05	24.60	27.18	27.30
2.37	59.99	27.95	27.57	27.57
2.82	59.33	32.58	27.79	27.87
3.17	59.37	37.25	28.29	28.37
3.58	58.13	43.18	28.77	28.95
4.35	59.67	54.53	30.21	30.25
5.04	59.47	65.85	31.60	31.66
5.66	59.67	76.94	32.96	33.00
6.50	59.56	93.94	35.39	35.44
7.12	59.50	108.0	37.56	37.62
7.66	58.42	122.8	39.60	39.79
8.55	58.42	147.9	43.96	44.15

Table 4.2.43

The thermal conductivity of Ethylene at T_{nom} = 371.15 K.

Pressure P/MPa	Ref. Temp. T_r/°C	Density at Ref. Temp. $\rho_r(T_r, P)$/Kgm^{-3}	Thermal conductivity $\lambda(T_r, \rho_r)$ mWm^{-1}K^{-1}	$\lambda(T_{nom}, \rho_r)$ mWm^{-1}K^{-1}
0.84	97.47	7.894	31.96	32.02
1.12	97.58	10.55	31.96	32.01
1.40	97.77	13.31	32.15	32.19
1.76	97.65	16.90	32.37	32.41
2.12	97.72	20.56	32.32	32.35
3.88	97.87	39.71	33.81	33.83
4.36	97.64	45.40	34.30	34.35
4.84	98.30	51.00	35.14	35.11
4.89	97.62	51.83	35.08	35.13
5.36	97.89	57.62	35.72	35.73
5.80	97.84	63.22	36.31	36.64
6.22	99.16	68.33	37.22	37.07
6.38	99.13	70.45	37.62	37.47
6.69	99.15	74.74	38.49	38.34

Table 4.2.44

The thermal conductivity of Ethylene at T_{nom} = 425.65 K.

Pressure P/MPa	Ref. Temp. T_r/°C	Density at Ref. Temp. $\rho_r(T_r, P)$/Kgm^{-3}	Thermal conductivity $\lambda(T_r, \rho_r)$ mWm^{-1}K^{-1}	$\lambda(T_{nom}, \rho_r)$ mWm^{-1}K^{-1}
1.39	152.98	11.29	41.94	41.88
1.72	152.99	14.00	41.98	41.91
2.03	153.06	16.69	42.21	42.13
2.38	152.94	19.70	42.02	41.96
2.69	153.00	22.39	42.38	42.31
3.04	152.98	25.35	42.52	42.45
3.46	153.00	29.14	42.61	42.54
3.77	153.26	31.90	42.52	42.42
4.16	152.83	35.44	43.13	43.09
4.51	152.82	38.68	43.16	43.12
4.97	152.79	42.98	42.61	43.54
5.42	152.81	47.21	43.78	43.74
5.79	152.80	50.76	44.01	43.97
6.14	152.90	54.14	44.43	44.37
6.49	152.71	57.53	44.62	44.60
6.73	152.90	59.86	45.19	45.13
7.00	152.79	62.54	45.18	45.14
7.60	152.84	68.59	45.82	45.77

Table 4.2.45

The thermal conductivity of Nitrogen at T_{nom} = 177.5 K.

Pressure P/MPa	Ref. Temp. T_r/K	Density at Ref. Temp. $\rho_r(T_r, P)$/Kgm^{-3}	Thermal conductivity $\lambda(T_r, \rho_r)$ mWm^{-1}K^{-1}	$\lambda(T_{nom}, \rho_r)$ mWm^{-1}K^{-1}
0.32	177.21	6.189	16.89	16.91
0.52	177.21	9.963	17.05	17.07
0.84	177.08	16.43	17.33	17.34
1.11	177.09	21.89	17.56	17.58
1.46	177.83	29.05	17.84	17.82
1.79	177.66	36.10	18.21	18.20
2.14	177.81	43.67	18.54	18.52
2.47	177.91	50.97	18.90	18.87
3.03	177.85	63.77	19.55	19.53
3.56	176.71	76.95	20.05	20.11
4.26	176.66	94.63	20.98	21.04
4.97	176.70	113.2	22.44	22.50
5.68	176.61	132.9	23.60	23.66
6.68	176.37	162.2	25.60	25.68
7.78	176.23	195.26	28.22	28.31
8.77	175.97	226.26	30.66	30.79

Table 4.2.46

The thermal conductivity of Nitrogen at T_{nom} = 223.15 K.

Pressure P/MPa	Ref. Temp. T_r/K	Density at Ref. Temp. $\rho_r(T_r, P)$/Kgm^{-3}	Thermal conductivity $\lambda(T_r, \rho_r)$ mWm^{-1}K^{-1}	$\lambda(T_{nom}, \rho_r)$ mWm^{-1}K^{-1}
0.48	222.50	7.327	20.74	20.78
0.79	222.70	12.10	20.95	20.98
1.07	222.74	16.48	21.14	21.17
1.45	222.75	22.41	21.39	21.42
1.85	222.86	28.60	21.63	21.05
2.31	223.05	35.94	21.95	21.96
2.86	222.61	44.93	22.34	22.38
3.55	222.69	56.21	22.87	22.90
4.24	222.81	67.60	23.44	23.57
4.93	222.86	79.14	24.06	24.08
5.69	222.58	92.19	24.73	24.77
6.36	222.71	103.6	25.52	25.56
7.42	222.66	121.9	26.47	26.51
8.42	222.63	139.2	27.58	27.62
9.48	222.68	157.3	28.67	28.71
10.53	222.57	175.4	29.90	29.94

Table 4.2.47

The thermal conductivity of Nitrogen at T_{nom} = 270.15 K.

Pressure	Ref. Temp.	Density at Ref. Temp.	Thermal conductivity $\lambda(T_r,\rho_r)$	Thermal conductivity $\lambda(T_{nom},\rho_r)$
P/MPa	T_r/K	$\rho_r(T_r,P)$/Kgm^{-3}	mWm^{-1}K^{-1}	mWm^{-1}K^{-1}
0.47	270.35	5.829	24.29	24.28
0.77	270.42	9.629	24.43	24.41
1.07	270.14	13.37	24.60	24.60
1.45	270.28	18.14	24.83	24.83
1.76	270.26	22.06	25.05	25.05
2.14	270.26	26.96	25.23	25.22
2.47	270.43	31.14	25.46	25.44
2.99	270.28	37.73	25.72	25.73
3.55	270.21	44.87	26.03	26.02
4.09	270.28	51.82	26.36	26.35
4.60	270.33	58.08	26.68	26.68
5.36	270.35	68.04	27.15	27.14
6.17	270.58	78.28	27.71	27.68
7.03	270.46	89.32	28.29	28.27
7.95	270.54	101.0	28.90	28.87
8.95	270.52	113.6	29.64	29.61

CHAPTER 5

THEORY

5.1 INTRODUCTION

In this chapter the kinetic theory of non-uniform gases is considered and extended. If a gas is subject to a macroscopic gradient of concentration, shear or temperature, which removes it from its equilibrium state, then associated with the macroscopic gradient is a macroscopic flux of mass, momentum or heat. If the gas is perturbed only slightly from equlibrium, the macroscopic gradient and flux are in direct proportion. The constant of proportionality is the transport coefficient (e.g. viscosity, thermal conductivity and diffusion coefficient). The kinetic theory of non-uniform gases is an attempt to understand how mass, momentum and energy are transported through the bulk of the gas by considering the microscopic behaviour of the gas and hence obtaining expressions for the transport coefficients in terms of microscopic properties. There are two microscopic phenomena of particular interest: the collisions between the constituent particles and the movement of the particles between the collisions. These two phenomena are dependent on the intermolecular force between the constituent particles of the gas. For a completely deterministic picture of the bulk gas, the position and momentum of each particle would also be required. The behaviour of the gas could then be predicted by application of Newton's laws of mechanics. This approach is not realistically possible so a statistical method is adopted. The most widely adopted statistical method is the Chapman Enskog kinetic theory [1].

Originally, the Chapman Enskog theory was applicable to structureless molecules interacting through spherically-symmetrical pair potentials. The gas is also considered to be sufficiently dilute so that only binary collisions occur. The Chapman Enskog kinetic theory provides kinetic theory expressions for the transport coefficients of monatomic gases in terms of fundamental properties of the atoms, physical constants and well-defined functions of the intermolecular potential. The intermolecular potentials are available for all the monatomic interactions and, in some cases, these potentials are very well known [2, 3]. Computer code is available for efficient calculation of the functionals [4].

The situation with respect to polyatomic gases is less well developed. This is because the molecules now possess internal energy and owing to the structure of the molecule the intermolecular potential is not spherically symmetric. These two features of polyatomic gases complicate the collision process. An extension of the kinetic theory of monatomic gases has been proposed [5, 6, 7] for polyatomic gases in which the transport coefficients are obtained from functionals of the intermolecular potential. Routine calculation of these functionals is, however, hampered by lack of sophisticated intermolecular potentials for polyatomic gases and the immense computational effort required. Attention has therefore been turned to approximate methods of calculation. Confidence in these approximate schemes can only be judged, for real systems, by comparison between theoretical predictions and accurate transport property data. Until recently, the kinetic theory of polyatomic gases has been limited to a first-order analysis. The advent of high accuracy transport property data has required further theoretical development to higher orders in order adequately to describe the

data. In the case of monatomic mixtures, a third–order analysis was found to be necessary [8]. In anticipation that this may also be necessary for polyatomic gases, second–order expressions are now available for most of the classical transport coefficients for pure polyatomic gases and their mixtures [7, 9]. This analysis is extended in this thesis to the thermal conductivity of a polyatomic gas mixture. (The previous analysis was restricted to the hypothetical thermal conductivity of a polyatomic gas mixture not subject to thermal diffusion).

So far the discussion has been limited to the dilute gas. This region is important because correlations of transport properties can be written in the form

$$X(\rho, T) = X_0(0, T) + \Delta X_{EXCESS}(\rho, T) + \Delta X_{crit}(\rho, T) \quad (5.1.1)$$

in which X represents a general transport property, X_0 represents the dilute gas contribution, ΔX_{EXCESS} represents the density dependence of the transport property and ΔX_{crit} represents the critical enhancement of the transport property. Therefore, as well as being able to predict the trasport properties of the dilute gas, the density dependence of the property must be considered. (The critical enhancemnt term is the subject of specialist study and is not considered from a theoretical point of view in this thesis). The statistical mechanical theory of the non–uniform dense gas indicates that the proper form for the density dependence of the transport coefficients is [6]

$$\Delta X_{EXCESS} = X_1\rho + X_2\rho^2 + X\rho^2\ell n\rho + \ldots \quad (5.1.2)$$

The theory of dense gas has been restricted to two main regions. There has been considerable development in the limit of very high density [10] and there has been some development in the moderately dense gas region. In the latter region, the equation for the density dependence (equation 5.1.2) is truncated at the first term and the transport properties are considered to be linear functions of density. Early work concentrated on extensions of the kinetic theory of dense hard spheres originally proposed by Enskog [6, 11]. Recent work has concentrated on a more realistic Lennard–Jones (12–6) potential model for which a microscopic treatment can be carried through [12, 13]. In the following sections a brief review of the available kinetic theory of monatomic and polyatmoic gases is presented. A more detailed analysis of the thermal conductivity of polyatomic gas mixtures is also presented to provide a new result. Finally, a brief account of the kinetic theory of moderately dense gas is given.

5.2 MONATOMIC GASES

The relevant kinetic theory expressions for the transport coefficients of dilute monatomic gases with reference to this work are those for thermal conductivity and viscosity. The gas is considered to be only slightly removed from equilibrium so the velocity distribution function can be written as a perturbation of its equilibrium value. This is referred to as the linear approximation

$$f(\underline{c}, r, t) = f^0(\underline{c}, r, t)(1 + \phi) \qquad (5.2.1)$$

Here, $f^0(\underline{c}, r, t)$ is the local equilibrium distribution function; $\underline{c}$

and $\underline{r}$ refer to the velocity and position of a particle; t refers to the time dependence of f and f^0 and ϕ is a perturbation function.

The spatial and temporal evolution of $f(\underline{c}, \underline{r}, \underline{t})$ is governed by the Boltzmann equation. From this point, and by considering the binary collision process, it is possible to derive expressions for the macroscopic fluxes when the gas is subject to a macroscopic gradient and hence obtain expressions for the transport coefficients. The mathematical solution for the transport coefficients involves the truncation of an expansion (see Appendix 5A). It is the number of terms taken in the expression that dictates the order of approximation. The first-order expressions are recovered if the first non-zero terms are taken. Details of this procedure can be found elsewhere [1, 2, 6, 11]. Hence, for the first-order viscosity and thermal conductivity in the linear approximation

$$[\eta^0]_1 = \frac{kT}{\langle v\rangle_0 \mathfrak{S}(2000)} \tag{5.2.2}$$

for the viscosity, and

$$[\lambda^0]_1 = \frac{5}{2}\frac{k^2T}{m\mathfrak{S}(1010)\langle v\rangle_0} \tag{5.2.3}$$

for the thermal conductivity. In the above expressions, k is Boltzmann's constant, T the absolute temperature, m the molecular mass,

$$\langle v\rangle_0 = 4\left[\frac{kT}{\pi m}\right]^{\frac{1}{2}} \tag{5.2.4}$$

and $\mathfrak{S}(1010)$ and $\mathfrak{S}(2000)$ are effective cross-sections related to the more usually employed collision integrals (note that these are the

collision integrals defined by Maitland *et al* [2] which differ from those used by Hirschfelder *et al* [11] by numerical factors) by the expressions

$$\mathfrak{S}(1010) = \frac{8}{15}\,\bar{\Omega}^{(2,2)} \tag{5.2.5}$$

$$\mathfrak{S}(2000) = \frac{4}{5}\,\bar{\Omega}^{(2,2)} \tag{5.2.6}$$

The collision integral contains the information about the binary collision process and is therefore dependent on the intermolecular potential. $\bar{\Omega}^{(2,2)}(T)$ is one of the functionals mentioned in the introduction. It is interesting to note that the first-order viscosity and thermal conductivity are functions of the same collision integral. Equations (5.2.2) and (5.2.3) can be combined to produce the exact kinetic theory relationship

$$\mathrm{Eu} = \frac{m[\lambda^{o}]_1}{C_v[\eta^{o}]_1} = 2.5 \text{ (exactly)} \tag{5.2.7}$$

Eu is known as the the Eucken factor.

The expression for the Eucken factor given by equation (5.2.7) involves the first-order approximations to the transport coefficients. By taking more terms in the series solution, higher-order expressions can be obtained in the form

$$[\lambda^{o}]_m = [\lambda^{o}]_1 f_{\lambda}^{m} \tag{5.2.8}$$

$$[\eta^{o}]_m = [\eta^{o}]_1 f_{\eta}^{m} \tag{5.2.9}$$

From which is obtained

$$Eu = \frac{m\ [\lambda^{o}]_1\ f_{\eta}^{m}}{C_v\ [\eta^{o}]_1\ f_{\lambda}^{m}} \qquad (5.2.10)$$

f_{η}^{m} and f_{λ}^{m} contain the higher-order corrections, which generally amount to about 1%, and are functions of generalised collision integrals similar to $\bar{\Omega}^{(2,2)}(T)$, defined by the equation

$$\bar{\Omega}^{(l,s)}(T) = \left[(s+1)!(kT)^{s+2}\right]^{-1} \int_0^{\infty} Q^{(l)}(E)\exp(-E/kT)E^{s+1}dE \qquad (5.2.11)$$

where E is the relative kinetic energy of two colliding particles and $Q^{(l)}$ is a transport cross-section [2]. The collision integral is therefore an energy-averaged transport cross-section. The transport cross-section contains the information about the binary collision and the intermolecular forces.

Explicit evaluation of the collision integrals is possible for rigid-sphere molecules. In this case

$$\bar{\Omega}^{(l,s)}(T) = \pi d^2 \qquad (5.2.12)$$

where d is the diameter of the rigid sphere. So for a rigid sphere the collision integrals are proportional to the cross-sectional area of the sphere. If the intermolecular potential is of the form

$$U(r) = \epsilon F(r/\sigma) \qquad (5.2.13)$$

where ϵ and σ are characteristic energy and size parameters, it is appropriate to define a reduced collision integral

$$\Omega^{(l,s)^*}(T^*) = \Omega^{(l,s)}(T)/\Omega_{rs}^{(l,s)}(T) \qquad (5.2.14)$$

where $\Omega_{rs}^{(l,s)}(T)$ refers to the collision integral of a rigid sphere of diameter σ and T^* is a reduced temperature defined by

$$T^* = T/(\epsilon/K) \qquad (5.2.15)$$

The transport coefficients can now be obtained in terms of these reduced collision integrals

$$[\eta^o]_1 = \frac{5}{16}\left[\frac{mkT}{\pi}\right]^{\frac{1}{2}} \frac{1}{\sigma^2\Omega^{(2,2)^*}(T^*)} \qquad (5.2.16)$$

$$[\lambda^o]_1 = \frac{75}{64}\left[\frac{k^3T}{m\pi}\right]^{\frac{1}{2}} \frac{1}{\sigma^2\Omega^{(2,2)^*}(T^*)} \qquad (5.2.17)$$

Equations (5.2.16) and (5.2.17) indicate that the viscosity and thermal conductivity are functions of a temperature-dependent cross-sectional area. The temperature dependence is derived from the temperature dependence of $\Omega^{(2,2)^*}(T^*)$. If the particle were a rigid sphere, the intermolecular potential is described schematically by Figure 5.1. When the particles come into contact there is an infinite potential barrier. There is no penetration of this barrier, no matter what the energy of the colliding particles. A real fluid has a different intermolecular potential, shown schematically in Figure 5.2. The potential barrier now has a finite slope and penetration into the repulsive region, beyond σ, is possible if the colliding particles have sufficient energy. Therefore, the effective size of the particle depends on the steepness of the potential barrier and the energy of the collision. Thus, all of the

Figure 5.1 The rigid sphere potential

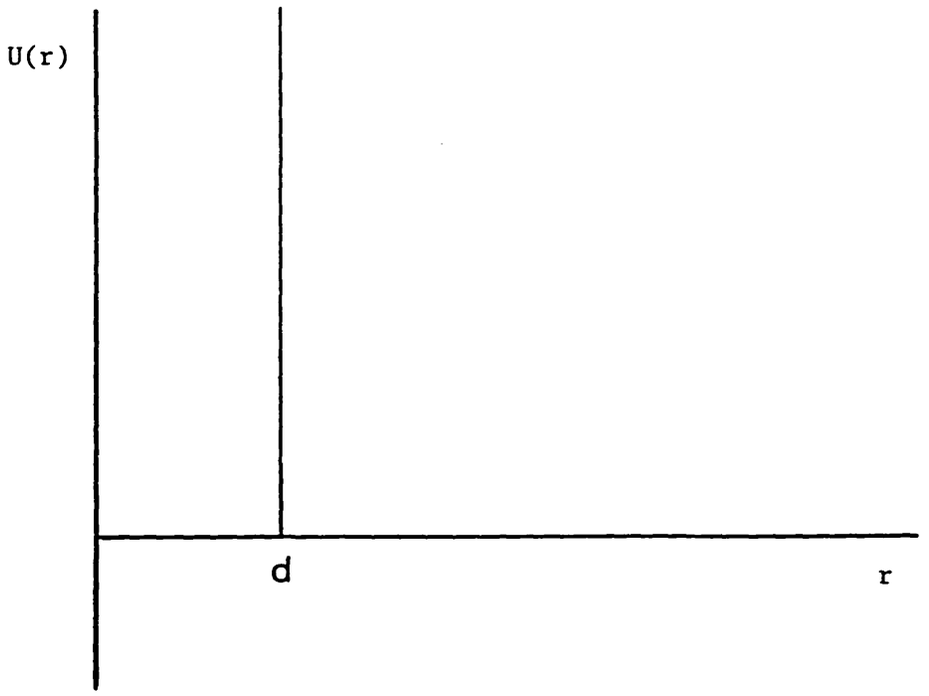

Figure 5.2 A real fluid potential.

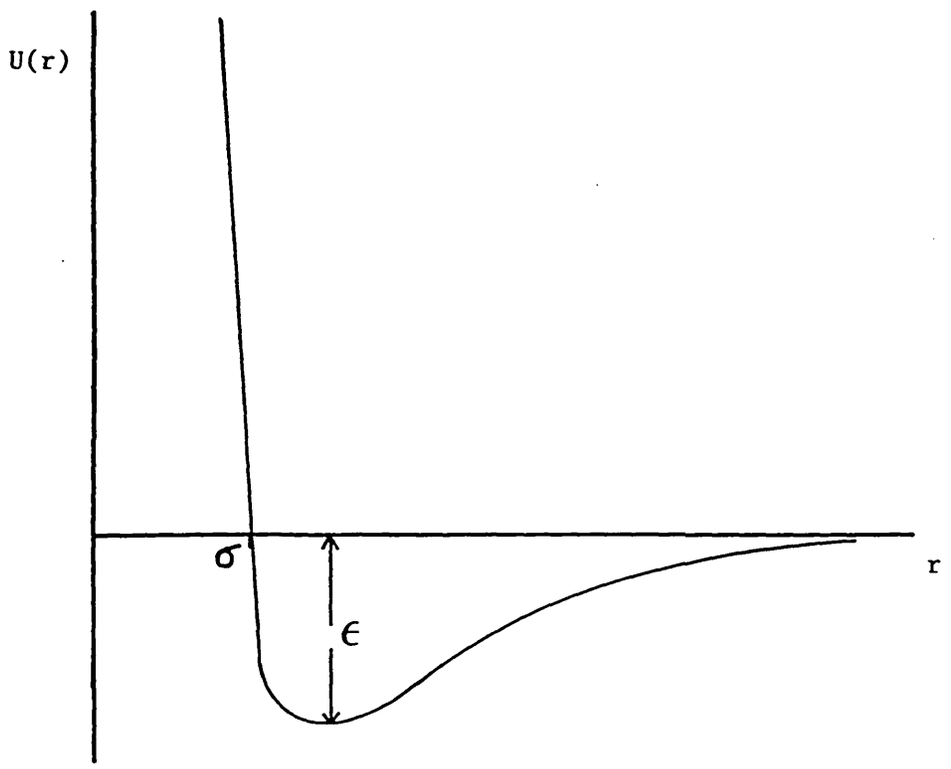

information about the pair potential is contained in $\Omega^{(2,2)^*}(T^*)$.

The kinetic theory expressions for monatomic gases can be used with effect in two main ways with respect to experimental thermal conductivity data. Fistly, in combination with high accuracy viscosity data, the Eucken factor expression can be used to verify the claimed accuracy of the thermal conductivity measurements, hence increasing the confidence in the performance of an instrument. Secondly, experimental themal conductivity data can be used as an independent test of proposed intermolecular potentials. Owing to the lack of high accuracy thermal conductivity data, potentials are generally constructed without recourse to thermal conductivity measurements. New independent data is therefore very useful to formulators of intermolecular potentials.

5.3 PURE POLYATOMIC GASES

The Chapman Enskog method provides a successful kinetic theory for monatomic gases. Polyatomic gases, however, possess features which are not present in the case of monatomic gases: (a) they have internal energy and (b) the intermolecular potential is not spherically symmetrical. These two features are coupled via the phenomena of inelastic collisions. In order to provide a formal theory for polyatomic gases, it is necessary to consider a distribution function similar to that of monatomic gases but also accounting for the internal energy state of the molecule. Additionally, the possibility of inelastic collisions must be incorporated into the binary collision dynamics.

The most widely-adopted formal theory for dilute polyatomic gases is the semi-classical kinetic theory of Wang Chang and Uhlenbeck. The translational energy of the molecules is treated

classically and the internal energy is treated quantum mechanically [5, 6]. The bulk gas is considered to be free from the influence of external fields. The single particle distribution function now refers to the distribution of velocity and internal energy in the gas. The spatial and temporal evolution of the distribution function is governed by an extension of the Boltzmann equation, the Wang Chang Uhlenbeck equation [5]

$$\frac{\partial f_i}{\partial t} + (\underline{c}.\nabla)f_i = \sum_{jkl} J_{ij}^{kl}(ff) \qquad (5.3.1)$$

where $f_i = f(\underline{c}, E_i, \underline{r}, t)$, and

$$J_{ij}^{kl}(ff) = \int\int\int (f_k'f_l' - f_if_j)gI(ij \to kl|\theta, \psi)\sin\theta d\theta d\psi d\underline{c}_1 \qquad (5.3.2)$$

Here E_i refers to the internal energy associated with quantum state i which represents a collection of quantum numbers necessary to define the internal state of the molecule. $I(ij \to kl|\theta, \psi)$ is the cross-section for scattering molecules in internal states i and j with relative speed g , such that after the collision, the molecules are in internal states k and l respectively and the relative velocity is rotated through polar angle θ and azimuthal angle ψ. Equations (5.3.1) and (5.3.2) are strictly applicable only to molecules that do not possess degenerate energy levels. This formation is considered to be justifiable in the absence of external fields and when there is no macroscopic angular momentum in the gas [14]. The inelastic collision cross-section is unknown but progress towards the transport coefficients is possible via an extension of the Chapman Enskog method [6]. The single particle distribution function of the non-uniform gas is considered to be a linear perturbation of the local

equilibrium distribution function

$$f_i = f_i^{(0)}[1 + \phi] \tag{5.3.3}$$

where

$$\phi = \frac{-1}{n} \underline{A}.\nabla \ell n\ T - \frac{1}{n} \underline{\underline{B}}:\nabla \underline{c}_0 - \frac{1}{n} \Gamma\nabla.\underline{c}_0 \tag{5.3.4}$$

and

$$f_i^{(0)} = \frac{n}{Q} \left[\frac{m}{2\pi kT}\right]^{3/2} \exp\ [-\mathscr{C}^2 + \epsilon_i] \tag{5.3.5}$$

Here n is the local number density, $\underline{c}_0$ is the local hydrodynamic velocity, T is the local temperature, m is the molecular mass, k is Boltzmann's constant and Q is the internal state partition function

$$Q = \sum_i \exp(-\epsilon_i) \tag{5.3.6}$$

in which ϵ_i is a reduced internal energy

$$\epsilon_i = E_i/kT \tag{5.3.7}$$

In addition, $\underline{\mathscr{C}}$ is the reduced pecular velocity

$$\underline{\mathscr{C}} = \left[\frac{m}{2KT}\right]^{\frac{1}{2}} \underline{C} \tag{5.3.8}$$

where

$$\underline{C} = \underline{c} - \underline{c}_0 \tag{5.3.9}$$

Linearisation of the Wang Chang–Uhlenbeck equation indicates that the quantities $\underline{A}$, $\underline{\underline{B}}$ and Γ obey the following integral equations [7]

$$\mathbb{R}\Gamma = \frac{2}{3}\left\{\left[\frac{C_{int}}{C_v}\right]\left[\mathscr{C}^2 - \frac{3}{2}\right] - \left[1 - \frac{C_{int}}{C_v}\right](\epsilon_i - \langle\epsilon\rangle_0)\right\} \quad (5.3.10)$$

$$\mathbb{R}\underline{A} = \left\{\left[\mathscr{C}^2 - \frac{5}{2}\right] + (\epsilon_i - \langle\epsilon\rangle_0)\right\}\underline{\mathscr{C}} \quad (5.3.11)$$

$$\mathbb{R}\underline{\underline{B}} = 2\,\underline{\mathscr{C}}^0\underline{\mathscr{C}} \quad (5.3.12)$$

($\underline{\mathscr{C}}^0\underline{\mathscr{C}} = \underline{\mathscr{C}}\underline{\mathscr{C}} - \frac{1}{3}\,\mathscr{C}^2\underline{\underline{I}}$), where $\mathbb{R}$ is the Wang Chang and Uhlenbeck collision operator defined by

$$n\, f_i^{(0)}\mathbb{R}(X) = \sum_{jkl}\int\int\int f_i^{(0)} f_j^{(0)}\,[X_i + X_j - X_k' - X_l']$$

$$g I_{ij}^{kl}(ij \to kl|\theta,\ \psi)\sin\theta d\theta d\psi d\underline{c}_1 \quad (5.3.13)$$

In the above equations C_{int} is the internal heat capacity of the gas per molecule, C_v is the constant volume heat capacity of the gas per molecule and the angle bracket $\langle..\rangle_0$ is defined by

$$\langle X\rangle_0 = \frac{\sum_i \int f_i^{(0)} X d\underline{c}}{\sum_i \int f_i^{(0)} d\underline{c}} \quad (5.3.14)$$

The unknown quantities Γ, $\underline{A}$ and $\underline{\underline{B}}$ are expanded in a series of orthonormal functions ϕ^{mosr} which are scalars, vectors or tensors respectively [7, 9, 15].

$$\Gamma = \sum_{r,s} c_{sr}\,\phi^{oosr} \quad (5.3.15)$$

$$\underline{A} = \sum_{r,s} a_{sr}\,\underline{\phi}^{1osr} \quad (5.3.16)$$

$$\underline{\underline{B}} = \sum_{r,s} b_{sr} \underline{\underline{\phi}}^{20sr} \tag{5.3.17}$$

The quantities ϕ^{mosr} are functions of Sonine and Wang Chang Uhlenbeck polynomials such that [9, 15]

$$\phi^{oosr} = A_{\frac{1}{2}}(s, r) S_{\frac{1}{2}}^{(s)}(\mathscr{C}^2) R^{(r)}(\epsilon_i) \tag{5.3.18}$$

$$\underline{\phi}^{1osr} = A_{3/2}(s, r) S_{3/2}^{(s)}(\mathscr{C}^2) R^{(r)}(\epsilon_i) \underline{\mathscr{C}} \tag{5.3.19}$$

$$\underline{\underline{\phi}}^{2osr} = A_{5/2}(s, r) S_{5/2}^{(s)}(\mathscr{C}^2) R^{(r)}(\epsilon_i) \underline{\underline{\mathscr{C}^0}}\,\underline{\underline{\mathscr{C}}} \tag{5.3.20}$$

In addition,

$$A_{\frac{1}{2}}(s, r) = \left[\frac{1}{2}\right]^{\frac{1}{2}} \left[\frac{k}{C_{int}}\right]^{r/2} \pi^{\frac{1}{4}} \left[\frac{s!}{(\frac{1}{2}+s)!}\right]^{\frac{1}{2}} \tag{5.3.21}$$

$$A_{3/2}(s, r) = \left[\frac{3}{2}\right]^{\frac{1}{2}} \left[\frac{k}{C_{int}}\right]^{r/2} \pi^{\frac{1}{4}} \left[\frac{s!}{(3/2+s)!}\right]^{\frac{1}{2}} \tag{5.3.22}$$

$$A_{5/2}(s, r) = \left[\frac{15}{4}\right]^{\frac{1}{2}} \left[\frac{k}{C_{int}}\right]^{r/2} \pi^{\frac{1}{4}} \left[\frac{s!}{(5/2+s)!}\right]^{\frac{1}{2}} \tag{5.3.23}$$

The Sonine polynomials are given by the expression

$$S_p^{(s)}(\mathscr{C}^2) = \sum_{L=0}^{s} \frac{(-\mathscr{C}^2)^L (p+s)!}{(p+L)(s-L)!L!} \tag{5.3.24}$$

and the first two terms of the Wang Chang Uhlenbeck polynomial defined by Wang Chang and Uhlenbeck are [5]

$$R^{(0)}(\epsilon_i) = 1 \quad \text{and} \quad R^{(1)}(\epsilon_i) = \epsilon_i - \langle \epsilon_i \rangle_0 \tag{5.3.25}$$

By following methods similar to those adopted for monatomic gases, the transport coefficients can be related to the first terms in the series expansions (i.e. equations 5.3.18–5.3.20).
Hence [6, 7, 9],

$$k^{o} = \frac{-2kT}{3}\left[\frac{C_{int}}{k}\right]^{\frac{1}{2}} C_{01} \qquad (5.3.26)$$

for the bulk viscosity

$$\lambda^{o} = \frac{2k^{2}T}{m}\left[-\left[\frac{5}{4}\right]^{\frac{1}{2}} a_{10} + \left[\frac{C_{int}}{k}\right]^{\frac{1}{2}} a_{01}\right] \qquad (5.3.27)$$

for thermal conductivity, and

$$\eta^{o} = \left[\frac{1}{2}\right]^{\frac{1}{2}} kTb_{00} \qquad (5.3.28)$$

for shear viscosity.

Using the expansion equations (5.3.18–5.3.20) in the integral equations (5.3.10–5.3.12) [9] or by using a variational procedure [6] a doubly infinite set of algebraic equations for the coefficients a_{sr}, b_{sr} and c_{sr} is obtained [6, 7, 9].

$$\sum_{s'=0}^{\infty}\sum_{r'=0}^{\infty} c_{s'r'}\langle\phi^{oosr}\mathbb{R}(\phi^{oos'r'})\rangle_{0} = -\left[\frac{2}{3}\right]^{\frac{1}{2}}\left[\frac{C_{int}}{C_{v}}\right]\delta s_{1}\delta r_{0} +$$

$$\left[\frac{C_{int}}{C_{v}} - 1\right]\frac{2}{3}\left[\frac{C_{int}}{k}\right]^{\frac{1}{2}}\delta s_{0}\delta r_{1} \qquad (5.3.29)$$

$$\sum_{s'=0}^{\infty}\sum_{r'=0}^{\infty} a_{s'r'}\langle \underline{\phi}^{1osr}\mathbb{R}(\phi^{1os'r'})\rangle_0 = -3\left[\frac{5}{4}\right]^{\frac{1}{2}}\delta s_1\delta r_0 + 3\left[\frac{C_{int}}{k}\right]^{\frac{1}{2}}\delta s_0\delta r_1 \tag{5.3.30}$$

$$\sum_{s'=0}^{\infty}\sum_{r'=0}^{\infty} b_{s'r'}\langle \underline{\phi}^{2osr}\mathbb{R}(\underline{\phi}^{2os'r'})\rangle_0 = 5\sqrt{2}\,\delta s_0\delta r_0 \tag{5.3.31}$$

in all cases r, s = 0 → ∞.

Expressions for the expansion coefficients c_{01}, a_{10}, a_{01} and b_{00} are obtained by solution of equations (5.3.29–5.3.31). The first–order expressions are recovered by retaining the first non–zero terms of equivalent order in the expansion. For viscosity only one term is required, i.e. s = 0, r = 0. For thermal conductivity and bulk viscosity the terms s = 1, r = 0 and r = 1, s = 0 are retained since $a_{00} = c_{00} = 0$ [9]. Finally, the expressions for the first–order transport coefficients are obtained

$$[k^o]_1 = \frac{2kT(C_{int}/C_v)^2}{3\langle v\rangle_0 \mathcal{S}(0010)} \tag{5.3.32}$$

$$[\lambda^o]_1 = [\lambda^o_{tr}]_1 +]\lambda^o_{int}]_1 \tag{5.3.33}$$

where

$$[\lambda^o_{tr}]_1 = \frac{5k^2T}{2m\langle v\rangle_0}\left\{\frac{\mathcal{S}(1001) + (\frac{2C_{int}}{5k})^{\frac{1}{2}}\mathcal{S}(\substack{1010\\1001})}{\mathcal{S}(1010)\mathcal{S}(1001) - \mathcal{S}(\substack{1010\\1001})^2}\right\} \tag{5.3.34}$$

and

$$[\lambda^o_{int}]_1 = \frac{5k^2T}{2m\langle v\rangle_0}\left\{\frac{(\frac{2C_{int}}{5k})^{\frac{1}{2}}\mathcal{S}(\substack{1010\\1001}) + (\frac{2C_{int}}{5k})\mathcal{S}(1010)}{\mathcal{S}(1010)\mathcal{S}(1001) - \mathcal{S}(\substack{1010\\1001})^2}\right\} \tag{5.3.35}$$

and

$$[\eta^o]_1 = \frac{kT}{\langle v\rangle_0}\,\frac{1}{\mathcal{S}(2000)} \tag{5.3.36}$$

Here

$$\langle v\rangle_0 = 4\left[\frac{kT}{\pi m}\right]^{\frac{1}{2}} \tag{5.3.37}$$

and the following effective cross-sections have been introduced

$$\mathcal{S}\begin{bmatrix} oosr \\ oos'r' \end{bmatrix} = \langle \phi^{oosr} \mathbb{R}(\phi^{oos'r'})\rangle_0 / \langle v\rangle_0 \tag{5.3.38}$$

$$\mathcal{S}\begin{bmatrix} 1osr \\ 1os'r' \end{bmatrix} = \langle \underline{\phi}^{1osr} . \mathbb{R}(\underline{\phi}^{1os'r'})\rangle_0 / 3\langle v\rangle_0 \tag{5.3.39}$$

$$\mathcal{S}\begin{bmatrix} 2osr \\ 2os'r' \end{bmatrix} = \langle \underline{\underline{\phi}}^{2osr} : \mathbb{R}(\underline{\underline{\phi}}^{2os'r'})\rangle_0 / 5\langle v\rangle_0 \tag{5.3.40}$$

These effective cross-sections contain all the information about the binary molecular collision process and the intermolecular potential. In order to increase the general accuracy of the result, it is possible to correct the above expression for thermal conductivity to account for the effects of spin polarisation [10] (see Appendix 5B). According to the Viehland-Mason-Sandler formalism [10]

$$[\lambda^0]_1 = [\lambda^0_{tr}]_1 + [\lambda^0_{int}]_1 \tag{5.3.41}$$

$$[\lambda^0_{tr}]_1 = \frac{5k^2T}{2m\langle v\rangle_0}\left\{\frac{\mathcal{S}(1001) + (\frac{2C_{int}}{5k})^{\frac{1}{2}}\mathcal{S}\binom{1010}{1001}}{\mathcal{S}(1010)\mathcal{S}(1001) - \mathcal{S}\binom{1010}{1001}}\right\} \tag{5.3.42}$$

$$[\lambda^0_{int}]_1 = \frac{5k^2T}{2m\langle v\rangle_0}\left\{\frac{(\frac{2C_{int}}{5k})^{\frac{1}{2}}\mathcal{S}\binom{1010}{1001} + (\frac{2C_{int}}{5k})\mathcal{S}(1010)}{\mathcal{S}(1010)\mathcal{S}(1001) - \mathcal{S}^2\binom{1010}{1001}}\right\} . S \tag{5.3.43}$$

where

$$S \simeq 1 - \frac{5}{3}\left[1 + \left[\frac{\lambda^0_{tr}}{\lambda^0_{int}}\right]\left[\frac{\Delta\lambda_n}{\lambda}\right]_{sat}\right] \tag{5.3.44}$$

Here $(\Delta\lambda_{\parallel}/\lambda)_{sat}$ is the fractional change in thermal conductivity of a gas parallel to a magnetic field observed at saturation.

An alternative formulation for the thermal conductivity was obtained by Thijsse *et al.* [17]. Rather than working with individual translation and internal contributions to the total heat flux, they attempted to describe the thermal conductivity starting from the total heat flux. In order to do this they used a different set of basis vectors for the expansion vector $\underline{A}$ in equation (5.3.16). The first of these is proportional to the total heat flux

$$\underline{\phi}^{101+1} = \left[\frac{4}{5\left[1 + \frac{2C_{int}}{5k}\right]}\right]^{\frac{1}{2}} \left\{\mathcal{C}^2 - 5/2 + \epsilon_i - \langle\epsilon\rangle_0\right\}\underline{\mathcal{C}} \qquad (5.3.45)$$

The second is proportional to the difference of the two fluxes

$$\underline{\phi}^{101-1} = \left[\frac{4}{5\left[1 + \frac{2C_{int}}{5k}\right]}\right]^{\frac{1}{2}} \left\{\left[\frac{2C_{int}}{5k}\right]^{\frac{1}{2}} (\mathcal{C}^2 - 5/2) - \left[\frac{5k}{2C_{int}}\right]^{\frac{1}{2}} (\epsilon_i - \langle\epsilon\rangle_0)\right\}\underline{\mathcal{C}} \qquad (5.3.46)$$

Using these new expansion vectors they found a second-order approximation to the thermal conductivity

$$[\lambda^0]_2^T = \frac{5k^2T}{2m\langle v\rangle_0} \frac{(1 + 2C_{int}/5k)}{\mathcal{S}(101+1)} \left\{1 - \frac{\mathcal{S}^2\binom{101+1}{101-1}}{\mathcal{S}(101+1)\mathcal{S}(101-1)}\right\} \qquad (5.3.47)$$

The superscript T indicates the Thijsse formalism.

A possible advantage of this formulation over the Viehland-Mason-Sandler formalism is that the coupling cross-section $\mathcal{S}\binom{101+1}{101-1}$ is often small compared with $\mathcal{S}(101+1)$ and $\mathcal{S}(101-1)$ [17].

Hence, the thermal conductivity may be well represented by the first–order expression

$$[\lambda^{o}]_1^T = \frac{5k^2T}{2m\langle v\rangle_0} \frac{(1 + 2C_{int}/5k)}{\mathfrak{S}(101+1)} \qquad (5.3.48)$$

The validity of this simple expression has been tested theoretically and experimentally [8] in addition to the study performed by Thijsse *et al.* This equation will be the subject for further investigation in the light of new high accuracy data. (See chapter 6.)

The task now is explicitly to evaluate the effective cross–sections given an intermolecular potenital. The difficulty is the immense computational effort required in order to evaluate the inelastic scattering cross–section. No exact calculations have been performed for realistic potentials. Attention has therefore been turned to either of two options. Firstly, the kinetic theory expressions could be simplified in order to facilitate routine calculation and, secondly, relationships between transport coefficients can be investigated.

It is worth noting that the kinetic theory expressions for thermal conductivity and viscosity contain different effective cross–sections. There is therefore no simple relationship relating the two coefficients as there was in the case of monatomic gases. Thermal conductivity and viscosity yield complementary information about the intermolecular forces. The polyatomic gas thermal conductivity also depends on many more effective cross–sections than the monatomic gases. However, the polyatomic gases have extra transport properties which can be related to the existing effective cross–sections. Two such transport properties are the collision number of internal energy relaxation [19]

$$\zeta_{int} = \frac{4kT}{\pi\eta\langle v\rangle_0} \mathcal{S}^{-1}(0001) \qquad (5.3.49)$$

and the so–called diffusion coefficient for internal energy [16]

$$D_{int} = \frac{kT}{nm\langle v\rangle_0} (\mathcal{S}(1001) - (\tfrac{1}{2})\mathcal{S}(0001))^{-1} \qquad (5.3.50)$$

These transport properties may be used to relate the viscosity and thermal conductivity to produce a result that is exact within the Wang Chang Uhlenbeck theory [20]

$$\frac{[\lambda^0]_1}{[\eta^0]_1} = \frac{([\lambda^0_{tr}]_1 + [\lambda^0_{int}]_1)}{[\eta^0]_1} \qquad (5.3.51)$$

$$\frac{[\lambda_{tr}{}^0]_1}{[\eta^0]_1} = \frac{5k}{2m}\left[\frac{3}{2} - \Delta\right] \qquad (5.3.52)$$

$$\frac{[\lambda^0_{int}]_1}{[\eta^0]_1} = \frac{\rho D_{int}}{[\eta^0]_1}\left[\frac{C_{int}}{k} + \Delta\right] \qquad (5.3.53)$$

with

$$\Delta = \frac{2C_{int}}{k\pi\zeta_{int}}\left[2.5 - \frac{\rho D_{int}}{[\eta^0]_1}\right]\left\{1 + \left[\frac{2}{\pi\zeta_{int}}\right]\left[\frac{5C_{int}}{3k} + \frac{\rho D_{int}}{[\eta^0]_1}\right]\right\}^{-1} \qquad (5.3.54)$$

Again the effects of spin polarisation can be included to produce, within the Viehland–Mason–Sandler formalism, a correction to the internal energy contribution

$$\frac{[\lambda^0_{int}]_1}{[\eta^0]_1} = \frac{\rho D_{int}}{[\eta^0]_1}\left[\frac{C_{int}}{k} + \Delta\right]\left\{1 - \frac{5}{3}\left[1 + \frac{\lambda^0_{tr}}{\lambda^0_{int}}\right]\left[\frac{\Delta\lambda_{\prime\prime}}{\lambda}\right]_{sat}\right\} \qquad (5.3.55)$$

Since D_{int} is not accessible to experiment, progress can be made via the kinetic theory result

$$\frac{\rho D_{int}}{[\eta^0]_1} = \frac{6}{5} A^* \frac{D_{int}}{D} \qquad (5.3.56)$$

where D is the hypothetical self-diffusion coefficient defined by

$$D = \frac{kT}{\rho \langle v \rangle_0} \mathfrak{S}^{-1}(1000) \qquad (5.3.57)$$

and A^* is a ratio of effective cross-sections [2] which is only a weak function of the intermolecular potential [9]. Equations (5.3.51)-(5.3.57) represent the most complete equations linking the thermal conductivity with other transport properties. They represent the usual method for calculation of thermal conductivity from viscosity and the other trransport property data. In order to carry through this calculation some statement about the ratio D_{int}/D must be made. It is general to assume that $D_{int}/D = 1$. It has been shown that making this assumption can lead to serious errors in the calculation of thermal conductivity. These errors may have arisen as a consequence of the first-order nature of the kinetic theory expressions. By retaining more terms in the equations for the expansion coefficients (5.3.29)-(5.3.31) higher-order expressions for the transport coefficients may be obtained [7, 9]. These expressions contain further cross-sections which are functions of the intermolecular potential. Model calculations using the rough hard-sphere model indicate that the second-order corrections are not greatly affected by the inelasticity of collisions and are generally of order 2% of the individual transport coefficients and about 1% for Eu [21].

It is the intention of this study to investigate the behaviour of individual cross-sections appearing in the kinetic theory expressions and also to investigate the value of the ratio D_{int}/D for

a number of gases over a range of temperatures. A detailed study of this type is only possible with the aid of high accuracy thermal conductivity and viscosity data since, as will be shown later, the value of D_{int}/D is sensitive to small errors in these quantities.

5.4 THE THERMAL CONDUCTIVITY OF POLYATOMIC GAS MIXTURES

5.4.1 The Formal Theory

A formal kinetic theory based on a generalised Boltzmann equation has been developed within the first-order Wang Chang-Uhlenbeck kinetic theory [14]. Experience with monatomic gas mixtures has indicated that first-order theory is insufficient adequately to describe the thermal conductivity of binary gas mixtures [8]. Expressions equivalent to a third-order Chapman Cowling approximation [1, 2, 8] were necessary properly to represent the thermal conductivity of a gas mixture consisting of molecules with molecular mass ratio very different from unity (e.g. helium and neon). Anticipating that a similar situation arises in the case of polyatomic gas mixtures, a formal theory for the thermal conductivity is presented.

The starting point for a formal theory is the single particle distribution function f_{qi} defined such that

$$f_{qi}\ d\underline{r}\ d\underline{c} = f_q(\underline{c}_q, E_{qi}, \underline{r}, t)\ d\underline{r}\ d\underline{c} \qquad (5.4.1.1)$$

is the probable number of molecules of component q of an N-component mixture, possessing internal energy E_i, occupying the elemental volume $d\underline{r}d\underline{c}$ in 6-D phase space. Once again, the subscript i denotes a collection of quantum numbers appropriate to describe the internal state of the molecule.

The spatial and temporal evolution of f_{qi} is governed by a proposed generalisation of the Boltzmann equation

$$\frac{\partial f_{qi}}{\partial t} + (\underline{c}_q.\nabla)f_{qi} = \sum_{q'} \sum_{jkl} qq' \, J_{ij}^{kl}(ff)$$

where

$$qq' J_{ij}^{kl}(ff) = \int \cdots \int (f'_{qk} f'_{q'l} - f_{qi} f_{q'j}) gI(ij \rightarrow kl|\theta, \phi)$$

$$\sin\theta d\theta d\phi d\underline{c}_{1q} \qquad (5.4.1.2)$$

and $I(ij \rightarrow kl|\theta, \phi)$ is the differential scattering cross-section. The subscript 1 differentiates between colliding molecules when they are of the same species. q' represents the q'th component and the other prime , on f , indicates conditions after the collision. Equation (5.4.1.2) exists for each quantum state i for each component of the mixture. It also implicitly assumes strict symmetry of inverse collisions [14] and that a single temperature is sufficient to describe the equilibrium between internal energy and translational energy of the molecules. Solution of equation (5.4.1.2), which is a generalised Wang Chang Uhlenbeck equation, can be obtained via application of the Chapman Enskog method. The distribution function is expanded as a perturbation of a local equilibrium distribution function. In the linear approximation

$$f_{qi} = f_{qi}^{(0)} (1 + \phi_{qi}) \qquad (5.4.1.3)$$

The macroscopic properties of the fluid may be obtained from f_{qi}

$$n_q(\underline{r}, t) = \sum_i \int f_{qi} \, d\underline{c}_q \qquad (5.4.1.4)$$

$$\rho \underline{c}_0(\underline{r}, t) = \sum_q \sum_i \int f_{qi}\, m_q\, \underline{C}_q\, d\underline{c}_q \qquad (5.4.1.5)$$

$$\rho U(\underline{r}, t) = \sum_q \sum_i \int f_{qi}(\tfrac{1}{2} m_q \underline{C}_q^2 + E_{qi}) d\underline{c}_q \qquad (5.4.1.6)$$

where

$$\rho = \Sigma\, n_q\, m_q \qquad (5.4.1.7)$$

and

$$\underline{C}_q = \underline{c}_q - \underline{c}_0 \qquad (5.4.1.8)$$

Identification of n_q, $\underline{c}_0$ and U as the local equilibrium number density, mass average velocity and energy per unit mass leads to the Chapman Enskog auxiliary conditions

$$\sum_i \int f_{qi}^{(0)}\, \phi_{qi}\, d\underline{c}_q = 0 \qquad (5.4.1.9)$$

$$\sum_q \sum_i \int f_{qi}^{(0)}\, \phi_{qi}\, m_q\, \underline{C}_q\, d\underline{c}_q = 0 \qquad (5.4.1.10)$$

$$\sum_q \sum_i \int f_{qi}^{(0)}\, \phi_{qi} (\tfrac{1}{2} m_q\, C_q^2 + E_{qi}) d\underline{c}_q = 0 \qquad (5.4.1.11)$$

The procedure is now the same as for pure polyatomic gases. The perturbation function is considered to be linear in the macroscopic gradients

$$\phi_{qi} = \frac{-1}{n} \underline{A}_q . \nabla\, \Omega n\, T - \frac{1}{n} \underline{\underline{B}}_q : \nabla \underline{c}_0 - \frac{1}{n} \Gamma_q\, \nabla . \underline{c}_0 - \frac{1}{n} \sum_{q'} \underline{F}_q^{q'} . \underline{d}_q \qquad (5.4.1.12)$$

where $\underline{A}_q$, $\underline{\underline{B}}_q$, $\underline{F}_q^{q'}$ and Γ_q are unknown coefficients and $\underline{d}_q$ is the qth component diffusion gradient given, in the absence of external forces, by

$$\underline{d}_q = \nabla\left[\frac{n_q}{n}\right] + \left[\left[\frac{n_q}{n}\right] - \frac{n_q m_q}{\rho}\right] \nabla \ell n\ P \qquad (5.4.1.13)$$

where P is the total pressure. Linearisation of the Wang Chang Uhlenbeck equation indicates that the unknown coefficients obey the following integral equations [9]

$$\sum_{q'} \frac{n_{q'}}{n^2} \mathbb{R}_{qq'}(\Gamma_q) = \frac{1}{n}\left[\frac{C_{int}}{C_v}\right]\left[\frac{2}{3}\left[\mathscr{C}_q^2 - \frac{2}{3}\right] + \left[\frac{k}{C_{int}}\right](\epsilon_{qi} - \bar{\epsilon}_q)\right] \qquad (5.4.1.14)$$

$$\sum_{q'} \frac{n_{q'}}{n^2} \mathbb{R}_{qq'}(\underline{A}_q) = \frac{1}{n}\left[\frac{2kT}{m_q}\right]^{\frac{1}{2}}\left[\left[\mathscr{C}_q - \frac{5}{2}\right] + (\epsilon_{qi} - \bar{\epsilon}_q)\right]\underline{\mathscr{C}}_q \qquad (5.4.1.15)$$

$$\sum_{q'} \frac{n_{q'}}{n^2} \mathbb{R}_{qq'}(\underline{\underline{B}}_q) = \frac{2}{n}\underline{\mathscr{C}}_q^{o}\underline{\mathscr{C}}_q \qquad (5.4.1.16)$$

$$\sum_{q'} \frac{n_{q'}}{n^2} \mathbb{R}_{qq'}(\underline{F}_q^k) = \frac{1}{n_q}(\delta_{qk} - \gamma_q)\left[\frac{2kT}{m_q}\right]^{\frac{1}{2}} \underline{\mathscr{C}}_q \qquad (5.4.1.17)$$

where

$$\bar{\epsilon}_q = Q^{-1} \sum \epsilon_{qi} \exp(-\epsilon_{qi}) \qquad (5.4.1.18)$$

and

$$n_{q'} f_{qi}^{(0)} \mathbb{R}_{qq'}(X) = \sum_{jkl} \int\!\!\ldots\!\int f_{qi}^{(0)} f_{q'j}^{(0)} gI(ij \rightarrow kl)|\theta, \psi)$$
$$[X_{qi} + X_{q'j} - X'_{qk} - X'_{q'i}]\sin\theta d\theta d\psi d\underline{c}_{1q'} \qquad (5.4.1.19)$$

Equation (5.3.17) contains the Kronecker delta function δ_{qk} and

$$\gamma_q = \frac{\rho_q}{\rho} \qquad (5.4.1.20)$$

This complication arises from the lack of linear independence of the diffusion gradients [6, 11]

$$\sum_q \underline{d}_q = 0 \qquad (5.4.1.21)$$

The integral equations can be solved for the unknown coefficients, the uniqueness of the solution is guaranteed by the auxiliary conditions (equations (5.4.1.9)–(5.4.1.11)) which imply the following conditions on Γ_q, $\underline{A}_q$ and $\underline{F}^k_q$. (The tensor $\underline{\underline{B}}_q$ automatically satisfies the auxiliary conditions).

$$\sum_i \int f^{(0)}_{qi} \, \Gamma_q \, d\underline{c}_q = 0 \qquad (5.4.1.22)$$

$$\sum_q \sum_i \int \sqrt{m_q} \, f^{(0)}_{qi} (\underline{A}_q \cdot \underline{\mathscr{C}}_q) d\underline{c}_q = 0 \qquad (5.4.1.23)$$

$$\sum_q \sum_i \int f^{(0)}_{qi} \, \Gamma_q \, (\tfrac{1}{2} m_q C_q^2 + E_{qi}) d\underline{c}_q = 0 \qquad (5.4.1.24)$$

$$\sum_q \sum_i \int \sqrt{m_q} \, f^{(0)}_{qi} (\underline{F}^k_q \cdot \underline{\mathscr{C}}_q) d\underline{c}_q = 0 \qquad (5.4.1.25)$$

5.4.2 Expressions for the Transport Coefficients

In this section the transport equations necessary for the evaluation of the thermal conductivity of the mixture are derived.

The average diffusion velocity of component q of the N–component mixture is

$$\langle \underline{C}_q \rangle_{AV} = \frac{1}{n_q} \sum_i \int f_{qi} \, \underline{C}_q \, d\underline{c}_q \qquad (5.4.2.1)$$

Substitution for the linear approximation to f_{qi} results in

$$\langle \underline{C}_q \rangle_A = \frac{1}{n_q} \sum_i \int f_{qi}^{(0)} \phi_{qi} \underline{C}_q \, d\underline{c}_q \qquad (5.4.2.2)$$

$$= \frac{-1}{3nn_q} \sum_i \sum_{q'} \int f_{qi}^0 \underline{F}_q^{q'} . \underline{C}_q \, d\underline{c}_q \, \underline{d}_{q'}$$

$$- \frac{-1}{3nn_q} \sum_i \int f_{qi}^0 \underline{A}_q . \underline{C}_q \, d\underline{c}_q \nabla \ell n \, T \qquad (5.4.2.3)$$

The equation for the diffusion velocity may be written in the form [6]

$$\langle \underline{C}_q \rangle_{AV} = - \sum_{q'} D_{qq'} \underline{d}_{q'} - D_q^T \nabla \ell n \, T \qquad (5.4.2.4)$$

The above allows identification of the multicomponent diffusion coefficient, $D_{qq'}$, and the thermal diffusion coefficient, D_q^T.

$$D_{qq'} = \frac{1}{3nn_q} \sum_i \int f_{qi}^{(0)} \underline{F}_q^{q'} . \underline{C}_q \, d\underline{c}_q \qquad (5.4.2.5)$$

$$D_q^T = \frac{1}{3nn_q} \sum_i \int f_{qi}^{(0)} \underline{A}_q . \underline{C}_q \, d\underline{c}_q \qquad (5.4.2.6)$$

It is useful to divide the collision operator $\mathbb{R}$ into partial operators such that

$$\sum_{q'} n_{q'} \mathbb{R}_{qq}(X) = \sum_{q'} n_{q'} [\mathbb{R}_{qq}^{(1)}(X) + \mathbb{R}_{qq}^{(2)}(X)] \qquad (5.4.2.7)$$

where

$$n_{q'} f_{qi}^{(0)} \mathbb{R}_{qq}^{(1)}(X) = \sum_{jkl} \int \ldots \int f_{qi}^{(0)} f_{qj}^{(0)} gI(ij \to kl | \theta, \psi)$$

$$[X_{qi} - X'_{qk}] \sin\theta d\theta d\psi d\underline{c}_{1q'} \qquad (5.4.2.8)$$

and

$$n_{q'} f^{(0)}_{q1} \mathbb{R}^{(2)}_{qq'}(X) = \sum_{jkl} \int \ldots \int f^{(0)}_{q1} f^{(0)}_{q'j} \, gI(ij \to kl|\theta, \psi)$$

$$[X_{q'j} - X'_{q'i}] \sin\theta d\theta d\psi d\underline{c}_{1q'} \qquad (5.4.2.9)$$

It is also useful to define the integral <<X>>:

$$\langle\langle \underline{X} \rangle\rangle = \sum_q \sum_{q'} \frac{n_q n_{q'}}{n^2} \{\langle\langle \underline{X}.\mathbb{R}^{(1)}(\underline{X})\rangle\rangle_0 + \langle\langle \underline{X}.\underline{\mathbb{R}}^{(2)}(X)\rangle\rangle_0\} \qquad (5.4.2.10)$$

where

$$\langle\langle \underline{X} \rangle\rangle_0 = \frac{1}{n_q} \sum_i \int f^{(0)}_{q1} \, \underline{X} \, d\underline{c}_q \qquad (5.4.2.11)$$

Using these definitions, the integral equations and the auxiliary conditions, the following equations have been derived

$$\langle\langle \underline{F}^{k'}_q . \mathbb{R}(\underline{F}^k_q) \rangle\rangle = \frac{1}{n_k} \sum_i \int f^{(0)}_{ki} \, \underline{F}^{k'}_k . \underline{C}_k \, d\underline{c}_k \qquad (5.4.2.12)$$

$$\langle\langle \underline{A}_q . \mathbb{R}(\underline{F}^k_q) \rangle\rangle = \frac{1}{n_k} \sum_i \int f^{(0)}_{ki} \, \underline{A}_k . \underline{C}_k \, d\underline{c}_k \qquad (5.4.2.13)$$

These equations can be compared with equation (5.4.2.5) and (5.4.2.6) in order to obtain the formal kinetic theory expressions for the multicomponent diffusion coefficient and thermal diffusion coefficient.

$$D_{qq'} = \frac{1}{3n} \langle\langle \underline{F}^{q'}_q . \mathbb{R}(\underline{F}^q_q) \rangle\rangle \qquad (5.4.2.14)$$

$$D^T_q = \frac{1}{3n} \langle\langle \underline{A}_q . \mathbb{R}(\underline{F}^q_q) \rangle\rangle \qquad (5.4.2.15)$$

A similar prcoedure may be carried out for the heat flux vector $\underline{q}$.

$$\underline{q} = \sum_q \sum_i \int f_{qi}(\tfrac{1}{2} m_q C_q^2 + E_{qi})\underline{C}_q \, d\underline{c}_q \qquad (5.4.2.16)$$

In the linear approximation to f_{qi}

$$\underline{q} = kT \sum_q \left[\frac{5}{2} + \bar{\epsilon}_q\right] n_q \langle \underline{C}_q \rangle_{AV} - \lambda^0 \nabla T - nkT \sum_q D_q^T \underline{d}_q \qquad (5.4.2.17)$$

where

$$\lambda^0 = \lambda^0_{int} + \lambda^0_{tr} \qquad (5.4.2.18)$$

and

$$\lambda^0_{tr} = \frac{k}{3n} \sum_q \left[\frac{2kT}{m_q}\right]^{\frac{1}{2}} \sum_i \int f^{(0)}_{qi}\left[\underline{\mathscr{C}}_q^2 - \frac{5}{2}\right] (\underline{A}_q \cdot \underline{\mathscr{C}}_q)\Big] d\underline{c}_q \qquad (5.4.2.19)$$

$$\lambda^0_{int} = \frac{k}{3n} \sum_q \left[\frac{2kT}{m_q}\right]^{\frac{1}{2}} \sum_i \int f^{(0)}_{qi}\left[\epsilon_{qi} - \bar{\epsilon}_q\right] (\underline{A}_q \cdot \underline{\mathscr{C}}_q)\Big] d\underline{c}_q \qquad (5.4.2.20)$$

Finally, ofter some manipulation [9]

$$\lambda^0 = \frac{k}{3} \langle\langle \underline{A}_q \cdot \mathbb{R}(\underline{A}_q) \rangle\rangle \qquad (5.4.2.21)$$

λ^0_{tr} and λ^0_{int} are the translational and internal contributions to the thermal conductivity of a gas of uniform composition. The first term in the heat flux vector (equation 5.4.2.17) represents a flux of energy due to the diffusion of molecules with respect to a coordinate system moving with the mass average velocity $\underline{c}_0$. The second term accounts for the flux of energy due to the temperature gradient. The third term represents the flux of energy due to the phenomena of thermal diffusion. λ^0 therefore is not the thermal conductivity measured by experiment because this always involves a gas of non-uniform composition. The diffusion terms must be eliminated from the heat flux vector, then the coefficient of an overall temperature

gradient is identified as the thermal conductivity measured by experiment. The elimination of the diffusion gradient from the heat flux vector is achieved using a matrix vector method which is a generalisation by Monchick, Mun and Mason [22] of a method originally used by Muckenfuss and Curtiss for monatomic mixtures [23] and applied by Monchick et al [22] to derive a generalised Stephan–Maxwell equation. The same method is applied here to the derivation of new higher–order expressions for thermal conductivity.

Equations (5.4.2.14), (5.4.2.15) and (5.4.2.21) are formal expressions for the transport coefficients of interest here. Explicit expressions for λ^0, D_q^T and $D_{qq'}$ are obtained by solution of the integral equations for the unknown vectors $\underline{A}_q$ and $\underline{F}_q^{q'}$. A method of solution has been used that recognises that a complete solution of the integral equations is not necessary. The formal expressions indicate that the equilibrium averages of the solutions of the integral equations are all that is required.

5.4.3 Explicit Solution for the Transport Coefficients

The unknown coefficients ($\underline{A}_q$, $\underline{F}_q^{q'}$) are expanded into a double series of orthonormal polynomials

$$\underline{F}_q^k = \sum_{s,r} F_{qsr}^k \, \underline{\phi}_q^{1osr} \qquad (5.4.3.1)$$

$$\underline{A}_q = \sum_{s,r} a_{qsr} \, \underline{\phi}_q^{1osr} \qquad (5.4.3.2)$$

where

$$\underline{\phi}_q^{1osr} = A_{3/2}(q, s, r) S_{3/2}^{(s)}(\mathscr{C}_q^2) R^{(r)}(\epsilon_{qi}) \underline{\mathscr{C}}_q \qquad (5.4.3.3)$$

$S_{3/2}^{(s)}(\mathscr{C}_q^2)$ are Sonine polynomials; $R^{(r)}(\epsilon_{qi})$ are Wang Chang Uhlenbeck

polynomials; $A_{3/2}(q, s, r)$ is a normalisation factor defined by

$$A_{3/2}(q, s, r) = \left[\frac{3}{2}\right]^{\frac{1}{2}} \left[\frac{k}{C_{int,q}}\right]^{r/2} \pi^{\frac{1}{4}} \left[\frac{S!}{\left[\frac{3}{2} + S\right]!}\right]^{\frac{1}{2}} \quad (5.4.3.4)$$

and F^{k}_{qsr} and a_{qsr} are expansion coefficients. Substitution of the expansion forms into the equations for the transport coefficients (equations (5.4.2.5), (5.4.2.6) and (5.4.2.18), (5.4.2.19)) expressions for the transport coefficients are obtained in terms of the expansion coefficients

$$D_{qq'} = \frac{1}{n} \left[\frac{kT}{m_q}\right]^{\frac{1}{2}} F^{q'}_{qoo} \quad (5.4.3.5)$$

$$D^{T}_{q} = \frac{1}{n} \left[\frac{kT}{m_q}\right]^{\frac{1}{2}} a_{qoo} \quad (5.4.3.6)$$

$$\lambda^{0}_{tr} = -\left[\frac{5}{4}\right]^{\frac{1}{2}} k \sum_{q} \left[\frac{2kT}{m_q}\right]^{\frac{1}{2}} x_q \, a_{q1o} \quad (5.4.3.7)$$

$$\lambda^{0}_{int} = \left[\frac{1}{2}\right]^{\frac{1}{2}} k \sum_{q} \left[\frac{2kT}{m_q}\right]^{\frac{1}{2}} \left[\frac{C_{q,int}}{k}\right]^{\frac{1}{2}} x_q \, a_{qo1} \quad (5.4.3.8)$$

where

$$x_q = \frac{n_q}{n} \quad (5.4.3.9)$$

As was the case for pure monatomic and pure polyatomic gases, the transport coefficients are functions of a single expansion coefficient. Explicit expressions for the expansion coefficients are obtained from the integral equations either by application of the variational principle [6] or by adopting the method used by Chapman and Cowling [1] ie substituting the expansion forms into

the integral equations and taking equilibrium averages. For $\underline{F}_q^k$ we have

$$\sum_{q'} \frac{n_q}{n^2} \mathbb{R}_{qq'}(\underline{F}_q^k) = \frac{1}{n_q} (\delta_{qk} - \gamma_q)\underline{C}_q \qquad (5.4.3.10)$$

Substituting the expansion for $\underline{F}_q^k$ we obtain

$$\sum_{q'} \sum_{sr} F^k_{q'sr} \left[\delta_{qq'} \sum_{\mu}^{N} \frac{n_\mu n_q}{n^2} \nu_{q\mu} \mathfrak{S}\begin{bmatrix} 1os'r' \\ 1osr \end{bmatrix}\begin{matrix} q \\ q \end{matrix}_{q\mu} \right.$$

$$\left. + \nu_{qq'} \frac{n_q n_{q'}}{n^2} \mathfrak{S}\begin{bmatrix} 1os'r' \\ 1osr \end{bmatrix}\begin{matrix} q \\ q' \end{matrix}_{qq'} \right]$$

$$= \frac{1}{3} (\delta_{qk} - \gamma_q) \langle\langle \underline{\phi}_q^{1os'r'} . \underline{C}_q \rangle\rangle_0 \qquad (5.4.3.11)$$

$$\Rightarrow \sum_{q'} \sum_{sr} F^k_{q'sr1} \mathbb{P}^{s'r'}_{qq'} = \left[\frac{kT}{m_q}\right]^{\frac{1}{2}} (\delta_{qk} - \gamma_q) \qquad (5.4.3.12)$$

where [9]

$$m\mathbb{P}^{s'r',sr}_{qq'} = \delta_{qq'} \sum_{\mu}^{N} \frac{n_q n_\mu}{n^2} \nu_{q\mu} \mathfrak{S}\begin{bmatrix} mos'r' \\ mosr \end{bmatrix}\begin{matrix} q \\ q \end{matrix}_{q\mu}$$

$$+ \nu_{qq'} \frac{n_q n_{q'}}{n^2} \mathfrak{S}\begin{bmatrix} mos'r' \\ mosr \end{bmatrix}\begin{matrix} q \\ q' \end{matrix}_{qq'} \qquad (5.4.3.13)$$

The $\mathbb{P}$ above are concentration dependent effective cross–sections. The concentration independent effective cross–sections relevant to mixtures are given by [9]

$$\mathfrak{S}\begin{bmatrix} mos'r' \\ mosr \end{bmatrix}\begin{matrix} q \\ q \end{matrix}_{q\mu} = \frac{\langle\langle T_q^{mos'r'} \circledR^{(1)}_{q\mu} (T_q^{mosr}) \rangle\rangle_0}{\gamma_{q\mu}^{(2m+1)}} \qquad (5.4.3.14)$$

$$\mathcal{G}\begin{bmatrix} mos'r' \\ mosr \end{bmatrix}\begin{matrix} q \\ q' \end{matrix}_{qq'} = \frac{<<T_q^{mos'r'} \mathcal{R}_{q\mu}^{(2)} (T_q^{mosr})>>_0}{\gamma_{qq'}(2m+1)} \quad (5.4.3.15)$$

where

$$\gamma_{qq'} = \left[\frac{8kT}{\pi\mu_{qq'}}\right]^{\frac{1}{2}} \quad (5.4.3.16)$$

with

$$\mu_{qq'} = \frac{m_q m_{q'}}{m_q + m_{q'}} \quad (5.4.3.17)$$

Uniqueness of solution is guaranteed by the auxiliary conditions. These can be expressed in terms of the expansion coefficients. In the case of $\underline{F}_q^k$ we have

$$\sum_q \sqrt{m_q}\, n_q\, F_{qoo}^k = 0 \quad (5.4.3.18)$$

Combining the auxiliary conditions (equation (5.4.3.18)) with the equation for the expansion coefficient (equation (5.4.3.12)) the final expression for the expansion coefficient $F_{q's'r'}^k$ is obtained

$$\sum_{q'} \sum_{s'r'} F_{q's'r'}^k \cdot {}_1\mathbb{P}_{qq'}^{sr,s'r'} = \left[\frac{kT}{m_q}\right]^{\frac{1}{2}} (\delta_{qk} - \gamma_q) \quad (5.4.3.19)$$

where

$${}_1\mathbb{P}_{qq'}^{sr,s'r'} = {}_1\mathbb{P}_{qq'}^{sr,s'r'} - \frac{n_{q'}\sqrt{m_{q'}}}{n_q \sqrt{m_q}} {}_1\mathbb{P}_{qq}^{sr,s'r'} \delta_{s'o}\delta_{r'o} \quad (5.4.3.20)$$

A similar equation is obtained for $a_{q's'r'}$ [9]

$$\sum_{q'} \sum_{s'r'} a_{q's'r'} {}_1\mathbb{P}_{qq'}^{sr,s'r'} = \frac{n_q}{n} \left[\frac{2kT}{m_q}\right]^{\frac{1}{2}} \left[-\left[\frac{5}{4}\right]^{\frac{1}{2}} \delta_{s1}\delta_{ro} + \left[\frac{C_{q,int}}{2k}\right]^{\frac{1}{2}} \delta_{so}\delta_{r1}\right] \quad (5.4.3.21)$$

The above expressions can be solved to any order for the expansion coefficients.

The transport coefficient of particular interest here is the thermal conductivity which is measured by experiment, λ^{∞}. In order to obtain this coefficient the diffusion gradient is eliminated from the heat flux vector. This elimination has been performed for polyatomic systems in a first and second **approximation**. This should not be confused with the first- and second-**order** solution of the Wang Chang Uhlenbeck equation.

Following the usual procedure for deriving explicit equations for the expansion coefficients, the first-order solution for λ^{0}_{tr}, λ^{0}_{int}, D^{T}_{q} and $D_{qq'}$ is obtained by retaining the first non-zero terms of equivalent order in the equation for the transport coefficients. Thus, for first-order expressions for λ^{0}_{tr}, λ^{0}_{int}, D^{T}_{q} terms up to and including a_{qoo}, a_{q1o} and a_{qo1} are retained in equation (5.4.3.21) and the first term, F^{k}_{qoo}, is retained in equation (5.4.3.19) to obtain the first-order expression for $D_{qq'}$. The first **approximation** to λ^{∞} is then obtained by eliminating the diffusion gradients from the heat flux vector using the expressions for λ^{0}_{tr}, λ^{0}_{int}, D^{T}_{q} and $D_{qq'}$ obtained in this manner. This procedure leads to a complicated expression for λ^{∞} [14] and contains an apparent inconsistency since different numbers of terms have been used in the derivation. The second approximation to λ^{∞} resolves this inconsistency by using the same number of terms in both expansions. The results obtained for λ^{∞} are simpler and are preferred for the calculation of thermal conductivity.

The second **approximation** is only first **order** with respect to the expansion coefficients for λ^{0}. In order to investigate the

contribution of higher–order terms in the expansion for λ^0, a general result is required, valid for any consistent set of sr,s′r′. The appropriate generalisation follows from the vector matrix method.

5.4.4 The Matrix Vector Method

The integral equations for the expansion coefficients $F^k_{q's'r'}$ and $a_{q's'r'}$,equations (5.4.3.19) and (5.4.3.20) , can be written in the form of a vector matrix. For $F^k_{q'sr'}$, considering an N–component mixture and an expansion up to and including the Mth term

$$P^{00}F_0 + P^{01}F_1 = G \qquad (5.4.4.1)$$

$$P^{10}F_0 + P^{11}F_1 = 0 \qquad (5.4.4.2)$$

where

P^{00} is an N x N matrix

P^{01} is an N x N(M–1) matrix

P^{10} is an N(M–1) x N matrix

P^{11} is an N(M–1) x N(M–1) matrix

G is an N x 1 vector

F_0 is an N x 1 vector

F_1 is an N(M–1) x 1 vector

Solving the matrix equations (5.4.4.1) and (5.4.4.2) for F_0 and F_1

$$F_0 = T^{-1}\, G \qquad (5.4.4.3)$$

$$F_1 = P^{11^{-1}}\, P^{10}\, T^{-1}\, G \qquad (5.4.4.4)$$

where

$$T^{-1} = (P^{00} - P^{01}P^{11^{-1}}P^{10})^{-1} \qquad (5.4.4.5)$$

Similarly, for the $a_{q's'r'}$

$$P^{00}\, a_0 + P^{01}\, a_1 = 0 \qquad (5.4.4.6)$$

$$P^{10}\, a_0 + P^{11}\, a_1 = R \qquad (5.4.4.7)$$

where R is an N(M–1) x 1 vector. Hence,

$$a_0 = - T^{-1}\, P^{01}\, P^{11^{-1}}\, R \qquad (5.4.4.8)$$

$$a_1 = P^{11^{-1}} R + P^{11^{-1}}\, P^{10}\, T^{-1}\, P^{01}\, P^{11^{-1}}\, R \qquad (5.4.4.9)$$

In order to proceed to eliminate the diffusion gradient from the heat flux vector the equation for the average diffusion velocity of the qth component is solved for the diffusion gradient

$$\langle \underline{c}_q \rangle_{AV} = - \sum_{q'} D_{qq'}\, \underline{d}_{q'} - D_q^T\, \ell n\, T \qquad (5.4.4.10)$$

Substituting for D_q^T and $D_{qq'}$ from equations (5.4.3.5) and (5.4.3.6) and rearranging

$$\sum_{q'} F_{qoo}^{q'}\, \underline{d}_{q'} = - n \langle \underline{c}_q \rangle_{AV} \left[\frac{m_q}{kT}\right]^{\frac{1}{2}} - a_{qoo}\, \nabla\, \ell n\, T \qquad (5.4.4.11)$$

From equation (5.4.4.3) in expanded form

$$\sum_{q'} T_{kq'} F_{qoo}^{q'} = \left[\frac{kT}{m_q}\right]^{\frac{1}{2}} (\delta_{qk} - \gamma_q) \qquad (5.4.4.12)$$

where T_{kq} is an element of the T matrix.

Hence multiplying equation (5.4.4.11) by T_{kq}, summing over all components and using the relation,

$$\sum_{q'} \underline{d}_{q'}(\delta_{q'k} - \gamma_k)\left[\frac{kT}{mk}\right]^{\frac{1}{2}} = -\sum_{q'} \underline{d}_{q'}\left[\frac{kT}{mk}\right]^{\frac{1}{2}} \delta_{q'k} \quad (5.4.4.13)$$

the following is obtained

$$-\left[\frac{kT}{m_k}\right]^{\frac{1}{2}} \underline{d}_k = -\sum_q T_{kq}\left\{n\,\langle C_q\rangle_{AV}\left[\frac{m_q}{kT}\right]^{\frac{1}{2}} + a_{qoo}\,\nabla\,\ell n\,T\right\} \quad (5.4.4.14)$$

The subsequent derivation assumes

$$\langle C_q\rangle_{AV} = 0 \quad (5.4.4.15)$$

which is the usual case when measuring λ^{∞} experimentally. The analysis will therefore not provide a general heat flux equation or diffusion equation but will recover the important information about λ^{∞}. Within this treatment

$$\underline{d}_k = \left[\frac{m_k}{kT}\right]^{\frac{1}{2}} \sum_q T_{kq}\,a_{qoo}\,\nabla\,\ell n\,T \quad (5.4.4.16)$$

From equation (5.4.4.8) we have

$$Ta_0 = -P^{01}\,P^{11^{-1}}\,R \quad (5.4.4.17)$$

and hence

$$\underline{d}_k = -\left[\frac{m_k}{kT}\right]^{\frac{1}{2}} \sum_q \sum_{sr} (P^{01}\,P^{11^{-1}})^{sr}_{kq}\,R_{qsr}\,\nabla\,\ell n\,T \quad (5.4.4.18)$$

where $(P^{01}\ P^{11^{-1}})^{sr}_{kq}$ is an element of the N x N(M–1) matrix $(P^{01}\ P^{11^{-1}})$ and R_{qsr} is an element of the N(M–1) x 1 vector R.

Substitution of the expansion forms for $F^{q'}_{q}$ and $\underline{A}_q$, the first-order heat flux vector, can be written in terms of the expansion coefficients

$$\underline{q} = kT \sum_q \left[\frac{5}{2} + \bar{\epsilon}_q\right] n_q \langle \underline{C}_q \rangle_{AV}$$

$$+ kT \sum_{q'} \sum_{q'} \frac{n_q}{n} \underline{d}_{q'} \left[\frac{kT}{m_q}\right]^{\frac{1}{2}} \left[\left[\frac{C_{int,q}}{k}\right]^{\frac{1}{2}} F^{q'}_{qo1} - \left[\frac{5}{2}\right]^{\frac{1}{2}} F^{q'}_{q10}\right]$$

$$- \left[- \left[\frac{5}{4}\right] \sum_q \frac{n_q}{n} \left[\frac{2kT}{m_q}\right]^{\frac{1}{2}} a_{q_{1o}} + \left[\frac{1}{2}\right]^{\frac{1}{2}} k \sum_q \left[\frac{2kT}{m_q}\right]^{\frac{1}{2}}\right.$$

$$\left. x \left[\frac{C_{int,q}}{k}\right]^{\frac{1}{2}} \frac{n_q}{n} a_{qo1} \right] \nabla T \qquad (5.4.4.19)$$

From equation (5.4.4.4) in expanded form we have

$$F^{q'}_{qrs} = - \sum_j (P^{11^{-1}}\ P^{10}\ T^{-1})^{rs}_{qj} \left[\frac{kT}{m_j}\right]^{\frac{1}{2}} (\delta_{jq} - \gamma_j) \qquad (5.4.4.20)$$

Substituting into the heat flux vector and neglecting terms proportional to $\langle \underline{C}_q \rangle_{AV}$

$$\underline{q} = - kT \sum_q \frac{n_q}{n} \left[\frac{kT}{m_q}\right]^{\frac{1}{2}} \left[\frac{C_{int,q}}{k}\right]^{\frac{1}{2}} \sum_{q'} (P^{11^{-1}} P^{10} T^{-1})^{01}_{qq'} \left[\frac{kT}{m_q}\right]^{\frac{1}{2}} \underline{d}_{q'}$$

$$+ kT \left[\frac{5}{2}\right]^{\frac{1}{2}} \sum_q \frac{n_q}{n} \left[\frac{kT}{m_q}\right]^{\frac{1}{2}} \sum_{q'} (P^{11^{-1}} P^{10} T^{-1})^{10}_{qq'} \left[\frac{kT}{m_q}\right]^{\frac{1}{2}} \underline{d}_{q'}$$

$$- \left[- \left[\frac{5}{4}\right]^{\frac{1}{2}} \sum_q \frac{n_q}{n} \left[\frac{2kT}{m_q}\right]^{\frac{1}{2}} a_{q1o} + \left[\frac{1}{2}\right]^{\frac{1}{2}} k \sum_q \left[\frac{2kT}{m_q}\right]^{\frac{1}{2}} \right.$$

$$\left. x \left[\frac{C_{int,q}}{k}\right]^{\frac{1}{2}} \frac{n_q}{n} a_{qo1} \right] \nabla T \qquad (5.4.4.21)$$

Further substitution for $\underline{d}_{q'}$ from equation (5.4.4.18) and using the relation (equation (5.4.4.9) in expanded form)

$$a_{qr's'} = \sum_{sr} \sum_{q'} (P^{11^{-1}})^{r's'} R_{q'sr} + \sum_{sr} \sum_{q'} (P^{11^{-1}} P^{10} T^{-1} P^{01} P^{11^{-1}})^{r's'} R_{q'sr} \qquad (5.4.4.22)$$

the following is obtained for the heat flux vector

$$\underline{q} = \left[\lambda^o_{int} - k \sum_q \sum_{q'} \sum_{sr} R_{qo1} (P^{11^{-1}})^{1o}_{qq'} R_{q'sr}\right] \nabla T - \lambda^0_{int} \nabla T$$

$$+ \left[\lambda^o_{tr} - k \sum_q \sum_{q'} \sum_{sr} R_{q1o} (P^{11^{-1}})^{01}_{qq'} R_{q'sr}\right] \nabla T - \lambda^0_{tr} \nabla T \qquad (5.4.4.23)$$

Equation (5.4.4.23) enables identification of λ^{∞}

$$\lambda^{\infty} = \lambda^{\infty}_{tr} + \lambda^{\infty}_{int} \qquad (5.4.4.24)$$

$$\lambda^{\infty}_{tr} = k \sum_{q}^{N} \sum_{q'}^{N} \sum_{sr\neq 0}^{M} R_{q_{10}} (P^{11^{-1}})^{10} R_{q'sr} \qquad (5.4.4.25)$$

$$\lambda^{\infty}_{int} = k \sum_{q}^{N} \sum_{q'}^{N} \sum_{sr\neq 0}^{M} R_{q_{01}} (P^{11^{-1}})^{01} R_{q'sr} \qquad (5.4.4.26)$$

Explicit equations for λ^{∞}_{tr} and λ^{∞}_{int} in the first-order Chapman Enskog solution are found in Appendix 5C. Comparing these expressions with the expressions for λ^{0}_{tr} and λ^{0}_{int} [9] indicate that the expressions for λ^{∞}_{tr} and λ^{∞}_{int} can be obtained from λ^{0}_{tr} and λ^{0}_{int} by deleting the set of top rows and left-hand columns from the determinants. This was also the observation in the first order theory of Monchick *et al* [14].

Equations (5.4.4.25) and (5.4.4.26) represent expressions for λ^{∞}_{tr} and λ^{∞}_{int} in the <u>second</u> approximation taken to infinite order in the expansion coefficients and as such constitute an extension of the first order and subsequent theories of Monchick et al [14,20,22]. The calculation of λ^{∞} requires inversion of an N(M-1) x N(M-1) matrix in which the elements are linear combinations of effective cross-sections. These effective cross-sections have never been evaluated for realistic potentials. Some progress may be made in the case of a binary mixture of a monatomic and polyatomic gas. In this case there are three possible interactions, i.e. monatomic-monatomic, polyatomic-monatomic and polyatomic-polyatomic. The monatomic-monatomic effective cross-sections can be calculated in a routine manner; the other cross-sections could be calculated via an

approximate method. Alternatively, model calculations could be made using, for example, a rough hard-sphere model in a similar manner to the case of pure polyatomic gases [21].

A complete derivation of the second approximation to the thermal conductivity of a polyatomic gas mixture has therefore been given. At present even the fastest computers are unable to evaluate rapidly the effective cross-sections for any realistic potential. In addition, there are, as yet, few reliable thermal conductivity data for mixtures containing polyatomic components. Consequently, the present work has been performed in the expectation that, following the experimental developments reported in this thesis, measurements on mixed systems will become available in the future. It is also expected that as computational speeds increase the evaluation of effective cross-sections will become feasible. The work performed here will ensure that the kinetic theory formulation itself will not provide a barrier to progress.

5.5 THE MODERATELY DENSE GAS

The statistical mechanical theory of the non-uniform, moderately dense gas suggests that the proper density dependence of the transport coefficients is

$$\Delta\lambda_{excess} = \lambda_1\rho + \lambda_2\rho^2 + \lambda_2'\rho^2\ell n\rho + \lambda_3\rho^3 + \ldots \qquad (5.5.1)$$

$$\Delta\eta_{excess} = \eta_1\rho + \eta_2\rho^2 + \eta_2'\rho^2\ell n\rho + \eta_3\rho^3 + \ldots \qquad (5.5.2)$$

The coefficients, λ_1, λ_2, etc. may be functions of temperature. The density dependence is therefore essentially a polynomial expansion in density with an additional logarithmic term. Careful experiments and

theoretical calculations [26] indicate that the coefficient of the logarithm term is so small that it has no practical significance. It is introduced later only to be complete, but is soon rejected and progress is made with the polynomial expansion only.

Most early work in the field of dense gases has been carried out with the Enskog theory of a dense hard-sphere gas. Although not strictly applicable to any real gaseous system, it does contain most of the important phenomena associated with such gases and thus can be used as the basis of a qualitative description of real gases, or can be employed as the starting point for empirical prediction schemes. More recently, some attention has been given theoretically to the first density coefficient of the transport properties of a more realistic potential model. In this work the experimental data are used to examine the gross features of the density dependence of thermal conductivity with some special attention being given to the first density coefficient which can be extracted from the present experimental results with more confidence than was possible earlier. The analysis of the results is reserved until later in Chapter 6. Here, a brief summary of the existing theory for the dense gases used in this analysis is given.

5.5.1 The Enskog Theory

Phenomenological kinetic theories of dilute gases stress the importance of the mean free path when explaining transport processes. The mean free path is the product of the average time between collisions and the average speed of a molecule. For a gas at equilibrium, the average speed is independent of the density but the average time between collisions is density dependent. The average

time between collisions is the inverse of the collision frequency, so in order to study the density dependence of the mean free path, the density dependence of the collision frequency must be determined.

Enskog considered that the collision frequency is affected by two important features of dense hard spheres. Firstly, the size of the molecules must be taken into account. The volume occupied by a molecule is of the same order as the molecular volume. That is, the average volume that the centre of mass has to move around in is reduced by the volume of the molecule. This will therefore increase the frequency of binary collisions. Secondly, the effects of multibody collisions must be considered. Instead of working with the complex dynamics of three–body collisions, Enskog considered that the presence of a third body modifies the binary collision frequency, via a sheilding effect. This change in the collision frequency is accommodated by the introduction of the radial distribution function χ which is a function of number density and is evaluated at the point of contact of two colliding molecules.

The radial distribution function is found in the exact equation of state for a hard–sphere fluid [1, 6, 11, 24]

$$\frac{PV}{RT} = 1 + b\rho\chi \qquad (5.5.1.1)$$

and

$$b = \frac{2\pi\sigma^3}{3m} \qquad (5.5.1.2)$$

where m is the mass of a molecule, σ is the hard–sphere diameter and ρ is the mass density of the gas. For hard spheres, χ is found to be [11]

$$\chi = 1 + 0.6250\ b\rho + 0.2869(b\rho)^2 + 0.115(b\rho)^3 \ldots \qquad (5.5.1.3)$$

For a hard-sphere fluid, the effects of the increased density on the collision frequency has been accommodated within χ. The increased density also contributes extra mechanisms to the fluxes. For example, in the case of momentum transfer, there are two mechanisms contributing The first is the movement of a molecule which carries its own momentum across the reference plane. The second occurs during a collision between one molecule with its centre of mass on one side of the reference plane and another molecule with its centre of mass on the other side of the reference plane. There is an instantaneous transfer of momentum from the centre of one molecule to the centre of the other without transfer of a centre of mass across the reference plane.

The theory leads to the following expressions for the viscosity, thermal conductivity and self-diffusion coefficient.

$$\eta = \eta^0 \rho b \left[\frac{1}{\chi \rho b} + 0.800 + 0.761\ \rho b \chi\right] \qquad (5.5.1.4)$$

$$\lambda_{tr} = \lambda^0_{tr} \rho b \left[\frac{1}{\chi \rho b} + 1200 + 0.755\ \rho b \chi\right] \qquad (5.5.1.5)$$

$$D = \frac{D^0}{\chi} \qquad (5.5.1.6)$$

where η, λ_{tr} and D are the dense gas viscosity, translational thermal conductivity and self-diffusion coefficient at mass density ρ and η^0, λ^0_{tr} and D^0 are the zero-density limits. These results are not exact even for hard spheres because they do not take into account the effects of correlated molecular velocities [10]. These effects arise when considering multiple collisions, but are not important for relatively low densities.

It is well known that the equation of state can be written as a virial expansion

$$\frac{PV}{RT} = 1 + \frac{B(T)}{V} + \frac{C(T)}{V^2} + \ldots \qquad (5.5.1.7)$$

where B, C, etc. are the virial coefficients which are related to integrals over the configurations of n molecules interacting simultaneously. The characteristic length associated with these integrals is the range of the molecular interaction. Substitution of equation (5.5.1.3) for the radial distribution function into equations (5.5.1.4)–(5.5.1.6) for the transport coefficients recovers a series expansion in density

$$\eta = \eta^0 + [-0.625 + 0.8]b\ \eta^0\ \rho + \ldots \qquad (5.5.1.8)$$

$$\lambda_{tr} = \lambda^0_{tr} + (-0.625 + 1.2)b\ \lambda^0_{tr}\ \rho + \ldots \qquad (5.5.1.9)$$

$$D = D^0 - 0.625\ b\ D^0\ \rho + \ldots \qquad (5.5.1.10)$$

To first order in density, the kinetic contributions are identified as $-0.625\ b_0\ \lambda^0_{tr}$, $-0.625\ b_0\ \eta^0$ and $-0.625\ b_0\ D^0$, the other contributions being due to collisional transfer. By analogy with the virial expansion equation (5.5.1.7) the kinetic contribution is due to three–body collisions. However, there are two general classifications of multibody collisions [25, 26]. Firstly, genuine multibody collisions in which all n molecules are interacting simultaneously. The characteristic length is the range of interaction and, secondly, collisions which consist of successive correlated binary collisions between the n particles. After the

binary collision the velocity of the colliding particles remain correlated until at least the next collision. The characteristic length between successive binary collisions is now the mean free path. The mean free path as we have seen is density dependent. The density dependence can now no longer be represented by a simple power series in density. In fact, a logarithmic term is introduced [25, 26]

$$\lambda = \lambda^0[1 + \lambda_1\rho + \lambda_2'\rho^2\ell n\rho + \lambda_2\rho^2 + \ldots] \qquad (5.5.1.11)$$

The logarithmic term is of order ρ^2, therefore if the development is restricted to terms proportional to density then the effect of correlated velocities will be minimal [10].

5.5.2 Modified Enskog Theories

The Enskog hard-sphere model has been used as the basis for *ad hoc* extensions to real fluids. The extensions assume that the mechanism for transfer for real fluids interacting through potentials with repulsive and attractive regions is the same as that for a hard sphere. Also the methods assume that the radial distribution function χ for the non-uniform gas is approximated by the equilibrium radial distribution function. The application of the Enskog theory to real fluids requires selection of appropriate methods for estimating χ and b. Hanley *et al.* [24] used a method in which b and χ are estimated from the equilibrium properties of the fluid. The hydrodynamic pressure in the equation of state of the hard-sphere fluid (equation (5.5.1.1)) is replaced by the thermal pressure $T(\partial P/\partial T)_V$ which is identical to P for a hard-sphere fluid, i.e.

$$PV = RT[1 + b\rho\chi] \tag{5.5.2.1}$$

$$\Rightarrow T\left[\frac{\partial P}{\partial T}\right]_V = \frac{RT}{V}[1 + b\rho\chi] \tag{5.5.2.2}$$

[Note: this assumes $\chi \neq \chi(T)$] and hence

$$T\left[\frac{\partial P}{\partial T}\right]_V = P \tag{5.5.2.3}$$

$$\therefore \frac{1}{R}\left[\frac{\partial PV}{\partial T}\right]_V = 1 + b\rho\chi \tag{5.5.2.4}$$

which can be written as

$$T\frac{\partial}{\partial T}\left[\frac{PV}{RT}\right]_V + \frac{PV}{RT} = 1 + b\rho\chi \tag{5.5.2.5}$$

Using the virial equation of state in the form

$$\frac{PV}{RT} = 1 + \frac{B(T)}{V} + \frac{C(T)}{V^2} + \ldots \tag{5.5.2.6}$$

implies from equation (5.5.2.5) that

$$1 + b\rho\chi = 1 + \frac{1}{V}\frac{d}{dT}(TB(T)) + \frac{1}{V^2}\frac{d}{dT}(TC(T)) + \tag{5.5.2.7}$$

$$\Rightarrow b\chi = \frac{1}{\rho V}\frac{d}{dT}(TB(T)) + \frac{\rho}{(\rho V)^2}\frac{d}{dT}(TB(T)) + \ldots \tag{5.5.2.8}$$

In equation (5.5.1.6) V is the molar volume which is related to the number density via Avogadro's number, i.e.

$$V = \frac{N_A}{n} \tag{5.5.2.9}$$

Hence

$$b\chi = \frac{1}{mN_A}\frac{d}{dT}(TB(T)) + \frac{nm}{(mN_A)^2}\frac{d}{dT}(TC(T)) + \ldots \quad (5.5.2.10)$$

Taking the limit as $n \to 0$, $\chi \to 1$,

$$b = \frac{1}{mN_A}\frac{d}{dT}(TB(T)) = \frac{1}{RMM}\frac{d}{dT}(TB(T)) \quad (5.5.2.11)$$

where RMM is the relative molecular mass and m is the molecular mass. For a hard sphere

$$B(T) = \frac{2}{3}\pi N_A \sigma^3$$

Hence

$$b_{HS} = \frac{2\pi\sigma^3}{3m} \quad (5.5.2.12)$$

which is consistent with the previous definition of b (equation (5.5.2.10)). Having obtained b from the compressibility data, the radial distribution function can be obtained from equation (5.5.12)

$$\chi = 1 + \frac{\rho}{RMM}\frac{\gamma}{\beta} + O(\rho^2) \quad (5.5.2.13)$$

where

$$\beta = \frac{d}{dT}(TB(T)) \quad (5.5.2.14)$$

and

$$\gamma = \frac{d}{dT}(TC(T)) \quad (5.5.2.15)$$

Substituting for χ and b into equations (5.5.1.4)–(5.5.1.6) the following is obtained

$$\eta = \eta^0 [1 + \eta_1^I n + \eta_2^I n^2 + \ldots] \quad (5.5.2.16)$$

$$\lambda_{tr} = \eta^0[1 + \lambda^I_{1,tr}n + \lambda^I_{2,tr}n^2 + \ldots] \qquad (5.5.2.17)$$

$$D = D^0[1 + D^I_1 n + D^I_2 n^2 + \ldots] \qquad (5.5.2.18)$$

where

$$\eta^I_1 = \frac{1}{N_A}\left[-\frac{\gamma}{\beta} + 0.8\ \beta\right] \qquad (5.5.2.19)$$

$$\lambda^I_{1,tr} = \frac{1}{N_A}\left[-\frac{\gamma}{\beta} + 1.2\ \beta\right] \qquad (5.2.2.20)$$

$$D^I_1 = \frac{1}{N_A}\left[-\frac{\gamma}{\beta}\right] \qquad (5.5.2.21)$$

and n is the nunber density. The superscript I indicates that the MET-I theory was used.

The MET-I procedure may be extended to polyatomic gases by using some results of dilute polyatomic gas theory. The thoery indicates that the internal energy and occurrence of inelastic collisions have a small effect on the viscosity. Hence equations (5.5.2.16) and (5.5.2.19) can be applied directly to the viscosity of polyatomic gases. In the case of thermal conductivity in the limit of zero density, the total property is divided into internal and translational contributions.

$$\lambda^0 = \lambda^0_{int} + \lambda^0_{tr} \qquad (5.5.2.22)$$

Therefore, by analogy,

$$\lambda = \lambda_{int} + \lambda_{tr} \qquad (5.5.2.23)$$

If the internal energy is assumed to be transported by a diffusive

mechanism, then [27]

$$\lambda^0_{int} = \frac{\rho D^0 C_{v,int}}{m} \qquad (5.5.2.24)$$

So, also by analogy,

$$\lambda_{int} = \frac{\rho D C_{v,int}}{m} \qquad (5.5.2.25)$$

From equation (5.5.1.6)

$$D = \frac{D^0}{\chi} \qquad (5.5.2.26)$$

$$\therefore \lambda_{int} = \frac{\rho D^0 C_{v,int}}{m\chi} \qquad (5.5.2.27)$$

$\therefore$ using (5.5.2.24)

$$\lambda_{int} = \frac{\lambda^0_{int}}{\chi} \qquad (5.5.2.28)$$

Combining the internal and translational contributions

$$\lambda = \lambda^0_{tr} b\rho \left[\frac{1}{b\rho\chi} + 1.200 + 0.755\ b\rho\chi\right] + \frac{\lambda^0_{int}}{\chi} \qquad (5.5.2.29)$$

Using equation (5.5.2.11) for b and equation (5.5.2.13) for χ

$$\lambda = \lambda^0_{tr}\left[1 - \frac{\rho}{RMM}\frac{\gamma}{\beta} + 1.200\ \frac{1}{RMM}\beta\right] + \lambda^0_{int}\left[1 + \frac{\rho}{RMM}\frac{\gamma}{\beta}\right] + 0(\rho^2) \qquad (5.5.2.30)$$

$$= \lambda^0 + \frac{\lambda^0_{tr}}{N_A}\left[1.200\ \beta - \frac{\gamma}{\beta}\left[\frac{\lambda^0}{\lambda^0_{tr}}\right]\right]n + 0(\rho^2) \qquad (5.5.2.31)$$

In equation (5.5.2.31) use can be made of the following relationships

$$\frac{\lambda^0}{\lambda^0_{tr}} = 1 + \frac{24}{75}\frac{C_{v.int}}{k} A^* \qquad (5.5.2.32)$$

and

$$\lambda^0_{tr} = \left[\frac{15}{4}\right]\left[\frac{k}{m}\right]\eta^0 \qquad (5.5.2.33)$$

Equation (5.5.38) reduces to the monatomic equation when $\lambda_{int} = \lambda^0_{int} = 0$.

An alternative extension of the Enskog theory has been proposed [28, 29] where b is still obtained from the virial coefficient data but the radial distribution function is obtained using the equation for the hard sphere. This method, denoted MET–II, provides the following results for η_1 and λ_1.

$$\eta_1^{II} = \frac{0.175\beta\eta^0}{N_A} \qquad (5.5.2.34)$$

$$\lambda_1^{II} = \frac{1}{N_A}\left[1.200 - 0.625\left[\frac{\lambda^0}{\lambda^0_{tr}}\right]\right]\lambda^0_{tr}\,\beta \qquad (5.5.2.35)$$

5.5.3 The Microscopic Theories

The Enskog theory of dense hard spheres was an *ad hoc* extension of dilute gas theory where an explicit discussion of multibody collisions is avoided. The theory also does not allow the presence of dimers in the gas since they are not possible for purely repulsive potentials. Real fluids do, however, possess attractive parts to the potential and hence dimerisation is possible, particularly at low reduced temperatures. Systematic theories for the density dependence of transport properties strive to identify distinctive contributions to the first density coefficient. In general, these contributions are the collisional transfer, three–body collisions and the monomer–dimer contribution. Different authors have identified these

contributions in different ways. Stogryn and Hirschfelder [30] and Kim and Ross [31] approximate the triple collision by the collision between a monomer and a dimer. The triple-body contribution is calculated from the binary-collision contributions of a mixture of monomers and dimers using the Chapman Enskog theory of binary mixtures. The equilibrium constant k for the formation of dimers is used to obtain the respective concentrations of momomer and dimer. Stogryn and Hirschfelder relate k to the equilibrium second virial coefficients of the gas and Kim and Ross derive k via the partition functions for the free monomer and dimer. Stogryn and Hirschfelder approximate the collisional contribution of monomer-dimer collisions but Kim and Ross do not include this explicitly.

A recent microscopically-based theory of the density dependence of the transport coefficients was presented by Friend and Rainwater [12, 13]. They identified three distinct contributions to the first density coefficient such that

$$X = X^0[1 + (B_X^{(2)} + B_X^{(3)} + B_X^{(M-D)})n + \ldots] \qquad (5.5.3.1)$$

$$= X^0[1 + B_X n + \ldots] \qquad (5.5.3.2)$$

where X represents either viscosity or thermal conductivity. $B_X^{(2)}$ represents the two-monomer collisional transfer contribution first derived by Snider and Curtiss [32, 33].

Friend and Rainwater recalculated this contribution for a Lennard-Jones 12-6 potential performing integrations over that region of phase space for which only monomer exists [34]. The three-monomer term $B_X^{(3)}$ was calculated by an extension of the Enksog 'shielding' effect, which alters the binary collision frequency, originally

proposed by Hoffman and Curtiss [35], and later by Bennet and Curtiss [36]. The final contribution, $B_x^{(M-D)}$, is due to monomer–dimer interaction, which was calculated from the algorithm of Stogryn and Hirschfelder [30] and requires knowledge of the potential between monomer and dimer. This potential is characterised by potential parameter ratios

$$\delta = \sigma_{M-D}/\sigma_N$$

$$\theta = \epsilon_{M-D}/\epsilon_D$$

Friend and Rainwater calculated these parameters by fitting experimental data to their theoretical expressions.

The microscopically–based theory of Friend and Rainwater is not strictly rigorous and there remain some theoretical difficulties involved with the $B_x^{(M-D)}$ term but this theory provides the most comprehensive treatment of the density dependence of transport properties. Subsequent chapters will analyse the new body of thermal conductivity data with respect to this theory.

APPENDIX 5A

MONATOMIC GASES

Having defined the velocity distribution function for the non-uniform gas in the form

$$f = f^0(1 + \phi) \tag{5A.1}$$

where f^0 is the local equilibrium distribution function and ϕ is the perturbation function, the macroscopic properties of the gas may be obtained

$$n(\underline{r}, t) = \int f \, d\underline{c} \tag{5A.2}$$

$$\rho \underline{c}_0(\underline{r}, t) = \int f \, m\underline{c} \, d\underline{c} \tag{5A.3}$$

$$\rho U(\underline{r}, t) = \int f \, \tfrac{1}{2} \, mC^2 d\underline{c} \tag{5A.4}$$

where $\rho = n(\underline{r}, t)m$ and the following have been defined:

$n(\underline{r}, t)$ is the number density;

$\underline{c}_0(\underline{r}, t)$ is the hydrodynamic velocity;

$U(\underline{r}, t)$ is the average internal energy of the bulk gas per unit mass;

$\underline{C}$ is the peculiar velocity defined by

$$\underline{C} = \underline{c} = \underline{c}_0 \tag{5A.5}$$

The heat flux vector and pressure tensor may be defined

$$\underline{q} = \tfrac{1}{2} m \int f C^2 \underline{C} \, d\underline{c} \tag{5A.6}$$

$$\underline{\underline{P}} = m \int f \underline{C} \, \underline{C} \, d\underline{c} \tag{5A.7}$$

Substituting for f from (5A.1) provides first-order flux equations

$$\underline{q} = \tfrac{1}{2} m \int f^0 \phi C^2 \underline{C} d\underline{c} \tag{5A.8}$$

$$\underline{\underline{P}} = nkT \, \underline{\underline{I}} + m \int f^0 \phi \underline{C} \, \underline{C} \, d\underline{c} \tag{5A.9}$$

Instead of explicitly working with ϕ it is usual to assume that it has the following form

$$\phi = \frac{-1}{n} \left[\frac{2kT}{m}\right]^{\frac{1}{2}} \underline{A}.\nabla \, \ell n \, T - \frac{1}{n} \underline{\underline{B}} : \nabla \underline{C}_0 \tag{5A.10}$$

This definition of ϕ contains the unknown vector and tensor quantities $\underline{A}$ and $\underline{\underline{B}}$ but allows their treatment to proceed separately. The spatial and temporal evolution of the single particle distribution function is governed by the Boltzmann equation

$$\frac{\partial f}{\partial t} + (\underline{C}.\nabla) f = \int_0^{\infty} \int_0^{\infty} \int_0^{2\pi} (f' f_1' - f f_1) g b db d\underline{c}_1 d\psi \tag{5A.11}$$

Linearisation of the Boltzmann equation about a local equilibrium distribution function indicates that vector $\underline{A}$ and tensor $\underline{\underline{B}}$ obey the following equations

$$\mathbb{R}(\underline{A}) = (\mathscr{C}^2 - 5/2)\underline{\mathscr{C}} \tag{5A.12}$$

$$\mathbb{R}(\underline{\underline{B}}) = 2\underline{\mathscr{C}}^{o}\underline{\mathscr{C}} \tag{5A.13}$$

where

$$\underline{\mathscr{C}}^{o}\underline{\mathscr{C}} = \underline{\mathscr{C}}\,\underline{\mathscr{C}} - \frac{1}{3}\,\underline{\underline{I}}\,\mathscr{C}^2 \tag{5A.14}$$

and

$$\underline{\mathscr{C}} = \left[\frac{m}{2kT}\right]^{\frac{1}{2}} \underline{C} \tag{5A.15}$$

and $\mathbb{R}$ is the linearised collision operator

$$nf^{o}\mathbb{R}(X) = \int\int\int f^{o}f_1^{o}(X + X_1 - X' - X_1')gbdbd\psi dc_1 \tag{5A.16}$$

The vector $\underline{A}$ is proportional to $\underline{\mathscr{C}}$ and is expanded in a series of orthonormal polynomials $\underline{\phi}^{1oso}$

$$\underline{A} = \sum_{s} a_s\,\underline{\phi}^{1oso} \tag{5A.17}$$

The quantity $\underline{\phi}^{1oso}$ is a function of sonine polynomials such that

$$\underline{\phi}^{1oso} = A_{3/2}(S,\,0)S_{3/2}^{(s)}(\mathscr{C}^2)\underline{\mathscr{C}} \tag{5.A.18}$$

where

$$Sp^{(s)} = \sum_{L=0}^{S} \frac{(-\mathscr{C}^2)^L(P+S)!}{(P+L)(S-L)!L!} \tag{5A.19}$$

and, in addition,

$$A_{3/2}(s,\,0) = \left[\frac{3}{2}\right]^{\frac{1}{2}} \pi^{\frac{1}{4}} \left[\frac{S!}{\left[\frac{3}{2} + S\right)!}\right]^{\frac{1}{2}}$$

Using equations (5A.8), (5A.10) and (5A.17) the thermal conductivity is obtained in terms of the expansion coefficients as

$$\lambda^{0} = -\left[\frac{5}{4}\right]^{\frac{1}{2}} \frac{2k^2T}{m}\,a_1 \tag{5A.20}$$

Using the expansion equation (5A.17) in the integral equation for $\underline{A}$ and taking equilibrium averages, an infinite set of algebraic equations is obtained for the expansion coefficients

$$\sum_{s'=0}^{\infty} a_{s'} \langle \phi^{1oso} . \mathbb{R}(\phi^{1os'o}) \rangle_0 = -3 \left[\frac{5}{4}\right]^{\frac{1}{2}} \delta_{s1} \qquad (5A.21)$$

where the notation $\langle X \rangle_0$ means

$$\langle X \rangle_0 = \frac{\int f^0 X dc}{\int f^0 \, dc} \qquad (5A.22)$$

and δ_{s1} is the Kronecker delta

Successive approximations to a_1 may be obtained by using more and more terms in equation (5A.21). Retaining the first non-zero term recovers the first-order solution for a_1

$$a_1 = - \left[\frac{5}{4}\right]^{\frac{1}{2}} \frac{1}{\mathfrak{S}(1010)\langle v \rangle_0} \qquad (5A.23)$$

where $\mathfrak{S}(1010)$ is an effective cross-section defined by

$$\mathfrak{S}\begin{bmatrix} 1osr \\ 1os'r' \end{bmatrix} = \langle \underline{\phi}^{1osr} . \mathbb{R}(\underline{\phi}^{1os'r'}) \rangle_0 / 3\langle v \rangle_0 \qquad (5A.24)$$

where

$$\langle v \rangle_0 = 4 \left[\frac{kT}{\pi m}\right]^{\frac{1}{2}} \qquad (5A.25)$$

Hence the first-order thermal conductivity is given by

$$[\lambda^0]_1 = \frac{5}{2} \frac{k^2 T}{m\mathfrak{S}(1010)\langle v \rangle_0} \qquad (5A.26)$$

In a similar manner the tensor $\underline{\underline{B}}$ is expanded in a series of orthonormal polynomials $\underline{\underline{\phi}}^{2oso}$

$$\underline{\underline{B}} = \sum_s b_s \underline{\underline{\phi}}^{1oso} \tag{5A.27}$$

where

$$\underline{\underline{\phi}}^{1oso} = A_{5/2}(s, 0) S_{5/2}^{(s)}(\mathscr{C}^2) \underline{\mathscr{C}}^0 \underline{\mathscr{C}} \tag{5A.28}$$

and

$$A_{5/2}(s, 0) = \left[\frac{15}{4}\right]^{\frac{1}{2}} \pi^{\frac{1}{4}} \left[\frac{S!}{\left[\left(\frac{5}{2} + S\right)\right]!}\right]^{\frac{1}{2}} \tag{5A.29}$$

Equations (5A.7), (5A.10) and (5A.27) are used to obtain an expression for the shear viscosity coefficient.

$$\eta^0 = \left[\frac{1}{2}\right]^{\frac{1}{2}} kT\, b_0 \tag{5A.30}$$

In a similar manner to the case for thermal conductivity b_0 is obtained in terms of an effective cross-section in the first-order approximation

$$b_0 = \frac{\sqrt{2}}{\langle v \rangle_0 \mathfrak{S}(2000)} \tag{5A.31}$$

Hence

$$[\eta^0]_1 = \frac{kT}{\langle v \rangle_0 \mathfrak{S}(2000)} \tag{5A.32}$$

APPENDIX 5B

SENFTLEBEN–BEENAKKER EFFECTS

The semi–classical kinetic theory of Wang Chang and Uhlenbeck is deficient in that it does not allow for degenerate energy levels and does not predict the effects of magnetic fields on thermal conductivity and viscosity. The link between magnetic field effects and free field transport properties is not obvious. The thermal conductivity and viscosity are associated with constants of free motion (i.e. momentum and energy) so it is not easy to see how the presence of a field can affect these properties except via coupling between velocity and angular momentum which is not a constant of motion. This coupling is likely to be small and, in fact, the effect of a magnetic field on thermal conductivity is a small effect, usually 1–2% of the thermal conductivity. The coupling between angular momentum and velocity will also exist in the field–free case but, once again, will be small. The source of the coupling can be seen to derive from the angle dependence of the effective cross–sections and has the effect of correlating velocity and angular momentum polarisations. The velocity is polarised due to the transport property itself and, via the coupling of a velocity and angular momentum, there will be an associated polarisation of angular momentum. This spin polarisation can be destroyed by the collision processes for which there will be an associated relaxation time. It was via this relaxation time and the identification of two components of thermal conductivity that Coope and Snider [37] arrived at the result

$$\underline{\underline{\lambda}}^0 = \lambda^{(0)}\underline{\underline{U}} + \underline{\underline{\lambda}}^{anis} \qquad (5B.1)$$

Here $\lambda^{(0)}$ refers to an isotopic contribution to $\underline{\underline{\lambda}}$ associated with angular momentum independent polarisations. λ^{anis} is due to anisotropy of angular momentum. $\lambda^{(0)}$ has been found to be equivalent formally to the usual Wang Chang Uhlenbeck expression. The anisotropic contribution has been identified as being associated with the change in thermal conductivity of a gas parallel to a magnetic field observed at saturation

$$(\Delta\lambda_{\shortparallel})_{sat} = \left[-\frac{3}{5}\underline{\underline{\lambda}}^{anis}\right]_{H=0} \qquad (5B.2)$$

Hence the field-free thermal conductivity corrected for the effects of spin polarisation is given by

$$\lambda^0 = \lambda^{(0)} - \frac{5}{3}(\Delta\lambda_{\shortparallel})_{sat} \qquad (5B.3)$$

In an earlier paper Viehland, Mason and Sandler [16] obtained a similar expression using a more heuristic approach based on model calculations and experimental evidence. If the spin polarisation correction is small, the two expressions are identical. Thus, in the Viehland-Mason-Sandler formalism,

$$[\lambda^0]_1 = [\lambda^0_{tr}]_1 + [\lambda^0_{int}]_1 \tag{5B.4}$$

$$[\lambda^0_{tr}]_1 = \frac{5k^2T}{2m\langle v\rangle_0}\left\{\frac{\mathcal{S}(1001) + (\frac{2C_{int}}{5k})^{\frac{1}{2}}\mathcal{S}(\frac{1010}{1001})}{\mathcal{S}(1010)\mathcal{S}(10\ 01) - \mathcal{S}^2(\frac{1010}{1001})}\right\} \tag{5B.5}$$

$$[\lambda^0_{int}]_1 = \frac{5k^2T}{2m\langle v\rangle_0}\left\{\frac{(\frac{2C_{int}}{5k})^{\frac{1}{2}}\ \mathcal{S}(\frac{1010}{1001}) + (\frac{2C_{int}}{5k})\mathcal{S}(1010)}{\mathcal{S}(1010)\mathcal{S}(1001) - \mathcal{S}^2(\frac{1010}{1001})}\right\}.S \tag{5B.6}$$

where

$$S \simeq 1 - \frac{5}{3}\left[1 + \left[\frac{\lambda^0_{tr}}{\lambda^0_{int}}\right]\left[\frac{\Delta\lambda_{\shortparallel}}{\lambda}\right]_{sat}\right] \tag{5B.7}$$

The Viehalnd–Mason–Sandler formalism has been used throughout this work owing to the fact that the magnetic field effect data is presented in the form of the relative change in thermal conductivity observed in a magnetic field at saturation, i.e. $(\frac{\Delta\lambda_{\shortparallel}}{\lambda})_{sat}$.

APPENDIX 5C

FIRST ORDER RESULTS FOR MIXTURES

The general infinite order result for the thermal conductivity of mixtures is,

$$\lambda^{\infty} = \lambda^{\infty}_{tr} + \lambda^{\infty}_{int} \qquad 5C.1$$

with

$$\lambda^{\infty}_{tr} = \kappa \sum_{q}^{N} \sum_{q'}^{N} \sum_{sr \neq 0}^{M} R_{q10} \left(P^{11}\right)^{10} R_{q'sr} \qquad 5C.2$$

$$\lambda^{\infty}_{int} = \kappa \sum_{q}^{N} \sum_{q'}^{N} \sum_{sr=0}^{M} R_{q01} \left(P^{11}\right)^{01} R_{q'sr} \qquad 5C.3$$

In the first order approximation M=3 and P^{11} is a 2N x 2N matrix.

$$P^{11} = \begin{pmatrix} \tilde{P}^{10,10}_{qq'} & \tilde{P}^{10,01}_{qq'} \\ \tilde{P}^{01,10}_{qq'} & \tilde{P}^{01,01}_{qq'} \end{pmatrix} \qquad 5C.4$$

The solution can then be written in the form of a ratio of determinants such that,

$$\left[\lambda^{\infty}_{tr}\right]_1 = \left(\frac{5}{4}\right)^{1/2} K \begin{vmatrix} P'' & -\left(\frac{5}{4}\right)^{1/2} w_q x_q \\ w_q h_q x_q & \end{vmatrix} \begin{vmatrix} P'' \end{vmatrix}^{-1} \qquad 5C.5$$

$$\begin{vmatrix} w_q' x_q' & 0 & 0 \end{vmatrix}$$

$$\left[\lambda^{\infty}_{int}\right]_1 = -K \begin{vmatrix} P'' & \left(\frac{5}{4}\right)^{1/2} w_q x_q \\ w_q h_q x_q & \end{vmatrix} \begin{vmatrix} P'' \end{vmatrix}^{-1} \qquad 5C.6$$

$$\begin{vmatrix} 0 & w_q' x_q' & 0 \end{vmatrix}$$

where,

$$w_q = \left(\frac{2KT}{m_q}\right)^{1/2} \qquad 5C.7$$

$$h_q = \left(\frac{C_{q,int}}{2K}\right)^{1/2} \qquad 5C.8$$

REFERENCES

[1] S. Chapman and T.G. Cowling, The Mathematical Theory of Non-Uniform Gases (Cambridge University Press, 1970).

[2] G.C. Maitland, M. Rigby, E.B. Smith and W.A. Wakeham, Intermolecular Forces: Their Origin and Determination (Clarendon Press, Oxford, 1981).

[3] R.A. Aziz in Springer Series in Chemical Physics, 34, 5 (Springer-Verlag, Berlin, 1984).

[4] Barker, Fock and Smith, Phys. Fluids, 7, 897 (1964).

[5] C.S. Wang Chang, G.E. Uhlenbeck and J. de Boer, Studies in Statistical Mechanics, Vol. 2, Part C, (Ed. J. de Boer and G.E. Uhlenbeck), (North Holland, Amsterdam, 1964).

[6] J.H. Ferziger and H.G. Kaper, Mathematical Theory of Transport Processes in Gases (North Holland, Amsterdam, 1972).

[7] G.C. Maitland, M. Mustafa and W.A. Wakeham, J. Chem. Soc. Faraday Trans. II, 79, 1425 (1983).

[8] M.J. Assael, PhD Thesis, University of London (1980).

[9] M. Mustafa, PhD Thesis, University of London (1988).

[10] J.H. Dymond, Quart. Rev. Chem. Soc., 3, 317 (1985).

[11] J.O. Hirschfelder, C.F. Curtiss and R.B. Bird, The Molecular Theory of Gases and Liquids (Wiley, New York, 1954).

[12] D.G. Friend and J.C. Rainwater, Chem. Phys. Lett., 107, 590 (1984).

[13] J.C. Rainwater and D.G. Friend, Phys. Rev., 36, 8, 4062 (1987).

[14] L. Monchick, K.S. Yun and E.A. Mason, J. Chem. Phys. 39, 654 (1963).

[15] J.P.J. Heemskerk, F.G. van Kuik, H.F.P. Knaap and J.J.M. Beenakker, Physica 71, 484 (1974).

[16] L.A. Viehland, E.A. Mason and S.I. Sandler, J. Chem. Phys. 68, 5277 (1978).

[17] B.J. Thijsse, G.W. 'T. Hooft, D.A. Coombe, H.F.P. Knaap and J.J.M. Beenakker, Physica, 98A, 307 (1979).

[18] J. Millat, V. Vesovic and W.A. Wakeham, Physica 148A, 153 (1988).

[19] K.F. Herzfeld and T.A. Litowitz, Absorption and Dispersion of Ultrasonic Waves (Academic Press, New York, 1959).

[20] L. Monchick, A.N.G. Pereira and E.A. Mason, J. Chem. Phys., 42, 3241 (1965).

[21] M.J. Assael, F.R. McCourt, G.C. Maitland, M. Mustafa and W.A. Wakeham, High Temp.–High Press., 17, 291 (1985).

[22] L. Monchick, R.J. Munn and E.A. Mason, J. Chem. Phys., 45, 8, 3051 (1966).

[23] C. Muckenfuss and C.F. Curtiss, J. Chem. Phys., 29, 6, 1273 (1958).

[24] H.J.M. Hanley, R.D. McCarty and E.G.D. Cohen, Physica, 60, 322 (1972).

[25] J.V. Sengers, N.B.S. AEDC–TR–69–68 (1969).

[26] B. Kamgar–Parsi and J.V. Sengers, Phys. Rev. Lett., 51, 24, 2163 (1983).

[27] E.A. Mason and L. Monchick, J. Chem. Phys., 36, 1622 (1962).

[28] R. Di Pippo, J.R. Dorfman, J. Kestin, H.E. Khalifa and E.A. Mason, Physica, 86A, 205 (1977).

[29] E.A. Mason, H.E. Khalifa, J. Kestin, R. Di Pippo and J.R. Dorfman, Physica, 91A, 377 (1978).

[30] D.E. Stogryn and J.O. Hirschfelder, J. Chem. Phys., 31, 6, 1531 (1959).

[31] S.K. Kim, G.P. Flynn and J. Ross, J. Chem. Phys., 43, 11, 4166 (1965).

[32] R.F. Snider and C.F. Curtiss, Phys. Fluids, 1, 122 (1958).

[33] R.F. Snider and C.F. Curtiss, Phys. Fluids, 3, 903 (1960).

[34] J.C. Rainwater, J. Chem. Phys., 81, 1, 495 (1984).

[35] D.K. Hoffman and C.F. Curtiss, Phys. Fluids, 8, 890 (1965).

[36] D.E. Bennett and C.F. Curtiss, J. Chem. Phys., 51, 2811 (1969).

[37] J.A.R Coope and R.F. Snider, J. Chem. Phys., 70, 1075 (1979).

CHAPTER 6

DISCUSSION

6.1 INTRODUCTION

In Chapter 4 the thermal conductivity of a number of gases over a range of temperatures up to 10 MPa was reported. This new set of accurate thermal conductivity data can be used to examine the available kinetic theory expressions for the thermal conductivity of gases. Most theoretical development has been confined to the dilute gas region but, as explained earlier, there have been recent advances with respect to moderately dense gases. Each of these regions will be considered separately in this chapter.

For the most part, it is the dilute gas region which is considered in detail. The kinetic theory of dilute gases shows that their transport properties are related to the intermolecular potential via effective cross-sections. In principle, these cross-sections can be evaluated from an assumed intermolecular potential. For monatomic systems the evaluation of the effective cross-section has become routine and there exist sophisticated potentials for all of the monatomic gases studied here. It is therefore appropriate to make comparison between the experimentally-measured thermal conductivities and the values obtained using the most recently proposed intermolecular potentials. In this way, a degree of mutual confirmation may be obtained since the potentials are obtained from *ab initio* calculation and a large number of microscopic and macroscopic data, but generally **not** including thermal conductivity.

For polyatomic systems, the situation is more complicated. Firstly, the effective cross-sections cannot be calculated routinely from proposed anisotropic potentials, although this may soon be possible [1-3]. Secondly, the intermolecular potentials necessary for evaluation of effective cross-sections are either non-existent or rudimentary. It would therefore seem appropriate to use the present thermal conductivity data to obtain experimental values of the effective cross-sections, required for thermal conductivity evaluation, in anticipation of theoretical and computational advances. Previous studies have shown that some of the effective cross-sections appropriate to thermal conductivity are sensitive to the anisotropy of the potential [4, 5]. Evaluation of these cross-sections would aid those in search of realistic intermolecular potentials.

The immense computational effort required for evaluation of the effective cross-section leads inevitably to the search for successful approximate methods for both the evaluation of effective cross-sections and for the estimation of thermal conductivity from other transport property data. The experimental evaluation of effective cross-sections allows approximate methods in both cases to be reviewed.

The most widely-adopted expressions for the thermal conductivity of polyatomic gases are those derived from the semi-classical kinetic theory of Wang Chang and Uhlenbeck [6] corrected for the effects of spin polarisation (the Viehland-Mason-Sandler formalism [7]). The first-order expressions are of the form

$$[\lambda^0]_1 = [\lambda^0_{tr}]_1 + [\lambda^0_{int}]_1 \tag{6.1.1}$$

$$[\lambda^0_{tr}]_1 = \frac{5k^2T}{2m\langle v\rangle_0}\left\{\frac{\mathfrak{S}(1001) + (\frac{C_{int}}{5k})^{\frac{1}{2}}\mathfrak{S}(\substack{1010\\1001})}{\mathfrak{S}(1010)\mathfrak{S}(1001) - \mathfrak{S}^2(\substack{1010\\1001})}\right\} \tag{6.1.2}$$

$$[\lambda^0_{int}]_1 = \frac{5k^2T}{2m\langle v\rangle_0}\left\{\frac{(\frac{2C_{int}}{5k})^{\frac{1}{2}}\mathfrak{S}(\substack{1010\\1001}) + (\frac{2C_{int}}{5k})\mathfrak{S}(1010)}{\mathfrak{S}(1010)\mathfrak{S}(1001) - \mathfrak{S}^2(\substack{1010\\1001})}\right\}.S \tag{6.1.3}$$

$$S = 1 - \left[\frac{5}{3}\right]\left[1 + \frac{\lambda^0_{tr}}{\lambda^0_{int}}\right]\left[\frac{\Delta\lambda_{\shortparallel}}{\lambda}\right]_{sat} \tag{6.1.4}$$

Here, m is the molecular mass, k is Boltzmann's constant and C_{int} is the internal contribution to the heat capacity at constant volume per molecule. Additionally, $(\Delta\lambda_{\shortparallel}/\lambda)_{sat}$ is the change in thermal conductivity parallel to a magnetic field observed at saturation. The quantities $\mathfrak{S}(\substack{p,q,r,s\\p',q',r',s'})$ are effective cross-sections. In the case where the top and bottom row are identical, it is usual to adopt the notation

$$\mathfrak{S}\left[\substack{p,q,r,s\\p,q,r,s}\right] = \mathfrak{S}(p,q,r,s) \tag{6.1.5}$$

Finally,

$$\langle v\rangle_0 = 4\left[\frac{kT}{\pi m}\right]^{\frac{1}{2}} \tag{6.1.6}$$

and is the equilibrium average molecular velocity.

The expressions for the thermal conductivity contain a number of different effective cross-sections, hence the thermal conductivity alone is insufficient to determine any of the cross-sections. In order to proceed use is made of a number of exact relationships between effective cross-sections [8]. For the purpose of this

analysis, the following are employed.

$$\mathcal{S}\begin{bmatrix}1010\\1001\end{bmatrix} = \begin{bmatrix}5r\\6\end{bmatrix} \mathcal{S}(0001) \qquad (6.1.7)$$

$$\mathcal{S}(1010) = \frac{2}{3}\mathcal{S}(2000) + \frac{25r^2}{8}\mathcal{S}(0001) \qquad (6.1.8)$$

$$\mathcal{S}(0010) = \frac{5r^2}{3}\mathcal{S}(0001) \qquad (6.1.9)$$

where

$$r = \left[\frac{2C_{int}}{5k}\right]^{\frac{1}{2}} \qquad (6.1.10)$$

The expressions for the thermal conductivity, equations (6.1.1)–(6.1.4), can be used in conjunction with the above to show that in the first order the thermal conductivity may be determined by three effective cross-sections and the spin polarisation correction

$$[\lambda^0]_1 - f(\mathcal{S}(2000), \mathcal{S}(0001), \mathcal{S}(1001), S) \qquad (6.1.11)$$

This analysis indicates that four experimental quantities are necessary for explicit evaluation of a consistent set of effective cross-sections.

The cross-section $\mathcal{S}(2000)$ an be obtained from the zero-density viscosity, for which the first-order kinetic theory expression is

$$[\eta^0] = \frac{kT}{\langle v\rangle_0}\mathcal{S}(2000)^{-1} \qquad (6.1.12)$$

The cross-section $\mathcal{S}(0001)$ is related to the collision number, for internal energy relaxation [9]

$$\zeta_{int} = \frac{4kT}{\langle v\rangle_0[\eta^0]}\mathcal{S}(0001)^{-1} \qquad (6.1.13)$$

or may be obtained from measurement of thermo-molecular pressure

differences [10] which can also be used to evaluate the translational part of the thermal conductivity.

Having obtained values for all the effective cross-sections, the information can be put to good use. An alternative formulation for the thermal conductivity of a polyatomic gas has been derived by Thijsse *et al.* [11] in which they found that in what they refer to as the second approximation

$$[\lambda]_2^T = \frac{5k^2T(1+r^2)}{2m\langle v\rangle_0 \mathcal{S}(10E)} \left[1 - \frac{\mathcal{S}^2\binom{10E}{10D}}{\mathcal{S}(10E)\mathcal{S}(10D)}\right]^{-1} \qquad (6.1.14)$$

The new effective cross-sections are related to those introduced earlier by the expressions [11]

$$\mathcal{S}(10E) = (1+r^2)^{-1}\left[\mathcal{S}(1010) - 2r\mathcal{S}\begin{bmatrix}1010\\1001\end{bmatrix} + r^2\mathcal{S}(1001)\right] \qquad (6.1.15)$$

$$\mathcal{S}\begin{bmatrix}10E\\10D\end{bmatrix} = (1+r^2)^{-1}\left[r\mathcal{S}(1010) + (1-r^2)\mathcal{S}\begin{bmatrix}1010\\1001\end{bmatrix} - r\mathcal{S}(1001)\right] \qquad (6.1.16)$$

$$\mathcal{S}(10D) = (1+r^2)^{-1}\left[r^2(1010) + 2r\mathcal{S}\begin{bmatrix}1010\\1001\end{bmatrix} + \mathcal{S}(1001)\right] \qquad (6.1.17)$$

[Note: Here the more recent notation of McCourt *et al.* [12] is used in place of that introduced by Thijsse *et al.* [11]. They are simply related, i.e.

$$\mathcal{S}(10E) \equiv \mathcal{S}(101+1),\ \mathcal{S}(10D) \equiv \mathcal{S}(101-1),\ \mathcal{S}\begin{bmatrix}10E\\10D\end{bmatrix} \equiv \mathcal{S}\begin{bmatrix}101+1\\101-1\end{bmatrix}\ ]$$

Hence the effective cross-sections appropriate to the Thijsse formulation may be calculated directly.

The two formulations are not exactly equivalent since the Viehland–Mason–Sandler formalism accounts for spin polarisation effects in the gas in a way not yet possible for the Thijsse formulation. The subsequent re–evaluation of thermal conductivity using the Thijsse effective cross–sections will not reproduce the experimental thermal conductivity exactly. The error will, however, be small and will not effect the major conclusions concerning the Thijsse formulation.

Application of the Mason–Monchick approximation [13] implies the following for the Wang Chang and Uhlenbeck effective cross–sections found within the Viehland–Mason–Sandler formalism. (The subscript M denotes application of the Mason–Monchick approximation)

$$\mathfrak{S}_M(1010) = \frac{2}{3}\,\mathfrak{S}(2000) \tag{6.1.18}$$

$$\mathfrak{S}_M\begin{bmatrix}1010\\1001\end{bmatrix} = 0 \tag{6.1.19}$$

and

$$\mathfrak{S}_M(1001) = \frac{kT}{\rho D\langle v\rangle_0} \tag{6.1.20}$$

where D is the hypothetical self–diffusion coefficient of the gas defined by

$$D = \frac{kT}{\rho\langle v\rangle_0}\,\mathfrak{S}(1000)^{-1} \tag{6.1.21}$$

and ρ is the density.

The results above have been obtained by neglecting the inelastic aspects of the molecular collisions. The basis for this approximation is that the change in internal energy during a

collision is negligible compared with the kinetic energy of the colliding molecules. The result of this approximation is to recover from the Viehland–Mason–Sandler formulation, with the additional assumption that S = 1, the modified Eucken formula

$$\frac{\lambda^0 m}{\eta^0} = \frac{15}{4} k + C_{int} \frac{\rho D}{\eta} \qquad (6.1.22)$$

It is generally recognised that this formula gives very poor results when used to calculate thermal conductivity from viscosity. The effects of inelastic collisions must be retained in the expressions for thermal conductivity if they are to have any predictive power. The effects of inelastic collisions are retained if the expressions for thermal conductivity in the Viehland–Mason–Sandler equations are rearranged using the exact relations and the expressions for other transport properties. In this case, without any further approximation [7],

$$\frac{m[\lambda^0]_1}{[\eta^0]_1} = \frac{m[\lambda^0_{tr}]_1}{[\eta^0]_1} + \frac{m[\lambda^0_{int}]_1}{[\eta^0]_1} \qquad (6.1.23)$$

where

$$\frac{m[\lambda^0_{tr}]_1}{[\eta^0]_1} = \frac{5k}{2m}\left[\frac{3}{2} - \Delta\right] \qquad (6.1.24)$$

$$\frac{m[\lambda^0_{int}]_1}{[\eta^0]_1} = \frac{k\rho D_{int}}{\eta}\left[\frac{C_{int}}{k} + \Delta\right] . S \qquad (6.1.25)$$

and

$$\Delta = \frac{2C_{int}}{k\zeta_{int}}\left[\frac{5}{2} - \frac{\rho D_{int}}{[\eta^0]_1}\right]\left[1 - \frac{2}{\pi\zeta_{int}}\left[\frac{5}{3}\frac{C_{int}}{k} + \frac{\rho D_{int}}{[\eta^0]_1}\right]\right]^{-1} \qquad (6.1.26)$$

Equations (6.1.23)–(6.1.26) contain the symbol D_{int} which refers to

the so-called diffusion coefficient of internal energy, defined in terms of effective cross-sections as [4]

$$D_{int} = \frac{kT}{\rho \langle v \rangle_0} \left[\mathfrak{S}(1001) - \tfrac{1}{2}\mathfrak{S}(0001) \right]^{-1} \qquad (6.1.27)$$

D_{int} is the only quantity in the above expressions which is inaccessible to experimental measurement. Application of the Mason-Monchick approximation to this quantity alone indicates that $D_{int} = D$. For calculation of $\rho D_{int}/\eta^0$ use can be made of the kinetic theory relation [14]

$$\frac{\rho D_{int}}{[\eta^0]_1} = \frac{6}{5} A^* \frac{D_{int}}{D} \qquad (6.1.28)$$

A^* is a ratio of effective cross-sections generally considered to be insensitive to the pair potential used for its evaluation [86]. For calculation purposes the value of A^* is obtained from a correlated source [14] and D_{int}/D is assumed to be unity.

Previous studies have indicated that this calculation procedure can produce serious errors when the thermal conductivity is calculated from viscosity [15]. Some of the cause of these discrepancies must be due to incorrect calculation of A^* but the assignment $D_{int} = D$ must also be in error [15].

Having obtained experimental values for the effective cross-sections using the present thermal conductivity data, it is possible to investigate further the behaviour of the ratio D_{int}/D and to make some comparisons between different gases and with other theoretical predictions. Moraal, McCourt and Snider [8, 16] have been able to demonstrate that for diatomic molecules in the high temperature limit

$$S(1001) \rightarrow S(1000) + \frac{7C_{int}}{6k} S(0001) \qquad (6.1.29)$$

and hence in the same limit

$$\frac{D_{int}}{D} \rightarrow \frac{S(1000)}{S(1000) + \left[\left[\frac{7C_{int}}{6k}\right] - \frac{1}{2}\right] S(0001)} \qquad (6.1.30)$$

which implies that $D_{int}/D \rightarrow 1$ from below since $S(0001) \rightarrow 0$.

Within the Thijsse formulation the effective cross-section $S(^{10E}_{10D})$ couples the total flux and a difference flux. Neglecting the effect of the relative importance of the translational and internal heat flow corresponds to setting $S(^{10E}_{10D}) = 0$ in equation (6.1.14) [11]. A recent theoretical and experimental study [17] has confirmed that the term $\left[1 - \frac{S^2(^{10E}_{10D})}{S(10E)S(10D)}\right]$ has a value very close to unity for many gases. Hence a first-order equation of the form [18]

$$[\lambda]_1^T = \frac{5k^2T(1+r^2)}{2m\langle v\rangle_0 S(10E)} \qquad (6.1.31)$$

is a good approximation for many gases and has the advantage of far greater simplicity over that of the Viehland-Mason-Sandler formalism. The validity of the first-order expression is further tested with the aid of the cross-sections calculated using the new accurate thermal conductivity data.

Whilst the effective cross-sections appropriate to both formalisms have been evaluated for all the polyatomic gases measured, a complete analysis was not always possible owing to the lack of bulk viscosity or related data. In such cases the effective cross-

sections presented are for guidance only and quantitative agreement between theoretical calculations and experimental evaluations may not be realised. However, the behaviour of the derived quantities obtained from these effective cross-sections, particularly the temperature dependence of the ratio D_{int}/D, leads to some interesting conclusions.

In view of recent theoretical developments concerning the density dependence of the thermal conductivity of gases, the new set of experimental data is used to test the available theories for the first density coefficient in the expansion

$$\lambda = \lambda^0[1 + \lambda_1 n + \lambda_2 n^2 + \ldots] \qquad (6.1.32)$$

(where n is the number density) and to confirm that generally the excess thermal conductivity is independent of temperature. The most recent dense gas theory due to Rainwater and Friend [19, 20] is used as the basis for a semi-empirical correlation of the first density coefficient.

In the following sections the monatomic gases are studied together and the predictions of recent intermolecular potentials are compared with the new experimental data. The polyatomic gases are studied separately. This is because each molecule is different and has a different intermolecular force. The individual nature of each molecule is a major obstacle to a unified account of the thermal conductivity of polyatomic gases. In the final section the theories for the initial density dependence of thermal conductivity are discussed. The most recent theory is based on a Lennard-Jones potential so it is appropriate to consider its application to all the

gases studied as a whole.

6.2 THE DILUTE MONATOMIC GAS

In the limit of zero-density the thermal conductivity is determined by the interaction between just two molecules. It is not, however, possible to perform transient hot-wire measurements at very low pressures, hence it is necessary to obtain the zero-density thermal conductivity by extrapolation. This extrapolation is carried out using a statistical method, described in detail elsewhere [21], applied to the data for each isotherm, which seeks to obtain the optimum values of the coefficients in the density expansion of the thermal conductivity

$$\lambda = \lambda^0 + \lambda_1\rho + \lambda_2\rho^2 + \ldots \qquad (6.2.1)$$

where ρ is the density in kg m^{-3}. To do this the first five points, $\lambda(\rho)$ along an isotherm are fitted to a linear function of ρ. More data points are then added progressively until the standard deviation of the fit passes through an extremum. At this stage, a second-order fit is initiated and the process is repeated for succeeding orders of polynomial. Provided that the experimental data conform to a polynomial expansion this process will yield the optimum values of λ^0, λ_1, etc. which are consistent between various orders of polynomial.

Tables 6.2.1 and 6.2.2 show the results of this analysis for argon, helium and neon. The results for the analysis for argon provide convincing evidence for conformality with a polynomial exapnsion for $\lambda(\rho)$. The results for helium and neon show that a linear expression is generally all that is required for representing

$\lambda(\rho)$ over the entire density range studied.

The important property of interest in this section is λ^0. Tables 6.2.3 and 6.2.4 list the optimum values of λ^0 obtained for all the monatomic gases studied along with the experimental values of the group

$$Eu^* = \frac{2\lambda^0 m}{5\eta^0 C_v F(T)} \qquad (6.2.2)$$

derived using the independent viscosiy data of Kestin *et al.* [22, 23] and Vogel [24] above 0°C. At lower temperatures the viscosity data of Clarke and Smith was used [25]. The value of F(T) is obtained from a correlated source [4] and deviates from unity by about 1%, C_v is the heat capacity per molecule at constant volume and m is the mass of the molecule. F(T) is the contribution of high-order terms within the Chapman-Enskog theory and is found to be essentially independent of the intermolecular potential. Its function in equation 6.2.2 is to correct the experimental data for thermal conductivity and viscosity to the equivalant first order result. It can be seen from Tables 6.2.3 and 6.2.4 that there is broad consistency between the theoretical and experimental value of Eu^* within the uncertainty ascribed to the experimental value, which includes an allowance for interpolation within the viscosity data. The discrepancies using Vogel's viscosity data are slightly larger, especially at the highest temperature for helium where the discrepancy is 1.4%. On this basis, it may be concluded that the uncertainty of the reported thermal conductivity is consistent with that claimed in Chapter 4, i.e. generally 0.3% near room temperature and deteriorating to 0.5% at the extremes of the temperature range. It would be premature, however, to claim that it is possible to distinguish between the two sets of viscosity data

above room temperature.

Also included in Tables 6.2.3 and 6.2.4 are theoretical values for the thermal conductivity of the gases studied. For argon, a potential has been proposed by Aziz [26] which has been deduced from a large number of molecular and macroscopic properties. The thermal conductivity was calculated in the third-order Chapman-Cowling approximation [27] and presented in the form of a correlation covering the temperature range 100 to 6600 K. In the case of helium, a pair potential has also been proposed by Aziz *et al.* [28]. In order to assess the ability of this potential to reproduce the independent thermal conductivity data, the thermal conductivity for helium was calculated from this potential by standard methods in the second-order Kihara approximation to the Chapman-Enskog theory [4]. Finally, a potential for neon has been proposed by Aziz *et al.* [29] and the thermal conductivity calculated by Millat [92]

From Tables 6.2.3 and 6.2.4 the proposed potentials reproduce the thermal conductivity of the gas measured to within 1% except in the case of helium at the highest temperature of 155°C, where the deviation is 1.7%. This level of agreement between the theoretical and experimental thermal conductivity provides mutual confirmation of the experimental data and the proposed pair potentials.

6.3 THE DILUTE POLYATOMIC GAS

The results of the statistical analysis for hydrogen, nitrogen, carbon dioxide, nitrous oxide, methane and tetrafluoromethane are shown in Tables 6.3.1-6.3.5. A linear expression in density is all that is required for hydrogen in the density range studied. In the case of nitrogen, methane and tetrafluoromethane, the coefficients

are generally recovered within their statistical uncertainty when a higher-order fit is employed to represent the data in a higher density range. This observation confirms the validity of the polynomial expansion in density for the thermal conductivity of these gases. For tetrafluoromethane the range over which a linear expansion is valid is very limited, hence determination of the zero-density thermal conductivity and the first density coefficient is more uncertain. For this reason, a quadratic expansion was used for this gas to determine the optimum set of coefficients.

For carbon dioxide and nitrous oxide, the linear region is also restricted and in some cases may only just lie within the region covered by experiment. The determination of the zero-density thermal conductivity and the first density coefficient is further complicated by the proximity of the critical point. There is a considerable contribution to the thermal conductivity at high densities from critical enhancement, especially for the lowest isotherm. The total thermal conductivity is therefore not properly represented by a polynomial in density. This is manifest as less consistent agreement for the expansion coefficients between orders of polynomial which, in turn, results in an error in the zero-density thermal conductivity extracted from the statistical analysis amounting to ± 0.5% for these gases. The error claimed for each individual thermal conductivity measurement remains ± 0.3%.

A similar situation exists with respect to the gases ethane and ethylene. The linear region is again very restricted and critical enhancement complicates application of the statistical analysis. Consequently, the uncertainty in the derived values of the zero-density thermal conductivity and the first density coefficient is somewhat larger than that typical for a monatomic gas. Typically,

the overall uncertainty of the zero-density thermal conductivity for ethane and ethylene amounts to ± 0.5%. It is worth noting that the first density coefficient for ethylene is particularly small and the value of zero is occasionally included within the rather large uncertainty band.

Table 6.3.6 contains the best estimate of the zero-density thermal conductivity and the first density coefficient for the polyatomic gases studied. Having now obtained the best estimates of the zero-density for the polyatomic gases, it is possible to analyse the results with respect to the available kinetic theory of polyatomic gases.

6.3.1 Hydrogen

In order to implement the analysis described in the introduction, other properties in addition to the thermal conductivity must be found. For the ideal gas, isobaric heat capacity a representation of the tables compiled by McCarty [30] and developed by Armstrong [31] has been used. The correlation is valid in the temperature range 80–2500 K. The internal energy contribution to the heat capacity is obtained by application of the simple formula

$$\frac{C_{int}}{k} = \frac{C_p}{k} - \frac{5}{2} \qquad (6.3.1.1)$$

The zero-density viscosity of hydrogen is obtained from a recent correlation of a large set of experimental data [32] and is considered to have an uncertainty of ± 0.5% in the temperature range of interest. The collision number for rotational relaxation is obtained from the same source and is a corrrelation of the data for normal hydrogen compiled by Lambert [87]. When molecules have more

than one internal mode then it is usual to assume that these modes are decoupled, and apply the formula [33]

$$\frac{C_{int}}{\zeta_{int}} = \frac{C_{rot}}{\zeta_{rot}} + \frac{C_{vib}}{\zeta_{vib}} \qquad (6.3.1.2)$$

where

$$C_{int} = C_{rot} + C_{vib} \qquad (6.3.1.3)$$

For hydrogen $C_{vib} << C_{rot}$ and $\zeta_{vib} >> \zeta_{rot}$, hence the second term in equation (6.3.1.2) can be neglected for the purposes of this analysis. Finally, an experimental value of $(\Delta\lambda_{\prime\prime}/\lambda)_{sat}$ at 300 K has been obtained by Hermans *et al.* [34]. The value of $(\Delta\lambda_{\prime\prime}/\lambda)_{sat}$ is small (= 6 x 10^{-5}) and its temperature dependence is weak. Therefore, the value of $(\Delta\lambda_{\prime\prime}/\lambda)_{sat}$ can be kept constant without affecting the main conclusions.

Using this collection of experimental data, a consistent set of Wang Chang and Uhlenbeck effective cross-sections appropriate to the Viehland-Mason-Sandler formalism and a constant set of effective cross-sections appropriate to the Thijsse formalism were obtained. The results are shown in Tables 6.3.7 and 6.3.8. The order of magnitude of the effective cross-sections indicate that the translational and internal energy fluxes are essentially decoupled. In particular, ignoring the coupling cross-section within the Thijsse formalism and using the simplified expression equation (6.1.31) reproduces the thermal conductivity almost exactly. It is also important to note that the negative values of $\mathfrak{S}(^{10E}_{10D})$ found for hydrogen are consistent with the conclusions of a recent theoretical and experimental investigation [17]. The evidence here seems to suggest that the Mason-Monchick approximation is appropriate for hydrogen. But further investigation provides evidence which is

contradictory to this conclusion.

Using the effective cross-sections and the value of A^* calculated by standard methods from the recommended spherical part of the potential [35], experimental values of D_{int}/D may be obtained via application of equations (6.1.27) and (6.1.28). The values of A^* were obtained from the recommended spherical part of the potential because the calculation of the effective cross-sections necessary is of such complexity that they have only been calculated up to 200 K [36] using the full potential. Furthermore, the best anisotropic pair potential for hydrogen, which was employed for these calculations, is not available in the open literature [37, 38]. Table 6.3.9 shows the value of A^* used and the values for D_{int}/D obtained. The uncertainty in the values of D_{int}/D due to small errors in thermal conductivity and viscosity is estimated to be about 2%. The values of D_{int}/D obtained show significant departure from the expected value of unity. It therefore seems that neither small negative values of $\mathfrak{S}(^{10E}_{10D})$ nor small values of $\mathfrak{S}(^{1010}_{1001})$ and $\mathfrak{S}(0001)$ are a guarantee that D_{int}/D = 1.

If the assumption that D_{int}/D = 1 is made and the thermal conductivity is calculated using equations (6.1.23–6.1.26) with a value of A^* obtained as above, then the maximum deviation of the theoretical prediction from the experimental results is 1.7%. The error in assuming that D_{int}/D = 1 is attenuated in this case because the rotational relaxation number is large and the internal energy contribution to the thermal conductivity is only about 25% of the total.

Unfortunately, application of the asymptotic theory of Moraal *et al.* [8, 16] would be inappropriate because, even at the highest temperature studied here, the hydrogen molecule is far from being in

the high temperature limit, since the rotational energy level spacing is so large. In fact, the large energy level spacing would seem to invalidate the application of the Mason–Monchick approximation since it is based on the contrary assumption that the energy level spacing is small. However, application of the Mason–Monchick procedure does seem to enjoy a fair degree of success; this is due to the rarity of inelastic collisions rather than the amount of energy transferred during the collision. It would appear that further theoretical investigation of this special system is necessary before these puzzles are solved.

6.3.2 Carbon Dioxide

In order to apply the analysis of the previous section for carbon dioxide the zero–density viscosity of carbon dioxide may be calculated from the correlation of Trengove *et al.* [39] which has recently been improved [40] so as to include the precise measurements of Vogel [41]. The estimated uncertainty of the new correlation is 0.3% in the temperature range of interest [40]. The value of $(\Delta\lambda_{\text{II}}/\lambda)_{\text{sat}}$ has been measured by Hermans *et al.* [42] at low temperatures and is essentially temperature–independent with a value $(\Delta\lambda_{\text{II}}/\lambda)_{\text{sat}} = -0.0075$. This constant value was used throughout the entire temperature range since the effect of the correction term S is small. Finally, for the isochoric heat capacity of the ideal gas the correlated values of a new equation of state by Ely *et al.* [43] has been used.

In contrast to the case for hydrogen, there are significant contributions to the heat capacity from both vibrational and rotational modes.

Hence,

$$C_{int} = C_{rot} + C_{vib} \qquad (6.3.2.1)$$

and

$$\frac{C_{int}}{\zeta_{int}} = \frac{C_{rot}}{\zeta_{rot}} + \frac{C_{vib}}{\zeta_{vib}} \qquad (6.3.2.2)$$

However, $\zeta_{vib} >> \zeta_{rot}$. Measurements of ζ_{vib} [44–47] can be used to produce a correlation of the form [40]

$$\frac{1}{\zeta_{vib}} = 4.52234 \times 10^{-4} \exp(-948.148/T) \qquad (6.3.2.3)$$

Unfortunately, there are no reliable measurements of λ^{o}_{tr} over the temperature range for carbon dioxide. However, there is a reliable measurement of ζ_{rot} from thermomolecular pressure differences at 300 K (ζ_{rot} = 1.95) [48]. There is also considerable evidence that the formula due to Brau and Jonkman [49] provides a reasonable estimate of the temperature dependence of ζ_{rot} for linear molecules [48].

$$\zeta_{rot} = \zeta^{\infty}_{rot}\left[1 + \frac{\pi^{3/2}}{2}\left[\frac{1}{T^*}\right]^{\frac{1}{2}} + \left[2 + \frac{\pi^2}{4}\right]\left[\frac{1}{T^*}\right] + \pi^{3/2}\left[\frac{1}{T^*}\right]^{3/2}\right]^{-1} \qquad (6.3.2.4)$$

where

$$T^* = Tk/\epsilon, \quad \epsilon/k = 251.2 \text{ K} \quad [40] \qquad (6.3.2.5)$$

and ζ^{∞}_{rot} is a disposable parameter found from the one available reliable datum to be 22.53 [40]. Equation (6.3.2.4) and (6.1.13) are therefore used to obtain $\mathfrak{S}(0001)$ at all other temperatures.

Tables 6.3.10 and 6.3.11 show a consistent set of the various Wang Chang Uhlenbeck effective cross-sections and those present

within the Thijsse formalism. The tables demonstrate that the coupling cross-sections are considerably smaller than the other cross-sections and particularly in the case of the Thijsse formalism, the relation

$$\mathcal{S}^2\begin{bmatrix}10E\\10D\end{bmatrix} \ll \mathcal{S}(10E)\mathcal{S}10D) \qquad (6.3.2.6)$$

is confirmed. The use of the simplified first order result would constitute a maximum error of 0.3% in the thermal conductivity, which is of equivalent order to the experimental uncertainty.

The calculated values of the effective cross-sections have been used to calculate values for D_{int}/D in the usual way. The results of this calculation along with the value of A^* obtained from a universal correlation [14] are included in Table 6.3.12. The results indicate compliance with the theoretical prediction of Moraal *et al.* [8, 16] (i.e. $D_{int}/D \to 1$ at higher temperatures). As noted for hydrogen, the values of D_{int}/D obtained in this way are burdened by an error of perhaps 2% due to the value of D_{int}/D being sensitive to small errors in the viscosity and thermal conductivity. In addition, the value of A^* calculated by way of a corresponding states approach may be in error by, at most, a few percent.

These considerations do not detract from the confidence placed on the value of D_{int} or individual cross-sections. In particular, the evidence from Table 6.3.11 indicates quite clearly that the simplified Thijsse formulation may be used as the basis of a simple correlation of the thermal conductivity. Hence, a suitably-defined reduced effective cross-section has been obtained by fitting the present data and other older, but reliable, data in the temperature range $300 < T < 470$ K [40]

$$\lambda^0 = \frac{5k^2T(1+r^2)}{2m\langle v\rangle_0\pi\sigma^2\mathfrak{S}_c^*(10E)} \qquad (6.3.2.7)$$

where

$$\mathfrak{S}_c^*(10E) = 0.3726 + \frac{152.3}{T} \qquad (6.3.2.8)$$

and

$$\sigma = 0.3751 \text{ nm} \qquad (6.3.2.9)$$

Generally, this representation reproduces the thermal conductivity to within 1% , see figure 6.1 and ref. [40]. The success of this simple formulation seems to indicate that the method offers a concise description of the thermal conductivity for practical purposes.

In the case of carbon dioxide, the analysis of the new thermal conductivity results in terms of effective cross-sections represents construction of evidence for the validity and the subsequent use of the Thijsse formulation for correlation of thermal conductivity. It is not anticipated that the effective cross-sections can be of significant value in the testing of intermolecular potentials until further accurate measurements of the total thermal conductivity and of its translational part, or equivalently ζ_{rot}, are performed over an extended temperature range.

6.3.3 Nitrous Oxide

The analysis of the nitrous oxide measurements is based on a less complete data set than was available for carbon dioxide. For viscosity, use has been made of a recent critical examination of the available data [40]. The uncertainty in the viscosity is estimated to be a few parts in a thousand in the temperature range of interest [40].

Figure 6.1

Deviations, $\epsilon = ((\lambda_{EXP} - \lambda_{CORR})/\lambda_{CORR})$ X 100 %, of the thermal conductivity data at zero density for carbon dioxide and nitrous oxide from a correlation based on eqn. (6.3.2.7)

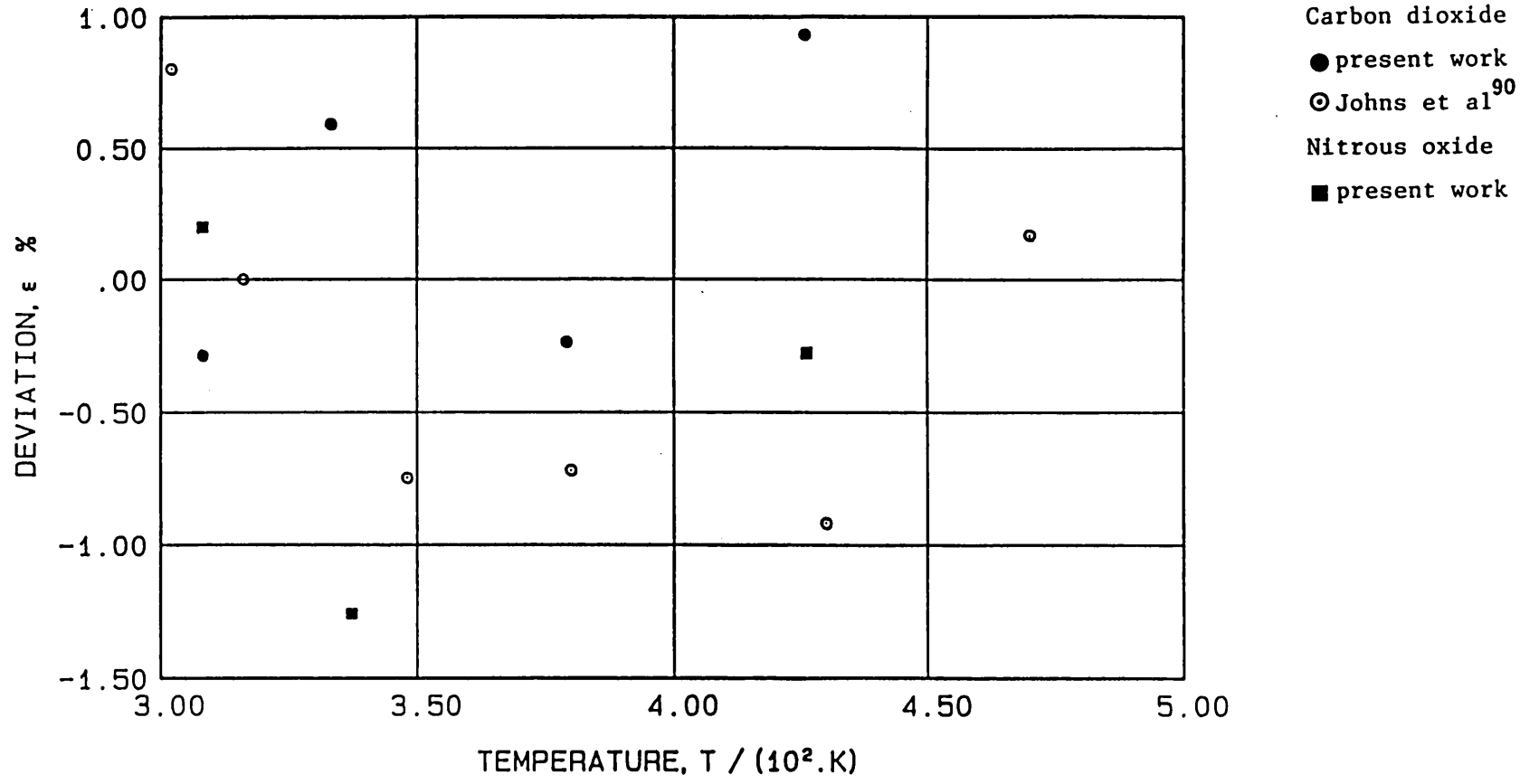

The ideal gas heat capacity is obtained from the tabulations of Glushko [50], while the vibrational collision number ζ_{vib}, has been obtained from the work of Eucken and Nümann [46] and found to be well-represented by a function of the form [40]

$$\frac{1}{\zeta_{vib}} = 12.44859 \times 10^{-4}\exp(-60.69039/T) \qquad (6.3.3.1)$$

There are no reported measurements for λ^0_{tr} for nitrous oxide so the available measurements of ζ_{rot}, which are reported to be the same as CO_2 at room temperature [51], have been used in conjunction with the Brau Jonkmann formula (equation (6.3.2.4)), with $\zeta^{\infty}_{rot} = 22.88$, to obtain the temperature dependence of $\mathfrak{S}(0001)$. The value of $(\Delta\lambda_{\eta}/\lambda)_{sat}$ for nitrous oxide has not been reported. The similarities between nitrous oxide and carbon dioxide and the small effect of this correction indicate that it is not unreasonable to adopt the value $(\Delta\lambda_{\eta}/\lambda)_{sat} = -0.008$ over the entire temperature range. Using all of this information, tabulations of the effective cross-sections are prepared. Table 6.3.13 shows the Wang Chang and Uhlenbeck effective cross-sections and Table 6.3.14 lists those appropriate to the Thijsse formalism. Owing to the lack of some experimental data for nitrous dioxide, the values contained within the tables are more uncertain than those for carbon dioxide.

A calculation of the ratio D_{int}/D is performed in the same way as for carbon dioxide. The results, along with the corresponding A^* values, are included in Table 6.3.15. It can be seen that whilst the ratio increases with temperature, it attains a value in excess of unity by a few percent at the highest temperatures. This result is in conflict with the expectation of theory and was not observed with CO_2. It would seem likely that the conflict arises from use of a

slightly incorrect value of A^*. It is, however, unclear why this should occur with N_2O and not CO_2.

Table 6.3.14 shows that the simplified Thijsse formalism is appropriate for representation of the thermal conductivity. Consequently, the present data and that of Kestin *et al.* [52] has been used to prepare a correlation, valid in the temperature range $300 \leq T \leq 430$ K, using equation (6.3.2.7) with $\mathfrak{S}_c^*(10E)$ given by

$$\mathfrak{S}_c^*(10E) = 0.2736 + \frac{183.21}{T} \qquad (6.3.3.2)$$

The deviations of the experimental data from this simple representation are shown in figure 6.1 and do not exceed ± 1.2%.

6.3.4 Methane

The zero-density viscosity for methane was obtained from a recent correlation, valid in the temperature range $110 < 1050$ K [39]. For the isochoric heat capacity, C_v, of the ideal gas the compilation given by Angus *et al.* [53] has been employed. The internal energy contribution to the heat capacity is obtained from the simple formula

$$\frac{C_v}{k} = \frac{3}{2} + \frac{C_{int}}{k} \qquad (6.3.4.1)$$

where

$$C_{int} = C_{rot} + C_{vib} \qquad (6.3.4.2)$$

These two modes of internal motion will, in general, relax at different rates. Adopting the usual separation

$$\frac{C_{int}}{\zeta_{int}} = \frac{C_{rot}}{\zeta_{rot}} + \frac{C_{vib}}{\zeta_{vib}} \qquad (6.3.4.3)$$

Measurement of ζ_{vib} has been made over the temperature range of interest by Cotrell and Matheson [54] and Eucken and Aybar [55]. Their results are best represented by the correlation [56]

$$\frac{1}{\zeta_{vib}} = 10.7445 \times 10^{-4}\exp(-841.5/T) \qquad (6.3.4.4)$$

The fractional change in thermal conductivity of methane parallel to a magnetic field $(\Delta\lambda_{\parallel}/\lambda)_{sat}$ has been determined [42] below room temperature and has been found to be essentially independent of temperature. Hence the value $(\Delta\lambda_{\parallel}/\lambda)_{sat} = -0.0017$ has been used over the whole temperature range.

The final piece of experimental information is provided by Millat *et al.* [10]. They have independently determined the translational part of the thermal conductivity of methane in the temperature range 300 to 650 K by measuring thermo-molecular pressure differences.

Table 6.3.16 contains the Wang Chang Uhlenbeck effective cross-sections and Table 6.3.17 the appropriate Thijsse effective cross-sections all calculated using the present thermal conductivity data and the other tranpsort property data. Having calculated the effective cross-sections, the usual derived quantities may be obtained. The value of the ratio D_{int}/D has been calculated using values of A^* obtained from the principle of corresponding states [14]. In addition to D_{int}/D the value of the rotational collision number may be obtained from equations (6.1.10) and (6.3.4.2). The values obtained may be considered to be experimental since they have been obtained from measurements of selected quantities and application of the appropriate kinetic theory results. The values of

A^*, D_{int}/D and ζ_{rot} are found in Table 6.3.18.

The results of Tables 6.3.16 and 6.3.17 demonstrate that the relaxation cross-section $\mathfrak{S}(0001)$ and the couplng cross-sections, $\mathfrak{S}\begin{bmatrix}1010\\1001\end{bmatrix}$ and $\mathfrak{S}\begin{bmatrix}10E\\10D\end{bmatrix}$ are much smaller than the transport cross-sections. Indeed, use of the simplified first-order Thijsse expression leads to an error of only 0.04% in the thermal conductivity. The results of Table 6.3.18 show quite clearly that $D_{int}/D \neq 1$. The use of $D_{int}/D = 1$ would, in the worst case, lead to an error of some 4% in the thermal conductivity. The temperature dependence of the ratio D_{int}/D is in qualitative agreement with the theory of Moraal *et al.* [8, 16]. The theoretical expectation that D_{int}/D tends towards unity at higher temperatures is valid for linear molecules. Even though the corresponding limit for other molecular shapes is unknown, the limit would intuitively be unity. The reason for the present limit being above unity is as yet not understood.

The success of the simplified Thijsse formalism has been used as the basis for a simple correlation of the zero-density thermal conductivity. The correlation is valid in the temperature range 300-425 K and has been obtained using the present data along with the earlier results of Clifford *et al.* [57] and Assael *et al.* [58]. In this case [56]

$$\mathfrak{S}_c^*(10E) = 0.3598 + \frac{100.49}{T} \qquad (6.3.4.5)$$

and

$$\frac{\epsilon}{k} = 163.6 \text{ K} \qquad (6.3.4.6)$$

$$\sigma = 0.3709 \text{ nm} \qquad (6.3.4.7)$$

The maximum deviation of the thermal conductivity data from this

equation as shown in figure 6.2 is 1.2% which is consistent with the scatter in the total set of experimental data.

6.3.5 Tetrafluoromethane

The analysis of tetrafluoromethane has been carried out using the viscosity data of Kestin *et al.* [23] and the compilation due to Glushko [50] for the heat capacity. The value of $(\Delta\lambda_{\mu}/\lambda)_{sat}$ was obtained by Hermans *et al.* [42] and a value of $(\Delta\lambda_{\mu}/\lambda)_{sat} = -0.0028$ has been used throughout the entire temperature range. The vibrational collision number has been measured by Corran *et al.* [59] and Jackson *et al.* [60]. Their results have been correlated by means of the equation [56]

$$\frac{1}{\zeta_{vib}} = 200.785 \times 10^{-4}\exp(-1120.04/T) \qquad (6.3.5.1)$$

Finally, the translational contribution to the thermal conductivity has been measured by Millat [10]. These data, together with the present thermal conductivity data, have been used to construct Tables 6.3.19 and 6.3.20 which contain a consistent set of effective cross-sections found within the Viehland-Mason-Sandler formalism (i.e. the Wang Chang-Uhlenbeck effective cross-sections) and the Thijsse formalism.

The results in Tables 6.3.19 and 6.3.20 show that for tetrafluoromethane, as for methane, the relaxation and coupling cross-sections are small compared with the transport cross-sections. This is most apparent in terms of the Thijsse formalism where use of the first-order Thijsse equation leads to an error of only 0.06%. Table 6.3.21 shows the derived quantities ζ_{rot} and D_{int}/D. The value of A^* used for the calculation of D_{int}/D was obtained from the

Figure 6.2

Deviations, $\varepsilon = ((\lambda_{EXP} - \lambda_{CORR})/\lambda_{CORR})$ X 100 %, of the thermal conductivity of methane and tetrafluoromethane at zero density from the correlation based on eqn. (6.3.2.7)

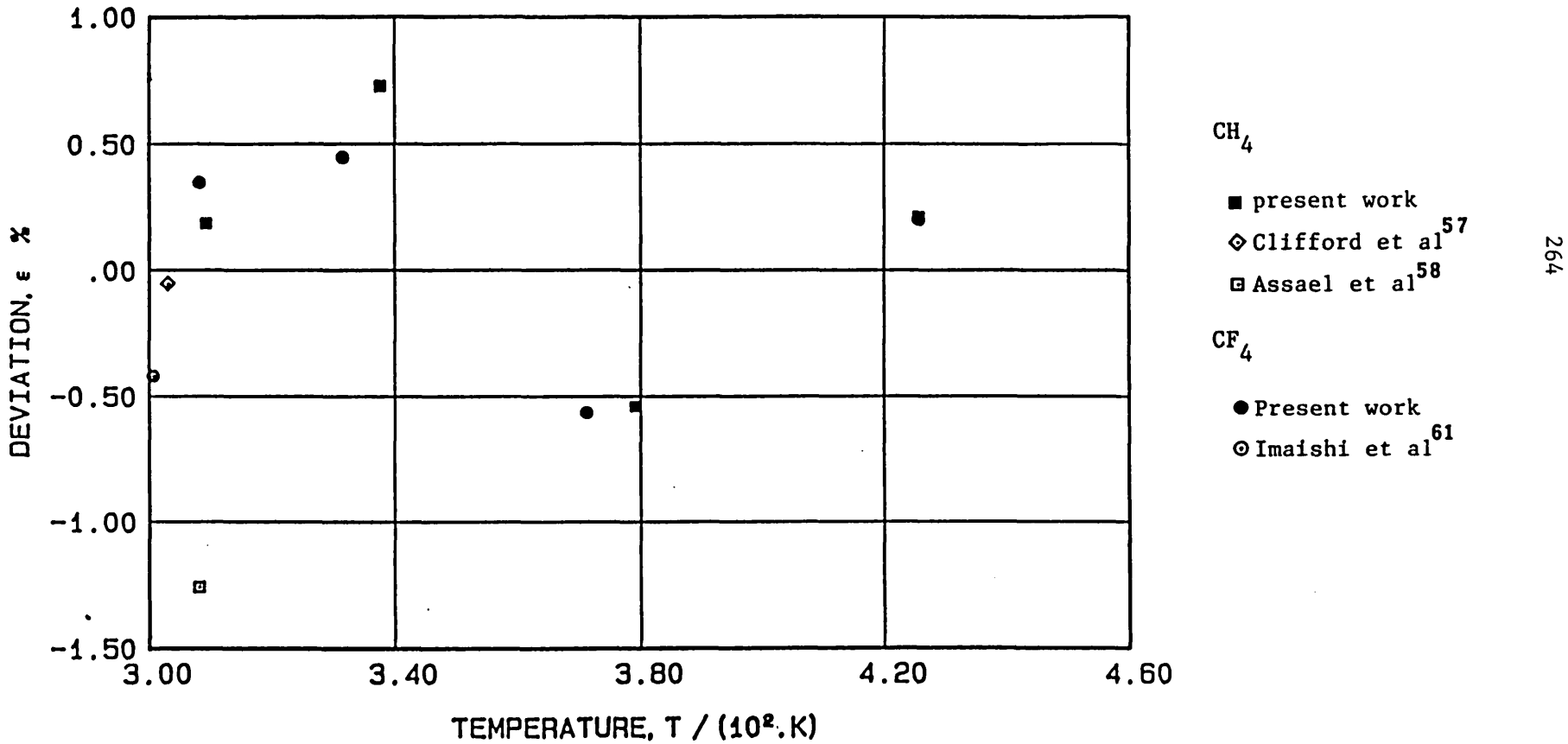

principle of coresponding states. The value of ζ_{rot} is a factor of two smaller for tetrafluoromethane than for methane which indicates that the frequency of rotationally–inelastic collisions is increased. The values of D_{int}/D obtained for tetrafluoromethane demonstrate considerably different behaviour than was observed for methane. The value of D_{int}/D is at all times slightly below unity (but by no more than 3%) and is essentially independent of temperature.

The success of the first–order Thijsse formulation leads in the usual way to a simple correlation for the zero–density thermal conductivity. The correlation is valid in the temperature range 300–425 K and includes the results of Imaishi *et al.* [61] in addition to the present data. In this case [56]

$$\mathfrak{S}_c^*(10E) = 0.4484 + \frac{80.894}{T} \qquad (6.3.5.2)$$

with

$$\sigma = 0.4579 \text{ nm} \qquad (6.3.5.3)$$

The data does not deviate form the correlation by more than ± 0.6%. (See figure 6.2.)

6.3.6 Ethylene

The analysis of the results for ethylene is similar to that of CO_2 and N_2O since the translational component of thermal conductivity has not been measured independently. In order to proceed, a less satisfactory route must be adopted. For ethylene, rotational and vibrational modes contribute substantially to the heat capacity. As usual the assumption is made that the two modes are decoupled for the purposes of identification of relaxation times.

$$\frac{C_{int}}{\zeta_{int}} = \frac{C_{rot}}{\zeta_{rot}} + \frac{C_{vib}}{\zeta_{vib}} \qquad (6.3.6.1)$$

The value of ζ_{vib} has been measured over a wide range of temperatures by Corran *et al.* [59]. Their results are well represented by the correlation [62]

$$\frac{1}{\zeta_{vib}} = 760.29 \times 10^{-4}\exp(-1264.8/T) \qquad (6.3.6.2)$$

The collision number is heavily temperature-dependent falling rapidly from 1000 near room temperature to nearly 100 at 570 K. The rotational collision number has been determined by Holmes *et al.* [63, 64] who quote a value between 1.3 and 2 collisions at 300 K. The value ζ_{rot} = 1.4 (at 300 K) adopted earlier [52] has been used along with the Brau Jonkman formula (equation 6.3.2.4) for the temperature dependence, as was the case for carbon dioxide. The internal energy contribution to the heat capacity may be obtained from the results of Jahangiri *et al.* [65] which also allows identification of the rotational and vibrational components. The viscosity in the limit of zero-density has been represented recently by Boushehri *et al.* [66] and their results have been used unaltered. The final quantity necessary for the evaluation of the effective cross-sections is the fractional change of thermal conductivity in a magnetic field. This has never been measured for ethylene so that in order to proceed, $(\Delta\lambda_{\eta}/\lambda)_{sat}$ is assigned the value zero. The effect of this assignment is unlikely to contribute more than 1 or 2% to the thermal conductivity and will not affect the final conclusions. It does, however, mean that the effective cross-sections are used for guidance only and are not likely to be in quantitative agreement with future calculations. The effective cross-sections appropriate to the

Viehland–Mason–Sandler and Thijsse formulations are listed in Tables 6.3.22 and 6.3.23.

From the tables it can be seen immediately that the use of the simplified Thijsse approximation leads to large errors of order 3% for ethylene. No attempt has been made to correlate the thermal conductivity using the Thijsse scheme at present, although this work will be a foundation for future developments. It is interesting to note that the value of D_{int}/D, calculated from the effective cross-sections and a value of A^* obtained from the principle of corresponding states, as shown in Table 6.3.24, is greater than unity at all the temperatures studied. This is in contrast with the expectation from the theoretical prediction for rigid rotors and will be discussed later.

6.3.7 Ethane

The analysis of the ethane results is similar to that performed for ethylene. The situation is, however, more complicated since in addition to the usual rotational and vibrational modes, ethane possesses a hindered rotation which contributes significantly to its heat capacity. This fact has led to considerable confusion in the literature as to the value of ζ_{vib}, which is variously quoted [64, 67, 68] as having values between 10 and 92 collisions near room temperature. This confusion seems to arise from the occasional failure to distinguish between the hindered rotation and the other vibratonal modes. For the purposes of this analysis, it is sufficient to use the value $\zeta_{vib} = 52$ at $T = 293$ K given by Lambert and Rowlinson [67] which represents the best estimate of the combined effect of both modes. This value has, indeed, been used at all the temperatures. To complete the data set the heat capacity data of

Younglove and Ely [69] has been used to provide the separate contributions to C_{rot} and C_{vib}. The viscosity has been taken from the correlation of Boushehri *et al.* [66]. As for ethylene, the spin polarisation correction is unknown and has therefore been assigned the value $(\Delta\lambda_{\mu}/\lambda)_{sat} = 0$. This assignment does not significantly affect the major conclusions. For ζ_{rot} there have been no direct measurements but, based on earlier analyses [52] and the basic similarity between the ethane and ethylene molecules, the value $\zeta_{rot} = 1.4$ at T = 300 K would seem reasonable. The formula of Brau and Jonkman [49] has been used to describe the temperature dependence of ζ_{rot}.

Using the above information and the present thermal conductivity data, a set of consistent effective cross-sections, appropriate to both the Viehland-Mason-Sandler and Thijsse formalism has been obtained. Tables 6.3.25 and 6.3.26 show the values of the effective cross-sections obtained. It is clear that the first-order Thijsse result is in error by approximately 3%. Therefore, no attempt has been made to correlate the data although, as for ethylene, it is expected that the present results will form the basis for a future correlation.

Table 6.3.27 lists the derived value of D_{int}/D calculated from the effective cross-sections and the value of A^*, which was obtained from the principle of corresponding states. The temperature dependence of the ratio D_{int}/D is similar to that of ethylene. It is never less than unity and rises to well above unity at the highest temperature.

6.3.8 Nitrogen

The final gas studied here is nitrogen. The present thermal

conductivities have been obtained below 0°C. The analysis of the present results also includes the earlier work of Haran *et al.* [70]. Thus the temperature range covered for nitrogen is 170–430 K. For the analysis an improved version [71] of a correlation due to Cole and Wakeham [72] was used which also included the new precise measurements made with an oscillating disc viscometer in Rostock [73, 74] and a new set due to Timrot *et al.* [75]. This new correlation has an ascribed accuracy of ± 0.3% near room temperature.

The ideal gas heat capacity C_p^o was taken from the recommendations of the IUPAC tables [76]. In general, the internal contribution to the heat capacity is composed of both rotational and vibrational components. Each of these components has its own relaxation time. However for nitrogen

$$\frac{C_{vib}}{\zeta_{vib}} \ll \frac{C_{rot}}{\zeta_{rot}} \qquad (6.3.8.1)$$

So by making use of the result

$$\frac{C_{int}}{\zeta_{int}} = \frac{C_{rot}}{\zeta_{rot}} + \frac{C_{vib}}{\zeta_{vib}} \qquad (6.3.8.2)$$

ζ_{int} is obtained from the expression

$$\zeta_{int} = \frac{C_{int}}{C_{rot}} \zeta_{rot} \qquad (6.3.8.3)$$

The collision number for internal energy relaxation may therefore be found from knowledge of the rotational contribution to the internal heat capacity and the rotational collision number.

The collision number, ζ_{rot}, has been shown [10] to be well

represented by the Brau and Jonkmann equation (equation (6.3.2.4)). In this case ϵ/k = 104.2 K and ζ_{rot} was found, by fitting the thermomolecular pressure data [10], to be ζ^{∞}_{rot} = 13.384. The final quantity necessary for the analysis is the fractional change in thermal conductivity observed in a magnetic field. The value of $(\Delta\lambda_{11}/\lambda)_{sat}$ has been determined by Hermans *et al.* [42] and was found to be essentially temperature independent

$$\left[\frac{\Delta\lambda_{11}}{\lambda}\right]_{sat} = -0.00777 \qquad (6.3.8.4)$$

All this information has been used along with the present and the older thermal conductivity data to prepare tables of the effective cross-sections appropriate to both the Viehland-Mason-Sandler formalism and the Thijsse formalism. The results are shown in Tables 6.3.28 and 6.3.29. These tables indicate that for nitrogen the coupling cross-sections are small compared with the transport cross-sections. Indeed, the first-order Thijsse approximation is useful above 300 K where the error never exceeds 1%. Below 300 K the error increases and reaches 2% at the lowest temperature. The deviation is overall not severe. Figure 6.3 shows the deviation of the new low temperature data from a recent correlation [71] ,which did not benefit from the use of primary low temperature data. The agreement is within about 1 % which is considered satisfactory. The comparison with a recent correlation due to Uribe et al is less satisfactory, with the maximum deviation being about 4 %, and demonstrates a different temperature dependence.

The Wang Chang Uhlenbeck effective cross-sections have been used together with an elastic value of A^*, from the principle of corresponding states, to calculate D_{int}/D over the entire temperature

Figure 6.3

Deviations, $\varepsilon = ((\lambda_{EXP} - \lambda_{CORR})/\lambda_{CORR})$ X 100 %, of the thermal conductivity of nitrogen at zero density from the correlation of Millat and Wakeham.[71]

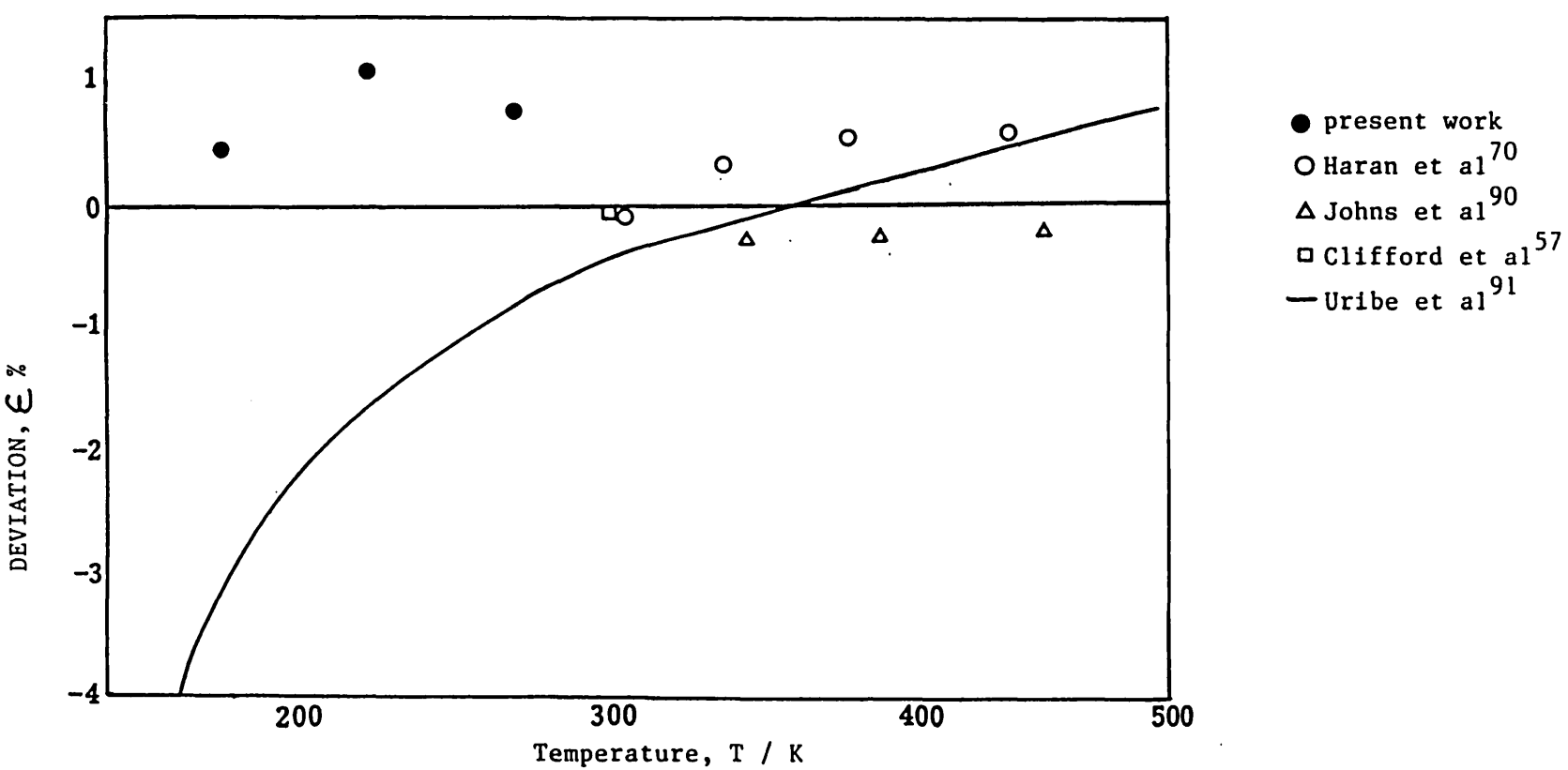

range. The results are presented in table 6.3.30. The temperature dependence of D_{int}/D is consistant with the theory of Moral *et al* [8,6].

6.4 SUMMARY

The preceding sections have detailed the analysis of both the monatomic and polyatomic gas thermal conductivity. In order to obtain the maximum information about the potential for inelastic systems, it is necessary to combine the thermal conductivity, viscosity and relaxation data to obtain effective cross-sections. These cross-sections may ultimately be of use to formulators of intermolecular potentials but, in the interim, they can be used to derive values for intermediate properties such as the collision number for rotational relaxation and, principally, the ratio D_{int}/D. The temperature dependence of the effective cross-sections are as yet unknown from *ab initio* calculations, but there are theories for the derived properties ζ_{rot} and D_{int}/D. The theory of Moraal *et al.* suggests that for rigid rotors the ratio D_{int}/D tends to unity in the high temperature limit. The evidence of this work suggests that this is true for some gases, e.g. carbon dioxide and tetrafluoromethane, but in the main the behaviour of D_{int}/D is to increase above unity.

This behaviour may be explained for some of the gases in the following way. The theory of Moraal *et al.* predicts the asymptotic behaviour of rigid rotors. Although there is no proof, it is reasonable to assume that the same asymptotic behaviour pertains for the diffusion coefficient of rotational energy for other molecules. For systems in which there are no inelastic collisions $D_{int}/D = 1$. Therefore, for gases in which $D_{int}/D > 1$ there must be transport of internal energy, other than that associated with rotation, ocurring more rapidly than the transport of the molecules themselves. This

transport is a result of inelastic collisions. Following Monchick *et al.* [33] when there is more than one mode of internal energy, then

$$\frac{C_{int}}{D_{int}} = \frac{C_{rot}}{D_{rot}} + \frac{C_{vib}}{D_{vib}} \qquad (6.4.1)$$

From this it is clear that the value of D_{int}/D depends on the value of D_{vib}/D if C_{vib} is significant. Thus, if $D_{int}/D > 1$ and even if $D_{rot}/D = 1$, then $D_{vib}/D > 1$. Therefore, it is concluded that for the gases where vibrational energy is significant, such as methane, ethane and ethylene, and $D_{int}/D > 1$, then the vibrational energy transport is more rapid than molecular mass transport.

There is, however, an alternative explanation of the phenomena. The use of equation (6.4.1) to tackle the problem of more than one mode of internal energy relaxation is a purely *ad hoc* extension of the theory for molecules with single relaxation modes and has no theoretical justification. The evidence of this work could therefore lead to the conclusion that equation (6.4.1) is unlikely to be correct.

The rather anomolous behaviour of hydrogen and nitrous oxide remains a puzzle. However, hydrogen is a quantum gas in the temperature range of interest and the asymptotic theories are totally inappropriate. For nitrous oxide, the estimation of A^* may be incorrect and hence cause a departure, by a few percent, from the expected behaviour.

6.5 THE DENSITY DEPENDENCE

The density dependence of the thermal conductivity may be studied in two ways, the first of which is the concept of the excess thermal conductivity

$$\Delta\lambda_{XS} = \lambda(T, \rho) - \lambda^0(T) \qquad (6.5.1)$$

This function has been found to be, in many cases, temperature independent far from the critical point [70, 77]. In the vicinity of the critical point the thermal conductivity is enhanced so it is more correct to consider a redefined excess function

$$\Delta\lambda_{XS} = \lambda(T, \rho) - \lambda_c(T, \rho) - \lambda^0(T) \qquad (6.5.2)$$

Use of the full definition for the excess function is restricted to carbon dioxide for which there has been a recent theoretically-based derivation of $\lambda_c(T, \rho)$ [78]. For the other gases no analogous treatment was possible but for some of the gases, the conditions are far removed from the critical point and it is expected that equation (6.5.1) is adequate.

The excess function is best presented in graphical form. Figures 6.4 to 6.6 show the excess function for argon, helium and neon respectively, calculated using equation (6.5.1), from which it can be seen that the excess function for these gases is essentially independent of temperature to a high degree of accuracy. The error bars indicate an error in the total thermal conductivity. Figures 6.7–6.14 show the excess function for hydrogen, carbon dioxide, nitrous oxide, methane, tetrafluoromethane, ethane, ethylene and nitrogen. The excess function for carbon dioxide was obtained from equation (6.5.2); in all other cases equation (6.5.1) was used.

The figures for hydrogen and carbon dioxide demonstrate that to a high level of precision the excess function is essentially independent of temperature. The figure for nitrous oxide, however, reveals considerable evidence of temperature dependence which is

Figure 6.4

The excess thermal conductivity of argon

▲ 174 K; ▼ 223.15 K; ◀ 266.65K; ▶ 308.15 K;

■ 333.15 K; ◆ 378.15 K; ● 428.15 K.

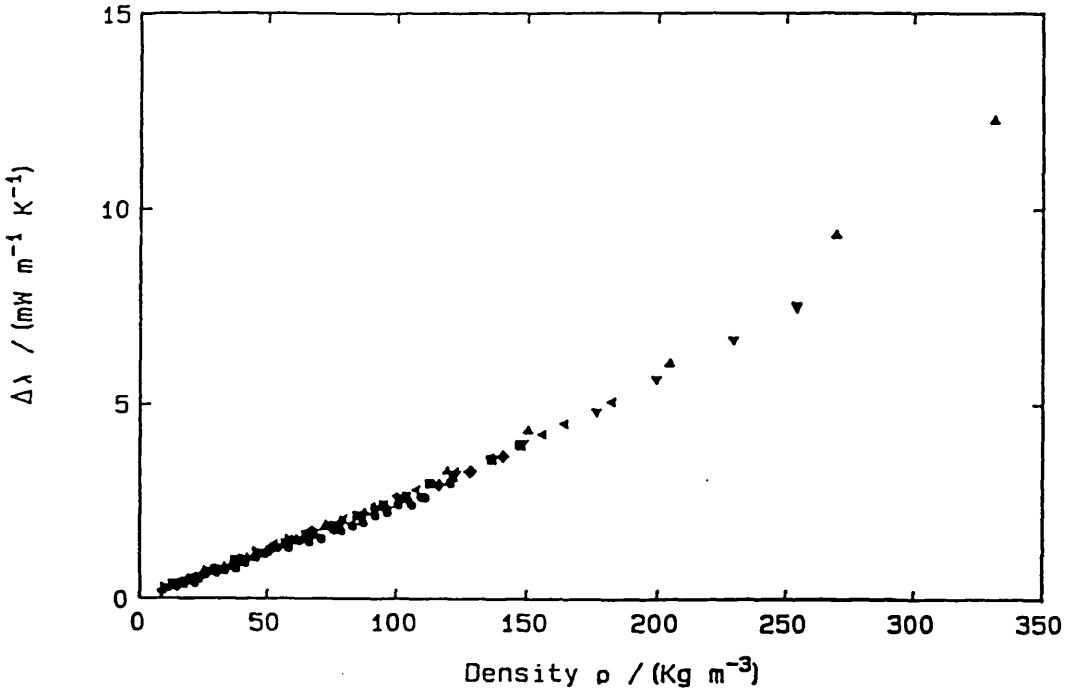

Figure 6.5

The excess thermal conductivity of helium.

▲ 308.15 K; ▼ 338.15 K; ◀ 379.65 K; ▶ 428.15 K.

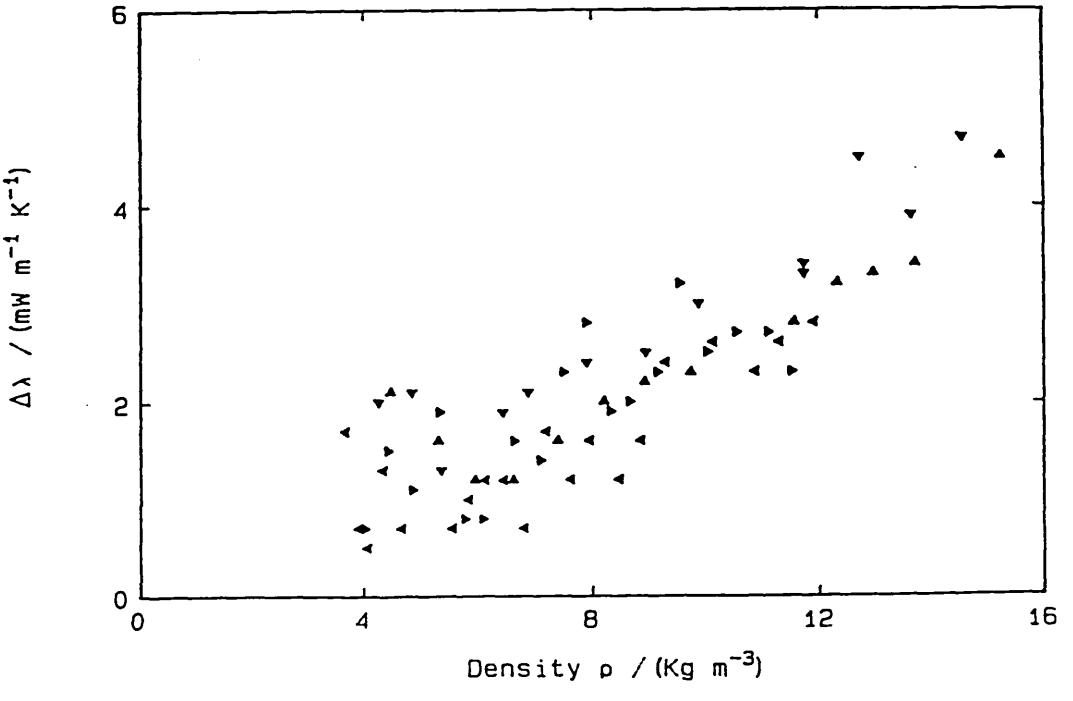

Figure 6.6

The excess thermal conductivity of neon.

◗ 308 K; • 337.65 K; ◆ 379.65 K; ■ 428 K.

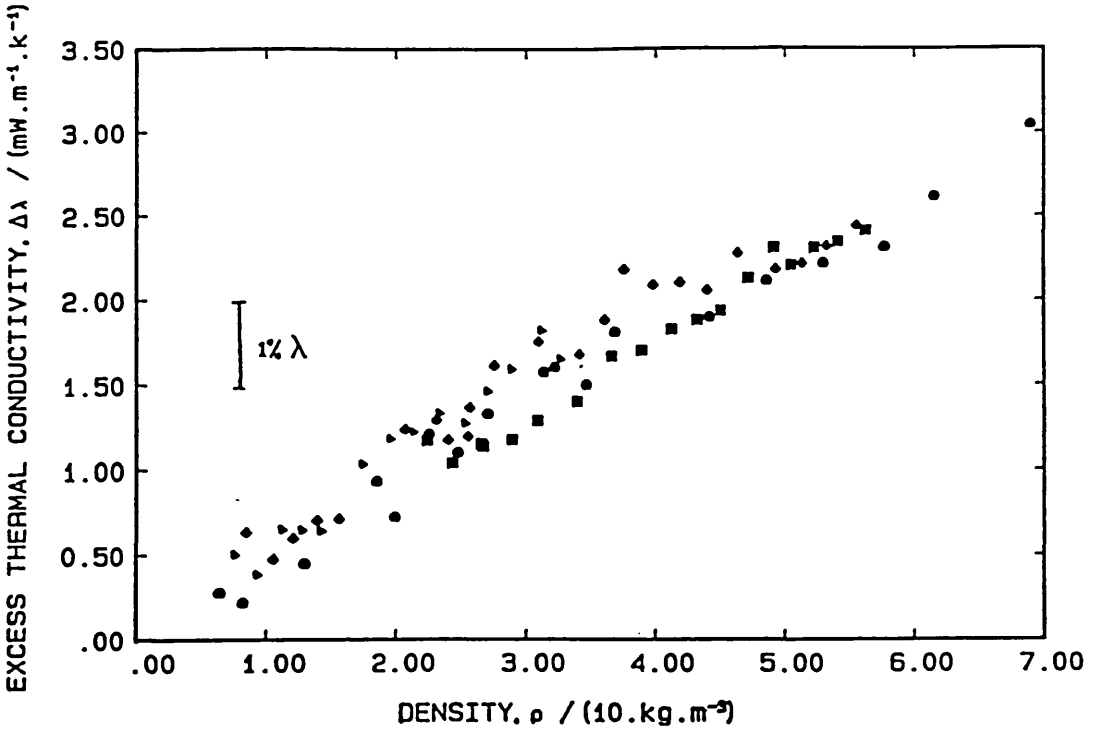

Figure 6.7

The excess thermal conductivity of hydrogen.

▲ 308.15 K; ▼ 337.65 K; ◀ 379.65 K; ▶ 428.15 K.

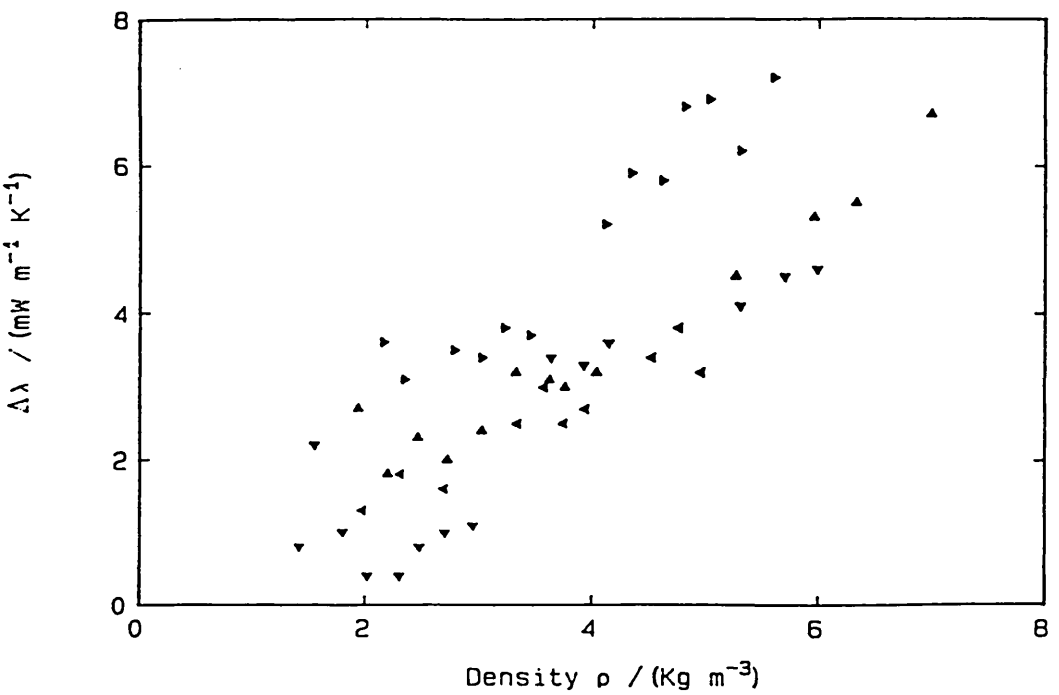

Figure 6.8

The excess thermal conductivity of CO_2

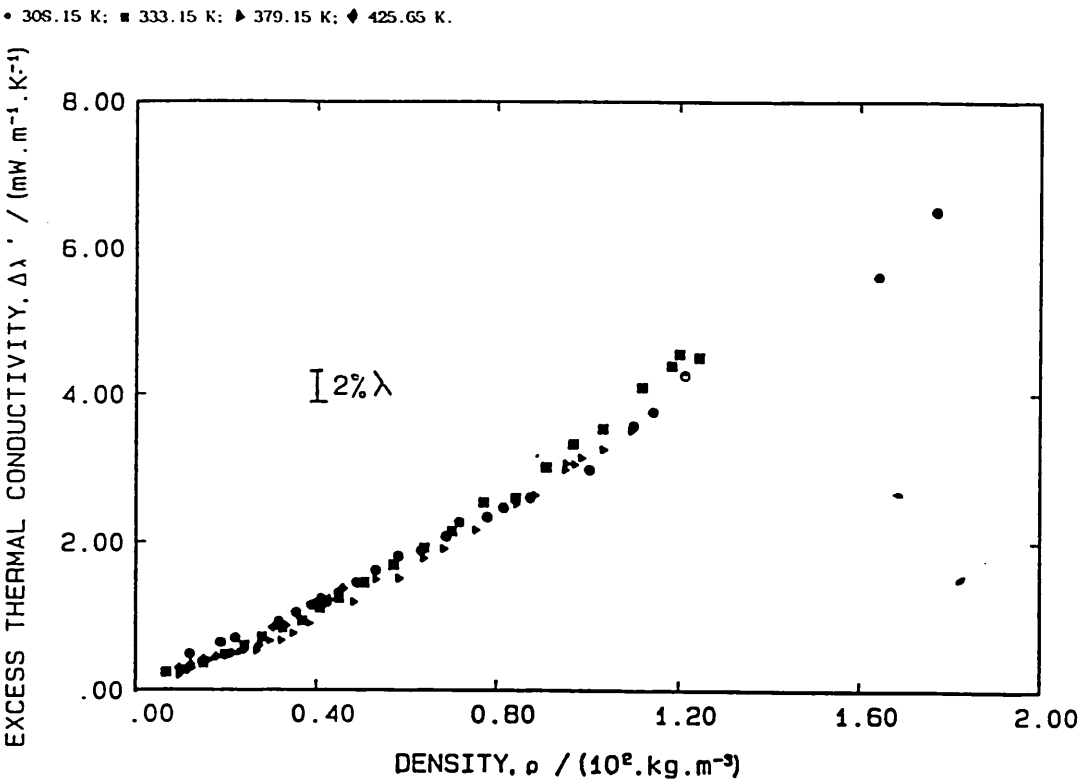

Figure 6.9

The excess thermal conductivity of N_2O

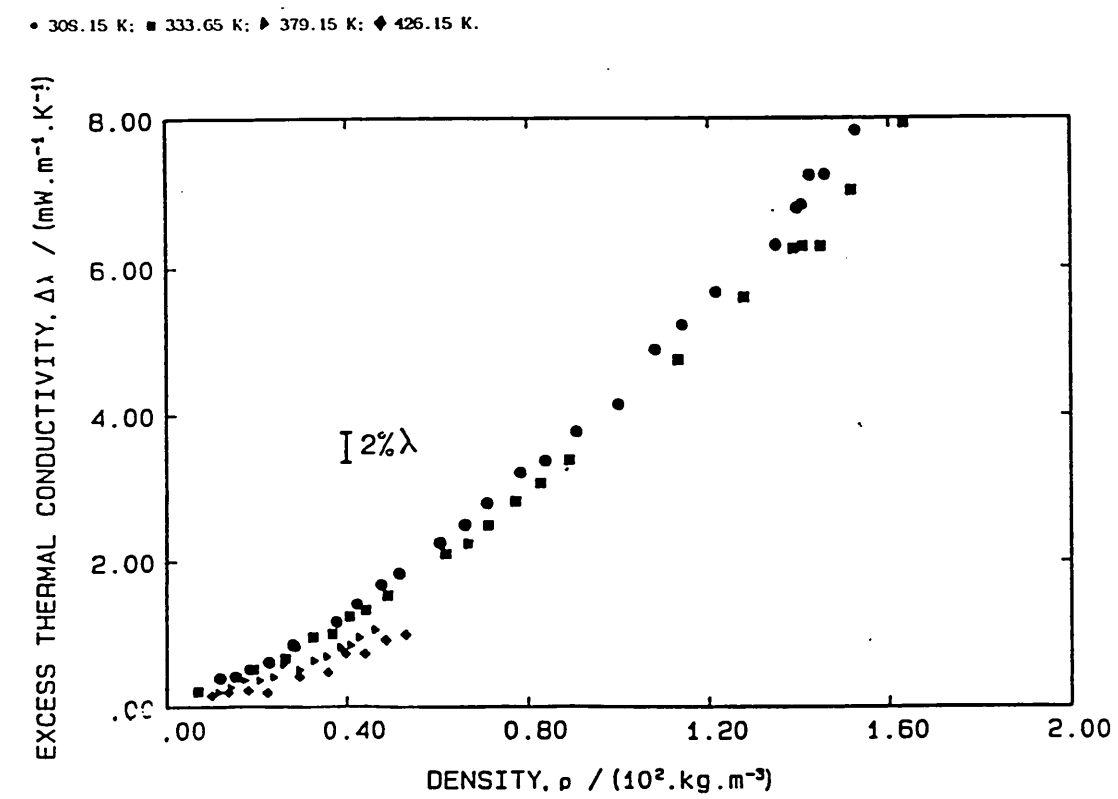

Figure 6.10

The excess thermal conductivity of methane.

▶ 309 K; • 337.65 K; ◆ 379 K; ■ 425.65 K.

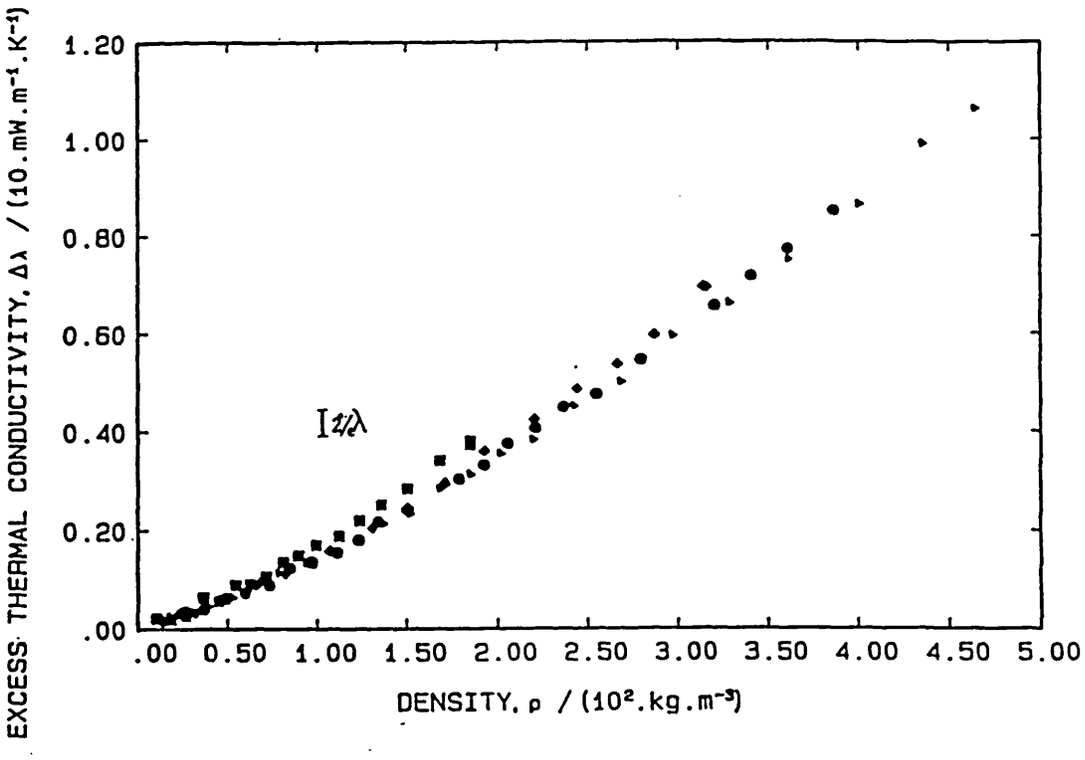

Figure 6.11

The excess thermal conductivity of tetrafluoromethane.

▶ 308 K; • 331.65 K; ◆ 371 K; ■ 425.65 K.

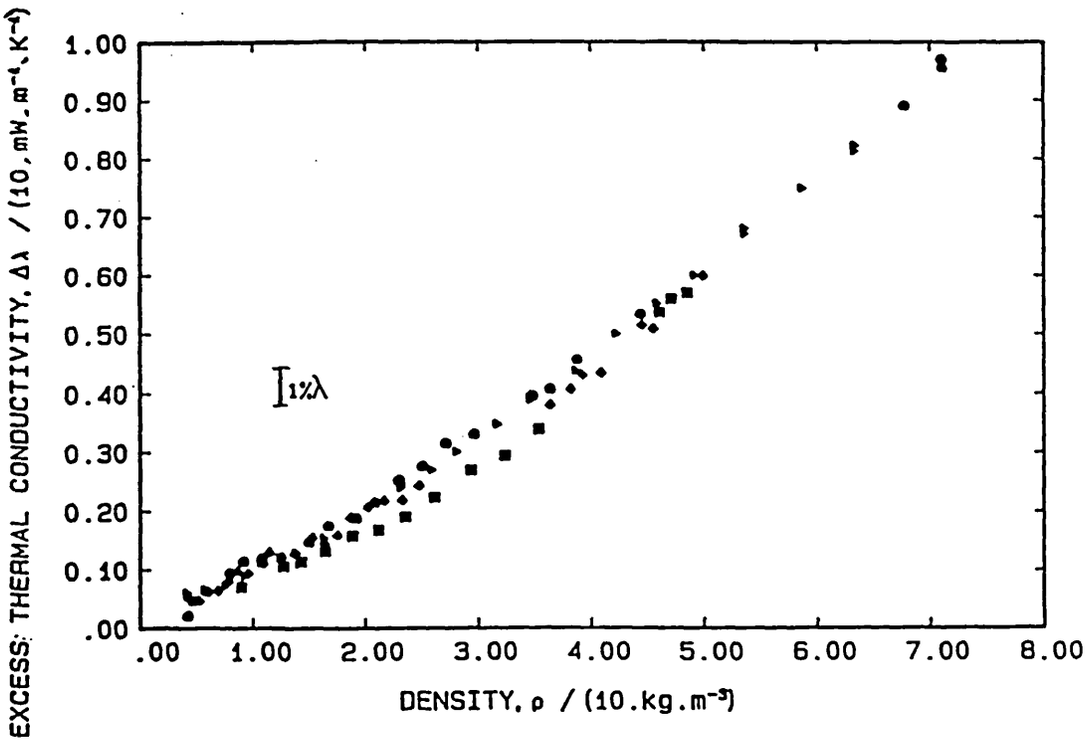

Figure 6.12

The excess thermal conductivity of ethane.

▲ 308.15 K; ■ 331.65 K; ♦ 380.15 K; • 425.65 K.

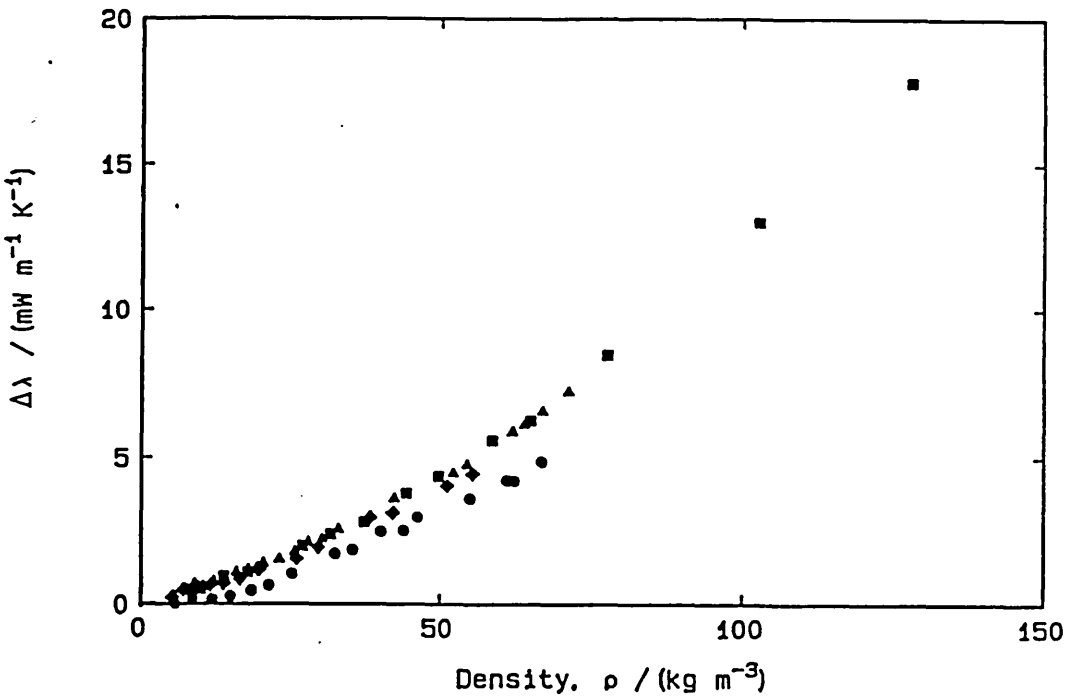

Figure 6.13

The excess thermal conductivity of ethylene.

▲ 308.15 K; ■ 333.15 K; ♦ 371.15 K; • 425.65 K.

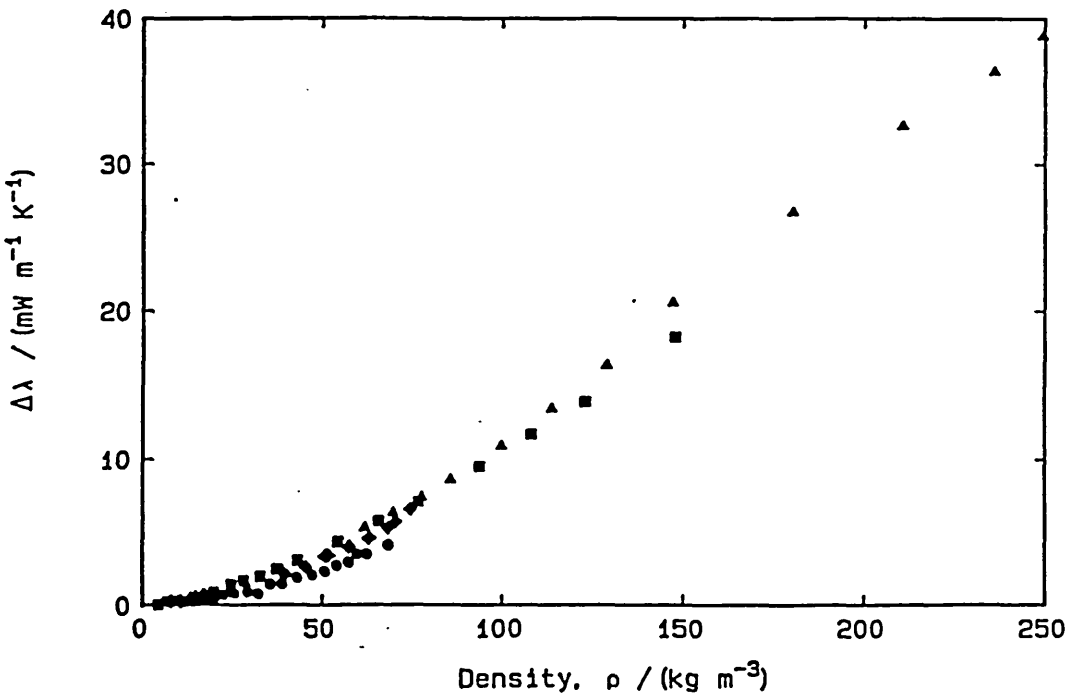

Figure 6.14

The excess thermal conductivity of nitrogen

Present work: ▲ 177.50 K; ▼ 225.15 K; ▶ 270.15 K.

Haran et al[70] ◀ 308.15 K; ■ 337.15 K; ◆ 378.15 K;

● 429.15 K.

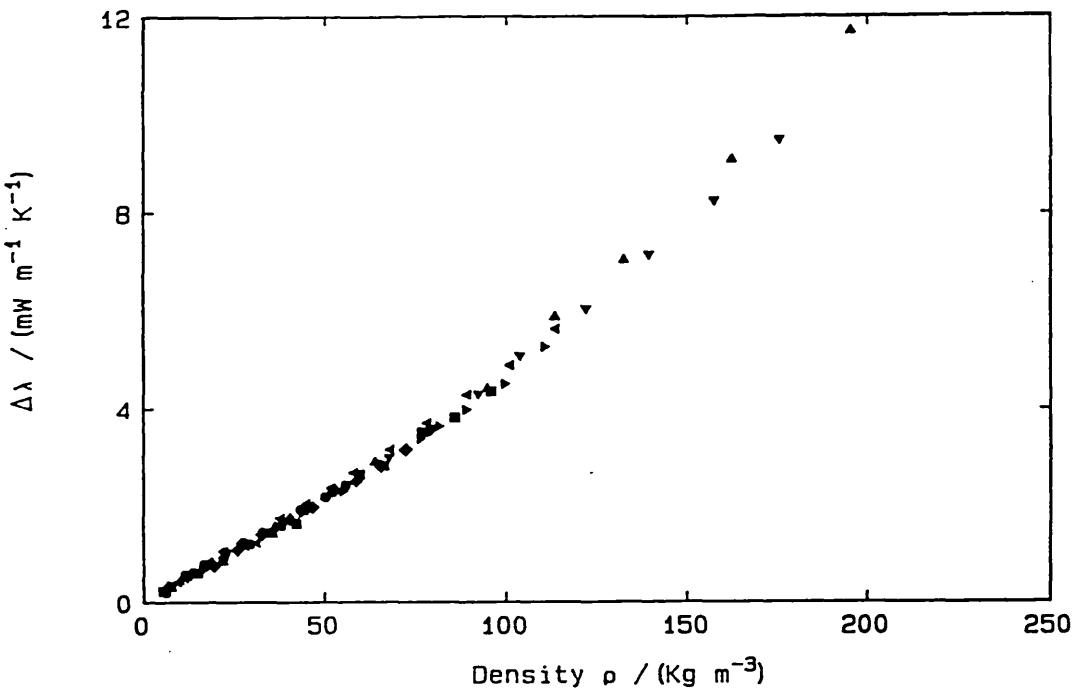

almost certainly attributable to the critical enhancement term. The contrast between the observations for carbon dioxide and nitrous oxide indicate that the concept of temperature–independent excess thermal conductivity is valid once allowance is made for the critical enhancement. This is important, not only for the prediction of thermal conductivity for engineering purposes, but also for the extraction of the critical enhancement itself from experimental data [78]. Figure 6.10 for methane shows a small but discernible trend with temperature, such that the excess thermal conductivity is lower at high temperatures. Conversely, for tetrafluoromethane (Figure 6.11) it is possible to discern the opposite trend. The density data for tetrafluoromethane is less certain than for methane, which results in a larger uncertainty in the plot for the excess thermal conductivity, but the trend does seem to be real. These relatively small departures from tempetature independnece have been noted previously [79, 61] but are not large enough to destroy confidence in the concept for the purposes of estimation. At the highest level of precision the concept of a temperature–independent excess function fails for both ethane and ethylene (Figures 6.12 and 6.13) . Both gases exhibit a decrease in the excess property with increasing temperature. The source of this temperature dependence is once again almost certainly the critical enhancement, which is unaccounted for in this analysis. It is still appropriate to use the temperature–independent excess function as a predictive tool of modest accuracy. The present results will no doubt contribute to a more complete study for these important industrial gases. Finally, Figure 6.14 shows the excess function for nitrogen over a wide temperature range, using the present results and those obtained earlier [70]. The results indicate that the concept of the

temperature–independent excess function is valid for nitrogen over a wide range of temperatures and pressures. There is, however, larger scatter at elevated pressures for the lower temperature isotherms. This must be due largely to experimental difficulties observed near the critical density [80].

One particular element of the density dependence of the thermal conductivity of gases that is of particular interest is the first density coefficient in the expansion

$$\lambda = \lambda^0 + \lambda_1\rho + \lambda_2\rho^2 + \ldots \qquad (6.5.3)$$

Here the density ρ is in mol/m^3. In the theory chapter some predictive schemes for the first coefficient were discussed. The first two of these schemes are based on the Enskog dense hard–sphere theory which require knowledge of the second and third virial coefficients and their temperature derivatives. In order to implement the two Modified Enskog Schemes the virial coefficients have been obtained using the compilation of Dymond and Smith [81]. Either the values recommended by them or those they consider most reliable have been employed. Table 6.5.1 shows a comparison between the experimental first density coefficient and those evaluated by the two Modified Enskog Schemes for a selection of gases at various temperatures.

The table shows that there are substantial discrepancies between the experimental values and those obtained from either of the Modified Enksog schemes. In some cases, this deviation may amount to more than a factor of 2 and, in some extreme examples, may be of the wrong sign. It is fair to conclude that neither of these schemes are particularly successful and that they are inadequate for predictive

purposes since an error in the first density coefficient propagates to an error in the thermal conductivity. It may be argued that at least part of the failure of these schemes is due to their reliance on the third virial coefficient which is generally rather poorly known.

As described previously in Chapter 5, there is now a microscopically-based theory for the first density coefficients [19, 20]. The comparison between the prediction of this dimer-collisional theory and the experimental results is shown in Figure 6.15. The calculations of Rainwater and Friend have been based on the Lennard-Jones 12-6 potential, so rather than compare direclty the predicted values of λ_1 of equation (6.5.3) for each gas, the comparison is made in terms of reduced units, thus

$$\lambda_1^* = \frac{\text{RMM } \lambda_1}{\left[\frac{2}{3} \pi \text{ Na } \sigma_c^3\right]} \quad , \quad T^* = kT/\epsilon_c \qquad (6.5.4)$$

were RMM is the relative molecular mass, Na Avagardro's number and σ_c and ϵ_c are the Lennard Jones parameters. For the original comparison, the polyatomic gases have been excluded since the theory is at present unable to account for the presence of internal energy and its exchange with translational energy. The value of σ_c used to produce the reduced density coefficient was taken from the corresponding states analysis of Kestin *et al.* [14, 82]. The reduced temperature has been obtained using a value of ϵ_c from the same source. It is expected that although these values are not identical to the optimum Lennard-Jones parameters for these systems, the differences will be small. The theoretical curve obtained from the results of Rainwater and Friend (the full line in Figure 6.15) is in good qualitative agreement with experiment. It is recognised that the Lennard-Jones (12-6) model

Figure 6.15

The reduced first density coefficient of thermal conductivity for monatomic gases.

——— Theoretical result for Lennard-Jones potential

- - - - - Empirical correlation of equation 6.5.5

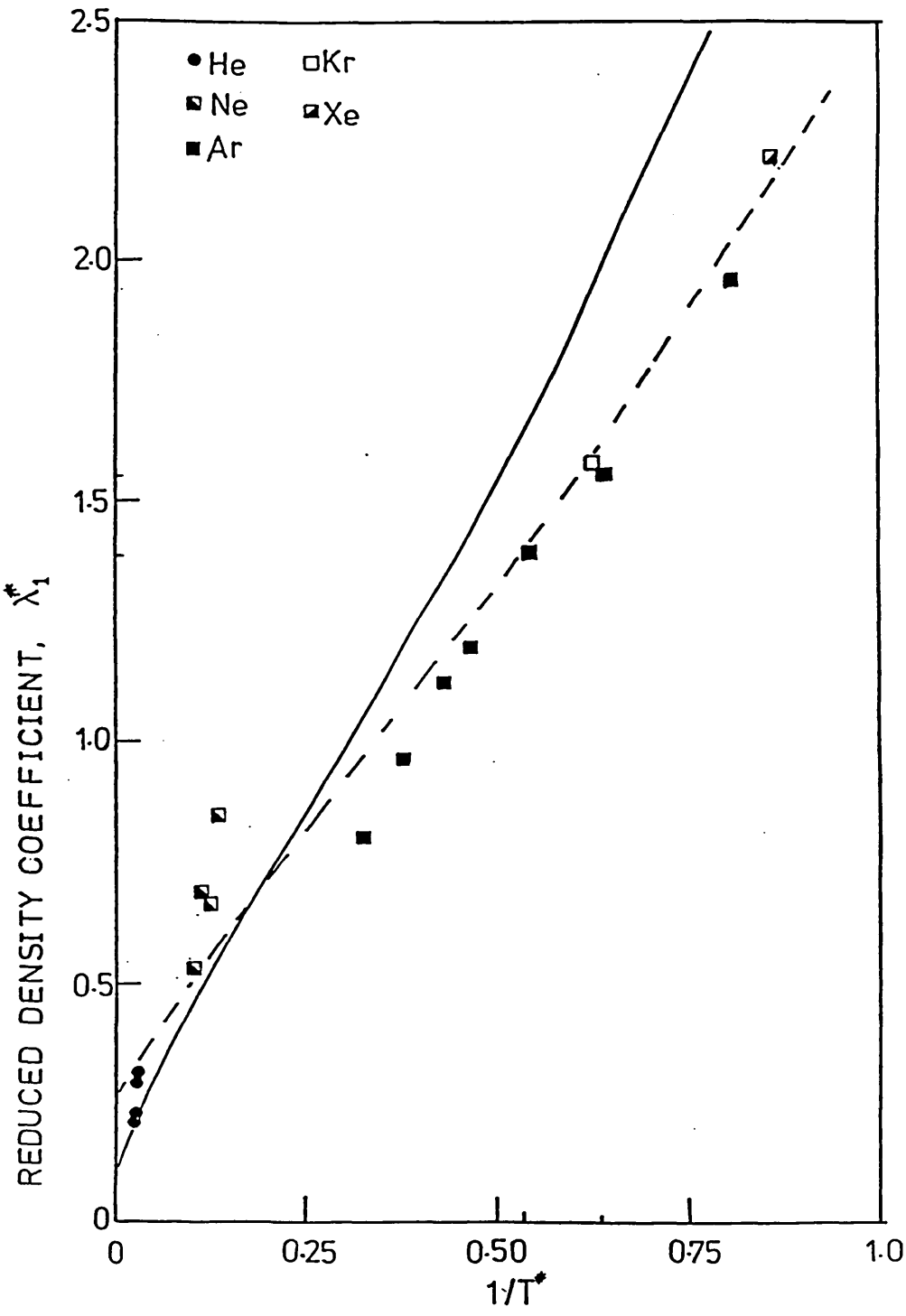

is not an appropriate pair potential for any molecular interaction [83] but at least among the monatomic gases there is a fair degree of conformality among the pair potentials and the functions of the pair potential [3]. It is therefore proposed that λ_1^* for the monatomic gases should be a universal function of T^* but that the functions are not those characteristic of the Lennard-Jones potential. The universal function found to be most appropriate was obtained from the optimum representation of the data. Hence for $1.2 < T^* < 40$

$$\lambda_1^* = 0.323 + \frac{1.638}{T^*} + \frac{0.563}{T^*} \qquad (6.5.5)$$

This curve is shown on Figure 6.15 as a dotted line. It can be seen that the new curve gives a better representation of the data. The effectiveness of this representation can be judged from Figure 6.16 which shows the deviations of selected data sets of thermal conductivity data from the correlations of equation (6.2.1) given in Chapter 4 with λ_1 calculated using equation (6.5.5) and the parameters of references [14, 82]. It can be seen that the deviations never exceed ± 1%.

The method may be extended to polyatomic gases when it is noted that although the pair potentials cannot be spherically symmetric and hence cannot be conformal, there is a considerable body of evidence that, to a reasonable degree, the dilute gas functionals of their pair potentials do obey a law of corresponding states with the monatomic gases [14]. It may therefore be possible to define a reduced first density coefficient for the polyatomic gases which is well represented by means of the function appropriate for the

Figure 6.16

Deviations of the experimental thermal conductivity data from the predictions of the present correlation.

Ne: ○ 425 K, ● 308 K This work

Ar: ▲ 429 K, △ 308 K ref 70

Kr: □ 308 K ref 89

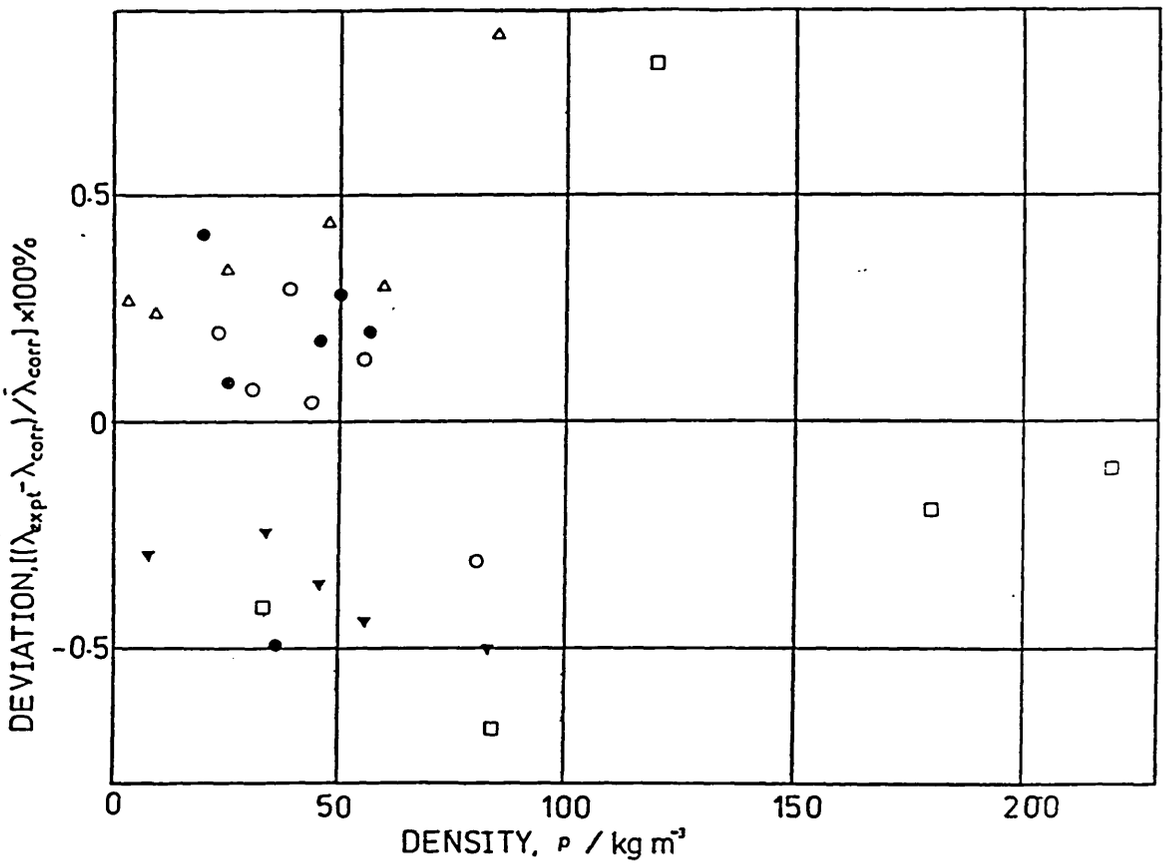

monatomic species. Such a definition follows from the MET-II scheme if it is used to construct a contribution to the translational energy contributions to the first density coefficient. Hence the first density coefficient for the polyatomic gases is reduced, thus

$$\lambda_1^* = \frac{\mathrm{RMM}(\lambda_1/\lambda_{tr}^0)}{\left[\frac{2}{3}\,\pi\,\mathrm{Na}\,\sigma_c^3\right]} + 0.625\left[\frac{\lambda^0}{\lambda_{tr}^0} - 1\right] \qquad (6.5.6)$$

Here λ_{tr}^0 is the translational contribution to the zero-density thermal conductivity. This quantity may be obtained from the zero-density viscosity of the gas by means of the simple equation

$$\lambda_{tr}^0 = \frac{15}{4}\,\frac{k}{m}\,\eta^0 \qquad (6.5.7)$$

Figure 6.17 shows the reduced first density coefficient of thermal conductivity for the polyatomic gases studied here. The dotted line is the representation for the monatomic gases given above (i.e. equation (6.5.5)). The figure shows that there is a remarkable degree of agreement. In general, the deviations are no worse than those of the monatomic gases. Figure 6.18 shows deviations for a selection of polyatomic gases. The maximum deviation never exceeds 1 %. However, at lower reduced temperatures, the agreement deteriorates as can be seen for ethane, ethylene and tetrafluoromethane. The original formulation of equation (6.5.5) relied on only one low reduced temperature measurement for xenon at around $T^* = 1.2$. The fact that equation (6.5.6) can no longer be used to represent all the polyatomic gases (the low temperature nitrogen is well represented by equation (6.5.6)) indicates that it is not universal at low reduced temperatures. This in turn leads to the conclusion that a rather

Figure 6.17

A comparison of the correlation of λ_1^* for monatomic gases with the values deduced for polyatomic gases from equation 6.5.6.

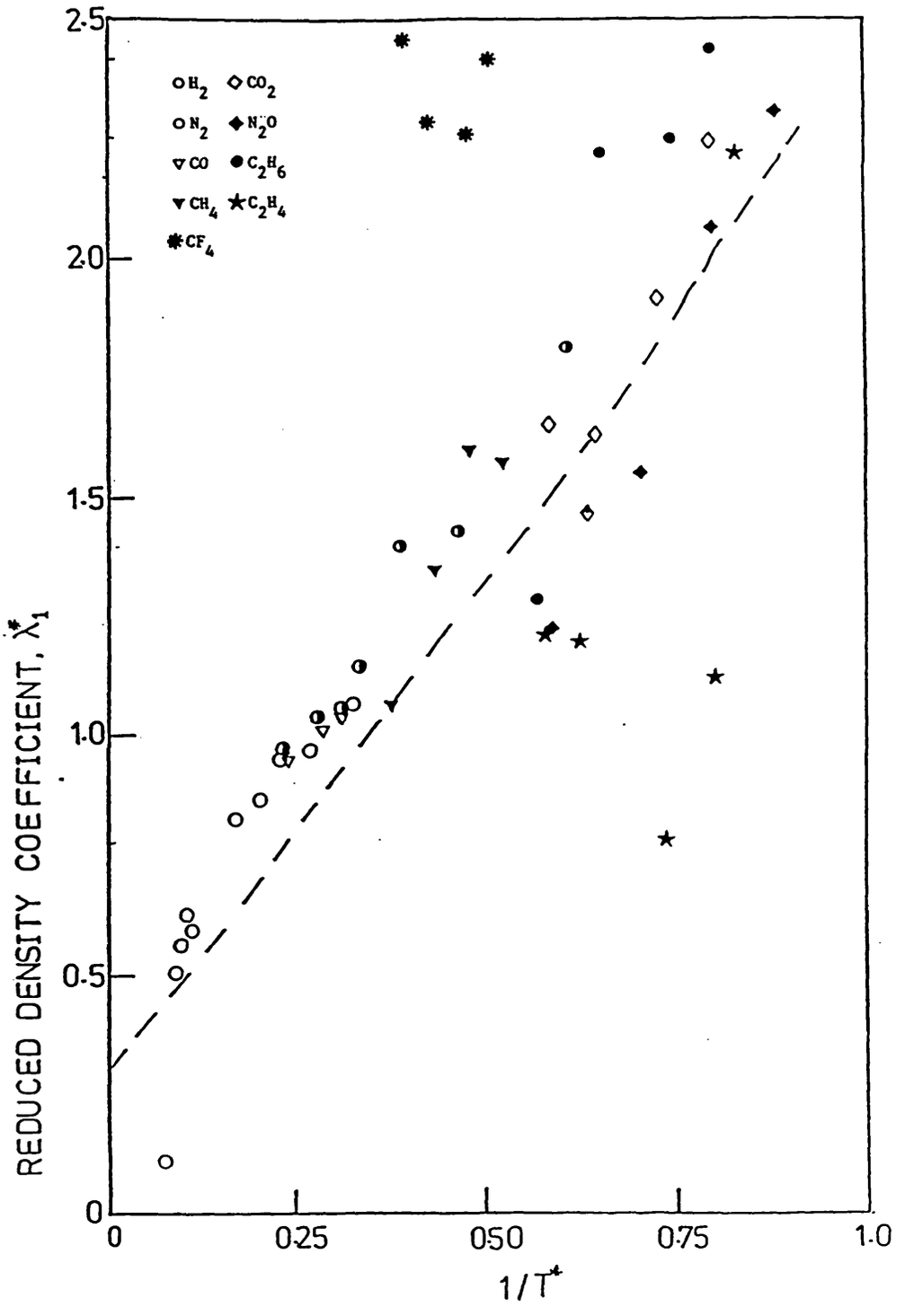

Figure 6.18

Deviations of experimental thermal conductivity data from the predictions of the present correlation for polyatomic gases.

N_2: ● 429 K, ○ 308 K ref

CH_4: ▲ 425.65 K, △ 309 K This work

CO_2: ■ 429 K, □ 308 K This work

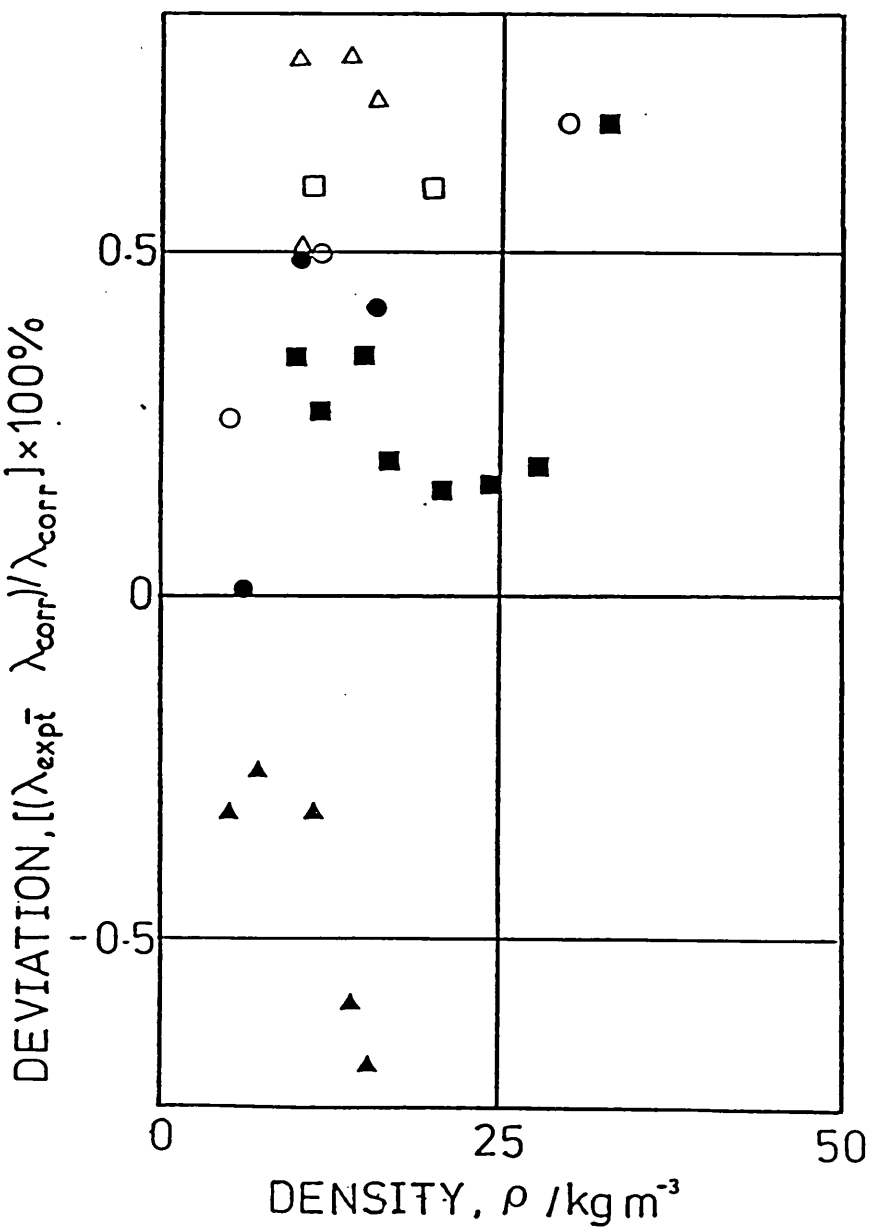

more rigorous theoretical treatment of energy transport in dense polyatomic gas systems is necessary if any further progress is made. A similar approach is also possible in the case of viscosity [84] although this is also less reliable near $T^* = 1$ [85].

6.6 SUMMARY

The concept of a temperature–independent excess thermal conductivity was found to be vindicated to within a high degree of accuracy for the monatomic, and some of the polyatomic, gases studied away from the critical region. When allowance is made for the critical enhancement, the temperature–independent excess function can be recovered as, for example, in the case of carbon dioxide. Near the critical point this concept can be maintained as a predictive tool of modest accuracy.

The macroscopically–based Modified Enskog theories were found to be inadequate for the prediction of the first density coefficient of thermal conductivity. The more systematic microscopic theory of Rainwater and Friend was found to be in qualitative agreement with experimental observation for the thermal conductivity of monatomic systems. An empirical extension was found to represent the density dependence of thermal conductivity well and was able to reproduce experimental thermal conductivities to within 1%. The initial density dependence of polyatomic systems was found to be represented with varying degrees of success by a redefined reduced first density coefficient and the correlation appropriate to monatomic systems. The function was found not to be universal at reduced temperatures near $T^* = 1$.

REFERENCES

[1] A. Dickenson and M.S. Lee, J. Phys. B: At. Mol. Phys. 18, 4177 (1985).

[2] A. Dickenson and M.S. Lee, J. Phys. B: At. Mol. Phys. 19, 3091 (1986).

[3] G.C. Maitland, M. Mustafa, W.A. Wakeham and F.R.W. McCourt, Mol. Phys. (to be published).

[4] G.C. Maitland, M. Mustafa, V. Vesovic and W.A. Wakeham, Mol. Phys. 57, 1015 (1986).

[5] E.B. Smith and A.R. Tindell, Faraday Discuss. Chem. Soc. 73, 221 (1982).

[6] C.S. Wang Chang and G.E. Uhlenbeck and J. de Boer, Studies in Statistical Mechanics, Vol. 2, Part C, (Eds. J. de Boer and G.E. Uhlenbeck) (North Holland, Amsterdam, 1964).

[7] L.A. Viehland, E.A. Mason and S.I. Sandler, J. Chem. Phys. 68, 5277 (1978).

[8] H. Moraal and R.F. Snider, Chem. Phys. Lett. 9, 401 (1971).

[9] K.F. Herzfeld and T.A. Litowitz, Absorption and Dispersion of Ultrasonic Waves (Academic Press, New York, 1959).

[10] J. Millat, A. Plantikas, D. Mathes and H. Nimz, Z. Phys. Chemie (Leipzig) (in press).

[11] B.J. Thijsse, G.W. 't Hooft, D.A. Coombe, H.F.P. Knaap and J.J.M. Beenakker, Physica 98A, 307 (1979).

[12] F.R.W McCourt, I. Kuscar, J.J.M Beenakker and W.Köhler (title to be announced, O.U.P).

[13] E.A. Mason and L. Monchick, J. Chem. Phys. 36, 1622 (1962).

[14] G.C. Maitland, M. Rigby, E.B. Smith and W.A. Wakeham, Intermolecular Forces: Their Origin and Determination (Clarendon

Press, Oxford, 1981).

[15] G.C. Maitland, M. Mustafa and W.A. Wakeham, J. Chem. Soc., Faraday Trans. I 79, 163 (1983).

[16] F.R.W. McCourt and H. Moraal, Phys. Rev. A45, 2000 (1972).

[17] J. Millat, V. Vesovic and W.A. Wakeham, Physica A148, 153 (1988).

[18] Millat *et al* (to be published)

[19] D.G. Friend and J.C. Rainwater, Chem. Phys. Lett. 107, 590 (1984).

[20] J.C. Rainwater and D.G. Friend, Phys. Rev. 36, 8, 4062 (1987).

[21] J.J. de Groot, J. Kestin, H. Sookiazian and W.A. Wakeham, Physica 100A, 349 (1980).

[22] J. Kestin, S.T. Ro and W.A. Wakeham, Physica 56, 4119 (1972).

[23] J. Kestin, H.E. Khalifa, S.T. Ro and W.A. Wakeham, Physica 88A, 242 (1977).

[24] E. Vogel, Ber. Bunsenges. Phys. Chem. 88, 997 (1984).

[25] A.G. Clarke and E.B. Smith, J. Chem. Phys. 48, 9, 3988 (1968).

[26] R.A. Aziz, Int. J. Thermo. 18, 2, 193 (1988)

[27] J.O. Hirschfelder, C.F. Curtiss and R.B. Bird, Molecular Theory of Gases and Liquids (John Wiley and Sons, New York, 1954).

[29] R.A. Aziz, V.P.S. Nain, J.S. Cordey, W.L. Taylor and G.T. McConville, J. Chem. Phys. 70, 4330 (1979).

[29] R.A. Aziz, W.J. Heath and A.R. Allnatt, J. Chem. Phys. 78, 295 (1983).

[30] R.D. McCarty, Hydrogen Technological Survey – Thermophysical Properties (NASA–SP–3089, Washington, 1975).

[31] B. Armstrong (private communication 1980)

[32] M.J.Assael, S. Mixafendi and W.A. Wakeham, J. Phys. Chem. Ref. Data, 15, 4, 1315 (1986).

[33] L. Monchick, A.N.G. Pereira and E.A. Mason, J. Chem. Phys. 42, 3241 (1965).

[34] L.J.F. Hermans, A. Schutte, H.F.P. Knaap and J.J.M. Beenakker, Physica 46, 491 (1970).

[35] U. Buck, F. Huisken, A. Kohlhase, D. Otten and J. Schaefer, J. Chem. Phys. 78, 4439 (1983).

[36] W.E. Kohler and J. Schaefer, J. Chem. Phys. 78, 4862 (1983).

[37] J. Schaefer and B. Lui (to be published).

[38] W. Meyer and J. Schaefer (to be published).

[39] R.D. Trengove and W.A. Wakeham, J. Phys. Chem. Ref. Data 16, ?? (1987).

[40] J. Millat, M. Mustafa, M. Ross, W.A. Wakeham and M. Zalaf, Physica 145A, 461 (1987).

[41] E. Vogel and L. Barkow, Z. Phys. Chemie (Leipzig) 267, 1038 (1986).

[42] L.J.F. Hermans, J.M. Koks, A.F. Hengeveld and H.F.P. Knaap, Physica 50, 410 (1970).

[43] J. Ely, J.M. Magee and W.M. Haynes, Thermophysical Properties of Carbon Dioxide from 217 K to 1000 K with Pressures up to 3000 bar (NBS Monograph – in press).

[44] K.M. Merrill and R.C. Amme, J. Chem. Phys. 51, 844 (1969).

[45] A. Eucken and R. Becker, Z. Phys. Chemie, B27, 235 (1934).

[46] A. Eucken and E. Nümann, Z. Phys. Chemie, B36, 163 (1937).

[47] L. Küchler, Z. Phys. Chemie B41, 192 (1938).

[48] J. Millat, Z. Phys. Chemie (Leipzig) (submitted).

[49] C.A. Brau and M. Jonkman, J. Chem. Phys. 52, 291 (1987).

[50] V.P. Glushko, L.V. Gurvich, G.A. German, I.V. Veyto, V.A. Medvedev, G.A. Khachkuruzov and V.S. Youngman, Thermodynamic Properties of Individual Substances, 3rd ed. (Nauka, Moscow, 1978).

[51] R. Holmes, G.R. Jones and R. Lawrence, J. Chem. Phys. 41, 2955 (1964).

[52] R. Fleeter, J. Kestin and W.A. Wakeham, Physica 103A, 521 (1980).

[53] S. Angus, B. Armstrong and K.M. de Reuck, International Thermodynamic Tables of the Fluid State – 5: Methane (Pergamon, Oxford, 1978).

[54] T.L. Cottrell and A.J. Matheson, Trans. Faraday Soc. 59, 824 (1963).

[55] A. Eucken and S. Aybar, Z. Phys. Chemie B46, 195 (1940).

[56] J. Millat, M. Ross, W.A. Wakeham and M. Zalaf, Physica 148A, 124 (1988)

[57] A.A. Clifford, J. Kestin and W.A. Wakeham, Physica 97A, 287 (1979).

[58] M.J. Assael and W.A. Wakeham, J. Chem. Soc. Faraday Trans. I 77, 697 (1981).

[59] P.G. Corran, J.D. Lambert, R. Salter and B. Warburton, Proc. Roy. Soc. (London) A244, 212 (1958).

[60] J.M. Jackson, P.A. Lewis, M.P. Skirrow and C.J.S.M. Simpson, J. Chem. Soc. Faraday Trans. II 75, 1341 (1979).

[61] N. Imaishi, J. Kestin and R. Paul, Int. J. Thermophys. 6, 3 (1985).

[62] J. Millat, M. Ross, W.A. Wakeham and M. Zalaf, Physica (to be published).

[63] R. Holmes, G.R. Jones and N. Pusat, Trans. Faraday Soc. 60, 1220 (1964).

[65] M. Jahangiri, R.T. Jacobsen, R.B. Stewart and R.D. McCarty, J. Phys. Chem. Ref. Data 15, 593 (1986).

[66] A. Boushehri, J. Bzowski, J. Kestin and E.A. Mason, J. Phys.

Chem. Ref. Data (in press).

[67] J.D. Lambert and J.S. Rowlinson, Proc. Roy. Soc. A214, 424 (1951).

[68] W. Griffith, J. Appl. Phys. 21, 1319 (1950).

[69] B.A. Younglove and J.F. Ely, J. Phys. Chem. Ref. Data 16, 577 (1987).

[70] E.N. Haran, G.C. Maitland, M. Mustafa and W.A. Wakeham, Ber. Bunsenges. Phys. Chem. 87, 657 (1983).

[71] J. Millat and W.A. Wakeham (to be published)

[72] W.A. Cole and W.A. Wakeham, J. Phys. Chem. Ref. Data 14, 209 (1985).

[73] E. Vogel, Ber. Bunsenges. Phys. Chem. 88, 997 (1984).

[74] E. Vogel, T. Srehlow, J. Millat and W.A. Wakeham, Z. Phys. Chem. (Leipzig) (submitted).

[75] D.L. Timrot, M.A. Seredrizkaja and S.A. Traktujeva, Teploenergetika 84, (1975).

[76] S. Angus, K.M. de Reuck and B. Armstrong, International Thermodynamic Tables of the Fluid State – 6: Nitrogen (Pergamon, Oxford, 1979).

[77] H.J.M. Hanley, R.D. McCarty and E.G. D. Cohen, Physica 60, 322 (1972).

[78] G.A. Olchowy and J.V. Sengers, University of Maryland, Institute for Physical Science and Technology Technical Report BN1052 (1986).

[79] H.M. Roder, Int. J. Thermophys. 6, 119 (1985).

[80] Millat *et al* (to be published).

[81] J.H. Dymond and E.B. Smith, The Virial Coefficients of Pure Gases and Mixtures (Clarendon, Oxford, 1980).

[82] J. Kestin, K. Knierim, E.A. Mason, B. Najafi, S.T. Ro and M. Waldman, J. Phys. Ref. Data 13, 229 (1984).

[83] M.J. Assael, C.A. Nieto de Castro and W.A. Wakeham, ChemPor '78, Braga, Portugal, 1978, pp. 16.1–16.9.

[84] M. Ross, R. Szczepanski, R.D. Trengove and W.A. Wakeham, Paper 96C presented at the Annual Winter Meeting of the AIChE, Miami, Florida, U.S.A. (November 1986).

[85] E. Vogel, B. Holdt and T.Strewhlow, Physica 148A, 46 (1988).

[86] M. Mustafa, PhD Thesis, University of London (1988).

[87] J.D. Lambert, 'Vibrational and Rotational Relaxation in Gases' (Clarendon, Oxford, 1981).

[88] H.M. Roder, Int. J. Thermophys., 5, 323 (1984).

[89] M.J. Assael, M. Dix, A. Lucas and W.A. Wakeham, J. Chem. Soc., Faraday Trans., I, 77, 439 (1981).

[90] A.I. Johns, S. Rashid, J.T.R Watson and A.A. Clifford, J. Chem. Soc., Faraday Trans., I, 82, 2235 (1986); A.C Scott, A.I. Johns, J.T.R Watson and A.A Clifford, J. Chem. Soc. Faraday Trans., I, 79, 733 (1983).

[91] Uribe,Mason and Kestin (to be published) (1988).

[92] J. Millat (private comunication) (1988).

Table 6.2.1

Statistical analysis of the Argon data.

T (K)	Max. Dens. Of fit. (Kgm^{-3})	Order of polynomial.	$\lambda_0 \pm\sigma_{\lambda_0}$ ($mWm^{-1}K^{-1}$)	$\lambda_1 \pm\sigma_{\lambda_1}$ ($\mu Wm^{2}Kg^{-1}K^{-1}$)	$\lambda_2 \pm\sigma_{\lambda_2}$ ($nWm^{5}Kg^{-2}K^{-1}$)	$\lambda_3 \pm\sigma_{\lambda_3}$ ($pWm^{8}Kg^{-3}K^{-1}$)	σ_{λ_3} (%)
174	71	1	10.96 ±0.01	25.2 ±0.2	——	——	±0.11
	150	2	11.01 ±0.01	21.4 ±0.4	46 ±3	——	±0.12
223.15	65	1	13.76 ±0.02	25.2 ±0.5	——	——	±0.15
	176	2	13.77 ±0.02	24.0 ±0.6	18 ±3	——	±0.16
266.65	66	1	16.06 ±0.01	26.4 ±0.3	——	——	±0.08
	182	2	16.11 ±0.03	23.4 ±0.7	21 ±3	——	±0.17
308.15	40	1	18.13 ±0.02	25.4 ±0.6	——	——	±0.16
	101	2	18.13 ±0.02	25.4 ±1.1	4.3 ±11	——	±0.16
333.15	104	1	19.43 ±0.02	25.2 ±0.3	——	——	±0.15
	148	2	19.48 ±0.02	22.3 ±0.8	27 ±5	——	±0.15
378.15	78	1	21.61 ±0.01	24.6 ±0.2	——	——	±0.06
	141	2	21.66 ±0.02	22.0 ±0.6	25 ±4	——	±0.07
428.15	96	1	23.87 ±0.03	22.8 ±0.5	——	——	±0.20
	120	2	23.94 ±0.04	19.0 ±1.4	38 ±10	——	±0.18

Table 6.2.2

Statistical analysis of the Helium and Neon data.

T (K)	Max. Dens. Of fit. (Kgm^{-3})	Order of polynomial.	$\lambda_0 \pm \sigma_{\lambda_0}$ ($mWm^{-1}K^{-1}$)	$\lambda_1 \pm \sigma_{\lambda_1}$ ($\mu Wm^{2}Kg^{-1}K^{-1}$)	$\lambda_2 \pm \sigma_{\lambda_2}$ ($nWm^{5}Kg^{-2}K^{-1}$)	σ_λ (%)
Helium						
308.15	15	1	159.6 ±0.3	257 ±33	———	0.25
337.65	15	1	170.2 ±0.3	304 ±26	———	0.18
379.65	12	1	183.6 ±0.3	211 ±37	———	0.22
428.15	12	1	201.9 ±0.4	255 ±48	———	0.20
Neon						
308.15	32	1	50.02 ±0.07	34 ±2	———	0.14
337.65	53	1	53.48 ±0.08	45 ±3	———	0.15
	69	2	53.41 ±0.10	52 ±7	-134 ±88	0.19
379.65	39	1	57.70 ±0.08	40 ±2	———	0.14
	56	2	57.37 ±0.13	76±9	-515 ±144	0.23
428.15	56	1	63.05 ±0.07	44±2	———	0.11

Table 6.2.3

Experimental reduced Eucken factors and theoretical thermal conductivities for Argon.

Temperature T(K)	Viscosity η^0 (μPa.s)	Viscosity η^0 (μPa.s)	λ^0_{exp} ($mWm^{-1}K^{-1}$)	λ^0_{th} ($mWm^{-1}K^{-1}$)	Eu_{exp}	Eu_{exp}
174	14.0[a]	———	10.96	10.89	1.003 ±0.01[a]	———
223.15	17.6[a]	———	13.76	13.70	1.001 ±0.01[a]	———
266.65	20.6[a]	———	16.06	16.02	0.998 ±0.01[a]	———
308.15	23.24[b]	23.22[c]	18.13	18.12	0.9996 ±0.004[b]	0.9992 ±0.004[c]
333.15	24.81[b]	24.76[c]	19.43	19.33	1.002 ±0.004[b]	1.004 ±0.004[c]
378.15	27.60[b]	27.40[c]	21.61	21.42	1.001 ±0.004[b]	1.009 ±0.004[c]
428.15	30.40[b]	30.19[c]	23.87	23.62	1.004 ±0.004[b]	1.011 ±0.004[c]

(a) ref.25 (b) ref.22 (c) ref.24

Table 6.2.4

Experimental reduced Eucken factors and theoretical thermal conductivities for Helium and Neon

Temperature T(K)	Viscosity η^0 (μPa.s)	Viscosity η^0 (μPa.s)	λ^0_{exp} ($mWm^{-1}K^{-1}$)	λ^0_{th} ($mWm^{-1}K^{-1}$)	Eu_{exp}	Eu_{exp}
Helium						
308.15	20.23[a]	20.30[c]	159.6	158.6	1.004 ±0.005[a]	1.005 ±0.005[c]
337.65	21.64[a]	21.64[c]	170.2	168.7	1.005 ±0.005[a]	1.006 ±0.005[c]
379.65	23.44[a]	23.43[c]	183.6	182.7	1.001 ±0.005[a]	1.002 ±0.005[c]
428.15	25.75[a]	25.45[c]	201.9	198.4	1.002 ±0.005[a]	1.014 ±0.005[c]
Neon						
308.15	32.46[b]	32.49[c]	50.02	50.32	0.9936 ±0.005[b]	0.9927 ±0.005[c]
337.15	34.57[b]	34.55[c]	53.48	53.53	0.9976 ±0.005[b]	0.9982 ±0.005[c]
379.65	37.48[b]	37.38[c]	57.70	57.91	0.9925 ±0.005[b]	0.9952 ±0.005[c]
428.15	40.66[b]	40.48[c]	63.05	62.76	0.9998 ±0.005[b]	1.0040 ±0.005[c]

(a) ref.23 (b) ref.22 (c) ref.24

Table 6.3.1 Statistical analysis of the Hydrogen and Nitrogen Data

T (K)	Max. Dens. Of fit. (Kgm^{-3})	Order of polynomial.	$\lambda_0 \pm \sigma_{\lambda_0}$ ($mWm^{-1}K^{-1}$)	$\lambda_1 \pm \sigma_{\lambda_1}$ ($\mu Wm^{2}Kg^{-1}K^{-1}$)	$\lambda_2 \pm \sigma_{\lambda_2}$ ($nWm^{5}Kg^{-2}K^{-1}$)	$\lambda_3 \pm \sigma_{\lambda_3}$ ($pWm^{8}Kg^{-3}K^{-1}$)	σ_λ (%)
Hydrogen							
308.15	7	1	193.7 ±0.3	893 ±60	———	———	0.21
337.65	6	1	209.0 ±0.4	813 ±110	———	———	0.29
379.65	5	1	226.7 ±0.4	724 ±99	———	———	0.13
428.15	6	1	245.3 ±0.5	1278 ±120	———	———	0.20
Nitrogen							
270.15	27	1	23.99 ±0.02	46.5 ±1.3	———	———	0.08
	114	2	24.04 ±0.04	40.9 ±1.5	70 ±13	———	0.19
225.15	45	1	20.47 ±0.01	41.9 ±0.5	———	———	0.06
	92	2	20.52 ±0.01	36.6 ±0.6	104 ±6	———	0.05
	175	3	20.54 ±0.03	34.7 ±1.7	146 ±23	-224 ±86	0.13
177.50	44	1	16.64 ±0.02	42.8 ±0.8	———	———	0.13
	95	2	16.66 ±0.02	40.0 ±1.2	66 ±11	———	0.13
	226	3	16.73 ±0.06	33.8 ±2.6	158 ±28	-130 ±82	0.32

Table 6.3.2

Statistical analysis of the Carbon dioxide data.

T (K)	Max. Dens. Of fit. (Kgm^{-3})	Order of polynomial.	$\lambda_0 \pm\sigma_{\lambda_0}$ ($mWm^{-1}K^{-1}$)	$\lambda_1 \pm\sigma_{\lambda_1}$ ($\mu Wm^{2}Kg^{-1}K^{-1}$)	$\lambda_2 \pm\sigma_{\lambda_2}$ ($nWm^{5}Kg^{-2}K^{-1}$)	$\lambda_3 \pm\sigma_{\lambda_3}$ ($pWm^{8}Kg^{-3}K^{-1}$)	σ_λ (%)
308.15	49	1	17.31 ±0.04	34.4 ±1.2	———	———	0.26
	100	2	17.40 ±0.04	25.5 ±1.7	172 ±16	———	0.22
	129	3	17.35 ±0.10	31 ±6	14 ±9	1.2 ±0.5	0.34
333.15	37	1	19.53 ±0.03	27.0 ±1.0	———	———	0.13
	118	2	19.58 ±0.04	20.2 ±1.4	199 ±11	———	0.26
	125	3	19.55 ±0.06	22 ±4	150 ±72	301 ±366	0.25
379.15	35	1	23.25 ±0.03	23 ±1	———	———	0.11
	109	2	23.23 ±0.04	20 ±2	152 ±14	———	0.21
425.65	37	1	27.34 ±0.05	26 ±2	———	———	0.19
	46	2	27.56 ±0.07	38 ±6	493 ±103	———	0.14

Table 6.3.3

Statistical analysis of the Nitrous oxide data.

T (K)	Max. Dens. Of fit. (Kgm^{-3})	Order of polynomial.	$\lambda_0 \pm\sigma_{\lambda_0}$ ($mWm^{-1}K^{-1}$)	$\lambda_1 \pm\sigma_{\lambda_1}$ ($\mu Wm^{2}Kg^{-1}K^{-1}$)	$\lambda_2 \pm\sigma_{\lambda_2}$ ($nWm^{5}Kg^{-2}K^{-1}$)	$\lambda_3 \pm\sigma_{\lambda_3}$ ($pWm^{8}Kg^{-3}K^{-1}$)	σ_λ (%)
308.15	28	1	18.21 ±0.05	29.5 ±2.5	———	———	0.18
	122	2	18.17 ±0.05	27.9 ±1.8	156 ±14	———	0.29
	153	3	18.16 ±0.09	28.8 ±1.5	146 ±73	5 ±300	0.35
337.65	37	1	20.62 ±0.04	27.7 ±2.0	———	———	0.17
	139	2	20.61 ±0.03	24.3 ±0.9	152 ±7	———	0.17
	163	3	20.63 ±0.08	23 ±4	179 ±62	-168 ±247	0.25
379.15	35	1	25.05 ±0.05	19.4 ±2	———	———	0.16
	46	2	25.17 ±0.08	7 ±7	283 ±117	———	0.15
425.65	36	1	29.32 ±0.05	13 ±2	———	———	0.15
	53	2	29.43 ±0.08	0.4 ±6	319 ±104	———	0.16

Table 6.3.4

Statistical analysis of the Methane data.

T (K)	Max. Dens. Of fit. (Kgm^{-3})	Order of polynomial.	$\lambda_0 \pm\sigma_{\lambda_0}$ ($mWm^{-1}K^{-1}$)	$\lambda_1 \pm\sigma_{\lambda_1}$ ($\mu Wm^{2}Kg^{-1}K^{-1}$)	$\lambda_2 \pm\sigma_{\lambda_2}$ ($nWm^{5}Kg^{-2}K^{-1}$)	$\lambda_3 \pm\sigma_{\lambda_3}$ ($pWm^{8}Kg^{-3}K^{-1}$)	σ_λ (%)
308.15	17	1	36.02 ±0.07	97 ±5	———	———	0.14
	43	2	36.07 ±0.04	83 ±1	780 ±50	———	0.11
	60	3	36.08 ±0.09	79 ±8	1034 ±241	-3663 ±2038	0.17
337.65	21	1	40.78 ±0.08	102 ±6	———	———	0.27
	45	2	40.77 ±0.07	98 ±7	425 ±134	———	0.27
	50	3	40.76 ±0.13	100 ±22	334 ±970	1170 ±12214	0.25
379.15	14	1	47.40 ±0.07	99 ±7	———	———	0.14
	47	2	47.55 ±0.07	74 ±7	716 ±140	———	0.16
	50	3	47.38 ±0.11	110 ±17	-1151 ±773	27510 ±9868	0.16
425.65	25	1	56.58 ±0.05	80 ±3	———	———	0.09
	35	2	56.87 ±0.13	39 ±12	1348 ±275	———	0.16

Table 6.3.5

Statistical analysis of the Tetrafluoromethane data.

T (K)	Max. Dens. Of fit. (Kgm^{-3})	Order of polynomial.	$\lambda_0 \pm\sigma_{\lambda_0}$ ($mWm^{-1}K^{-1}$)	$\lambda_1 \pm\sigma_{\lambda_1}$ ($\mu Wm^{2}Kg^{-1}K^{-1}$)	$\lambda_2 \pm\sigma_{\lambda_2}$ ($nWm^{5}Kg^{-2}K^{-1}$)	$\lambda_3 \pm\sigma_{\lambda_3}$ ($pWm^{8}Kg^{-3}K^{-1}$)	σ_λ (%)
308.15	17	1	16.76 ±0.03	12.4 ±0.8	———	———	0.18
	168	2	16.74 ±0.04	12.1 ±1.3	23 ±7	———	0.24
	464	3	16.78 ±0.05	10.4 ±1.2	39 ±7	-30 ±11	0.30
331.65	75	1	18.69 ±0.04	12.6 ±0.9	———	———	0.15
	240	2	18.70 ±0.04	10.6 ±0.8	35 ±3	———	0.24
	390	3	18.69 ±0.05	10.7 ±1.2	40 ±7	-30 ±12	0.27
371.15	69	1	21.70 ±0.07	15.0 ±1.4	———	———	0.17
	171	2	21.80 ±0.04	10.9 ±1.0	36 ±5	———	0.18
	287	3	21.87 ±0.06	7.8 ±1.8	67 ±13	-83 ±29	0.18
425.65	27	1	26.29 ±0.05	5.2 ±2.7	———	———	0.15
	185	2	26.16 ±0.04	12.4 ±1.1	44 ±6	———	0.27

Table 6.3.6

The derived density coefficients of thermal conductivity of the polyatomic gases.

T (K)	λ_0 ($mWm^{-1}K^{-1}$)	λ_1 ($\mu Wm^{-1}K^{-1}$)
Hydrogen		
308.15	193.7 ±0.3	893 ±60
337.65	209.0 ±0.4	813 ±110
379.65	226.7 ±0.4	724 ±99
428.15	245.3 ±0.5	1278 ±120
Nitrogen		
177.5	16.64 ±0.02	42.8 ±0.8
225.15	20.47 ±0.01	41.9 ±0.5
270.15	23.99 ±0.02	46.5 ±1.3
Carbon dioxide		
308.15	17.31 ±0.04	34.4 ±1.2
333.15	19.53 ±0.03	27.0 ±1.0
379.15	23.25 ±0.03	22.7 ±1.0
425.65	27.34 ±0.05	26.3 ±2.0
Nitrous oxide		
308.15	18.21 ±0.05	29.5 ±2.5
337.65	20.62 ±0.04	27.7 ±2.0
379.15	25.05 ±0.05	19.4 ±2.0
426.15	29.32 ±0.05	13.0 ±2.0

Table 6.3.6/cont.

Metane		
309.15	36.02 ±0.07	97 ±5
337.65	40.78 ±0.08	102 ±6
379.15	47.40 ±0.07	99 ±7
425.65	56.58 ±0.05	70 ±3
Tetrafluoromethane		
308.15	16.76 ±0.03	12.4 ±0.8
331.15	18.69 ±0.04	12.6 ±0.9
371.15	21.70 ±0.07	15.0 ±1.4
425.65	26.29 ±0.05	5.2 ±2.7
Ethylene		
308.15	22.59 ±0.12	20.8 ±4.1
335.15	25.93 ±0.18	4.6 ±18
371.15	31.78 ±0.18	16.6 ±5.4
425.65	41.67 ±0.25	8.1 ±9.0
Ethane		
308.15	22.87 ±0.14	55.5 ±6.5
331.15	26.14 ±0.15	50.6 ±3.2
380.15	34.01 ±0.18	46.0 ±7.7
425.65	42.29 ±0.25	-3.8 ±14

Table 6.3.7

Wang Chang Uhlenbeck effective cross-sections for Hydrogen.(All cross-sections have units $10^{-20}m^2$.)

T (K)	$\sigma(0001)$ $\times 10^{-2}$	$\sigma(1001)$	$\sigma(1010)$	$\sigma\binom{1010}{1001}$ $\times 10^{-2}$	$\sigma(2000)$
308.15	6.405	12.83	12.24	3.333	18.31
337.65	6.408	12.22	12.05	3.365	18.02
379.65	6.419	12.07	11.80	3.397	17.65
428.15	6.448	12.02	11.55	3.426	17.27

Table 6.3.8

Thijsse effective cross-sections for Hydrogen.
(All cross-sections hve units $10^{-20}m^2$.)

T (K)	$\sigma(10E)$	$\sigma(10D)$	$\sigma\binom{10E}{10D}$	$\dfrac{\sigma^2\binom{10E}{10D}}{\sigma(10E)\,\sigma(10D)}$
308.15	12.38	12.69	-0.2497	0.9996
337.65	12.21	12.20	-0.0637	1.0000
397.65	11.85	12.02	-0.1077	0.9999
428.15	11.65	11.92	-0.1987	0.9997

Table 6.3.9

Values of A^* and D_{int}/D for Hydrogen.

T (K)	A^*	D_{int}/D
308.15	1.154	1.03 ±0.02
337.65	1.158	1.07 ±0.02
397.65	1.162	1.05 ±0.02
428.15	1.165	1.03 ±0 02

Table 6.3.10

Wang Chang Uhlenbeck effective cross-sections for Carbon dioxide (All cross-sections have units $10^{-20}m^2$.)

T (K)	$\mathfrak{S}(0001)$	$\mathfrak{S}(1001)$	$\mathfrak{S}(1010)$	$\mathfrak{S}\binom{1010}{1001}$	$\mathfrak{S}(2000)$
308.15	15.99	50.06	51.71	11.97	50.69
333.15	13.42	46.05	48.64	10.37	48.91
379.65	10.14	41.91	44.21	8.24	46.22
425.65	8.00	37.73	40.86	6.78	44.06

Table 6.3.11

Thijsse effective cross-sections for Carbon dioxide.

(All cross-sections have units $10^{-20}m^2$.)

T (K)	$\mathcal{S}(10E)$	$\mathcal{S}(10D)$	$\mathcal{S}(^{10E}_{10D})$	$\frac{\mathcal{S}^2(^{10E}_{10D})}{\mathcal{S}(10E)\,\mathcal{S}(10D)}$
308.15	38.63	62.15	2.59	0.9972
338.15	36.65	57.07	2.54	0.9969
379.15	34.44	50.85	1.77	0.9982
425.65	32.12	45.74	1.82	0.99778

Table 6.3.12

Values of A^* and D_{int}/D for Carbon dioxide.

T (K)	A^*	D_{int}/D
308.15	1.114	0.901
338.15	1.107	0.936
379.15	1.101	0.950
425.65	1.096	0.993

Table 6.3.13

Wang Chang Uhlenbeck effective Cross-sections for Nitrous oxide.(All cross-sections have units $10^{-20}m^2$.)

T (K)	$\sigma(0001)$	$\sigma(1001)$	$\sigma(1010)$	$\sigma(^{1010}_{1001})$	$\sigma(2000)$
308.15	14.70	48.28	51.83	11.49	50.81
337.65	12.02	45.05	48.05	9.71	48.53
379.15	9.42	38.89	43.96	7.92	45.96
426.15	7.47	35.77	40.54	6.52	43.74

Table 6.3.14

Thijsse effective cross-sections for nitrous oxide (All cross-sections have uints $10^{-20}m^2$.)

T (K)	$\sigma(10E)$	$\sigma(10D)$	$\sigma(^{10E}_{10D})$	$\frac{\sigma^2(^{10E}_{10D})}{\sigma(10E)\,\sigma(10D)}$
308.15	38.24	60.88	3.00	0.9961
337.65	36.43	55.73	2.27	0.9975
379.15	33.08	48.98	2.86	0.9950
426.15	31.15	44.44	2.22	0.9957

Table 6.3.15

Values of A^* and D_{int}/D for nitrous oxide

T (K)	A^*	D_{int}/D
308.15	1.121	0.92
337.65	1.113	0.93
379.15	1.105	1.01
426.15	1.099	1.04

Table 6.3.16

Wang Chang Uhlenbeck effective cross-sections for methane. (All cross-sections have units $10^{-20} m^2$.)

T (K)	$\sigma_{(0001)}$	$\sigma_{(1001)}$	$\sigma_{(1010)}$	$\sigma_{\binom{1010}{1001}}$	$\sigma_{(2000)}$
309.15	5.15	34.04	32.71	3.69	41.15
337.65	4.41	31.67	31.46	3.28	39.85
379.15	3.58	30.09	30.01	2.82	38.32
425.65	2.89	27.68	28.77	2.44	36.99

Table 6.3.17

Thijsse effective cross-sections for methane.

(All cross-sections have units $10^{-20} m^2$.)

T (K)	$\sigma(10E)$	$\sigma(10D)$	$\sigma(^{10E}_{10D})$	$\frac{\sigma^2(^{10E}_{10D})}{\sigma(10E)\,\sigma(10D)}$
309.15	29.54	37.00	-0.002	1.0000
337.65	28.21	34.74	0.35	0.9999
379.15	27.15	32.79	0.19	1.0000
425.65	25.71	30.60	0.58	0.9996

Table 6.3.18

Values of A^*, D_{int}/D and ξ_{rot} for Methane.

T (K)	A^*	D_{int}/D	ξ_{rot}
309.15	1.094	1.00	8.3
337.65	1.093	1.03	8.6
379.15	1.092	1.03	9.1
425.65	1.093	1.08	9.6

Table 6.3.19

Wang Chang Uhlenbeck effective cross-sections for Tetrafluoromethane.(All cross-sections have units $10^{-20}m^2$.)

T (K)	$\sigma(0001)$	$\sigma(1001)$	$\sigma(1010)$	$\sigma\binom{1010}{1001}$	$\sigma(2000)$
308.15	6.78	51.71	59.91	7.99	61.63
331.65	5.98	49.91	57.78	7.28	60.07
371.15	5.01	48.21	54.92	6.40	57.89
425.65	4.15	45.31	51.99	5.57	55.55

Table 6.3.20

Thijsse effective cross-sections for Tetrafluoromethane. (All cross-sections have units $10^{-20}m^2$.)

T (K)	$\sigma(10E)$	$\sigma(10D)$	$\sigma\binom{10E}{10D}$	$\dfrac{\sigma^2\binom{10E}{10D}}{\sigma(10E)\,\sigma(10D)}$
308.15	46.70	64.60	1.36	0.9994
331.65	45.42	61.96	1.17	0.9995
371.15	44.15	58.68	0.63	0.9998
425.65	41.98	55.05	0.64	0.9998

Table 6.3.21

Values of A^*, D_{int}/D and ξ_{rot} for Tetrafluoromethane.

T (K)	A^*	D_{int}/D	ξ_{rot}
308.15	1.093	0.97	3.5
331.15	1.092	0.98	3.6
371.15	1.092	0.97	3.8
425.65	1.093	0.98	4.0

Table 6.3.22

Wang Chang Uhlenbeck effective cross-sections for Ethylene. (All cross-sections have units 10^{-20} m^2)

T (K)	$\mathcal{C}(0001)$	$\mathcal{C}(1001)$	$\mathcal{C}(1010)$	$\mathcal{C}(^{1010}_{1001})$	$\mathcal{C}(2000)$
308.15	28.31	57.19	82.70	24.82	58.74
333.15	22.86	52.52	76.68	21.10	56.61
371.15	17.13	46.58	69.51	16.95	53.95
425.65	12.08	39.97	62.03	13.01	51.01

Table 6.3.23

Thijsse effective cross-sections for Ethylene.

(All cross-section have units $10^{-20}m^2$.)

T (K)	$\sigma(10E)$	$\sigma(10D)$	$\sigma\binom{10E}{10D}$	$\frac{\sigma^2\binom{10E}{10D}}{\sigma(10E)\,\sigma(10D)}$
308.15	44.50	95.39	11.47	0.9969
333.15	42.38	86.81	9.87	0.9974
371.15	39.39	76.70	8.41	0.9977
425.65	35.64	66.36	7.41	0.9977

Table 6.3.24

Values of A^* and D_{int}/D for Ethylene.

T (K)	A^*	D_{int}/D
308.15	1.113	1.02
333.15	1.108	1.04
371.15	1.102	1.07
425.65	1.096	1.14

Table 6.3.25

Wang Chang Uhlenbeck effective cross-sections for Ethane.
(All cross-sections have units $10^{-20}m^2$.)

T (K)	$\sigma(0001)$	$\sigma(1001)$	$\sigma(1010)$	$\sigma\binom{1010}{1001}$	$\sigma(2000)$
308.15	23.72	62.41	97.08	24.87	67.39
331.65	19.78	58.18	90.79	21.65	65.10
380.15	14.28	50.92	81.06	16.94	61.31
425.65	11.07	46.05	74.55	14.01	58.58

Table 6.3.26

Thijsse effective cross-sections for Ethane.
(All cross-sections have units $10^{-20}m^2$.)

T (K)	$\sigma(10E)$	$\sigma(10D)$	$\sigma\binom{10E}{10D}$	$\dfrac{\sigma^2\binom{10E}{10D}}{\sigma(10E)\,\sigma(10D)}$
308.15	51.60	107.88	11.27	0.9977
331.65	49.28	99.70	9.96	0.9980
380.15	44.94	87.04	8.43	0.9982
425.65	41.78	78.80	7.55	0.9983

Table 6.3.27

Values of A^* and D_{int}/D for Ethane

T (K)	A^*	D_{int}/D
308.15	1.114	1.00
331.65	1.108	1.01
380.15	1.100	1.06
425.65	1.096	1.10

Table 6.3.28

Wang Chang Uhlenbeck effective cross-sections for Nitrogen.(All cross-sections have units $10^{-20}m^2$.)

T (K)	$\mathcal{S}(0001)$	$\mathcal{S}(1001)$	$\mathcal{S}(1010)$	$\mathcal{S}\binom{1010}{1001}$	$\mathcal{S}(2000)$
177.50	31.98	47.77	44.93	16.86	40.71
225.15	23.92	41.21	38.28	12.61	37.46
270.15	19.46	36.88	34.44	10.27	35.40
308.15	16.91	34.95	32.17	8.93	34.12
337.15	15.40	33.09	30.82	8.14	32.39
378.15	13.69	31.20	29.30	7.26	32.39
429.15	12.03	29.44	27.84	6.42	31.47

Table 6.3.29

Thijsse effective cross-sections for Nitrogen.

(All cross.sections have units $10^{-20} m^2$.)

T (K)	$\mathfrak{S}(10E)$	$\mathfrak{S}(10D)$	$\mathfrak{S}(^{10E}_{10D})$	$\frac{\mathfrak{S}^2(^{10E}_{10D})}{\mathfrak{S}(10E)\,\mathfrak{S}(10D)}$
177.50	30.21	61.48	6.39	0.9780
225.15	27.44	51.08	4.51	0.9855
270.15	25.60	44.81	3.70	0.9881
308.15	24.64	41.58	2.96	0.9914
337.15	23.86	39.18	2.84	0.9914
378.15	23.03	36.63	2.59	0.9920
429.15	22.23	34.23	2.33	0.9929

Table 6.3.30

Values of A^* and D_{int}/D for Nitrogen.

T (K)	A^*	D_{int}/D
177.50	1.097	0.974
225.15	1.092	0.978
270.15	1.092	0.995
308.15	1.094	0.981
337.15	1.096	0.999
378.15	1.098	1.010
429.15	1.102	1.017

Table 6.5.1

The first density coefficient of thermal conductivity

Temperature T/(K)	Source	$10^5\lambda$ mol^{-1} Experiment	MET–I	MET–II
Helium				
428	This work	0.51 ± 0.1	1.36	0.75
379.6		0.46 ± 0.05	1.35	0.75
338		0.71 ± 0.06	1.33	0.75
308		0.64 ± 0.07	1.32	0.75
Hydrogen				
428	This work	0.10 ± 0.01	1.81	0.99
379.6		0.64 ± 0.08	1.30	0.52
337.6		0.78 ± 0.09	1.11	0.35
308		0.92 ± 0.07	0.87	0.15
300	[88]	1.20 ± 0.02	1.32	0.60
200		1.80 ± 0.03	1.14	0.73
175		2.10 ± 0.04	1.12	0.83
150		2.50 ± 0.04	1.04	0.98
125		2.70 ± 0.03	0.82	1.12
100		3.30 ± 0.05	0.38	1.32

Continued.

Temperature T/(K)	Source	$10^5\lambda$ mol^{-1} Experiment	MET–I	MET–II
Nitrogen				
429	[70]	3.46 ± 0.04	2.59	1.27
378		3.83 ± 0.08	2.88	0.41
333		3.95 ± 0.04	3.23	0.37
308		4.54 ± 0.08	3.59	0.34
Methane				
425.6	This work	1.8 ± 0.1	2.11	–0.062
379.1		3.1 ± 0.1	3.69	0.30
337.6		4.5 ± 0.1	5.07	0.59
309.1		4.9 ± 0.1	6.09	0.92
Krypton				
308	[89]	8.30 ± 0.04	8.54	3.76
Xenon				
308	[89]	16.9 ± 0.2	18.7	7.27
Argon				
428	[70]	4.10 ± 0.04	5.23	2.25
378		4.60 ± 0.04	5.89	2.32
333		5.20 ± 0.04	6.29	2.41
308		5.50 ± 0.04	6.29	2.49

Continued.

Temperature T/(K)	Source	$10^5\lambda$ mol^{-1} Experiment	MET–I	MET–II
Carbon dioxide				
426	This work	4.1 ± 0.3	10.5	0.24
379.6		4.5 ± 0.3	13.4	0.74
337.6		6.2 ± 0.6	10.3	1.32
308		8.7 ± 0.3	6.99	1.83
Neon				
428	This work	1.41 ± 0.05	1.42	0.94
379.6		1.84 ± 0.1	1.34	0.97
337.6		1.75 ± 0.11	1.25	0.99
308		2.24 ± 0.15	1.17	1.01
Carbon monoxide				
429	[70]	2.89 ± 0.03	2.48	1.43
378		3.49 ± 0.03	4.52	1.63
337		3.76 ± 0.03	8.65	1.69
Ethylene				
425.6	This work	2.7 ± 0.5	15.0	–1.75
379.1		2.7 ± 0.5	7.93	–0.96

CHAPTER 7

CONCLUSION

In response to the need for high accuracy thermal conductivity data over a wide thermodynamic range measurements have been made on a variety of monatomic and polyatomic gases between 170K and 430K and at pressures up to 10 MPa. It has been demonstrated that the data is accurate to within ± 0.3% in most cases except near the critical density. Further, the data are believed to be the most reliable currently available.

The aquisition of the high accuracy data required significant modification of the existing instrument which provided data near room temperature only. It is hoped that the modified instrument will be used to provide more low temperature gas and liquified gas data so that the theories of the transport properties of gases and liquids can be tested further. The low temperature capability also means that industrially important refrigerant gases can be studied in the gas phase. It is anticipated that an insulated wire instrument would be appropriate and in addition, measurements near to saturation will require further development of the rig.

Full advantage has been taken of the new data in order to test existing theories concerning transport properties. Particularly successful was the comparison between experiment and theory in the case of monatomic gases in the limit of zero density both with respect to high accuracy viscosity measurements and the predictions of various proposed intermolecular potentials. In the limit of zero density the polyatomic gas data has been used to obtain experimental effective cross–section information of a greater or lesser uncertainty depending on the availability of the relaxation data. It is expected that this information will be useful to those who wish to construct realistic anisotropic potentials and also for

those who wish to test approximate methods.

In the mean time the Wang Chang and Uhlenbeck effective cross–sections have been used to calculate intermediate molecular properties, notably the ratio of diffusion coefficients D_{int}/D. These calculations have demonstrated that approximating this ratio to unity is in considerable error for most gases. The approximation is more successful for gases in which internal energy relaxation is slow (eg Hydrogen and Methane). The basis for the approximation is that the internal energy exchanged during an inelastic collision is small compared to the kinetic energy of the colliding molecules. This is not the case for Hydrogen and Methane. The reason for the success of the approach for these gases is obscure except that the frequency of inelastic collisions is so low that their effect on the bulk gas is small regardless of the energy exchanged.

The only theoretical guidance available regarding the ratio of diffusion coefficients is that for rigid rotors the classical limit is unity. Some gases studied here tend to confirm the validity of this limit. In other cases the limit appears to be well in excess of unity. In these instances there is a significant vibrational contribution to the heat capacity of the molecules. It has not been proven but it seems reasonable to suppose that D_{int}/D for such systems also tends to unity in the classical limit. It would however be premature to discount this idea since the way in which multi–mode systems are treated within the kinetic theory is by way of an *ad hoc* extension without a theoretical basis. It therefore seems appropriate to make a further theoretical and experimental study of multi–mode systems in order to clarify the situation. Progress in this area is hampered by lack of high quality relaxation time or thermo–molecular pressure difference data so attention should be turned in these directions before the physics of polyatomic systems can be fully understood.

In addition to serving an important theoretical function the new data represents a considerable increase in the volume of high quality data available for inclusion in physical properties data bases. The foundation for such data bases is often the zero density thermal conductivity and what is required is a temperature function for this property. The Wang Chang Uhlenbeck effective cross–sections have been used to obtain the effective cross–sections appropriate to the Thijsse formalism. It has been shown that the first order Thijsse result can be used as a simple form for representing the data to within ± 1% in general. This simplified representation enjoys the advantage that viscosity and relaxation time data are not required for its implimentation. It is believed that as the basis of a practical correlation the Thijsse formalism is the most appropriate so long as the first order result is applicable within a few percent.

For pure component systems an analysis equivalent to a first order Chapman and Cowling approximation is considered to be adequate. In the case of monatomic mixtures earlier work has demonstrated the need to extend the analysis to third order. The effect of higher order corrections in the case of polyatomic systems is at present unknown. The existing theory is only equivalent to a first order analysis and is known to fail in binary mixtures containing molecules with a large mass ratio. In this thesis new expressions have been derived which allow calculation of the thermal conductivity of mixtures to arbritrary order within the Wang Chang Uhlenbeck theory as generalised to mixtures. It is hoped that calculation of the relevant effective cross–sections required will soon be possible either exactly or by way of approximation. This will allow progress to be made in an area of considerable theoretical and industrial importance.

Further to the study of zero density thermal conductivity progress has been made in the moderately dense gas region where the thermal

conductivity is a linear function of density. The new data have allowed the first really rigorous test of the available theory. Sadly, the modified Enskog schemes have been found to be wholly inadequate and do not provide reliable prediction of the thermal conductivity. A new microscopically based theory shows considerable promise. The agreement between theory and experiment is good considering the Lennard–Jones 12–6 potential was used for the calculations. Encouraged by this success the theory was used as the basis of a semi–empirical scheme which reproduces the data well for most systems except at low reduced temperatures. Further low temperature measurements will help to improve the prediction. Also calculations based on more realistic potentials may give greater theoretical guidance.

It is evident that the problems associated with polyatomic systems abound and that low temperature experimental data of high accuracy is still needed. This must be accompanied by improved and new relaxation data and further theoretical developement. It is hoped that the Thijsse formalism can be applied to mixtures to provide simplified expressions for representing the data and that it may form the basis of a corresponding states approach for polyatomic systems. The method of application remains obscure. Significant progress is still required before a concise corresponding states approach is available as in the case for monatomic systems.

LIST OF PUBLICATIONS

1. Transient hot-wire measurements of the thermal conductivity of gases at elevated temperatures.
   G.C. Maitland, M. Mustafa, M. Ross, R.D. Trengove, W.A. Wakeham and M. Zalaf,
   Int. J. Thermophys. 7, 245 (1986).
2. The initial density dependence of the transport properties of gases.
   M. Ross, R. Szczepanski, R.D. Trengove and W.A. Wakeham.
   Paper WA86/23 presented at the AIChE Annual Winter Meeting, Miami, Florida, November 1986.
3. Absolute measurements of the thermal conductivity of helium and hydrogen.
   M. Mustafa, M. Ross, R.D. Trengove, W.A. Wakeham and M. Zalaf.
   Physica 141A, 233 (1987).
4. The thermal conductivity of argon, carbon dioxide and nitrous oxide.
   J. Millat, M. Mustafa, M. Ross, W.A. Wakeham and M. Zalaf.
   Physica 145A, 461 (1987).
5. The thermal conductivity of neon, methane and tetrafluoromethane.
   J. Millat, M. Ross, W.A. Wakeham and M. Zalaf.
   Physica 148A, 124 (1988).
6. The thermal conductivity of ethylene and ethane.
   J. Millat, M. Ross, W.A. Wakeham and M. Zalaf.
   Physica (in press).